SYNTHESIS AND CHARACTERIZATION OF NOVEL ETHYLENE COPOLYMERS BY PALLADIUM-DIIMINE CATALYSTS

By

PENG XIANG

Thesis Submitted as A Partial

Requirement in the

Doctor of Philosophy

in Materials Science

School of Graduate Studies

Laurentian University

Sudbury, Ontario, Canada

THESIS DEFENCE COMMITTEE/COMITÉ DE SOUTENANCE DE THÈSE
Laurentian Université/Université Laurentienne
Faculty of Graduate Studies/Faculté des études supérieures

Title of Thesis
Titre de la thèse SYNTHESIS AND CHARACTERIZATION OF NOVEL ETHYLENE COPOLYMERS BY PALLADIUM-DIIMINE CATALYSTS

Name of Candidate
Nom du candidat Xiang, Peng

Degree
Diplôme Doctor of Philosophy

Department/Program
Département/Programme Materials Science

Date of Defence September 24, 2015
Date de la soutenance

APPROVED/APPROUVÉ

Thesis Examiners/Examinateurs de thèse:

Dr. Zhibin Ye
(Supervisor/Directeur(trice) de thèse)

Dr. Louis Mercier
(Committee member/Membre du comité)

Dr. Ramesh Subramanian
(Committee member/Membre du comité)

Dr. M'Hamed Chahma
(Committee member/Membre du comité)

Dr. Robin A. Hutchinson
(External Examiner/Examinateur externe)

Dr. Joy Elizabeth Gray-Munro
(Internal Examiner/Examinateur interne)

Approved for the Faculty of Graduate Studies
Approuvé pour la Faculté des études supérieures
Dr. David Lesbarrères
Monsieur David Lesbarrères
Acting Dean, Faculty of Graduate Studies
Doyen intérimaire, Faculté des études supérieures

ACCESSIBILITY CLAUSE AND PERMISSION TO USE

ABSTRACT

Late transition metal catalysts, especially Pd-diimine catalysts, have been extensive studied for olefin polymerization. The unique characteristics of Pd–diimine catalysts, including chain walking mechanism, highly electrophilic cationic metal center with reduced oxophilicity, the capability of initiating and catalyzing olefin "living" polymerization, and the sterically tunable–diimine ligands, allow the synthesis of a range of polyolefins and olefin copolymers with special pedant functionalities and unique microstructures. The main objective of this thesis research is to synthesize different new types of polymers and polymer-grafted nanoparticles with Pd–diimine catalysts by utilizing above unique characteristics.

A broad class of low-polydispersity ethylene–norbornene (E–NB) copolymers having various controllable comonomer composition distributions, including gradient, alternating, diblock, triblock, and block-gradient, was synthesized through “living”/quasi-living E–NB copolymerization facilitated with a single Pd–diimine catalyst. This synthesis benefits from two remarkable features of the Pd–diimine catalyst, its high capability in NB incorporation and high versatility in rendering E–NB “living” copolymerization at various NB feed concentrations ($[NB]_0$) while under an ethylene pressure of 1 atm and at 15 °C.

A class of hyperbranched polyethylene ionomers containing positively charged tetralkylammonium ions and different counter anions were first synthesized by direct

one-pot copolymerization of ethylene with tetralkylammonium-containing acrylate-type ionic liquid comonomers. The use of a Pd–diimine catalyst, which shows excellent stability towards the highly polar ionic group, is key to the direct synthesis. The resulting ionomers properties including structural, thermal, and melt rheological properties have also been demonstrated.

In a further study, HBPE ionomers encapsulating self-supported Pd(0) nanoparticles (NPs) as efficient and recyclable supported Pd catalysts were synthesized with a Pd–diimine catalyst. The Pd(0) NPs were immobilized on the ionomer matrix through ionic interaction directly during the copolymerization of ethylene with polymerizable ionic liquid comonomer. The resulting ionomer supported Pd(0) nanocatalysts have been utilized to catalyze carbon-carbon cross coupling reactions (Suzuki and Heck reactions) and semi-hydrogenation of alkynes.

Moreover, the successful tuning of structural parameters of PE brushes in surface-initiated ethylene "living" polymerization from two types of silica nanoparticles were studied. The brush parameters that are controlled herein include brush length, density, and topology. The PE-grafted silicas with varying brush density and length are also used as nanofillers to construct polymer nanocomposites with an elastomeric ethylene-olefin copolymer (EOC) as the matrix polymer. The effects of brush length and density on the nanofiller dispersion, rheological properties, and tensile properties of the composites are examined (The preparation and characterization of the nanocomposites were carried out by K. Petrie and M. Kontopoulou at Queen's University).

ACKNOWLEDGEMENTS

First I would like to thank my supervisor, Professor Zhibin Ye, for his direction, assistance, and guidance. I also thank Professor Ramesh Subramanian, Professor Louis Mercier, Professor Hélène Joly, and Professor Gerardo Ulibarri for their guidance and help.

Second I would like to thank faculties and staffs including Natalie Boutet, Claudine Beausoleil, Henry Ylitalo, Greg Lakanen, Luc Beaudet, Linda Weber, Louise Cooper, and Professor David Lesbarreres, in Engineering, Chemistry, and Graduate Studies, who helped me greatly in my university life.

I would also like to thank my colleagues, both past and present, Dr. Xuewei Xia, Dr. Lixin Xu, Dr. Yuanqing Xu, Dr. Shiyun Li, Dr. Meixiu Wan, Dr. Pingwei Liu, Dr. Zhongmin Dong, Dr. Zhichao Zhang, Dr. Patakamuri Govindaiah, Dr. Vimal Tiwari, Shawn Morgan, Wei Liu, Patrick Campeau, John-Wesley McGraw, Yitan Chen, Eric Landry, Bienvenu Muboyayi, Zhe Chen, Hui Su, Lingqi Huang, Mark Grundy, and Jose Otavio Santos who provided tremendous help and support during my study.

Lastly, and most importantly, I would thank my parents and my wife for their constant support during my study. Without their support and understanding, I would not have been able to achieve so much as I have so far.

TABLE OF CONTENTS

Abstract **iii**

Acknowledgement **v**

Table of Contents **vi**

List of Figures **xii**

List of Schemes **xxiii**

List of Tables **xxv**

Nomenclature **xxvii**

Chapter 1: Introduction, Background and Research Objectives **1**

1.1 Introduction to Polyethylenes **1**

1.2 Ethylene Polymerization Techniques 3

1.2.1 Free Radical Polymerization 3

1.2.2 Ethylene Polymerization with Phillips Catalyst and Ziegler-Natta (Z-N) Catalysts 4

1.2.3 Ethylene Polymerization with Single-Site Metallocene Catalysts 7

1.2.4 Ethylene Polymerization with Single-Site Late Transition Metal Catalysts 9

1.2.4.1 Chain Walking 11

1.2.4.2 Copolymerization of Ethylene with Olefin 16

1.2.4.3 Copolymerization of Ethylene with Functional Monomers Containing Polar Groups 23

1.2.4.4 "Living" Ethylene Polymerization with Pd-Diimine Catalysts 27

1.3 Thesis Research Objectives and Outlines 29

1.4 References 31

Chapter 2: Alternating, Gradient, Block, and Block-Gradient Copolymers of Ethylene and Norbornene by Pd-Diimine-Catalyzed "Living" Copolymerization 38

Abstract 38

2.1 Introduction 39

2.2 Experimental Section 43

2.2.1 Materials 43

2.2.2 General Procedure for E-NB Copolymerizations 44

2.2.3 Characterizations and Measurements 45

2.3 Results and Discussion 47

2.3.1 Alternating and Gradient E-NB Copolymers by Single-Stage "Living" Copolymerization 48

2.3.2 Thermal Properties of Alternating and Gradient E-NB Copolymers 58

2.3.3 Diblock/Block-Gradient Copolymers by Two-Stage "Living" Copolymerization 63

2.3.4 Triblock Copolymers by Three-Stage "Living" Copolymerization 79

2.4 Conclusions 75

2.5 References 76

2.6 Supporting Information 80

2.7 Sample Calculation of NB Content in Each Block of The Block Copolymers 87

Chapter 3: Hyperbranched Polyethylene Ionomers Containing Cationic Tetralkylammonium Ions Synthesized by Pd–Diimine-Catalyzed Direct One-Pot Ethylene Copolymerization with Ionic Liquid

Comonomers **89**

Abstract 89

3.1 Introduction 90

3.2 Experimental Section 94

3.2.1 Materials 94

3.2.2 Synthesis of [2-(acryloyloxy)ethyl]trimethylammonium tetrafluoroborate 95

3.2.3 Synthesis of [2-(acryloyloxy)ethyl]trimethylammonium hexafluorophosphate 96

3.2.4 Synthesis of [2-(acryloyloxy)ethyl]trimethylammonium bis(trifluoromethane)sulfonamide 96

3.2.5 Synthesis of [2-(acryloyloxy)ethyl]trimethylammonium trifluoromethanesulfonate 97

3.2.6 Synthesis of [2-(acryloyloxy)ethyl]trimethylammonium hexafluoroantimonate 97

3.2.7 Copolymerization of Ethylene with Polymerizable Ionic Liquid Comonomers 98

3.2.8 General Procedure for Basic Hydrolysis of Ionomers 99

3.2.9 Characterization and Measurements 99

3.3 Results and Discussion 101

3.3.1 HBPE Ionomer Synthesis by Direct Ethylene Copolymerization and Macromolecular Characterizations 101

3.3.2 Solid State Strucure and Thermal Properties of HBPE Ionomers 113

3.3.3 Melt Rheological Properties of HBPE Ionomers 118

3.4 Conclusions 124

3.5 References 125

Chapter 4: Hyperbranched Polyethylene Ionomers Containing Self-Encapsilated Palladium Nanoparticles as Catalysts for C–C Cross Coupling and Alyne Semi-hydrogenation Reactions 131

Abstract 131

4.1 Introduction 132

4.2 Experimental Section 135

4.2.1 Materials 135

4.2.2 Synthesis of [2-(acryloyloxy)ethyl]trimethylammonium tetrafluoroborate 137

4.2.3 Copolymerization of Ethylene with 2 for Synthesis of HBPE Ionomers (HBIs) Encapsulating Self-Supported Palladium Nanoparticles (Pd NPs) 137

4.2.4 Synthesis of Graphene Oxide 138

4.2.5 Synthesis of GO/HBI Supported Pd NP Catalyst 138

4.2.6 Mizoroki-Heck Reactions Catalyzed with HBI2 139

4.2.7 Suzuki-Miyaura Reactions Catalyzed with HBI2 140

4.2.8 Semi-Hydrogenation Reactions Catalyzed with HBI2 141

4.2.9 General Procedure for Pd Conetent Measurement 142

4.2.10 General Procedure for Cleavage of HBIs 142

4.2.11 Characterization and Measurements 143

4.3 Results and Discussion 144

4.3.1 Synthesis and Characterization of HBPE Ionomers (HBIs) Encapsulating Self-Supported Pd(0) Nanoparticles (NPs) 144

4.3.2 Catalytic Application of HBIs in Semi-Hydrogenation of Alkynes 151

4.3.3 Catalytic Application of HBIs in Heck and Suzuki Reactions 158

4.4 Conclusions 162

4.5 References 163

4.6 Supporting Information 168

Chapter 5: Tuning Structural Parameters of Polyethylene Brushes in Surface-Initiated Ethylene "Living" Polymerization from Silica Nanoparticles and Effects on Nanocomposite Properties 182

Abstract 182

5.1 Introduction 183

5.2 Experimental Section 187

5.2.1 Materials 187

5.2.2 Preparation of Acryloyl-Functionalized Silicas 188

5.2.3 Preparation of Catalyst-Immobilized Silicas 189

5.2.4 Ethylene Polymerization with Homogeneous and Immobilized Catalysts 189

5.2.5 General Procedure for Cleavage of PE Brushes 191

5.2.6 Compounding of Polymer Nanocomposites 191

5.2.7 Characterization and Measurements 192

5.3 Results and Discussion 195

5.3.1 Surface Functionalization of Bare Silicas and Covalent Catalyst Immobilization 195

5.3.2 Surface-Initiated Ethylene “Living” Polymerization at 27 atm and 5 °C for Synthesis of Silicas Grafted with Linear PE Brushes at Different Length and Density 202

5.3.3 Surface-Initiated Ethylene Polymerization at 1 atm and 25 ℃ for Synthesis of Silicas Grafted with Hyperbranched PE Brushes 210

5.3.4 Thermal Properties of PE-Grafted Silicas 214

5.3.5 Effect of PE Brushes on Silica Dispersion in Solution and Particle Size 214

5.3.6 Compounding of Elastomer Nanocomposites and Effect of PE Brushes on Nanofiller Dispersion 215

5.3.7 Rheological Properties of Nanocomposites 221

5.3.8 Tensile Properties of Nanocomposites 225

5.4 Conclusions 226

5.5 References 228

5.6 Supporting Information 233

Chapter 6: Significant Research Contributions and Recommendations for Future Developments 238

6.1 Significant Research Contributions of Thesis Work 238

6.2 Recommendations for Future Research 240

6.2.1 Mechanical and Rheological Property of E-NB copolymer 240

6.2.2 Synthesis of Artificial-Nacre Nanocomposites 241

LIST OF FIGURES

Figure 2.1 GPC elution curves (recorded from DRI detector) of the polymers synthesized in single-stage polymerizations (runs 1–5, see Table 2.1) at different NB feed concentrations (0.64–0 M). GPC measurement condition: toluene (for runs 1 and 2) or THF (for runs 3–5) as the eluting phase at 1 mL/min and 33 °C. 51

Figure 2.2 Dependences of M_n and overall NB content ($F_{NB,0}$) on polymerization time in runs 1–5 (see Table 2.1). Fitting lines are plotted for the purpose of guiding eyes. 52

Figure 2.3 ^{13}C NMR (125 MHz) spectra of some selected polymers obtained in single-stage polymerizations: (a) run 1, 2 h (polymerization time) polymer; (b) run 2, 2 h polymer; (c) run 3, 1 h polymer; (d) run 3, 3 h polymer; (e) run 3, 5 h polymer; and (f) run 5, 2 h hyperbranched PE. D-chloroform was used as the solvent. The signal marked with an asterisk (*) arises from trace residual THF. 54

Figure 2.4 DSC heat flow curves (in black) and 1st derivatives (in red) of heat flow curves of the 6 h polymers synthesized in runs 1, 2, and 5, respectively. The heat flow curves were collected during a second heat ramp at 10 °C/min in DSC measurements. The width for each glass transition (ΔT_g) is illustrated with an arrow in each derivative curve. 59

Figure 2.5 DSC heat flow curves (a) and derivatives of the heat flow curves (b) for the set of gradient copolymers synthesized in run 3. The heat flow curves were collected during the second heat ramp at 10 °C/min in DSC measurements. The width for each glass transition (ΔT_g) is illustrated with an arrow in the derivative curve. 61

Figure 2.6 DSC heat flow curves (in black) and 1st derivatives (in red) of heat flow curves of the 1h and 6 h polymers synthesized in run 4. The heat flow curves were collected during a second heat ramp at 10 °C/min in DSC measurements. The width for each glass transition (ΔT_g) is illustrated with an arrow in each derivative curve. 63

Figure 2.7 M_n of block polymer and NB molar fraction in the second block ($F_{NB,2}$) vs. polymerization time in the second stage (t_2) in the two-stage E-NB copolymerizations (runs 6 and 7 in Table 2.2). Fitting lines are plotted for the purpose of guiding eyes. 66

Figure 2.8 DSC heat flow curves (a) and derivatives of the heat flow curves (b) for the set of polymers synthesized in run 6 (see Table 2.2). The heat flow curves were collected during the second heat ramp at 10 °C/min in DSC measurements. The width for each glass transition (ΔT_g) is illustrated with an arrow in the derivative curve. 70

Figure 2.9 Dependences of M_n and overall NB content ($F_{NB,0}$) on overall polymerization time in three-stage copolymerization run 8 (see Table 2.3). Fitting lines are included for the purpose of guiding eyes. 73

Figure 2.10 DSC heat flow curves (a) and derivatives of the heat flow curves (b) for the set of polymers synthesized in three-stage run 8 (see Table 2.3). The heat flow curves were collected during the second heat ramp at 10 °C/min in DSC measurements. The width for each glass transition (ΔT_g) is illustrated with an arrow in the derivative curve. 74

Figure S2.1 ^{13}C NMR (125 MHz) spectra of copolymers synthesized in run 4 (see Table 1) at different polymerization time: (a) 1 h of polymerization; (b) 2 h; (c) 3 h; (d) 4 h; (e) 5 h; and (f) 6 h. 80

Figure S2.2 GPC elution curves (recorded from DRI detector) of the polymers synthesized in two-stage polymerizations (runs 6 and 7, see Table 2). In the figure, t_2 represents the polymerization time in the second stage polymerization. GPC measurement condition: THF as the eluting phase at 1 mL/min and 33 °C. 81

Figure S2.3 ^{13}C NMR spectra (125 MHz) of polymers obtained in run 6 at different polymerization time: (a) t_1=1 h, t_2=0 h, hyperbranched PE block; (b) t_2=1 h; (c) t_2=2 h; (d) t_2=3 h; (e) t_2=4 h; (f) t_2=5 h. 82

Figure S2.4 ^{13}C NMR spectra (125 MHz) of polymers obtained in run 7 at different polymerization time: (a) t_1=2 h, t_2=0 h, hyperbranched PE block; (b) t_2=1 h; (c) t_2=2 h; (d) t_2=3 h; (e) t_2=4 h. 83

Figure S2.5 DSC heat flow curves (a) and derivatives of the heat flow curves (b) for the set of polymers synthesized in run 7. The heat flow curves were collected during the second heat ramp at 10 °C/min in DSC measurements. The T_g breadth for each glass transition is illustrated with an arrow in the derivative curve. 84

Figure S2.6 GPC elution curves (recorded from DRI detector) of the polymers synthesized in three-stage run 8 (see Table 2.3). In the figure, t_1, t_2, and t_3 represent the polymerization time in the first, second, and third stage, respectively. GPC measurement condition: THF as the eluting phase at 1 mL/min and 33 °C. 85

Figure S2.7 ^{13}C NMR spectra (125 MHz) of polymers obtained in run 8 at different polymerization time: (a) t_1 = 1 h, t_2 = 0 h, first block; (b) t_2 = 1 h, t_3 = 0 h, diblock polymer; (c) t_3 = 1 h; (d) t_3 = 2 h; (e) t_3 = 3 h; (f) t_3 = 4 h. 86

Figure 3.1 ^{1}H NMR spectra of (a) homopolyethylene HPE, (b) ionomer I-B-2, (c) I-B-2 after hydrolysis, (d) ionomer I-P-1, and (e) ionomer I-T-1. The peak denoted with an asterisk (*) results from trace THF residue present in the polymer. 107

Figure 3.2 GPC elution curves of HPE and the hydrolyzed ionomers recorded with the refractive index detector in their characterization with triple-detection GPC (undertaken with THF as mobile phase at 1 mL/min and 33 °C). 112

Figure 3.3 Mark-Houwink plot of the hydrolyzed I-B set of ionomers and HPE. 112

Figure 3.4 X-ray scattering of I-B-1, I-B-3, and a hyperbranched polyethylene homopolymer synthesized in our earlier work. 115

Figure 3.5 DSC heat flow curves of the ionomers and homopolyethylene HPE. The curves were taken from the second heating ramp at 10 °C/min. 117

Figure 3.6 Master curves of (a and b) dynamic moduli G′ and G″; (c and d) complex viscosity (η*) and phase angle (δ) for the ionomers and HPE at the reference temperature of 95 °C. All the master curves were constructed with the data measured at minimum five different temperatures in the general temperature range of 35–135 °C. 120

Figure 4.1 UV-Vis spectra of HBIs encapsulating Pd(0) NPs in THF. 149

Figure 4.2 TEM micrographs of HBI1 encapsulating Pd NPs (scale bar = 50 nm). 150

Figure 4.3 Time course for hydrogenation of phenylacetylene (a) entry 4, using HBI2 (394 ppm), (b) entry 13, using Pd/Carbon (2070 ppm), and (c) entry 14, Pd/carbon (376 ppm). 155

Figure 4.4 TGA curves of GO supported HBI2 before and after recycling semi-hydrogenation. 158

Figure 4.5 Conversion of IPh as a function of reaction time in the Heck reactions of IPh and BA with HBI2 at different Pd amounts. 160

Figure S4.1 ^{1}H NMR spectrum of (a) HBI1, (b) cleaved HBI1, (c) HBI2, (d) HBI3, and (e) HBI4. 168

Figure S4.2 ^{1}H NMR spectrum of semi-hydrogenation of PA entry 4 after 150 min 169

Figure S4.3 ^{1}H NMR spectrum of semi-hydrogenation of 4-phenyl-1-butyne after 120 min 170

Figure S4.4 ^{1}H NMR spectrum of semi-hydrogenation of 1-ethynylcyclohexene after 150 min 171

Figure S4.5 ^{1}H NMR spectrum of Heck reaction with 6.1 ppm Pd catalyst after 18 h 172

Figure S4.6 ^{1}H NMR spectrum of recycling Suzuki reaction entry 2 after 1h 173

Figure S4.7 ^{1}H NMR spectrum of Suzuki coupling of aryl bromides and phenylboronic acid entry 2 after 24 h 174

Figure S4.8 ^{1}H NMR spectrum of Suzuki coupling of aryl bromides and phenylboronic acid entry 3 after 24 h 175

Figure S4.9 ^{1}H NMR spectrum of Suzuki coupling of aryl bromides and phenylboronic acid entry 4 after 24 h 176

Figure S4.10 ^{1}H NMR spectrum of Suzuki coupling of aryl bromides and phenylboronic acid entry 5 after 8 h 177

Figure S4.11 ^{1}H NMR spectrum of Suzuki coupling of aryl bromides and phenylboronic acid entry 6 after 24 h 178

Figure S4.12 ^{1}H NMR spectrum of Suzuki coupling of aryl bromides and phenylboronic acid entry 7 after 24 h 179

Figure S4.13 ^{1}H NMR spectrum of Suzuki coupling of aryl bromides and phenylboronic acid entry 9 after 24 h 180

Figure S4.14 ^{1}H NMR spectrum of Suzuki coupling of aryl bromides and phenylboronic acid entry 10 after 24 h 181

Figure 5.1 Thermogravimetric curves of bare silicas and surface-functionalized silicas. 200

Figure 5.2 Thermogravimetric curves of PE-grafted silicas synthesized with Pd-Silica-I-1 (a) and Pd-Silica-I-3 (b) for different polymerization time (2, 4, and 6 h) at 27 atm and 5 ℃ (runs 1–3 with Pd-Silica-I-1 and runs 8–10 in Table 2). The corresponding curves for bare Silica-I, functionalized silica, and catalyst-

immobilized silica are included for comparison. The final percentage weight retention data at 700 ℃ are listed. 205

Figure 5.3 Dependencies of relative mass of PE brushes on polymerization time at the polymerization condition of 27 atm and 5 ℃. 206

Figure 5.4 GPC elution traces (recorded from DRI detector) of cleaved PE brushes from PE-grafted silicas obtained with Pd-Silica-I-1 in runs 1, 2, and 3 carried out at 27 atm and 5 ℃, and in run 4 carried out 1 atm and 25 ℃. GPC eluent: THF at 1 mL/min and at 33 ℃. 206

Figure 5.5 Dependencies of M_n on polymerization time for the cleaved PE brushes synthesized with the six different catalyst-immobilized silicas and the polymers synthesized with catalyst **1** at 27 atm/5 ℃. The M_n data were determined with light scattering detector in triple-detection GPC characterization. 208

Figure 5.6 Mark-Houwink plot (intrinsic viscosity vs. molecular weight) for cleaved PE brushes. Two reference curves ($[\eta]= 0.0646M^{0.603}$ and $[\eta]= 0.0525M^{0.548}$) for PEs synthesized with homogeneous catalyst **1** at 27 atm/5 ℃ and 1 atm/25 ℃, respectively, are included for comparison. 211

Figure 5.7 TEM images of the EOC composites with bare Silica-I (a), PE-grafted Silica-I synthesized in run 1 (see Table 5.2) (b), run 2 (c), run 3 (d), run 8 (e), run 9 (f), and run 10 (g). The content of dry bare silica in the composites is

7 wt%. All images were taken at a magnification of 19,000 at 200 kV. Scale bar = 500 nm. 218

Figure 5.8 Average aggregate area and Feret diameter of the EOC composites with bare Silica-I, PE-grafted Silica-I samples synthesized in runs 1–3 and 8–10. The results were obtained by performing image analysis on the TEM images shown in Figure 5.7. Error bars correspond to standard deviation. 219

Figure 5.9 TEM images of the EOC composites with bare Silica-II (a), PE-grafted Silica-II sample in run 12 (see Table 2) (b), run 13 (c), run 18 (d), run 19 (e), and run 20 (f). The content of dry bare silica in the composites is 5 wt%. All images were taken at a magnification of 50,000 at 200 kV. Scale bar = 100 nm. 220

Figure 5.10 Average aggregate area and Feret diameter of the EOC composites with bare Silica-II, PE-grafted Silica-II samples synthesized in runs 12, 13, and 18–20. The results were obtained by performing image analysis on the TEM images shown in Figure 9. Error bars correspond to standard deviation. 221

Figure 5.11 Storage modulus (G′) curves (at 190 ℃) for the EOC composites compounded with various PE-grafted Silica-I samples as fillers: (a) PE-grafted Silica-I samples synthesized in runs 1–3; (b) PE-grafted Silica-I samples synthesized in runs 8–10. The curves for pure EOC and the composite compounded with bare Silica-I are also included. The filler

loading is designed with the dry bare silica content in the composites being 7 wt%. 222

Figure 5.12 Storage modulus (G′) curves (at 190 ℃) for the EOC composites compounded with various PE-grafted Silica-II samples (synthesized in runs 12, 13, and 18–20) as fillers. The curves for pure EOC and the composite compounded with bare Silica-II are also included. The filler loading is designed with the dry bare silica content in the composites being 5 wt%. 223

Figure 5.13 G ´values at 6.28×10^{-2} rad/s (at 190 °C) for the two sets of composites: (a) the set with Silica-I series of samples as fillers; (b) the set with Silica-II series of samples as fillers. 224

Figure 5.14 Elongation at breakage and tensile modulus of the composites compounded with Silica-II series samples (bare Silica-II, runs 12 and 14 samples) as fillers. 226

Figure S5.1 Derivative thermogravimetric curves of bare silicas and surface-functionalized silicas. 233

Figure S5.2 GPC elution curves (recorded from DRI detector) of cleaved PE brushes from PE-grafted silicas obtained in runs 5–18 with the various catalyst-immobilized silicas. GPC eluent: THF at 1 mL/min and at 33 ℃. 234

Figure S5.3 ^{1}H nuclear magnetic resonance spectra of cleaved polyethylene brushes from run 1 synthesized with Pd-Silica-I-1 (a), from run 8 synthesized with

Pd-Silica-I-3 (b), from run 12 synthesized with Pd-Silica-II-1 (c), from run 18 synthesized with Pd-Silica-II-3. These runs were all carried out at 27 atm and 5 ℃ (see Table 2). The signals marked with an asterisk (*) result from trace solvent residue (methanol or THF) present in the cleaved brushes. 235

Figure S5.4 DSC thermograms of the PE-grafted silicas synthesized with Pd-Silica-I-1 and Pd-Silica-I-3, respectively. 236

Figure S5.5 Particle size distribution of bare silicas and PE-grafted silicas determined from their dispersions with DLS at room temperature. The dispersions of bare silicas were prepared in THF and those of PE-grafted silicas were prepared in toluene. 237

LIST OF SCHEMES

Scheme 1.1 Initiation and chain propagation in radical polymerization. 3

Scheme 1.2 A typical structure of metallocene catalyst. 7

Scheme 1.3 Ethylene polymerization with metallocene catalyst. 8

Scheme 1.4 Pd– and Ni–diimine catalysts. 11

Scheme 1.5 Chain waling mechanism with Pd-diimine catalysts. 12

Scheme 1.6 Chain walking strategy for controlling polymer topology. 14

Scheme 1.7 Schematic effects of ring incorporation on polymer chain topology in chain walking polymerization. 16

Scheme 1.8 Functional 1-alkene comonomers used for synthesis of functionalized HBPEs via ethylene copolymerization. 26

Scheme 1.9 Functional acrylate comonomers used for synthesis of functionalized HBPEs via ethylene copolymerization. 26

Scheme 2.1 E–NB alternating, gradient, block, and block-gradient copolymers by "living" E–NB copolymerization with **1**. 48

Scheme 3.1 One-step synthesis of hyperbranched polyethylene ionomers containing tetralkylammonium ions by direct chain walking copolymerization of ethylene with polymerizable ionic liquid comonomers. 102

Scheme 4.1 Synthesis of hyperbranched ionomers (HBI) encapsulating self-supported Pd(0) nanoparticles. 146

Scheme 5.1 Homogeneous and covalently immobilized Pd–diimine catalysts. 186

Scheme 5.2 Three-step procedure for surface modification of silica nanoparticles with polyethylene brushes via surface-initiated ethylene polymerization. 197

LIST OF TABLES

Table 1.1 The global demand of the five largest thermoplastic materials in 2010. 1

Table 1.2 Polyethylene types, and their properties and applications. 2

Table 2.1 Single-stage "living" copolymerizations of ethylene and norbornene (NB) at different NB feed concentrations. 50

Table 2.2 Two-stage "living" copolymerizations consisting of 1st-stage ethylene "living" homopolymerization and second-stage "living" copolymerization of ethylene and norbornene (NB). 65

Table 2.3 Three-stage "living" copolymerization (run 8) of ethylene and norbornene (NB). 71

Table 3.1 Summary of the polymerization results and the characterization data for all polymers. 104

Table 3.2 Rheological parameters of the ionomers and HPE at reference temperature of 95 ℃. 123

Table 4.1 Summary of the copolymerization conditions, results, and the characterization data for all hyperbranched polyethylene ionomers. 148

Table 4.2 Semi-hydrogenation of phenylacetylene to styrene using HBI supported Pd catalysts. 153

Table 4.3 Semi-hydrogenation of terminal alkynes using HBI2 Pd catalyst. 156

Table 4.4 Recycling semi-hydrogenation of PA with GO/HBI2 Pd catalyst. 157

Table 4.5 Heck reaction of iodobenzene (IPh) and n-butyl acrylate (BA) using HBI2. 159

Table 4.6 Eight-Cycle Recycling Heck Reactions with HBI2. 160

Table 4.7 Suzuki reaction of iodobenzene (IPh) and phenylboronic acid (PBA) using HBI2. 161

Table 4.8 Suzuki coupling of aryl bromides and phenylboronic acid. 162

Table 4.9 Recycling Suzuki Reactions with HBI2. 162

Table 5.1 Synthesis of surface-functionalized silicas and corresponding catalyst-immobilized silicas. 198

Table 5.2 Surface-initiated ethylene polymerizations with catalyst-immobilized silicas and characterization results. 204

NOMENCLATURE

AETH	[2-(acryloyloxy)ethyl]trimethylammonium hexafluorophosphate
AETS	[2-(acryloyloxy)ethyl]trimethylammonium bis(trifluoromethane)sulfonamide
AETT	[2-(acryloyloxy)ethyl]trimethylammonium tetrafluoroborate
ATCS	3-Acryloxypropyltrichlorosilane
ATRP	Atom Transfer Radical Polymerization
BA	Butyl Acrylate
$CDCl_3$	Chloroform
CHE	Cyclohexene
CHP	Cycloheptene
C_p	Cyclopentadienyl
CPE	Cyclopentene
COE	Cyclooctene
DEDAM	Diethyl Diallylmalonate

DRI	Differential Refractive Index
DSC	Differential Scanning Calorimetry
E–NB	Ethylene–Norbornene
EOC	Ethylene-Olefin Copolymer
ETCS	Ethyltrichlorosilane
ΔH_m	Melting Enthalpy
GO	Graphene Oxide
GPC	Gel Permeation Chromatography
HBPE	Hyperbranched Polyethylene
HBI	Hyperbranched Polyethylene Ionomer
HDPE	High Density Polyethylene
LDPE	Low Density Polyethylene
LLDPE	Linear Low Density Polyethylene
LS	Light Scattering

MAO	Methylaluminoxane
MMA	Methyl Methacrylate
MWCNTs	Multi-Wall Carbon Nanotubes
MWD	Molecular Weight Distribution
M_w	Weight-Average Molecular Weight
NB	Norbornene
NMR	Nuclear Magnetic Resonance
NP	Nanoparticle
^{13}C NMR	Carbon-13 Nuclear Magnetic Resonance
^{1}H NMR	Proton Nuclear Magnetic Resonance
IPh	Iodobenzene
PBA	Phenylboronic Acid
PDI	Polydispersity Index
PE	Polyethylene

PET	Polyethylene Terephthalate
PA	Phenylacetylene
PMMA	Polymethyl Methacrylate
PNB	Polynorbornene
POSS	Polyhedral Oligomeric Silsesquioxane
PP	Polypropylene
PPA	Polymer Processing Aid
PS	Polystyrene
PVC	Polyvinylchloride
RCS	Refrigerated Cooling System
ROMP	Ring-Opening Metathesis Polymerization
R_p	Chain Propagation Rate
R_w	Chain Walking Rate
SAM	Self-Assembled Monolayer

THF	Tetrahydrofuran
TOF	Turnover Frequency
T_g	Glass Transition Temperature
T_m	Melting Temperature
TEM	Transition Electron Microscopy
TOF	Turnover Frequency
UHMWPE	Ultra High Molecular Weight Polyethylene
VLDPE	Very Low Density Polyethylene
$[\eta]$	Intrinsic Viscosity
$[\eta]_w$	Weight-Average Intrinsic Viscosity
η_0	Zero-Shear Viscosity
UHMWPE	Ultra High Molecular Weight Polyethylene
XRD	X-ray diffraction
Z-N	Ziegler-Natta

Chapter 1

Introduction, Background and Research Objectives

1.1 Introduction to Polyethylenes

Polyethylene having industrially useful properties was first synthesized in 1933 by the British chemists Dr. E. W. Fawcett and Dr. R. O. Gibson in the laboratories of ICI (Imperial Chemical Industries).[1–3] After 80 years of development, PE has become an essential component in everyday life. Each year, over 75 million metric tons of PE is manufactured, making it the world's most important thermoplastic material.[3] Table 1.1 shows the global demand of the five largest thermoplastic materials in 2010.[3]

Table 1.1 The global demand of the five largest thermoplastic materials in 2010.[3]

Thermoplastic Type	Global Demand (billions of pounds)	Market Share (%)
Polyethylene (PE)	154	31.2
Polypropylene (PP)	112	22.7
Polyvinylchloride (PVC)	75	15.2
Polyethylene terephthalate (PET)	119	24.1
Polystyrene (PS)	34	6.9
Total	494	100

Generally, depending on manufacturing process and polymer properties, PE can be classified into three major types: high density polyethylene (HDPE), low density polyethylene (LDPE), and linear low density polyethylene (LLDPE). Each type of PE possesses its own properties that address different market applications, as summarized in Table 1.2.

Table 1.2 Polyethylene types, and their properties and applications.[1,3]

PE type	Branches [a]	Property [b]						Applications	Market share in 2004
		Density	Degree of crystallinity (% from density)	Tensile modulus (psi)	Tensile yield stress (psi)	Tensile strength at break (psi)	Melting temperature (℃)		
LDPE	40–150 short branches and with long branches	0.91–0.94	42–62	25,000–50,000	1,300–2,800	1,200–4,500	98–115	toys, containers, corrosion-resistant surfaces, parts, packaging, plastic wraps	28%
HDPE	<15 short branches and no long branches	0.94–0.97	62–82	155,000–200,000	2,600–4,500	3,200–4,500	125–132	bottles, cans, bags, films, caps, toys, pipes, wire	44%
LLDPE	numerous short branches	0.90–0.94	34–62	38000–130,000	1,100–2,800	1,900–6,500	100–125	plastic bags, sheets, toys, wire, cables, pipes, tubing, drum liners	28%

[a] The unit of short chain branching density is 1/(1000 ethylene units).

[b] Other properties including flexural modulus, tensile elongation at break, shore hardness Type D, izod impact strength, heat distortion temperature, heat of fusion, thermal expansivity can be found in reference 1.

1.2 Introduction to Ethylene Polymerization Techniques

To manufacture above mentioned PEs, different polymerization techniques have been developed. In this section, all ethylene polymerization techniques including free radical polymerization, early transition metal-based Phillips, Ziegler-Natta (Z-N) and metallocene catalyst systems, and late transition metal-based Pd/Ni catalyst systems will be reviewed.

1.2.1 Free Radical Polymerization

The earliest commercial available PE known as LDPE is produced exclusively through free radical polymerization which requires very high ethylene pressure (1,000–3,000 bar) and high reaction temperature (100–350 ℃). In this process, initiators (oxygen or organic peroxides) are firstly decomposed to generate free radicals under appropriate conditions. The free radical species then attach themselves to ethylene molecules, while unpaired electrons relocate to the opposite end of the monomers. Growth of the polyethylene will proceed when the free radical on the end of the growing chain reacts with another ethylene molecule (Scheme 1.1). This chain propagation will continue to grow a polyethylene chain until chain transfer or chain termination occurs.

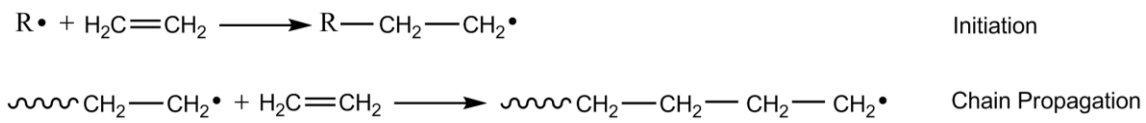

Scheme 1.1 Initiation and chain propagation in radical polymerization.[1]

1.2.2 Ethylene Polymerization with Phillips Catalyst and Ziegler-Natta (Z-N) Catalysts

In 1953, new linear-type PE, HDPE, was discovered in two separate research laboratories.[1,3] In one laboratory of the Phillips Petroleum Company in the United States, J. P. Hogan and R. L. Banks utilized a chromium-based catalyst supported on porous silica to synthesize HDPE, while the other group lead by Karl Ziegler in Germany produced a similar HDPE with organometallic compounds based on aluminum alkyls and transition metal compounds with titanium chloride compound (the 1st generation Z-N catalyst). In both cases, the preparation of HDPE only required much lower ethylene pressures (10–80 bar) and temperatures (80–150 ℃) compared to those used for radical polymerization of ethylene.

From 1955 to 1975, HDPE was produced commercially with both the Phillips catalyst and the Z-N catalyst. However, the structure and properties of HDPE produced with each type catalyst were not identical. For instance, the HDPE produced with Phillips catalyst had a relatively higher molecular weight and broader molecular weight distribution, which could be used to fabricate plastic bottles using the blow-molding technique. On the other hand, HDPE produced with Z-N catalyst had a relatively narrow molecular weight distribution and its molecular weight can be controlled in a much wider range, which was useful for items fabricated using the injection-molding fabrication technique.

In the Phillips-type catalyst chromium (VI) oxide on silica is prepared by roasting a Cr (III) compound at ca. 1000 K in oxygen. The polymerization mechanism using this catalyst is unclear, but one model system described it as the classic coordination polymerization. The polymerization mechanism herein involves three steps: (1) the reduction of Cr (VI) to Cr (II) species to provide catalyst active center; (2) the coordination of ethylene with Cr at the vacant site; and (3) the insertion of ethylene between the metal and the alkyl.

The 1st generation Z-N catalyst consists of a transition metal salt and a base metal alky. The transition metal salts including $TiCl_4$, $TiCl_3$, VCl_3, $ZrCl_4$, etc. are mainly chosen from the group IVB to VIIIB, and the base metal alkyls are chosen from the group IA to IIIA like $(C_3H_5)_3Al$, $(C_2H_5)_2Mg$, C_4H_9Li, etc. In the most common Z-N catalyst system ($AlEt_3$ with $TiCl_4$ catalyst), a titanium atom is coordinated with four chlorine atoms and an alkyl group with an empty site. Similar to the mechanism described for ethylene polymerization with Phillips catalysts, the ethylene molecule coordinates with the titanium at the vacant site, then inserts between the metal and the alkyl.

Comparing the two catalyst systems, the Cr-based, Phillips catalyst had relatively higher catalytic activity and yielded HDPE with better mechanical and physical properties. In the industry, Phillips catalyst was usually supported on amorphous silica. These supported-catalysts provide templates for the growth of the small HDPE particles into large granular HDPE particles which were insoluble in the

organic solvents used in the polymerization process. These allowed the use of a commercialized Phillips loop reactor which had lower manufacturing costs. Thus, during the period from 1955 to 1975, Phillips catalyst was the preferred catalyst for manufacturing HDPE.[3]

In the early 1970s, it was found that Ti-based Z-N catalysts could be supported onto inorganic supports, such as $MgCl_2$ to significantly improve catalyst activity (increased by a factor of 10 to 50 compared to the 1st generation Z-N catalyst). With this 2nd generation Z-N catalyst, high density polyethylene (HDPE) and a new type of PE, linear low density polyethylene (LLDPE) with improved properties over LDPE can be synthesized. In the polymerization, small amounts of a α-olefin comonomer (such as propylene, 1-butene, 1-hexene, or 1-octene) are added to the feedstock to synthesize LLDPE. These α-olefin comonomers are randomly polymerized and introduced small branches into the linear PE chains with comonomer incorporation concentration of 0.2–20 mol%. The structure of LLDPE is essentially linear but with a low density because of the short branches. Moreover, the properties of LLDPE can be varied by adjusting the proportion of ethylene and comonomer and by using different comonomers which allow it to be used for various applications. However, the Phillips catalyst and loop reactor were not as good as 2nd generation Z-N catalysts because it was only beneficial in producing LLDPE with a relatively lower level of comonomer. LLDPE with higher levels of comonomer having high solubility in the slurry solvent in this case would result in process problems. Later, in 1977, Union Carbide further developed a high-

activity, silica-supported Z-N catalyst that was utilized to manufacture LLDPE in a gas-phase, fluidized-bed process, which made LLDPE commercially more important.

1.2.3 Ethylene Polymerization with Single-Site Metallocene Catalysts

Different from heterogeneous Z-N catalysts, metallocene catalysts are homogenous catalysts with single-type active sites, which have been considered as a new generation of Z-N catalysts. The first metallocene, ferrocene, was discovered in 1951 by Keally and Pauson,[4] and Miller et al.[5] Deriving from ferrocene, various metallocene catalysts have been synthesized. A common metallocene contains a transition metal and two cyclopentadienyl (Cp) ligands coordinated in a sandwich structure with the general form $[L_2MX_2]$ as shown in Scheme 1.2. The L herein represents ligand (e.g. cyclopentadienyl, fluorenyl, indenyl, or their substituted structures) which helps to stabilize the active metal species by providing electrons to a vacant site on the metal; M is the transition metal (e.g., titanium, zirconium, hafnium); and X is either halogen or an alkyl group.

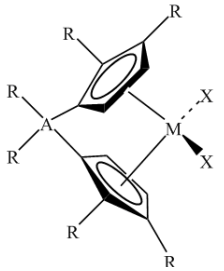

Scheme 1.2 A typical structure of metallocene catalyst.

In 1957, the metallocene catalyst consisted of titanocene (Cp_2TiCl_2) with triethylaluminum (Et_3Al) or diethylaluminum chloride (Et_2AlCl), and was first discovered for catalyzing ethylene polymerization by Natta et al.[6], and Breslow and Newburg.[7] However, these catalysts had much lower catalytic activity than those of Z-N catalysts, which did not attract more attention at that time. In the late 1970s, a breakthrough in this area was made by Walter Kaminsky and Hansjörg Sinn who discovered that methylaluminoxane (MAO) acted as an effective co-catalyst to dramatically increase the catalyst activities of metallocene catalysts.[8]

MAO is an unusual oligomer that has Al atoms in the backbone, which helps in the dialkylation of the metallocene catalyst. After dialkylation, the MAO complex seizes one of methyl groups on the $L_2M(Me)_2$ to form an anion which can distribute the electron over the structure, stabilizing the charged system. On the other hand, the cation $L_2M(CH_3)^+$ is formed, which provides the active site for olefin polymerization. The mechanism of ethylene polymerization with a metallocene catalyst is shown in Scheme 1.3.

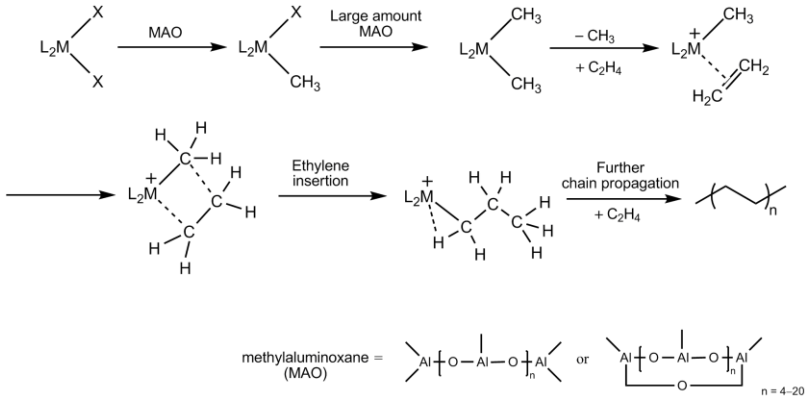

Scheme 1.3 Ethylene polymerization with metallocene catalyst

Compared to Z-N catalysts, metallocene catalysts have many advantages that offer unprecedented control over polymer structure and property. Firstly, metallocene catalysts have well defined chemical structures that can be characterized. These uniform structures provide single-site active centers which result in polymer chain with uniform architecture and a narrow molecular weight distribution. Secondly, metallocene catalysts have good stability compared to Z-N catalysts. For example, metallocene catalysts can be active at temperatures over 200 ℃, while Z-N catalysts start to lose their activity at temperatures as low as 60 ℃. Thirdly, metallocene catalysts can efficiently polymerize ethylene with α-olefins (e.g., 1-butene, 1-hexene, and 1-octene) with a broader range of compositions. However, Z-N catalysts can only produce polymers with much lower concentrations of α-olefin. Furthermore, cyclic olefins have also been successfully copolymerized with ethylene by using metallocene catalysts with controlled structures, while Z-N catalysts were found to have very low activity for these kinds of ethylene copolymerizations.

Hence, because of the above mentioned advantages, the use of metallocene catalysts greatly expand the versatility of polyolefins in the research area and allowed the commercial production of LLDPE with lower density, higher molecular weight and with superior mechanical properties for use in industry.

1.2.4 Ethylene Polymerization with Single-Site Late Transition Metal Catalysts

Early transition metal (Ti, Zr, V, and Cr) based Phillips, Z-N and metallocene catalysts with high activities are widely used in industry nowadays. However, these catalysts have the limitation of producing PE with pendant functional groups. The main reason herein is that early transition metal catalysts exhibit high oxophilicity which can be easily poisoned by most commercially available polar comonomers preventing the polymerization. Despite the ability to use protecting groups on the polar comonomers to somewhat solve this problem, the complex commoner synthetic procedure add significant cost to polymer production in the industry. Hence, functionalized polyolefins with polar groups, for example polyolefin ionomers, are still mainly produced commercially through free radical polymerization.

In the mid 1990s, late-transition metal catalysts were discovered as a new generation of single-site catalysts for olefin polymerization. The typical late transition metal catalysts, Pd (II) and Ni (II) α–diimine catalysts were first reported by Brookhart for the polymerization of ethylene and α–olefins in 1995.[9] Scheme 1.4 shows the structures of Pd– and Ni–diimine catalysts used by Brookhart. Since then, these unique late-transition metal catalysts have been extensively studied for the polymerization of ethylene, α-olefins, and cyclic olefins and the copolymerization of nonpolar olefins with functionalized olefins.[10, 11] In particular, the polyethylenes synthesized with Pd–diimine catalysts were amorphous polymers having high branching densities (ca. 90 branches per 1000 carbons). On the other hand, Ni–diimine catalysts produced polyethylenes with structures ranging from linear semicrystalline to moderately branched amorphous with extremely high activities comparable to those of metallocene catalysts.

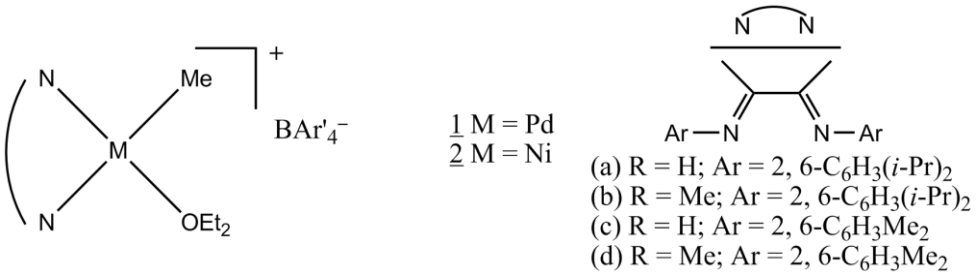

Scheme 1.4 Pd– and Ni–diimine catalysts.[9]

Despite the above differences, Pd and Ni–diimine catalysts showed several unique characteristics which are concluded as follows: (1) chain walking mechanism which allows the synthesis of new type of PE, hyperbranched polyethylene (HBPE) and the control of HBPE chain microstructure (i.e. polymer chain topology) by adjusting the polymerization conditions (ethylene pressure and reaction temperature); (2) highly electrophilic cationic metal centers with reduced oxophilicity, which allow the copolymerization of ethylene with comonomers having polar functionalities; (3) the capability of initiating and catalyzing olefin "living" polymerization; and (4) sterically tuneable α–diimine ligands which allow the convenient control on HBPE molecular weight. Benefiting from these features, a novel range of homo-polyolefins and olefin copolymers with polar functional groups with unique polymer microstructures have been synthesized successfully. In this section, a detailed comparison between these late transition metal catalysts and other existing catalysts will be discussed. Meanwhile, each feature of these late-transition Pd– and Ni– diimine catalysts will also be summarized and discussed.

1.2.4.1 Chain Walking

Different from early-transition metal catalysts (Z-N and metallocene catalysts) which can only synthesize HDPE and LLDPE from ethylene and α-olefins, late transition Pd– and Ni– diimine catalysts were found to give rise to high-molecular-weight polymers with unique hyperbranched chain microstructures.[9] Especially, the polyethylenes synthesized with Pd–diimine catalysts were shown to have dendrimer-like branch-on-branch structures with branching densities *ca.* 100 branches per 1000 carbons. These unique chain microstructures were found to be attributed to the unprecedented chain walking mechanism of Pd–diimine catalysts described by Guan et al. in 1999.[12] They reported that during chain propagation, the Pd metal active centers can walk along the polymer chain at the ethylene dissociated state. The detailed chain walking process can be described as three sequential processes: β–hydride elimination, bond rotation, and subsequent readdition, as shown in Scheme 1.5.[12]

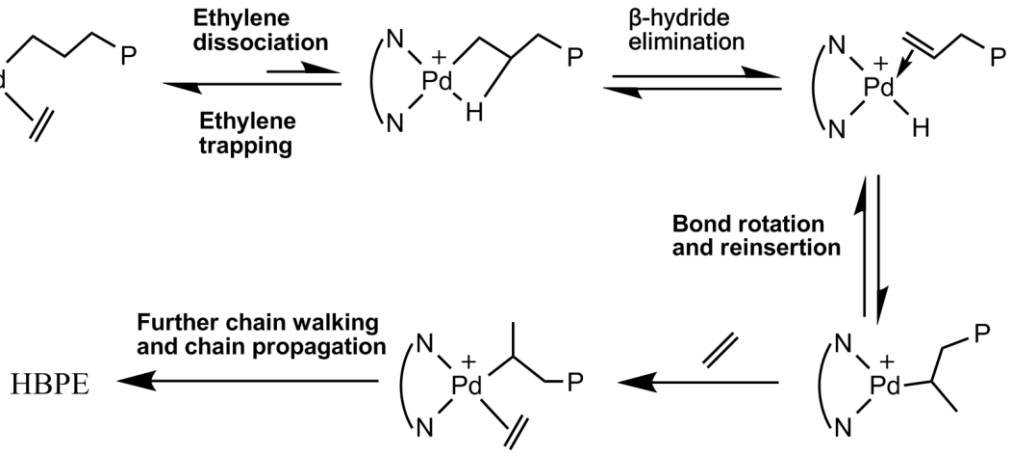

Scheme 1.5 Chain waling mechanism with Pd-diimine catalysts.[12]

Compared to the Ni analogs, the Pd–diimine catalysts usually show significantly higher chain walking capability with much longer walking distance, rendering

polyethylenes with high branching densities. On the other hand, the Ni–diimine catalysts usually produce polyethylene with relative linear chain architecture containing short branches. Thus, the control of chain topology of hyperbranched polyethylene (HBPE) were mainly studied by utilizing Pd–diimine catalysts.[12–14] Guan et al. firstly demonstrated that the concept of using catalyst chain walking to tune polyethylene chain topologies in ethylene polymerization with Pd–diimine catalyst.[12] They found that the polyethylene chain topology could be controlled by simply tuning ethylene pressure. In this case, although the overall branching density and short-chain branching distribution had barely changed, the chain topology of HBPE changes from linear with moderate branches at high ethylene pressures to hyperbranched at low pressure. Meanwhile, Brookhart et al. have elucidated their nuclear magnetic resonance (NMR) studies on the detailed mechanism of the chain walking process in ethylene polymerization with Pd–diimine catalysts.[13] They found that the chain propagation rate (R_p) in this case actually was independent of ethylene concentration, while the chain walking rate (R_w) had an inverse first-order dependence on ethylene pressure. Thus, without affecting the R_p, reducing ethylene pressure can increase R_w and produce polyethylene with hyperbranched architecture, while increasing ethylene pressure will yield polyethylene with relatively linear chain topology.

Other than ethylene pressure (i.e., ethylene concentration), polymerization temperature is another parameter that can affect polymer chain topology. At an ethylene pressure of 1 atm, it was found that increasing the polymerization temperature lead to enhanced polymer the chain compactness.[14] That is, as the temperature increases, the

increase of the chain walking rate (R_w) is faster than that of the chain propagation rate (R_p), resulting in longer chain walking distance, With longer chain walking distance, more hyperbranched polyethylene can be produced. Scheme 1.6 shows the chain walking strategy for controlling polymer chain topology by adjusting the chain propagation rate (R_p) and the chain walking rate (R_w).

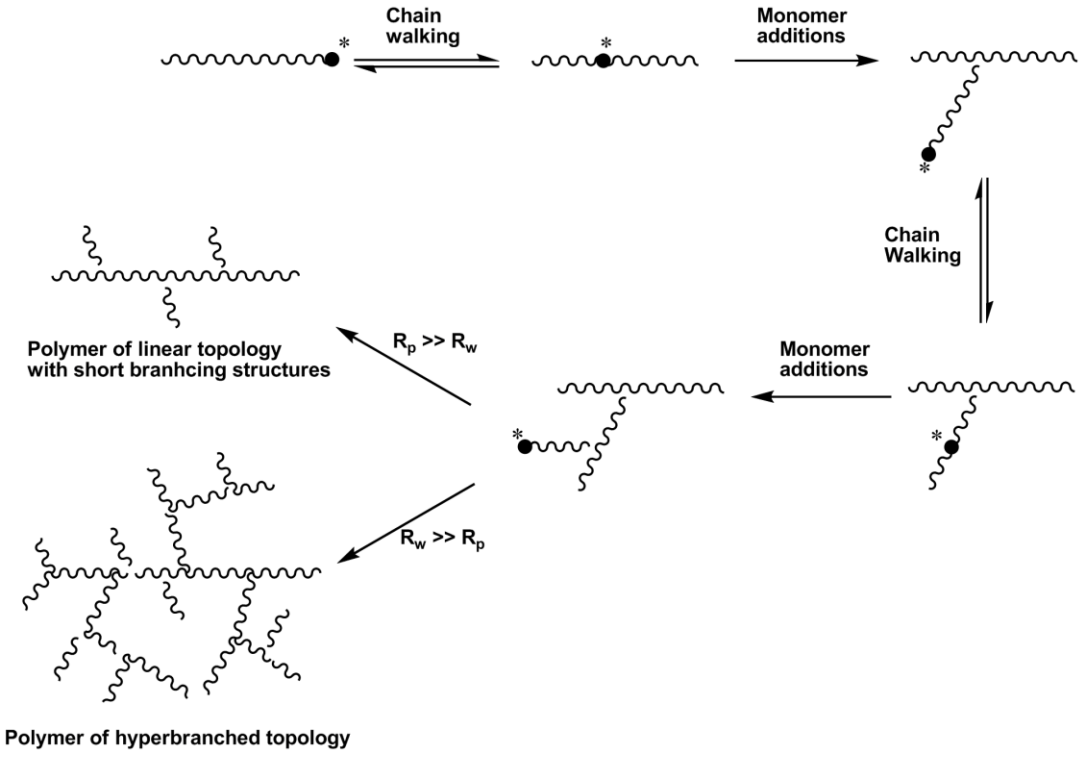

Scheme 1.6 Chain walking strategy for controlling polymer topology.[12]

Different from two mentioned parameters (ethylene pressure and polymerization temperature), the ring incorporation discovered by our group can also effectively change the polyethylene chain topology in the polymerization with Pd–diimine catalyst.[15] It was found that the incorporated ring structures can block catalyst chain walking to restrict chain walking distance and render HBPEs with more linear chain topology. Two five-

membered aliphatic ring structures have been demonstrated to be able to block catalyst chain walking. In one case,[15a] 1,2-disubstituted *cis*-fused five-membered rings containing a quaternary carbon on the 4th position are incorporated through ethylene copolymerization with diethyl diallylmalonate (DEDAM). In the polymerization, DEDAM underwent cyclo-addition resulting in five-membered rings incorporated on the polymer backbone at various low contents (0.26–3.6 mol %). On the basis of the consistent increase in intrinsic viscosity in the Mark-Houwink plots with the increase of ring content, polymer chain topology was confirmed to be linearized with the incorporation of the rings. The "blocking" mechanism herein was believed to be that 1,2-disubstituted rings block or minimize Pd–diimine catalyst from walking back through the ring to prior chain segments. In another study by Morgan et al.,[15b] cyclopentene (CPE) was used as the ring-forming commoner to give primarily 1,3-enchained *cis*-fused five-membered rings on polymer backbone. Similar to the use of DEDAM, the increase of ring content linearized the polymer chain topology. However, the linearization effect of CPE rings was weaker compared to those of DEDAM possibly due to the difference in their ring structures. For instance, chain walking can only occur through one side of the rings formed by DEDAM, while it can occur through both sides of the rings formed by CPE. The effects of ring incorporation on polymer chain topology in chain walking polymerization are shown schematically in Scheme 1.7.

Moreover, Guan had also found that catalyst ligand electronics can affect the polymer chain topology.[16] They synthesized a series of α–diimine catalysts with different ligands for the ethylene polymerization. Based on the polymers obtained,

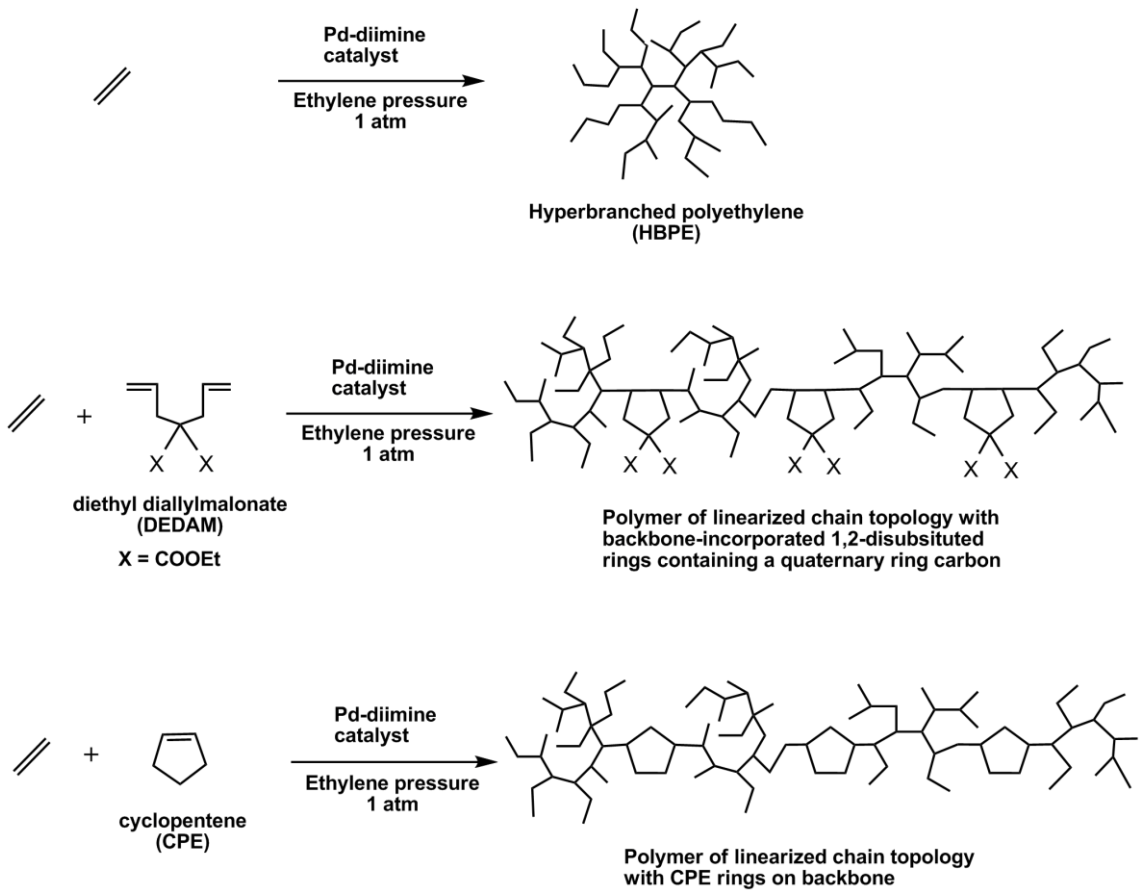

Scheme 1.7 Schematic effects of ring incorporation on polymer chain topology in chain walking polymerization.[15]

they demonstrated that electron-deficient ligands tend to enhance catalysts chain walking capability and render polymers with more branched chain topology. However, this strategy involved the changing of the catalyst structure which is totally different from the previous examples. Moreover, the changing of polymer chain topology through this approach is not as effective as the changing of ethylene pressure, polymerization temperature and the ring incorporation content.

1.2.4.2 Copolymerization of Ethylene with Olefin

Commercially, ethylene has been copolymerized with different comonomers including α-olefins, acylic acids, dienes, vinyl acetate, vinyl alcohol, styrene, acrylate, etc. using free radical polymerization, Z-N catalysts, or metallocene catalysts.[17] Table 1.3 summarizes commercial ethylene copolymers with their structures and manufacturing techniques. From the table, it is obvious to see that copolymerization of ethylene with comonomers containing polar groups are commercially carried out using free radical polymerization, which is also used for the production of LDPE. Incorporation of the polar functionality in this case is random. On the other hand, the early transition metal catalysts (Z-N catalysts and metallocene catalysts) are commercially used for the copolymerization of ethylene with other olefins (α-olefins, styrene, and dienes). The main reason herein is that the early transition metal based Z-N and metallocene catalysts with high oxophilicity are easily poisoned by the monomers containing functional groups.

As previously mentioned, Z-N and metallocene catalysts can be used for the copolymerization of ethylene and α-olefins (i.e., 1-butene, 1-hexene, 1-octene) to produce LLDPE.[1–3] Actually, early transition metal catalysts can also be utilized for copolymerization of ethylene with cyclo-olefins (i.e., cyclopentene, norbornene) selectively without ring opening, however, with low activity. In the case of using Z-N catalysts, because of the multiple active centers, the control of polymer structures such as molecular weight, molecular weight distribution, and composition distribution is hard to achieve. Thus, even though Natta et al. reported the first successful copolymerization of ethylene with a monocyclic olefin monomer such as cyclopentene (CPE),

Table 1.3 Common ethylene copolymers with their structures and manufacturing techniques.[17]

Ethylene copolymer	Structure	Polymerization Technique	Comonomer	Note
Ultra-low-density polyethylene (ULDPE)	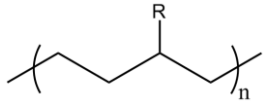	Metallocene catalyst (not Z-N catalyst)	1-olefin (1-butene, 1-hexene, 1-octene)	
Metallocene linear low-density polyethylene (mLLDPE)	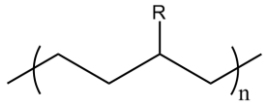	Metallocene	Butane, hexane, octene, 4-methyl-1-pentene, cyclic and bicyclic groups	
Ethylene-acrylic acid copolymers, carboxylated ethylene copolymers (ionomers)	$-(CH_2-CH_2)_n-[CH_2-C(CH_3)(CO_2Na^+)]_m-[CH_2-CH_2-CCH_3(CO_2H)]_l-$	Free radical polymerization, Ceiling temperature 550 K	Methacrylic acid	Post-synthesis adducts sodium, lithium, zinc
Poly(ethylene-co-acrylate)	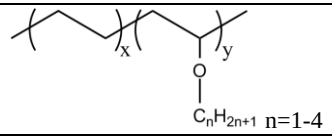	Free radical polymerization	Methyl acrylate, ethyl acrylate, butyl acrylate	
Ethylene-propylene-diene monomer elastomers	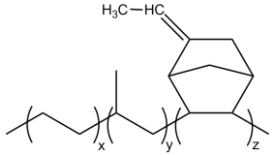	Ziegler-Natta or metallocene (e.g., $VOCl_3/Et_3Al_2Cl_3$, 30–70 ℃, or Cp_2Zr/methalumonxane, 80–120 ℃)	Propene, ethylidene norbornene or dicyclopentadiene, 1,4 hexadiene, vinyl norbornene, norbornadiene	Z-N gives better incorporation of bycylic dienes than metallocenes, for straight-chain dienes it is reversed
Ethylene-vinyl acetate copolymer	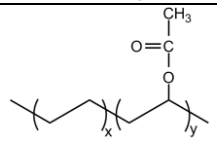	Free radical polymerization	Vinyl acetate	
Ethylene-vinyl alcohol copolymer	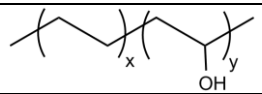	Free radical polymerization	Vinyl acetate	Post-synthesis hydrolysis
Styrene-ethylene-butylene-styrene triblock copolymer	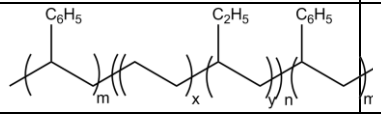	Free radical polymerization	Styrene, butylene	

cycloheptene (CHP), cyclooctene (COE), or cyclohexene (CHE) in the presence of vanadium precatalysts and alkylaluminum cocatalysts, the products were polymer mixture with crystalline and elastomeric copolymers and the detailed microstructure of ethylene-cycloolefin copolymers were not reported.[18] In the case of the single-site metallocene catalyst, the precise control of molecular structure becomes possible. More types of PE such as LLDPE, very low density polyethylene (VLDPE) or ultra low density polyethylene (ULDPE) can be produced. Most common cycloolefins, cyclopentene and norbornene have been extensively used as the cyclic comonomers in olefin polymerization with metallocene catalysts to prepare high-performance cycloolefin copolymers. Moreover, metallocene catalysts also show a unique feature of polymerizing cycloolefin monomers homogeneously.

In 1989, a significant breakthrough in the synthesis of cylic olefin copolymers was achieved by Kaminsky et al.[19] They prepared copolymers of CPE and ethylene with up to 37 mol % CPE incorporation through 1,2- and 1,3-enchainment with a zirconocene catalyst, *rac*-ethylene-bis(indenyl)zirconium dichloride, combined with MAO. Since then, a wide variety of metallocene catalysts have started to be used for the copolymerization of ethylene with CPE.[20,21] Some examples for synthesis of ethylene/CPE copolymers with different metallocene catalysts will be given. For example, Müller et al. reported the copolymerization of ethylene and CPE with zirconocene catalyst, *rac*-dimethylsilylene(ferroceno[2,3]indenyl)(cyclopentadienyl)zirconium dichloride with MAO, as well as the assignment of the ^{13}C NMR spectrum of the copolymer.[22] Both

1,2-enchained and 1,3-enchained CPE units were detected and the ratio of 1,2- to 1,3-units increased as the CPE content in the copolymer increased. Fujita and Coates reported the synthesis and characterization of copolymers from ethylene and CPE using a living bis (phenoxyimine)titanium catalyst.[23] The resulting copolymers with *cis*-1,2 cyclopentane units, high molecular weights and low polydispersities have CPE incorporation of 47 mol % indicating a nearly perfect alternating polymer macrostructure. Naga and Imanishi reported the copolymerization of ethylene and CPE with various non-bridged and bridged zirconocene catalysts with MAO.[24] All of the bridged catalysts produced ethylene homopolymer without incorporation of CPE, while all of bridged catalysts yielded copolymer. Among them, *rac*-Et$(Ind)_2ZrCl_2$ showed the highest reactivity toward CPE, producing a copolymer with 38 mol % CPE incorporation. Later Naga reported the copolymerization of ethylene and twelve cycloolefins with a constrained-geometry catalyst, dimethylsilylene(tetramethylcyclopentadienyl)(N-tert-butyl)titanium dichloride, with methyl isobutyl aluminoxanes as a cocatalyst.[25] Tang et al. successfully copolymerized ethylene and cyclopentene with bis(β-enaminoketonato) titanium complexes activated with modified MAO.[26] Napoli et al. also copolymerized ethylene with cyclopentene using half titanocenes.[27]

Norbornene is another cyclic comonomer for ethylene copolymerization which has been widely studied in last two decades. The earliest copolymerization of ethylene with NB and some of its derivatives was disclosed in patents as early as 1960s. However, the major breakthrough was made by Kaminsky et al. who reported the first

copolymerization of ethylene with norbornene using zirconocene catalysts in 1991.[19b] Later, various zirconium and titanium based metallocene catalysts were used for the copolymerization of ethylene with NB.[28] A few representative examples for synthesis of ethylene/norbornene (NB) copolymers with different metallocene catalysts will be given. For instance, Tritto et al. reported the synthesis of ethylene-norbornene copolymers by using *ansa*-zirconocene catalysts [29] and titanium-based ($Me_2Si(Me_4Cp)(N^tBu)TiCl_2$) [30] catalysts. The polymerization was carried out at 30 ℃ and yielded ethylene-NB copolymers with high molecular weights and narrow molecular weight distributions. A similar catalyst ($Me_2SiFlu(N^tBu)TiMe_2$) was also used for ethylene/NB copolymerization by Shiono et al.[31] Fujita et al. demonstrated high-performance "living" ethylene-NB alternating copolymerization with bis(pyrrolide-imine) titanium catalysts.[32] Li et al. synthesized high-molecular-weight narrow-distributed copolymers containing primary alternating and isolated NB units with bis(enaminoketonato)titanium catalysts.[33] Nomura and Wang also synthesized ultrahigh-molecular-weight E-NB copolymers containing primarily isolated and alternating NB units with (arylimido)(aryloxo)vanadium/Et_2AlCl catalyst systems.[34]

Late transition metal Pd and Ni catalysts have also been used for the copolymerization of ethylene with cycloolefins. For example, Zou et al. synthesized high-molecular-weight branched ethylene/cyclopentene copolymers by three α-diimine nickel(II) complexes in the presence of MAO.[36] In the resulting copolymers, the CPE was entirely incorporated via *cis*-1,3-enchainment, and various branches such as methyl, ethyl, propyl, butyl, and long branches were showing in polyethylene segments.

However, the CPE content in the copolymer can only reach about 23% and the branching density varied from 13 to 51 braches per 1000 carbons. In the previous section, we have also mentioned that CPE was successfully copolymerized with ethylene by using Pd–diimine catalyst by our group.[15b] In 1998, Goodall et al. reported on ethylene-norbornene copolymerization with a variety of late transition Pd and Ni catalysts on two patents.[37] Then, Benedikt et al. synthesized the copolymers of ethylene with NB derivatives, as well as their terpolymers with1-alkenes using a series of neutral, square-planar nickel complexes containing anionic P∼O chelates.[35] Later in 2003, Kaminsky et al. investigated screening-like procedure for the copolymerization of ethylene with norbornene with sixteen Pd–diimine catalysts having different ligand sterics.[38] Two catalysts, [(ArN=CHCH=NAr)Pd(Me)–(CH_3CN)]BAr^f_4 (1b'; Ar = 2,6-$Me_2C_6H_3$, BAr^f_4 = B[3,5–$C_6H_3(CF_3)_2]_4$) and [(ArN=C(CH_3)C(CH_3)=NAr)Pd(Me)–(CH_3CN)]BAr^f_4 (2c'; Ar = 2,6–*i*$Pr_2C_6H_3$) were synthesized as discrete catalytically active species, and their copolymerization behavior was investigated in detail. They discussed the influence of feed composition, polymerization temperature, and ligand structure on copolymer properties and microstructures with selected Pd–diimine catalysts.[39] More recently, lots of late transition metal catalysts including palladium complexes with an anionic P∼O chelate,[40] cationic organopalladium complexes bearing hemilabile bidentate ligands of α–amino-pyridines,[41] β–diketiminato nickel/MAO,[42] neutral salicylaldiminato-ligated palladium(II),[43] neutral aryl phosphin sulfonate palladium catalyst [44] were also investigated for the ethylene/NB copolymerization.

1.2.4.3 Copolymerization of Ethylene with Functional Monomers Containing Polar Groups

Despite the fact that early transition metal catalysts with high oxophilicity are easily poisoned by functional polar groups in the comonomers during the copolymerization, some successful examples have been reported.[45] For example, halogen-containing monomers may be directly homopolymerized or copolymerized with olefins using Z-N and metallocene catalysts. In one case, Basckai synthesized a terpolymer of ethylene, propylene, and 8-bromo-1-octene having 22% halomonomer incorporation with $TiCl_3/Et_2AlCl$.[46] However, the products were not homogeneous and no characterization of tacticity or cross-linking was carried out. In another one, Galimberti et al. synthesized ethylene/propylene/4-iodo-1-butene terpolymers with $V(acac)_3/AlEt_2X$ catalyst (X = Cl, I). The resulting copolymers were amorphous and processed a bimodal molecular weight distribution of high-molecular-weight polymer and oligomers.[47] Metallocene catalysts such as *rac*-$Et(Ind)_2ZrCl_2$/MAO catalyst were also used to synthesize terpolymers of ethylene, propylene, and 11-chloro-1-undecene.[48] The resulting well defined polymers have up to 2 mol % incorporation of the halogenated monomer with molecular weight of 40,000 to 60,000 g/mol and PDI of 1.7–2.0. Beside halogen-containing monomers, certain oxygen-containing ester monomers can also be copolymerized with ethylene. For instance, Amiard et al. copolymerized methyl 5-norbornene-2-yl ester with ethylene, propylene, 1-butene, and dicyclopentadiene using vanadium-based Z-N catalysts.[49] Direct copolymerizations of

ethylene with nitrogen-containing amines are difficult with early-transition metal catalysts, and few examples were described in the review articles.[45]

In most cases, the reactivity of functional groups toward the metal catalysts require protection-deprotection strategies. For compatibility with Z-N and metallocene catalysts, the most commonly employed protecting groups are based on aluminum, boron, and silicon.[45] For example, Mülphaupt et al. copolymerized the ethylene with the protected monomer *N*,*N*-bis(trimethylsilyl)-1-amino-10-undecene using a zirconocene/MAO initiating system.[50] The protecting groups were later removed with HCL followed by a sodium hydroxide wash. The resulting copolymers having 6–19 wt % amine showed decreased T_m (101–116 °C) and crystallinities compared to the parent polyolefin. In the case of oxygen-containing groups such as alcohol, acid, and ester, an aluminum-based Lewis acid was usually used as chemical protection for successful polymerization.

In addition to the use of chemical protection, the proper steric protection of the active site from the oxygenated functionality is also required. For example, Aaltonen et al. used MAO to protect 1-hydroxy-10-undecene in situ and then directly synthesized polyethylene and polypropylene polymers containing hydroxyl side groups using $Et(Ind)_2ZrCl_2$ and $MeSi(Ind)_2ZrCl_2$ with MAO.[51] Kashiwa et al. also copolymerized ethylene and 1-hydroxy-10-undecene pre-treated with trimethyl aluminum to produce polyethylene functionalized with hydroxyl side groups using a special *ansa*-zirconocene catalyst structurally featured by a large steric hindrance.[52]

Previous examples using early transition metal catalysts to directly copolymerize ethylene with other polar functional comonomers are challenging due to catalytic poisoning. The protecting group method provided an alternative route to avoid the catalytic poisoning but added complex synthetic steps which were not convenient. Late transition metal based Pd–/Ni– diimine catalysts, owing to their remarkable low oxophilicity, show great capability for copolymerization of ethylene with comonomers containing polar functionalities. A range of functionalized HBPEs containing various valuable functionalities have been synthesized through chain walking polymerization with Pd–diimine catalysts.[53]

Usually, two main classes of functional comonomers, acrylates and 1-alkenes, can be employed for synthesis of functionalized HBPEs. Both comonomers are important and have their own advantages. For example, acrylate-type comonomers are usually commercially available or easy to synthesize, while HBPEs synthesized with 1-alkenes are more stable under acidic and alkaline application conditions. The functionalities that can be designed into comonomers usually contain oxygen such as ester, ketone, epoxide, ether, alcohol, carboxylic acid, which Pd–diimine catalysts can tolerate. Some comonomers containing fluoro, phosphorous, and sulfone groups can also be copolymerized. Scheme 1.8 summarized functionalized 1-alkene comonomers that have been used for synthesis of functionalized HBPEs.[53b,54,55] These comonomers were usually designed to have a quaternary carbon or a long spacing between the olefinic double bond and the functionality to avoid the possible catalytic poisoning

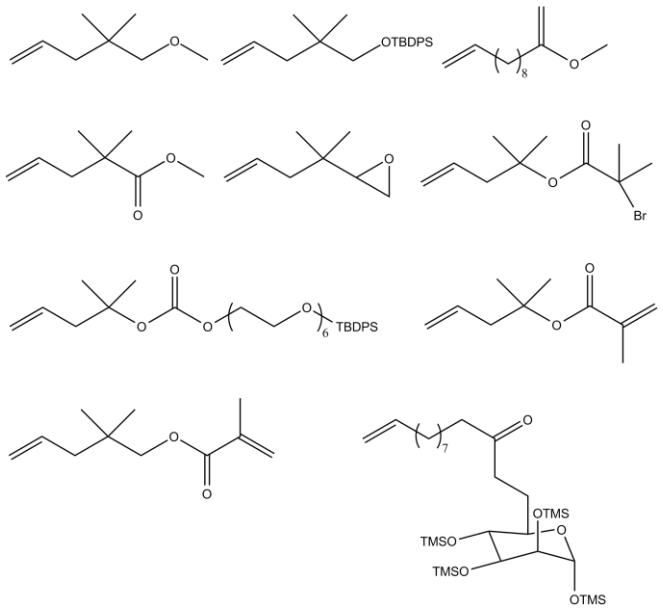

Scheme 1.8 Functional 1-alkene comonomers used for synthesis of functionalized HBPEs via ethylene copolymerization.[53–55]

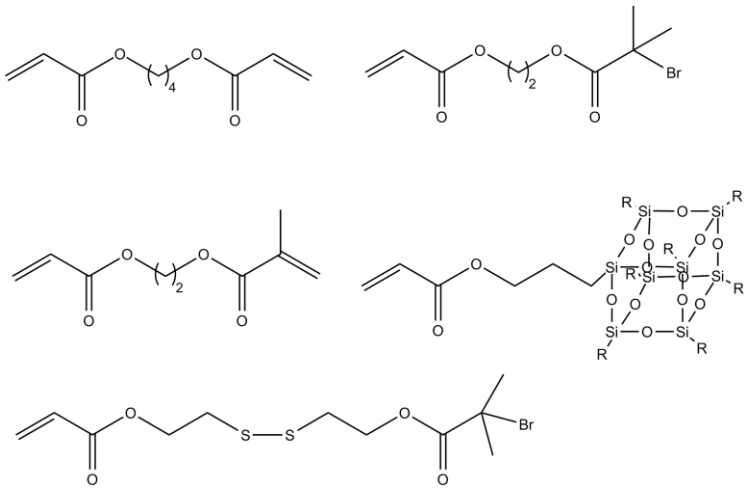

Scheme 1.9 Functional acrylate comonomers used for synthesis of functionalized HBPEs via ethylene copolymerization.[53,56]

during the copolymerization. Different from the use of 1-alkenes, our group utilized various functional acrylate comonomers for the synthesis of functionalized HBPEs via

ethylene copolymerization as shown in Scheme 1.9.[53b,56] For example, in a study by Wang et al., HBPEs containing covalently tethered polyhedron oligomeric silsesquioxane (POSS) nanoparticles at different contents have been successfully synthesized by chain walking ethylene copolymerization with acryloisobutyl-POSS a using Pd–diimine catalyst.[56b] In another study, Zhang et al. synthesized HBPEs containing 2-bromoisobutyryl groups which were subsequently used for the atom-transfer radical polymerization.[56a] The resulting polymers possess a novel core-shell architecture with HBPE core grafted with linear side arms of poly(methyl methacrylate) (MMA). More recently, HBPEs containing pendant disulfide groups at controllable content have also been synthesized by chain walking copolymerization of ethylene with an acrylate comonomer containing disulfide functionality.[56e] The Pd(II) catalysts in this case were immobilized in situ onto the polymers by coordinative binding with the pendant disulfide and form the homogeneous self-supported Pd(II) catalysts. These resulting polymers were subsequently used as effective catalysts for various carbon-carbon coupling reactions.

1.2.4.4 "Living" Ethylene Polymerization with Pd-Diimine Catalysts

In "living" polymerization, the polymer chains retain their ability to propagate and grow to a desired size while their degree of termination or chain transfer is still negligible. Common living polymerization techniques including living anionic polymerization, living cationic polymerization, living ring-opening metathesis

polymerization, living free radical polymerization, and living chain-growth polycondensations.[57]

In 1955, the initial work of living polymerization was done by Szware who proved the livingness of the anionic polymerization of styrene. Later, Morton and Bywater made a critical contribution in this field.[57] Since then, the research on living polymerizations has been extensively developed. Kennedy has reviewed the living cationic polymerization in 1999.[58] At the same time, the living/controlled group transfer polymerization of (meth)acrylates was developed by Webster.[59] More recently, the controlled/living radical polymerization has been discovered. The detailed discussions of this polymerization technique were shown in some review papers.[60]

Single-site transition metal catalysts including metallocene and Pd/Ni catalysts have also been used for the living polymerization of α-olefins. Among all transition metal catalysts, Pd–diimine catalysts have been developed and discussed mostly in the last two decades. Brookhart et al. who discovered the late-transition Pd–diimine catalysts have done extensive work with Pd–diimine catalysts for living α-olefin polymerizations. [61,] Meanwhile, our group has also designed and developed a series of new Pd-diimine catalysts for synthesis of new classes of novel polyethylene with unprecedented chain architectures by utilizing their "living" feature.[62] For example, Zhang et al reported the synthesis of a POSS–supported Pd–diimine catalyst which were subsequently used for the ethylene "living" polymerization. A range of polyethylenes containing a POSS with controllable length were successfully synthesized.[62a] In further

extended work, Zhang et al. synthesized polymer-inorganic hybrid nanoparticles through surface-initiated ethylene "living" polymerization with the silica supported catalyst.[62b] Zhang et al. also reported the synthesis of ATRP initiator containing polyethylene through ethylene "living" polymerization.[62c] The functionalized polyethylenes have been used as macroinitiator for the synthesis of block copolymers through chain extension via ATRP. We have also demonstrated the first "core-first" synthesis of three-arm and multiarm star polyethylene by using novel trinuclear and multinuclear Pd–diimine catalysts through the "living" polymerization.[62d] Xu et al. demonstrated the synthesis of a novel class of diblock and triblock treelike hyperbranched-linear polyethylene block polymers comprised of chemically identical but topologically different chain blocks utilizing the "living" polymerization feature of Pd–diimine catalyst.[62e] Liu et al. reported the "arm-first" synthesis of core–shell-structured multiarm polyethylene star polymers having multiple linear-but-branched PE arms joined at a cross-linked polydivinylbenzene core. In this case, coordinative ethylene "living" polymerization was first carried out using a functionalized Pd–diimine catalyst. Then, polyethylene containing an end-capping 2-bromoisobutyryl group was subsequently used for initiating ATRP.[62f] Moreover, Zhang and Ye reported the synthesis of a range of well-defined treelike (hyperbranched polyethylene)-*b*-(linear polyketone) block polymers by utilizing "living" ethylene polymerization with ligand switchable Pd catalyst.[62g]

1.3 Thesis Research Objectives and Outlines

Late-transition Pd–diimine catalysts have been demonstrated to have many advantages and unique features compared to early-transition metal catalysts (Z-N and metallocene catalysts). Their outstanding characteristics including chain walking, the capability for copolymerizing ethylene with cycloolefins and comonomers containing polar functionalities, and the capability of initiating and catalyzing olefin "living" polymerization attracted me to explore and synthesize polyethylene copolymers with different comonomers and polyethylene-inorganic hybrid nanoparticles. Thus, the overall objectives of this thesis are: (1) to synthesize a range of ethylene–norbornene (E–NB) copolymers having various controllable comonomer composition distributions, (2) to synthesize HBPE ionomer containing ionic functional group, (3) to characterize the synthesized polymers (4) to evaluate the performance of HBPE ionomers containing Pd nanoparticles in carbon-carbon coupling reactions and semi-hydrogenation reactions of alkynes, (5) to synthesize polyethylene-grafted silica nanoparticles with controllable polymer density, length and chain topology utilizing "living" feature of Pd–diimine catalysts, and (6) to evaluate the effects on polymer-grafted silica dispersion in a polyolefin matrix (this work has been done by K. Petrie and Professor M. Kontopoulou at Queen's University).

In Chapter 2, a broad class of low-polydispersity ethylene–norbornene (E–NB) copolymers having various controllable comonomer composition distributions, including gradient, alternating, diblock, triblock, and block-gradient, have been synthesized through "living"/quasiliving E–NB copolymerization facilitated with a single Pd–diimine catalyst.

In Chapter 3, HBPE ionomers containing ammonium ions have been synthesized via one-pot chain walking copolymerization of ethylene with polymerizable acrylate type ionic liquid comonomers by using Pd–diimine catalyst.

In Chapter 4, HBPE ionomer containing Pd(0) nanoparticles have been synthesized via copolymerization of ethylene with polymerizable acrylate ionic liquid comonomer. The polymer-supported Pd(0) nanoparticle catalysts have shown outstanding catalytic performances for the Heck and Suzuki cross-coupling reactions, and semi-hydrogenation of alkynes.

In Chapter 5, the successful tuning of various structural parameters including brush length, density, and topology of polyethylene brushes in the surface-initiated polymerization have been achieved. The effects of brush length and density on the nanofiller dispersion and physical properties of the composites are also examined. (This part of work on nanofiller dispersion in the nanocomposites and physical properties of the nanocomposites was done by the Queen's group through collaboration).

1.4 References

1. Peacock, A. J. *Handbook of Polyethylene Structures, Properties, and Applications* Marcel Dekker, Inc.: New York, USA, 2000.
2. Charles E. Carraher, Jr. *Polymer Chemistry* Sixth Edition; Marcel Dekker, Inc.: New York, USA, 2003.

3. Nowlin, T. E. *Business and Technology of the Global Polyethylene Industry: An In-depth Look at the History, Technology, Catalysts, and Modern Commercial Manufacture of Polyethylene and Its Products*, Wiley-Scrivener, 2014.
4. Kealy, T. J.; Pauson, P. L. *Nature* **1951**, *168*, 1039–1040.
5. Miller, S. A.; Tebboth, J. A.; Tremaine, J. F. *J. Chem. Soc.* **1952**, 632–635.
6. Natta, G.; Pino, P.; Mazzanti, G.; Giannini, U. *J. Am. Chem. Soc.* **1957** *79*, 2975–2976.
7. Breslow, D. S.; Newburg, N. R. *J. Am. Chem. Soc.* **1957**, *79***,** 5072–5073.
8. (a) Andresen, A.; Cordes, H. G.; Herwig, J.; Kaminsky, W.; Merck, A.; Mottweiler, R.; Pein, J.; Sinn, H; Vollmer, H. J. *Angew Chem. Int. Ed.* **1976**, *15*, 630–632; (b) Kaminsky, W. *J. Polym. Sci. Part A: Polym. Chem.* **2004**, *42*, 3911–3921.
9. Johnson, L. K.; Killian, C. M.; Brookhart, M. *J. Am. Chem. Soc.* **1995**, *117*, 6414–6415.
10. Ittel, S. D.; Johnson, L. K. *Chem. Rev.* **2000**, *100*, 1169–1203.
11. Camacho, D. H.; Guan, Z. *Chem. Commun.* **2010**, 46, 7879–7893.
12. Guan, Z.; Cotts, P. M.; McCord, E. F.; McLain, S. J. *Science*, **1999**, *283*, 2059–2062.
13. (a) Tempel, D. J.; Johnson, L. K.; Huff, R. L.; White, P. S.; Brookhart, M. *J. Am. Chem. Soc.* **2000**, *122*, 6686–6700; (b) Shultz, L. H.; Tempel, D. J.; Brookhart, M. *J. Am. Chem. Soc.*, **2001**, *123*, 11539–11555.
14. (a) Ye, Z.; Zhu, S. *Macromolecules* **2003**, *36*, 2194–2197; (b) Ye, Z.; AlObaidi, F.; Zhu, S. *Macromol. Chem. Phys.* **2005**, *24*, 897–906.
15. (a) Xiang, P.; Ye, Z.; Morgan, S.; Xia, X.; Liu, W. *Macromolecules* **2009**, *42*, 4946–4949; (b) Morgan, S.; Ye, Z.; Subramanian, R.; Wang, W.; Ulibarri, G. *Polymer*,

2010, *51*, 597–605.

16. Popeney, C.; Guan, Z. *Organiometallics* **2005**, *24*, 1145–1155.
17. Mark, J. E. *Polymer Data Handbook*; Oxford University Press, New York, 1999.
18. (a) Natta, G.; Dell'Asta, G.; Mazzanti, G.; Pasqunn, I.; Valvassori, A.; Zambelli, A. *Makromol. Chem.* **1962**, *54*, 95–101; Dall'Asta, G.; Mazzanti, G. *Makromol. Chem.* **1963**, *61*, 178–197; (c) Natta, G.; Dell'Asta, G.; Mazzanti, G. *Angew. Chem. Int. Ed.* **1964**, *3*, 723–729.
19. (a) Kaminsky, W.; Spiehl, R. *Makromol. Chem.* **1989**, *190*, 515–526; (b) Kaminsky, W.; Bark, A. *Makromol. Chem. Macromol. Symp.* **1991**, *47*, 83–93.
20. Baugh, L. S.; Canich, J. A. M. Stereoselective Polymerization with Single-Site Catalysts; CRC Press, 2007.
21. Li, X.; Hou, Z. *Coordination Chemistry Reviews* **2008**, *252*, 1842–1869.
22. Jerschow, A.; Ernst, E.; Hermann, W.; Müller, N. *Macromolecules* **1995**, *28*, 7095–7099.
23. Fujita, M.; Goates, G. W. *Macromolecules* **2002**, *35*, 9640–9647.
24. Naga, N.; Imanishi, Y. *Macromol. Chem. Phys.* **2002**, *203*, 159–165.
25. Naga, N. *J. Polym. Sci. Part A: Polym. Chem.* **2005**, *42*, 1285–1291.
26. Tang, L.-M.; Duan, Y.-Q.; Li P.; Li, Y.-S. *J. Polym. Sci. Part A: Polym. Chem.* **2005**, *43*, 1681–1689.
27. Napoli, M.; Mariconda, A.; Immediata, I.; Longo, P. *J. Polym. Sci. Part A: Polym. Chem.* **2008**, *46*, 4725–4733.
28. See representative reviews: (a) Tritto, L.; Boggioni, L.; Ferro, D. R. *Coord. Chem. Rev.* **2006**, *250*, 212–241; (b) Janiak, C.; Lassahn, P. G. *J. Mol. Catal., Chem.* **2001**,

166, 193–209; (c) Makovetskii, K. L. *Polym. Sci, Ser. C* **2008**, *50*, 22–38.

29. (a) Jansen, J. C.; Mendichi, R.; Locatelli, P.; Tritto, I. *Macromol. Rapid Commun.* **2001**, *22*, 1394–1398; (b) Jansen, J. C.; Mendichi, R, Sacchi, M. C.; Tritto, I. *Macromol. Chem. Phys.* **2003**, *204*, 522–530.
30. Thorshaug, K.; Mendichi, R.; Boggioni, L.; Tritto, I.; Trinkle, S.; Friedrich, C.; Mulhaupt, R. *Macromolecules* **2002**, *35*, 2903–2911.
31. (a) Hasan, T.; Shiono, T.; Ikeda, T. *Macromol. Symp.* **2004**, *213*, 123–129; (b) Hasan, T.; Ikeda, T.; Shiono, T. *Macromolecules* **2004**, *37*, 8503–8509.
32. (a) Yoshida, Y.; Saito, J.; Mitani, M.; Takagi, Y.; Mastsui, S.; Ishili, S. I.; Nakano, T.; Kashiwa, N.; Fujita, T. *Chem. Commun.* **2002**, 1298–1299; (b) Yoshida, Y.; Mohri, J.-I.; Ishii, S.-I.; Mitani, M.; Saito, J.; Matsui, S.; Makio, H.; Nakano, T.; Tanaka, H.; Onda, M.; Yamamoto, Y.; Mizuno, A.; Fujita, T. *J. Am. Chem. Soc.* **2004**, *126*, 12023–12032.
33. Li, X.-F.; Dai, K.; Ye, W. P.; Pan, L.; Li, Y.-S. *Organometallics* **2004**, *23*, 1223–1230.
34. Wang, W.; Nomura, K. *Macromolecules* **2005**, *38*, 5905–5913.
35. Benedikt, G. M.; Elce, E.; Goodall, B. L.; Kalamarides, H. A.; McIntosh, III, L. H.; Rhodes, L. F.; Selvy, K. T. *Macromolecules* **2002**, *35*, 8978–8988.
36. Zou, H.; Zhu, F.; Wu, Q. *J. Polym. Sci. Part A: Polym. Chem.* **2008**, *46*, 2186–2192.
37. (a) Makovetsky, K. L.; Finkelstein, E. S.; Bykov, V. I.; Bagdasaryan, A. K. Goodall, B. L.; Rhodes, L. F. WO Patent No. 9856837, 1998; (b) Goodall, B. L.; McIntosh, L. H., WO Patent No. 9856839, 1998.
38. Kiesewetter, J.; Kaminsky, W. *Chem. Eur. J.* **2003**, *9*, 1750–1758.

39. Kiesewetter, J.; Arikan, B.; Kaminsky, W. *Polymer* **2006**, *47*, 3302–3314.

40. Liu, S.; Borkar, S.; Newsham, D.; Yennawar, H.; Sen, A. *Organometallics* **2007**, *26*, 210–216.

41. Lin, Y.-C.; Yu, K.-H.; Huang, S.-L.; Liu, Y.-H.; Wang, Y.; Liu, S.-T.; Chen, J.-T. *Dalton Trans.* **2009**, 9058–9067.

42. Li, Y.; Gao, M.; Gao, H.; Wu, Q. *European Polymer Journal* **2011**, *47*, 1964–1969.

43. Pong, F. Y.; Mandal, S.; Sen, A. *Organometallics* **2014**, *33*, 7044–7051.

44. Tritto, I.; Boggioni, L.; Ravasio, A.; Scalcione, G. *Macromol. React. Eng.* **2013**, *7*, 91–97.

45. See some review articles: (a) Gibson, V. C.; Spitzmesser, S. K. *Chem. Rev.* **2003**, *103*, 283–315; (b) Dong, J.-Y.; Hu, Y. *Coordination Chemistry Reviews* **2006**, *250*, 47–65.

46. Bacskai, R. *J. Polym. Sci., Part A* **1965**, *3*, 2491–2510.

47. Galimberti, M.; Giannini, U.; Albizzati, E.; Caldari, S.; Abis, L. *J. Mol. Catal. A: Chem.* **1995**, *101*, 1–10.

48. Bruzaud, S.; Gramail, H.; Duvignac, L.; Deffieux, A. *Macromol. Chem. Phy.* **1997**, *198*, 291–303.

49. Amiard, Y.; Bellissent, J.-P.; Marie, G. U.S. Patent 3,723,399, March 27, 1973.

50. Schneider, M. J.; Schäfer, R.; Mülhaupt, R. *Polymer* **1997**, *38*, 2455–2459.

51. (a) Aaltonen, P, Lofgren, B. *Macromolecules* **1995**, *28*, 5353–5357; (b) Aaltonen, P.; Fink, G.; Lofgren, B.; Seppala, J. *Macromolecules* **1996**, *29*, 5255–5260.

52. Imuta, J.; Toda, Y.; Kashiwa, N. *Chem. Lett.* **2001**, *30*, 710–711.

53. See some review articles: (a) Ye, Z.; Li, S. Macromol. React. Eng. 2010, 4, 319–332;

(b) Dong, Z.; Ye, Z. Polym. Chem., 2012, 3, 286–301.

54. (a) Chen, G.; Ma, X.; Guan, Z. J. Am. Chem. Soc., 2003, 125, 6697–6704; (b) Chen, G.; Guan, *J. Am. Chem. Soc.*, **2004**, *126*, 2662–2663; (c) Chen, G.; Huynh, D.; Felgner, P. L.; Guan, Z. *J. Am. Chem. Soc.*, **2006**, *128*, 4298–4302.
55. Wang, J.; Zhang, K.; Ye, Z. *Macromolecules* **2008**, *41*, 2290–2293.
56. (a) Zhang, K.; Wang, J.; Subramanian, R.; Ye, Z.; Lu, J.; Yu, Q. *Macromol. Rapid Commun.*, **2007**, *28*, 2185–2191; (b) Wang, J.; Ye, Z.; Joly, H. *Macromolecules*, **2007**, *40*, 6150–6163; (c) Morgan, S.; Ye, Z.; Zhang, K.; Subramanian, R. *Macromol. Chem. Phys.* **2008**, *209*, 2232–2240; (d) Xu, Y.; Campeau, P.; Ye, Z. *Macromol. Chem. Phys.* **2011**, *212*, 1255–1262; (e) Liu, P.; Ye, Z.; Wang, W.-J.; Li, B.-G. *Macromolecules* **2013**, *46*, 72–82.
57. See some review articles: (a) Hadjichristidis, N.; Iatrou, H.; Pitsikalis, M.; Mays, J. *Prog. Polym. Sci.* **2006**, *31*, 1068–1132; (b) Lopez, R. G.; D'Agosto, F.; Boisson, C. *Prog. Polym. Sci.* **2007**, *32*, 419–454.
58. Kennedy, J. P. *J. Polym. Sci., Polym. Chem.* **1999**, *37*, 2285–2293.
59. Webster, O. W. *J. Polym. Sci., Polym Chem.* **2000**, *38*, 2855–2860.
60. See some review articles: (a) Matyjaszewski, K. *Chem. Rev.* 2001, **101**, 2921–2990; (b) Kamigaito, M.; Ando, T. *Chem. Rev.* 2001, **101**, 3689–3745; (c) Hawker, C. J.; Bosman, A. W.; Harth, E. *Chem. Rev.* 2001, **101**, 3661–3688; (d) Chiefari J.; Rizzardo, E. In: Matyjaszewski, K.; Davis, T. P. editors. *Handbook of radical polymerization* Hoboken: Wiley-interscience, 2002.
61. (a) Gottfried, A. C.; Brookhart, M. *Macromolecules* **2001**, *34*, 1140–1142; (b) Gottfried, A. C.; Brookhart, M. *Macromolecules* **2003**, *36*, 3085–3100.

62. (a) Zhang, Y.; Ye, Z. *Chem. Commun.* **2008**, *10*, 1178–1180; (b) Zhang, Y.; Ye, Z. *Macromolecules* **2008**, *41*, 6331–6338; (c) Zhang, K.; Ye, Z.; Subramanian, R. *Macromolecules* **2008**, *41*, 640–649; (d) Zhang, K.; Ye, Z.; Subramanian, R. *Macromolecules* **2009**, *42*, 2313–2316; (e) Xu, Y.; Xiang, P.; Ye, Z.; Wang, W.-J. *Macromolecules* **2010**, *43*, 8026–8038; (f) Liu, P.; Landry, E.; Ye, Z.; Joly, H.; Wang, W.-J.; Li, B.-G. *Macromolecules* **2011**, *44*, 4125–4139; (g) Zhang, Z.; Ye, Z. *Chem. Commun*, **2012**, *48*, 7940–7942.

Chapter 2

Alternating, Gradient, Block, and Block-Gradient Copolymers of Ethylene and Norbornene by Pd–Diimine-Catalyzed "Living" Copolymerization

This chapter is organized based on a paper published by P. Xiang and Z. Ye in J. Polym. Sci., Part A: Polym. Chem. 2013, 51, 672–686*

Abstract

This chapter demonstrates the facile synthesis of a broad class of low-polydispersity ethylene–norbornene (E–NB) copolymers having various controllable comonomer composition distributions, including gradient, alternating, diblock, triblock, and block-gradient, through "living"/quasi-living E–NB copolymerization facilitated with a single Pd–diimine catalyst (**1**). This synthesis benefits from two remarkable features of catalyst **1**, its high capability in NB incorporation and high versatility in rendering E–NB "living" copolymerization at various NB feed concentrations ($[NB]_0$) while under an ethylene pressure of 1 atm and at 15 °C. At higher $[NB]_0$ values between 0.42–0.64 M, E–NB copolymerization with **1** renders nearly perfect alternating copolymers. At lower $[NB]_0$ values (0.11–0.22 M), gradient copolymers yield due to gradual reduction in NB concentration, with the starting chain end containing primarily alternating segments and the finishing end being hyperbranched polyethylene segments. Through two-stage or three-stage "living" copolymerization with sequential NB feeding, diblock or triblock copolymers containing gradient block(s) have been designed. This work thus greatly expands the family of E–NB copolymers. All the copolymers have

controllable molecular weight and relatively low polydispersity (with polydispersity index below 1.20). Most notably, some of the gradient and block-gradient copolymers have been found to exhibit the characteristic broad glass transitions as a result of their possession of broad composition distribution.

2.1 Introduction

Describing the distribution of different repeat units within a chain, the composition distribution of copolymers is an important chain parameter intrinsically governing the physical properties of the copolymers and their end applications. Its design and control have been one of the key themes in modern polymer chemistry. Random, alternating, block, and graft are the classical composition distributions often found in conventional copolymers, and their synthesis has been extensively studied with the use of various polymerization techniques.[1] In particular, the tremendous advancements in "living"/controlled polymerization techniques, most notably controlled radical polymerization techniques, in the past two decades have further enabled the precision synthesis of well-defined, narrow-distributed copolymers having these classical composition distributions.[2] Meanwhile, novel copolymers having new composition distributions have also been made possible with the use of these advanced polymerization techniques. The synthesis of gradient copolymers (also known as tapered copolymers) is the most prominent example.[3] While random/alternating copolymers have no gradient in composition (or average composition) in a chain and block copolymers have an abrupt change in composition at the block joint location, gradient copolymers show a gradual continuous change in composition from one to the other

chain end. Gradient copolymers cover a material space between random/alternating and block copolymers, with some unique properties (e.g., extremely broad glass transition temperature range) and featured applications (e.g., damping materials) demonstrated.[4] In addition, some hybrid composition distributions, such as block-gradient and graft-gradient copolymers where a block or graft contains gradient composition, have also been successfully synthesized.[3]

Ethylene–norbornene (E–NB) copolymers synthesized through metal-catalyzed copolymerization are an important class of high-performance ethylene copolymers with many remarkable properties, such as high transparency, high glass transition temperature, good heat resistance, and high refractive index.[5] Their synthesis and control of composition distribution have been extensively studied since the first report of E-NB copolymerization with zirconocene catalysts by Kaminsky et al. in 1991.[6] In this copolymerization system, the transition metal catalysts play the key role in determining the copolymer composition distribution and polymerization behavior. A large number of high-performance catalysts based on both early and late transition metals have been investigated for the copolymerization.[5] However, there are only a few well-behaved catalysts that can facilitate the desired "living" or quasi-living copolymerization for synthesis of E–NB copolymers of controlled composition distribution and molecular weight while at narrow molecular weight distribution.[7] These "living" catalysts and their enabled copolymer composition distributions are briefly summarized as follows.

Though Cherdron et al. had briefly noted "living" E–NB copolymerization as early as in 1994,[8] the first detailed investigation was reported by Tritto et al. in 2001 with the use of three *ansa*-zirconocene catalysts at 30 ℃ and at high NB/E feed ratios (12.5–28.4).[9] The copolymers possessed relatively narrow molecular weight distribution (polydispersity index, PDI, in the range of 1.16–1.50), with a significant increase of number-average molecular weight (M_n) for up to one hour. Similar quasi-living behavior was also noted later on with a constrained geometry catalyst ($Me_2Si(Me_4Cp)(N^tBu)TiCl_2$)[10] and its analogue ($Me_2SiFlu(N^tBu)TiMe_2$)[11] by Tritto et al., and Shiono et al., respectively. Subsequently, Fujita et al. demonstrated in 2002 high-performance "living" E–NB alternating copolymerization with bis(pyrrolide-imine)titanium catalysts at 25 ℃.[12] Narrow-distributed E–NB alternating copolymers and diblock copolymers were successfully synthesized therein with controllable molecular weight. With bis(enaminoketonato)titanium catalysts, Li et al.[13] synthesized high-molecular-weight narrow-distributed copolymers containing primary alternating and isolated NB units and polyethylene-*b*-poly(E-*co*-NB) diblock copolymers. Using (arylimido)(aryloxo)vanadium/Et_2AlCl catalyst systems, Nomura and Wang obtained ultrahigh-molecular-weight copolymers containing primarily isolated and alternating NB units.[14] With a "living" fluorinated-bis(phenoxyimine) titanium catalyst, Coates et al. synthesized a E–NB copolymer containing random NB units and a high-molecular-weight poly(E-*co*-propylene)-*b*-poly(E-*co*-NB) diblock copolymer for application as self-assembled photonic band gap materials.[15] In addition, Fujita et al. also showed the synthesis of narrow-distributed copolymers containing primarily alternating NB units by

"living" E–NB copolymerization with nonfluorinated bis(phenoxyimine) titanium catalysts at 25 ℃.[16]

Besides early transition metal catalysts, a class of high-performance neutral α-iminocarboxamidato Ni catalysts (via activation with bis(1,5-octadiene)Ni) has also been developed by Bazan et al. for catalyzing quasi-living copolymerization of ethylene and functionalized NB comonomers.[17] A series of narrow-distributed copolymers having various composition distributions has been obtained, including tapered, pseudo-diblock, pseudo-tetrablock, triblock, and pentablock copolymers. Containing both semicrystalline and amorphous blocks, the block copolymers synthesized in their works have been shown to possess self-assembled morphology and some remarkable mechanical properties.[17] In addition, Kaminsky et al.[18] reported E–NB copolymerization with Pd–diimine catalysts at 30 °C having various ligand sterics. These catalysts show significantly higher ability for NB incorporation compared to metallocene catalysts based on early transition metals. Though overall NB content data in the copolymers were determined, the copolymer composition distribution was not elucidated in their study and the copolymers likely contained complex mixed composition distributions. "Living" feature of the copolymerization was not demonstrated therein. The synthesis of narrow-distributed copolymers of various controllable composition distributions has not yet been presented with this series of late transition metal catalysts.

Further to but different from all above studies, the versatile synthesis of a broad class of E–NB copolymers having various composition distributions through one-pot

"living" copolymerization is reported in this Chapter with a single Pd–diimine catalyst, $[(ArN=C(Me)–(Me)C=NAr)Pd(CH_3)(N\equiv CMe)]^+SbF_6^-$ (Ar = 2,6–(iPr)$_2$C$_6$H$_3$) (**1**). Previously shown to enable "living" ethylene homopolymerization (at temperature below or around 15 °C),[19,20] this catalyst is also demonstrated herein to show remarkable "living" characteristics in E–NB copolymerization in addition to high capability of NB incorporation. These features facilitate the convenient design of copolymers of different composition distributions by simply adjusting the polymerization parameters, such as NB feed concentration, stagewise polymerization, and sequential addition of NB. The composition distributions achieved herein include alternating, gradient, diblock, triblock, and block-gradient structures, whose synthesis greatly expands the family of E-NB copolymers.

2.2 Experimental Section

2.2.1 Materials

The Pd–diimine catalyst, $[(ArN=C(Me)–(Me)C=NAr)Pd(CH_3)(N\equiv CMe)]^+SbF_6^-$ (Ar = 2,6–(iPr)$_2$C$_6$H$_3$) (**1**), was synthesized by following a literature procedure.[21] Its synthesis and manipulations were all carried out in a N_2-filled glove box or using Schlenk technique. Ultra-high-purity N_2 (> 99.97%) and polymer-grade ethylene (both from Praxair) were purified by passing through a 3Å/5Å molecular sieve column and an Oxiclear column in series to remove moisture and oxygen, respectively, before use. Chlorobenzene (99.5%, Aldrich) was deoxygenated and dried using a solvent

purification system (Innovative Technology) before use. Norbornene (99%) was obtained from Aldrich and was used as received. Other solvents, including methanol (> 99%), tetrahydrofuran (THF, HPLC grade, > 99%), toluene (HPLC grade), etc., were obtained from Fisher Scientific and were used as received.

2.2.2 General Procedure for E-NB Copolymerizations

All copolymerizations were carried out in a 500 mL jacketed glass reactor equipped with a magnetic stirrer and a refrigerating circulator. Prior to the polymerization, the oven-dried reactor was sealed with a rubber septum, and was immediately vacuumed and purged with ethylene for several cycles. It was then filled with ethylene at 1 atm (absolute pressure). The reactor temperature was set at 15 °C by passing water through the jacket using the circulator. Anhydrous chlorobenzene and a prescribed amount of NB dissolved in chlorobenzene (total chlorobenzene volume: 40 mL) were then injected into the reactor. After thermal equilibrium for about 10 min, catalyst **1** (80 mg, 0.1 mmol) dissolved in 10 mL chlorobenzene was injected to start the polymerization. During the polymerization, ethylene pressure was maintained at 1 atm by continuous feed from a cylinder. The polymerization temperature was controlled constant with the circulator. A prescribed amount of the polymerization solution was sampled periodically (generally, every hour) to monitor polymer growth. In the case of two-stage or three-stage copolymerization runs involving sequential NB addition, a prescribed volume of the polymerization solution was sampled followed with the addition of the desired amount of NB dissolved in the same volume of chlorobenzene.

At the end of polymerization, ethylene pressure was released and the reactor was emptied.

The polymer in each sampled polymerization solution was precipitated out using 2%-acidified methanol. To remove Pd black resulting from the deactivated catalyst, the polymer product was redissolved in THF, followed with the addition of H_2O_2 solution (50 wt%, ca. 0.5 mL) under stirring. After ca. 1 h, the polymer was precipitated in a methanol, and was further washed with methanol for several times. Finally, the polymer sample was dried under vacuum at ca. 70 °C overnight, weighed, and subsequently characterized.

2.2.3 Characterizations and Measurements

^{13}C nuclear magnetic resonance (NMR) spectra of the polymers were all obtained on a Bruker AV500 spectrometer (125 MHz) at ambient temperature with $CDCl_3$ as the solvent. Polymer characterization with gel permeation chromatography (GPC) was carried out on a Polymer Laboratories PL-GPC220 system equipped with a differential refractive index (DRI) detector (from Polymer Laboratories) and a three-angle light scattering (LS) detector (high-temperature miniDAWN from Wyatt Technology). The detection angles of the light scattering detector were 45, 90, and 135°, and the laser wavelength was 687 nm. One guard column (PL# 1110-1120) and three 30 cm columns (PLgel 10 μm MIXED-B 300 × 7.5 mm) were used. This GPC system has

been used extensively in our earlier works [20,22] for polymer characterization and a similar methodology is used herein.

Except the polymers synthesized in runs 1 and 2 (see Table 2.1) that could not dissolve well in THF due to high overall NB content, HPLC-grade THF was used as the mobile phase at a flow rate of 1 mL/min for the characterization of all polymers. For those synthesized in runs 1 and 2, HPLC-grade toluene was used instead at 1 mL/min since they could dissolve completely in toluene at room temperature. The complete GPC system, including columns and detectors, was maintained at 33 °C. The mass of the polymers injected into the columns varied with polymer molecular weight; typically 200 μL of 4–7 mg/mL solution was injected. Astra software from Wyatt Technology was used for data collection and analysis. Two narrow polystyrene standards (from Pressure Chemicals) with weight-average molecular weight (M_w) of 30 and 200 kg/mol were used for the normalization of light scattering signals at the three angles, and the determination of inter-detector delay volume and band broadening, respectively. The DRI increment dn/dc value of 0.078 mL/g was used for all hyperbranched polyethylene homopolymers,[20,22] The dn/dc values of all E–NB copolymers were determined on-line from their injected mass data by assuming complete polymer recovery. The dn/dc value of 0.185 mL/g was used for polystyrene. With this characterization methodology, the two polystyrene standards were measured to have a typical M_w value of 30.1 and 201.3 kg/mol, respectively, with a polydispersity index (PDI) of 1.00 for both, which are in good agreement with the data provided from the supplier.

Thermal characterization of the polymers with differential scanning calorimetry (DSC) was carried out on a TA Instruments Q100 DSC equipped with a refrigerated cooling system (RCS) under N_2 atmosphere. The instrument was operated in the standard DSC mode and was calibrated with an indium standard. A N_2 purging flow of 50 mL/min was used. In a typical run, the polymer sample (ca. 5 mg) was heated from room temperature to 200 °C at 10 °C/min and cooled down to –90 °C at 5 °C /min, and the data were collected on a subsequent heating ramp from –90 °C to 200 °C at 10 °C/min. In a typical thermogram, glass transition temperature (T_g) was read as the peak-maximum temperature of the glass transition peak in the 1st-derivative heat flow curve and the width of glass transition (ΔT_g) was read as the difference between the peak onset temperature and peak end temperature of the transition peak in the derivative heat flow curve. Melting temperature (T_m) was read as the peak-maximum temperature of the melting endotherm in the heat flow curve.

2.3 Results and Discussion

2.3.1 Alternating and Gradient E–NB Copolymers by Single-Stage "Living" Copolymerization

Our group has previously shown that **1** facilitates successfully "living" ethylene homopolymerization at various ethylene pressures (1–30 atm) as long as the polymerization temperature is sufficiently low (ca. 15 °C or lower). Though not fulfilling strictly the linear growth required for a perfect living polymerization due to

minor catalyst deactivation, the M_n data in the polymerization increase continuously over time but at a decaying rate within a period of 6 h.[20] Herein, a similar "living" behavior is found in the case of E-NB copolymerization with **1** at 15 °C under different NB feed concentrations ($[NB]_0$). Meanwhile, a range of low-polydispersity copolymers of alternating or gradient composition distribution can be synthesized by controlling $[NB]_0$ (see Scheme 2.1).

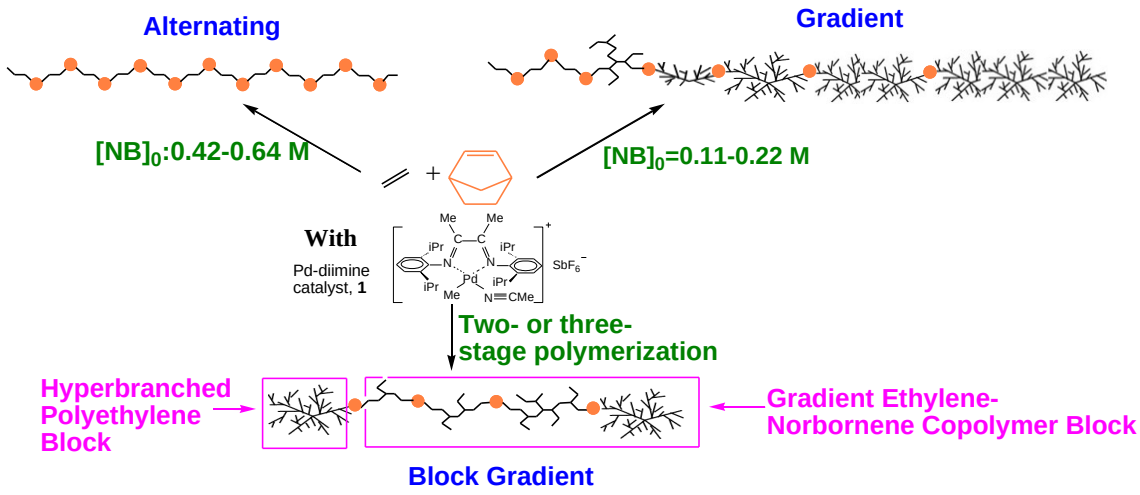

Scheme 2.1 E–NB alternating, gradient, block, and block-gradient copolymers by "living" E–NB copolymerization with **1**.

Four single-stage E-NB copolymerizations (runs 1–4 in Table 2.1) were carried out with **1** at different $[NB]_0$ (0.64–0.11 M) at 15 °C and ethylene pressure of 1 atm. In these single-stage runs, NB was fed at the beginning of the polymerization while ethylene pressure was maintained at 1 atm throughout the polymerization. In each run, polymer solution was sampled every hour. Each resulting copolymer was characterized with GPC incorporating on-line DRI and LS detectors for molecular weight

development, and with ^{13}C NMR for chain microstructures and overall NB molar fraction ($F_{NB,0}$). For the purpose of comparison, a "living" ethylene homopolymerization run (run 5) was also conducted as a control run. Table 2.1 summarizes these single-stage polymerizations and polymer characterization results.

GPC characterization of the polymers was performed with either THF or toluene as the eluting phase at 33 °C. The dn/dc values of these polymers, which were critical for molecular weight quantification with LS detector, were calculated using an online method from the mass of the injected polymer and the integration of the DRI peak. All the polymers synthesized in runs 3–5 were soluble in both THF and toluene at room temperature due to zero or low $F_{NB,0}$ values, which are to be shown below. However, their dn/dc values in toluene are very small (close to 0), rendering weak LS and DRI signals and in turn inaccurate molecular weight data in toluene. Their GPC characterization was thus carried out in THF. Differently, the copolymers synthesized in runs 1 and 2 at higher $[NB]_0$ (0.64 and 0.42 M, respectively) were characterized in toluene since they had complete solubility only in toluene at room temperature and their dn/dc values in toluene were high enough (0.056 mL/g) for accurate quantification due to higher $F_{NB,0}$

Figure 2.1 shows the evolution of GPC elution curves (recorded from the DRI detector) in each run. Like the control run, the elution peaks in each set of copolymers move progressively towards left (i.e., reduced elution time) with the increase of polymerization time, but with increasingly pronounced low-molecular-weight tails.

Table 2.1 Single-stage "living" copolymerizations of ethylene and norbornene (NB) at different NB feed concentrations[a]

Run	$[NB]_0$[b] (M)	Time (h)	Product[c] (kg/mol Pd h)	NMR characterization[d]		GPC characterization[e]				Thermal transitions[f]	
				$F_{NB,0}$	Alternat. NB (%)	dn/dc (mL/g)	M_n (kDa)	M_w (kDa)	PDI	T_g and width (ΔT_g in bracket) (°C)	T_m (°C) & ΔH_m (J/g, in bracket)
1	0.64	1	7.1	0.45	94	0.056	12	15	1.20	116 (16)	
		2	4.6	0.46	94		19	21	1.12	118 (17)	
		3	3.6	0.45	94		21	23	1.10	115 (20)	
		4	3.0	0.46	94		24	26	1.09	110 (22)	
		5	4.5	0.51	94		23	26	1.13	117 (19)	
		6	2.7	0.49	93		26	30	1.15	122 (16)	
2	0.42	1	7.5	0.46	93	0.056	13	16	1.18	106 (19)	
		2	4.9	0.44	92		18	20	1.11	115 (13)	
		3	4.0	0.45	93		21	23	1.10	114 (15)	
		4	3.5	0.44	92		24	26	1.09	108 (16)	
		5	2.7	0.44	93		26	28	1.10	115 (12)	
		6	3.5	0.45	94		30	34	1.16	109 (19)	
3	0.22	1	9.7	0.38	78	0.136	13	14	1.03	101 (37)	
		2	6.6	0.27	65	0.135	19	19	1.05	68 (34)	
		3	4.3	0.22	63	0.126	22	23	1.04	48 (119)	
		4	5.2	0.17	64	0.119	23	25	1.10	–56 (24); 74 (59)	–25 (0.5)
		5	3.8	0.15	65	0.114	27	29	1.09	–56 (22); 74 (47)	–25 (2)
		6	4.4	0.12	65	0.110	30	34	1.13	–60 (19); 77 (35)	–28 (3)
4	0.11	1	6.9	0.19	57	0.116	12	12	1.01	13 (52)	
		2	4.3	0.09	55	0.104	20	21	1.04	–63 (18)	–29 (8)
		3	6.3	0.06	54	0.096	27	29	1.06	–61 (16)	–28 (6)
		4	6.0	0.05	54	0.093	32	34	1.06	–62 (16)	–29 (8)
		5	5.3	0.04	55	0.091	36	39	1.09	–64 (15)	–30 (8)
		6	4.4	0.04	56	0.089	41	44	1.09	–64 (15)	–31 (10)
5	0	1	11.4	0	N/A	0.078	15	15	1.01	–68 (15)	–32 (17)
		2	13.7				25	26	1.03	–67 (13)	–31 (15)
		3	11.1				38	41	1.08		
		4	9.1				44	49	1.12	–65 (16)	–26 (17)
		5	9.2				47	54	1.16		
		6	8.2				55	62	1.12	–70 (15)	–28 (19)

[a] Other conditions: Pd catalyst, 0.1 mmol; solvent, chlorobenzene (50 mL); ethylene pressure, 1 atm; temperature, 15 °C.

[b] NB feed concentration.

[c] Polymer productivity.

[d] Overall NB molar fraction ($F_{NB,0}$) and the percentage of alternating units among all incorporated NB units in the copolymers were determined from ^{13}C NMR spectra.

[e] Triple-detection GPC were carried out with THF (runs 3–5 polymers) or toluene (runs 1 and 2 polymers) as eluent at 33 °C. M_n, M_w, and PDI were determined with light scattering detector. Polymer dn/dc values were determined on-line from the mass of polymer injected.

[f] Thermal transitions were determined with differential scanning calorimetry (DSC).

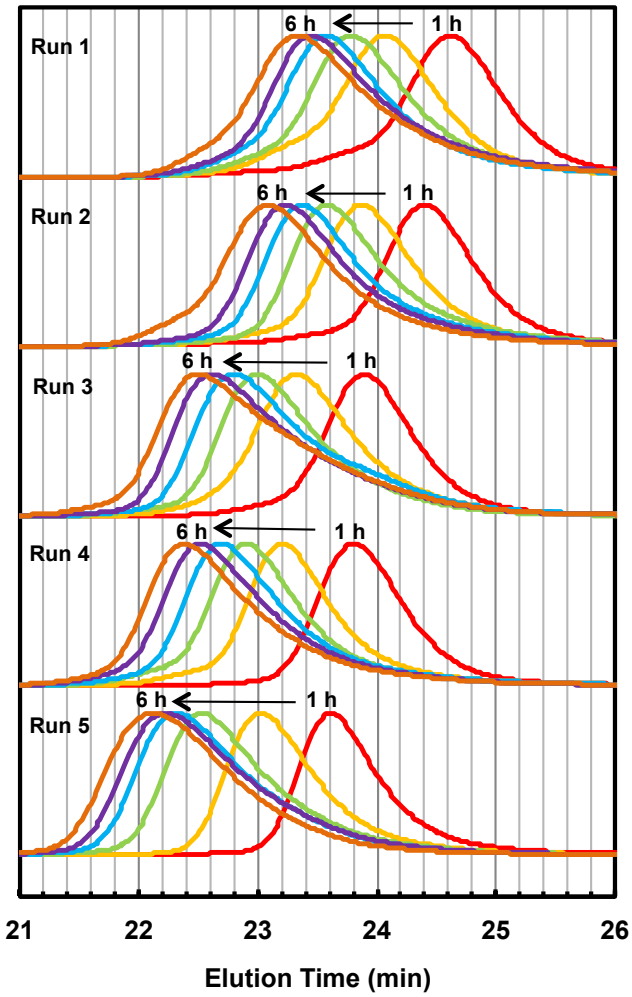

Figure 2.1 GPC elution curves (recorded from DRI detector) of the polymers synthesized in single-stage polymerizations (runs 1–5, see Table 2.1) at different NB feed concentrations (0.64–0 M). GPC measurement condition: toluene (for runs 1 and 2) or THF (for runs 3–5) as the eluting phase at 1 mL/min and 33 °C.

In Figure 2.2, the dependencies of M_n on the polymerization time are plotted for the five runs. Generally, the M_n value increases over time but at a gradually reduced rate in each run. This trend becomes more pronounced with the increasing $[NB]_0$. Meanwhile, by comparing the five runs, the M_n value at any given time tends to decrease with the

increase of $[NB]_0$. These indicate that the incorporation of NB slows down the chain growth. Nevertheless, the PDI values of the polymers are maintained low, generally in the range of 1.01–1.20 with slight increase over time in each run. The increasing M_n and relatively low PDI data confirm that the E–NB copolymerizations are typically "living" but with the presence of increasingly pronounced chain termination due to catalyst deactivation with the increasing $[NB]_0$ value.

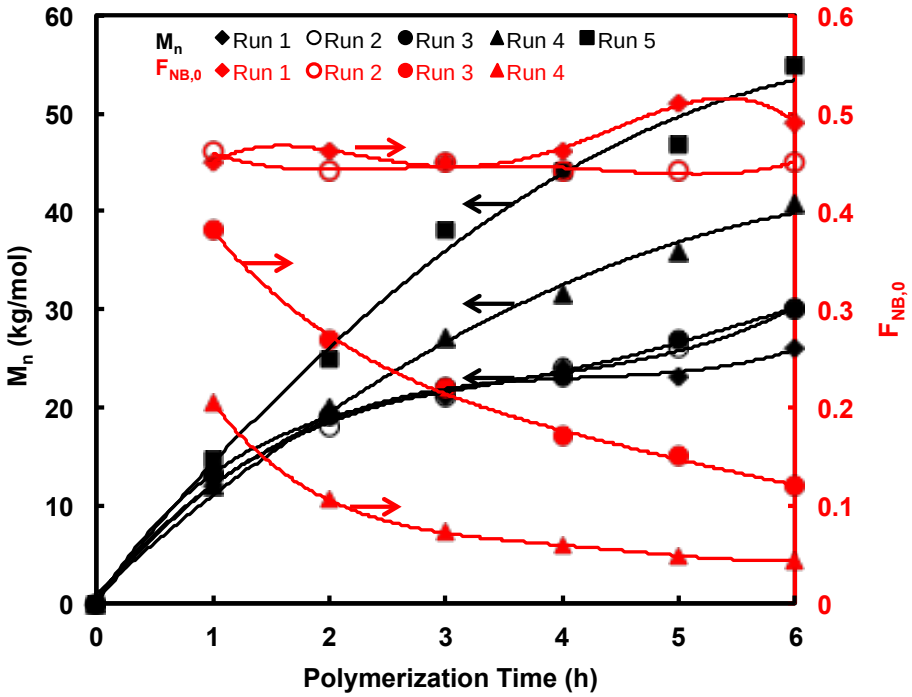

Figure 2.2 Dependences of M_n and overall NB content ($F_{NB,0}$) on polymerization time in runs 1–5 (see Table 2.1). Fitting lines are plotted for the purpose of guiding eyes.

Figure 2.3 displays ^{13}C NMR spectra of some selected polymers from runs 1–3, along with peak assignment and identified microstructures. Additional spectra for copolymers synthesized in run 4 are presented in Figure S2.1 in Supporting Information.

As extensively studied in our previous works, the polyethylene (PE) homopolymers synthesized in run 5 should possess hyperbranched topology with numerous complex branch-on-branch structures due to catalyst chain walking.[23-25] For the purpose of comparison, the spectrum of a representative PE homopolymer (2 h polymerization time) is included in Figure 2.3 (Figure 2.3f) and the signals arising from various short branches (methyl to hexyl and longer) are assigned as per literature reports.[23-25]

It is interesting to find that all the copolymers synthesized in runs 1 and 2 have nearly identical spectra (representatively, see Figure 2.3a,b) despite the different polymerization time (in turn, different molecular weight) and $[NB]_0$ in the two runs. This indicates their virtually very similar chain microstructure, NB content, and copolymer composition distribution. By comparison with the chemical shifts reported in the literature,[5a,12b,26] these copolymers contain primarily alternating E-NB units (ca. 94%, see Table 2.1) with a very small quantity of isolated NB units (ca. 6%) but virtually with no NB diads/triads/blocks. The NMR peaks confirming this structural feature have been labeled in Figure 2.3a. The peaks at 47.4 and 46.8 ppm are assigned to the C2 and C3 carbons (see the microstructures drawn in Figure 2.1a for the definition of the carbons) in the alternating isotactic and alternating syndiotactic units, respectively. The peak at 46.7 ppm is for the C2 and C3 carbons in the isolated NB units and it is generally very weak in the copolymers in runs 1 and 2. The peaks at 41.4 and 40.9 ppm are attributed to the C1 and C4 carbons in the alternating isotactic units and in the alternating syndiotactic & isolated units, respectively. The peak at 32.8 ppm should derive from the C7 carbon of NB units, whose sole presence at this chemical shift indicates the

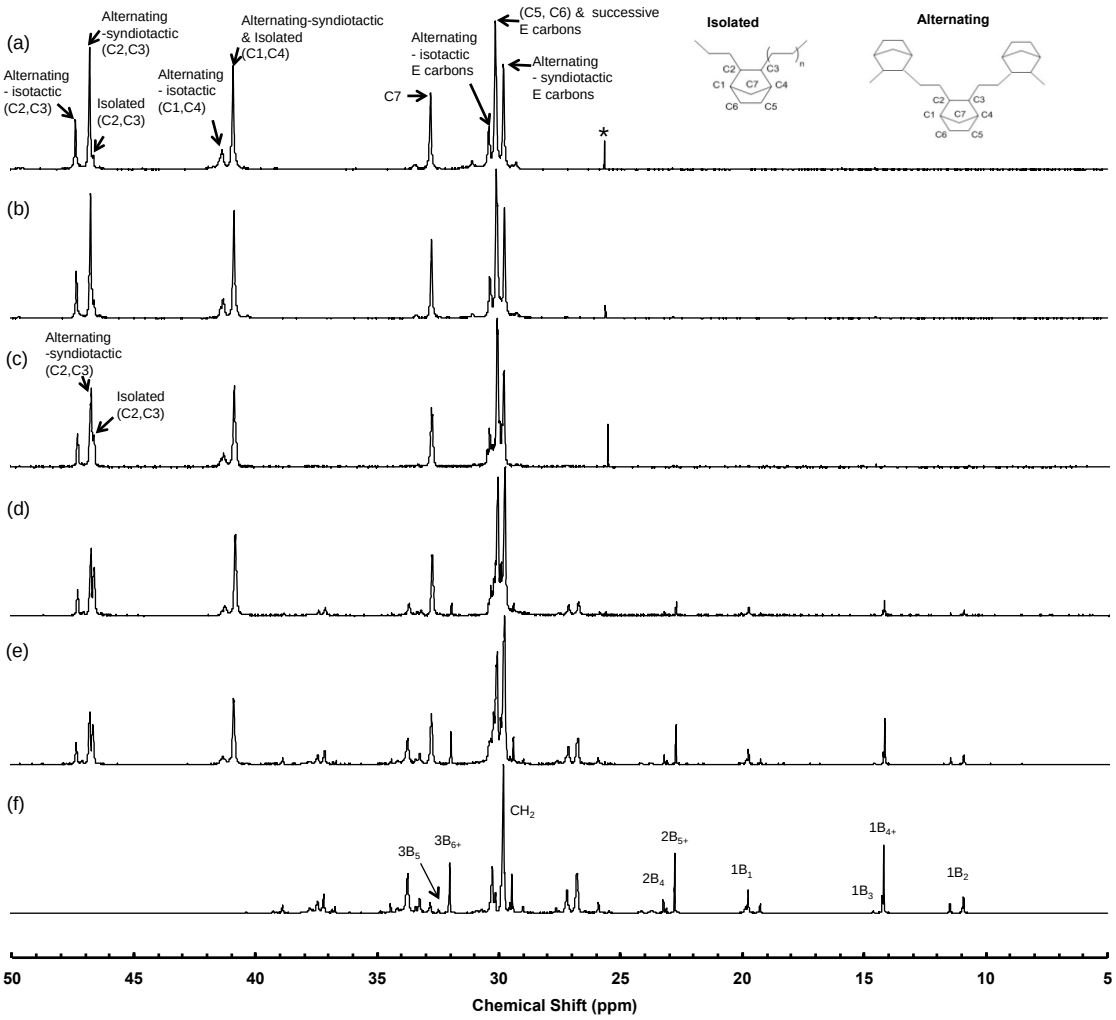

Figure 2.3 ^{13}C NMR (125 MHz) spectra of some selected polymers obtained in single-stage polymerizations: (a) run 1, 2 h (polymerization time) polymer; (b) run 2, 2 h polymer; (c) run 3, 1 h polymer; (d) run 3, 3 h polymer; (e) run 3, 5 h polymer; and (f) run 5, 2 h hyperbranched PE. D-chloroform was used as the solvent. The signal marked with an asterisk (*) arises from trace residual THF.

exclusive *exo-exo* enchainment of the NB units. Additionally, the peaks at 30.4 and 29.8 ppm are the ethylene carbons in the alternating isotactic and alternating syndiotactic units, respectively. The peak at 30.2 ppm is assigned to C5 and C6 carbons in the NB

units and carbons in the successive ethylene units. All these assignments match well with the literature reports.[5a,12b,26]

These NMR results indicate that catalyst **1** has a high tendency to form alternating E-NB copolymers. Meanwhile, the isotactic and syndiotactic units have a ratio of about 33/67 on the basis of their relative peak intensities, indicating that the catalyst has a certain level of tacticity control with syndiotactic units enriched most possibly through chain end control mechanism. This differs from the random tacticity with a syndiotactic/isotactic ratio of 48/52 achieved with bis(pyrrolide-imine)titanium catalysts by Fujita et al. in "living" alternating E–NB copolymerization.[12b] In addition, no branching structures in the ethylene sequences are observed in these copolymers, confirming the absence of catalyst chain walking during the alternating copolymerization. The $F_{NB,0}$ value of each copolymer synthesized in these two runs has been calculated from their ^{13}C NMR spectra according to literature methods[18] and it is generally fixed at about 0.45 with only small negligible variations among the two sets of copolymers (see Figure 2.2). These narrow-distributed copolymers thus possess uniform, predominant alternating E-NB units along the whole chain and their molecular weight can be controlled by changing the polymerization time.

Different from runs 1 and 2, evolving NMR spectra (see Figure 2.3c–e for run 3 and Figure S2.1 for run 4), with decreasing $F_{NB,0}$, are observed with the increase of polymerization time in runs 3 and 4 performed at lower $[NB]_0$ (0.22 and 0.11 M, respectively). Comparing Figure 2.3c–e for run 3 polymers, the peaks attributed to the

alternating E-NB units and isolated NB units are the sole ones in the 1 h polymer with no signals corresponding to hyperbranched PE segments; subsequently, peaks attributed to hyperbranched PE segments appear in the 3 h polymer and their relative intensities gradually increase over time (e.g., see Figure 2.5e for 5 h polymer). Similar trend is also observed in the spectra for run 4 polymers though at lower $F_{NB,0}$ data. Quantification of the NMR spectra indicates that alternating units are still the primary NB structure (75%) in the 1 h polymer in run 3 but with more isolated NB units (25%) compared to those in runs 1 and 2. With the increase of polymerization time, the percentage of isolated NB units is enhanced from 25% at 1 h to 35% at 6 h. Meanwhile, $F_{NB,0}$ decreases in run 3 from 0.38 at 1 h to 0.12 at 6 h (see Figure 2.2). The $F_{NB,0}$ values in run 4 polymers are generally lower than those in run 3 due to a lower $[NB]_0$. With the increase of time from 1 to 6 h, $F_{NB,0}$ also decreases from 0.19 to 0.04. However, the percentage of isolated NB units in run 4 stays at around 46% with only negligible variations from 1 to 6 h.

The decreasing $F_{NB,0}$ over time in runs 3 and 4, accompanied by the parallel "living" increase of M_n, confirms the presence of gradient NB composition along the polymer chain due to the gradual reduction of NB concentration during the chain growth. In particular, the starting end of the polymer chain should be featured mainly with alternating E–NB units given the observation of their NMR peaks in the 1 h samples in both runs. When NB concentration is reduced to a threshold value, subsequent NB incorporation should occur primarily in the form of isolated NB units segregated between hyperbranched PE segments and the NB content should accordingly decrease following the gradual reduction in NB concentration. We estimate that the threshold NB

concentration should be slightly below the $[NB]_0$ value (i.e., 0.11 M) in run 4, since alternating units are observed in the beginning of run 4. Above this threshold concentration, NB is incorporated primarily as alternating units. This very low threshold NB concentration (with the corresponding [NB]/[E] ratio estimated to be around 1 herein) warranting alternating E–NB copolymerization is highly remarkable as high [NB]/[E] feed ratios are often required with most previously reported catalysts to achieve alternating copolymers. For example, a ratio of ca. 10 is needed to achieve alternating E-NB copolymerization with bis(pyrrolide-imine)titanium catalysts, which were claimed to have very high norbornene incorporation capability.[12b] In consistency with Kaminsky's reports,[18] these results herein also demonstrate the high capability of catalyst **1** in NB incorporation.

Given their very different $F_{NB,0}$ data, we reason that the gradient profile is different in the two sets of polymers synthesized in runs 3 and 4, respectively. In the run 3 polymers, the composition gradient should be relatively more persistent throughout the whole chain since $F_{NB,0}$ decreases continuously from 1 h (0.38) to 6 h (0.12). In run 4 polymers, the gradient profile should be featured primarily in the starting end of the chain (chain segments grown in the first 1 h) because $F_{NB,0}$ is quickly reduced from 0.19 at 1 h to 0.09 at 2 h. Extension of the polymerization time from 2 h to 6 h leads to only marginal changes in $F_{NB,0}$ (0.04 at 6 h). This indicates the predominant incorporation of ethylene units in the latter period (2–6 h) to form hyperbranched PE segments. Except the short gradient segment at the starting end, the majority of the chain in the 2 h to 6 h

polymers should thus be composed of hyperbranched PE sequences with few isolated NB units.

2.3.2 Thermal Properties of Alternating and Gradient E-NB Copolymers

DSC characterization was performed on copolymers obtained above in runs 1–4 to further elucidate their differences in composition distribution and meanwhile to investigate the effect of composition distribution on their thermal properties. Figure 2.4 shows the DSC heat flow curves of representative alternating copolymers synthesized in runs 1 and 2 (at 6 h of polymerization), as well as that of a corresponding hyperbranched PE hompolymer synthesized in run 5 (6 h). Because of their uniform composition distribution, the polymers in each set (runs 1, 2, and 5) have very similar heat flow curves despite at different molecular weights. Therefore, only a representative polymer is selected from each set in the figure. In the figure, the first derivatives of corresponding heat flow curves with respect to temperature are also included. Such derivatives of heat flow curves have often been applied to characterize complex thermal behaviors in polymer blends, block copolymers, and gradient copolymers for the more precise determination of the width of glass transition (ΔT_g).[4] In the analysis of the DSC curves, glass-transition temperature (T_g) is read as the peak-maximum temperature of the glass transition peak in the derivative curve and ΔT_g is calculated as the difference between the on-set point (T_0) and the end point (T_e) of the transition peak in the derivative curve (see Figure 2.4 for illustration). All the DSC results are summarized in Table 2.1. The hyperbranched PEs in run 5 have a glass transition with T_g = –68 °C and

ΔT_g = 13–16 °C, and a weak but broad melting endotherm centered at around –30 °C (T_m) with a melting enthalpy (ΔH_m) of about 17 J/g, in consistency with those reported in our previous studies.[25] Due to their possession of identical uniform composition distribution, all the alternating copolymers in runs 1 and 2 have similar T_g (at around 110 °C) and ΔT_g (12–20 °C, see the data listed in Table 2.1) despite their different molecular weights.

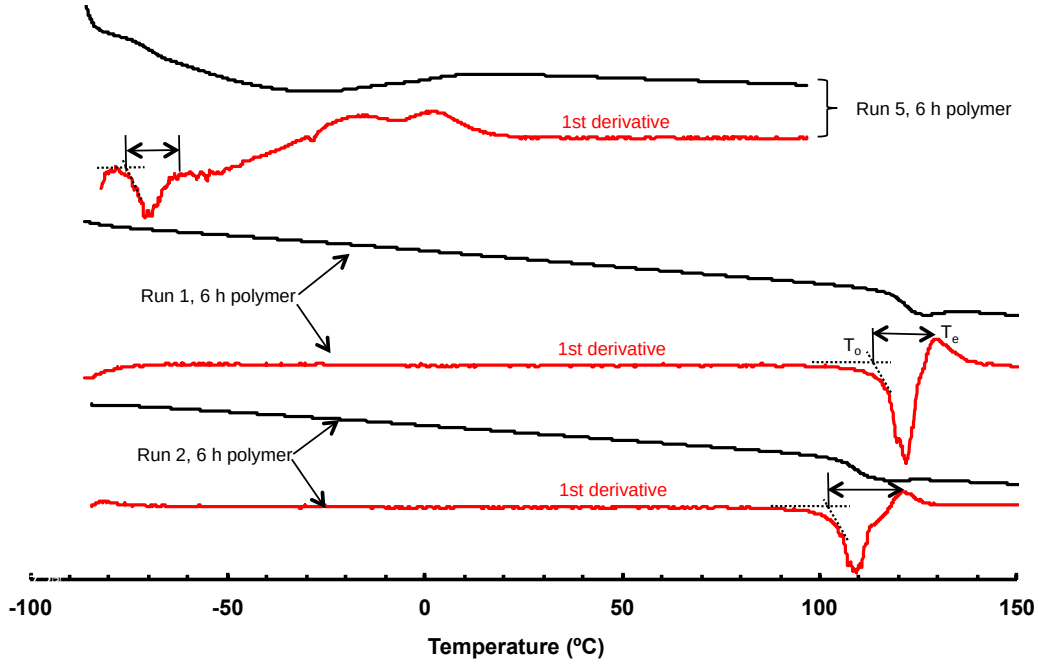

Figure 2.4 DSC heat flow curves (in black) and 1st derivatives (in red) of heat flow curves of the 6 h polymers synthesized in runs 1, 2, and 5, respectively. The heat flow curves were collected during a second heat ramp at 10 °C/min in DSC measurements. The width for each glass transition (ΔT_g) is illustrated with an arrow in each derivative curve.

The gradient copolymers synthesized in run 3, somehow, show dramatically evolving DSC curves with the increase of polymerization time due to the continuous reduction in NB content from the starting end (enriched with alternating units) to the finishing end (i.e., ethylene-rich end) of the chain. Figure 2.5 shows the DSC heat flow curves and their associated derivative curves for this set of polymers. For the 1 h to 3 h polymers, a single glass transition is observed without the occurrence of micro-phase separation, but with decreased T_g and significantly enhanced ΔT_g. The T_g value decreases from 101 °C (1 h) to 48 °C (3 h). The ΔT_g value increases substantially from 37 °C (1 h) to 119 °C (3 h), which are much greater than the typical value (12–20 °C) of the alternating copolymers in runs 1 and 2. The high ΔT_g values, indicative of very broad glass transition, prove solidly the gradient composition distribution featured in the copolymer.[4] While the high-temperature end of the broad glass transition corresponds to the starting end of the gradient polymer chain containing relatively higher NB content, the low-temperature end corresponds to the ethylene-rich finishing end. Meanwhile, the increase of ΔT_g from 1 to 3 h also confirms the elevated broadening of the NB content range covered with the gradient profile. In particular, the high ΔT_g value of 119 °C for the 3 h polymer (with the transition covering from –41 to 78 °C) is remarkably striking as it is even greater that the highest ΔT_g values of 80 °C reported in the literature for styrene/4-hydroxystyrene gradient copolymers.[4]

Further extension of the polymerization time to 4–6 h in run 3 leads to clear micro-phase separation with the appearance of two glass transitions (see Figure 2.5). In all three polymers, a glass transition corresponding to hyperbranched PE segments near

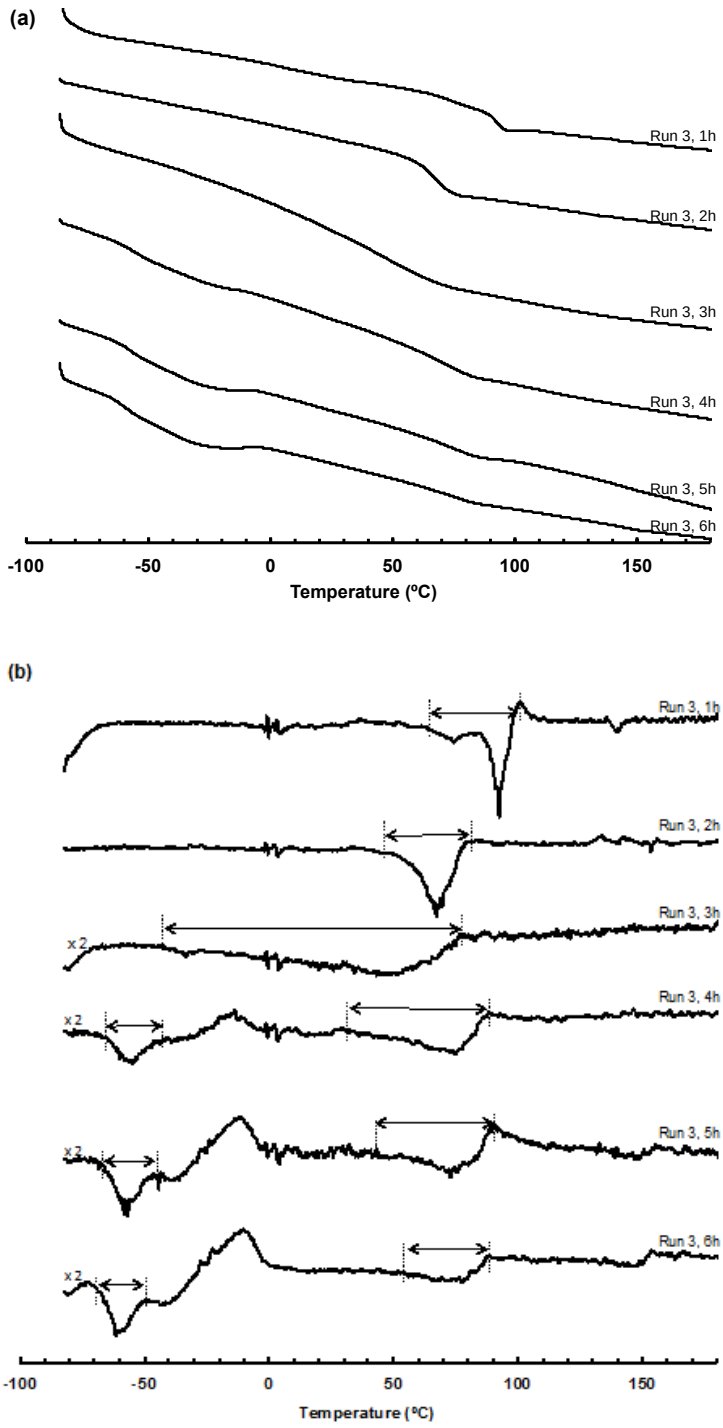

Figure 2.5 DSC heat flow curves (a) and derivatives of the heat flow curves (b) for the set of gradient copolymers synthesized in run 3. The heat flow curves were collected during the second heat ramp at 10 °C/min in DSC measurements. The width for each glass transition (ΔT_g) is illustrated with an arrow in the derivative curve.

the finishing chain end is clearly present at ca. –56 °C (ΔT_g at around 22 °C), along with a very weak accompanying melting endotherm centered at around –25 °C. With the increase of the polymerization time, ΔH_m, though small, shows a trend of gradual increase from 0.5 J/g at 4 h to 3 J/g at 6 h, indicating the increase in the mass content of hyperbranched PE segments. A relatively broad second glass transition is present at ca. 74–77 °C in all three copolymers and its ΔT_g shows a continuous reduction from 59 °C at 4 h to 35 °C at 6 h due to enhanced phase separation.[4] This transition should correspond to a pseudo gradient block containing significant average NB content at the beginning end. The presence of two glass transitions indicates that these gradient copolymers with the local NB content spanning over a broader range along the chain (from alternating units in the beginning to nearly pure hyperbranched PE sequences at the end) evolve to behave as pseudo-block copolymers constructed with chain blocks having very different average NB contents.

For the other set of gradient copolymers synthesized in run 4, a change in their DSC curves is only observed from the 1 h polymer to the 2 h polymer while the other polymers obtained from 2 h to 6 h have nearly identical DSC curves. Figure 2.6 shows the DSC heat flow curves and the associated derivative curves for the 1 h and 6 h copolymers in this run. The 1 h polymer has only a single glass transition at 11 °C with a relatively broad width (ΔT_g = 48 °C) resulting from the gradient structure. Differently, all the other polymers show only transitions attributed to the hyperbranched PE sequences (T_g = ca. –62 °C with ΔT_g = ca. 16 °C, T_m = –30 °C with ΔH_m = ca. 8 J/g). In consistency with their low $F_{NB,0}$ data, these polymers thus approach to behave like pure

hyperbranched PEs. Meanwhile, it agrees well with our previous reasoning that the gradient profile is primarily featured in the short starting end of the chain while the majority of the chain is comprised of hyperbranched PE segments with negligible NB units.

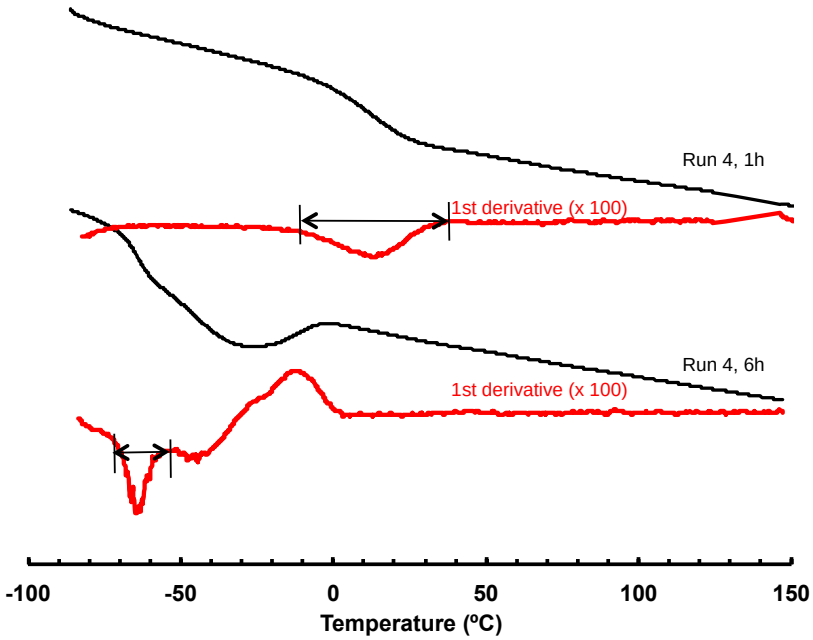

Figure 2.6 DSC heat flow curves (in black) and 1st derivatives (in red) of heat flow curves of the 1h and 6 h polymers synthesized in run 4. The heat flow curves were collected during a second heat ramp at 10 °C/min in DSC measurements. The width for each glass transition (ΔT_g) is illustrated with an arrow in each derivative curve.

2.3.3 Diblock/Block-Gradient Copolymers by Two-Stage "Living" Copolymerization

We have further extended this "living" polymerization protocol for two-stage E-NB copolymerizations, which consist of a first stage for ethylene homopolymerization

and a second stage for E-NB copolymerization. As a demonstration, two runs (runs 6 and 7 in Table 2.2) were carried out. In these two runs, the first ethylene homopolymerization was carried out at 15 °C under 1 atm for a prescribed time (t_1 = 1 h for run 6, and 2 h for run 7), followed with the addition of NB ($[NB]_0$ = 0.22 M for both runs) to start the second-stage copolymerization, which lasted 5 or 4 h for runs 6 and 7, respectively. This two-stage copolymerization is expected to give rise to block-gradient copolymers, with the first stage rendering a hyperbranched PE block and the second stage giving a E-NB copolymer block of gradient composition profile (see Scheme 2.1). In each run, the polymerization solution was sampled at the end of the first stage and every hour during the second stage. The resulting polymers were similarly characterized with GPC, NMR, and DSC. Table 2.2 summarizes the polymerization data and polymer characterization results.

Figure S2.2 in Supporting Information shows the GPC elution curves in both runs. Successful chain extension from the first hyperbranched PE block is achieved in both runs. With the increase of second-stage polymerization time (t_2), the elution curve in each run moves progressively towards reduced elution time though with the presence of increasingly pronounced tail at the high-elution-time end. The change of M_n as a function of t_2 is plotted in Figure 2.7. The hyperbranched PE block in the two runs has a M_n value of 11 and 21 kg/mol, respectively, and is narrow distributed with low PDI (around 1.01). Gradual increase of M_n of the resulting block copolymer is observed in the second stage in both runs. But like the singe-stage runs, the rate of increase slows down over time resulting from incremental catalyst deactivation. Nevertheless,

Table 2.2 Two-stage "living" copolymerizations consisting of 1st-stage ethylene "living" homopolymerization and second-stage "living" copolymerization of ethylene and norbornene (NB) [a]

Run	t_1 [b] (h)	t_2 & $[NB]_0$ [c]	Product[d] (kg/mol Pd h)	NMR Characterization[e]			GPC characterization (THF as eluent)[f]					Thermal transitions[g]	
				$F_{NB,0}$	$F_{NB,2}$	Alternat. NB (%)	dn/dc (mL/g)	M_n (kDa)	M_w (kDa)	PDI	$M_{n,2}$ (kDa)	T_g and width (ΔT_g in bracket) (°C)	T_m (°C) & ΔH_m (J/g, in bracket)
6	1	0	7.7	0	N/A	N/A	0.078	11	11	1.01	0	–68 (13)	–32 (16)
		1h;0.22M	6.2	0.12	0.25	71	0.110	27	28	1.04	16	–59 (22); 80 (36)	–25 (3)
		2h	5.4	0.15	0.27	67	0.115	34	36	1.05	23	–59 (21); 73 (44)	–26 (2)
		3h	5.2	0.15	0.24	64	0.115	39	42	1.07	28	–59 (19); 56 (57)	–27 (2)
		4h	3.9	0.14	0.21	62	0.111	43	47	1.10	32	–54 (23); 66 (30)	–22 (1)
		5h	4.5	0.12	0.18	64	0.108	47	53	1.14	36	–56 (22); 66 (30)	–22 (1)
7	2	0	7.5	0	N/A	N/A	0.078	21	21	1.02	0	–67 (14)	–31 (16)
		1h;0.22M	5.9	0.07	0.21	74	0.097	35	37	1.03	15	–65 (15)	–30 (8)
		2h	4.5	0.10	0.27	71	0.103	41	43	1.04	21	–63 (20); 78 (39)	–29 (6)
		3h	4.1	0.11	0.25	63	0.105	45	48	1.05	25	–63 (17); 65 (39)	–28 (4)
		4h	4.7	0.11	0.23	64	0.107	48	52	1.07	28	–60 (21); 66 (35)	–27 (4)

[a] Other conditions: Pd catalyst, 0.1 mmol; solvent, chlorobenzene (50 mL); ethylene pressure, 1 atm; temperature, 15 °C.

[b] t_1 is the time for 1st-stage ethylene polymerization.

[c] t_2 is the time for second-stage copolymerization and $[NB]_0$ is the NB feed concentration in the beginning of the second-stage polymerization. [d] Polymer productivity.

[e] NB molar fraction in the overall block copolymer ($F_{NB,0}$) and 2nd block ($F_{NB,2}$), and the percentage of alternating NB units among all incorporated NB units determined from ^{13}C NMR spectra.

[f] Triple-detection GPC were carried out with THF as eluent at 33 °C. M_n, M_w, and PDI were determined with light scattering detector. $M_{n,2}$, the size for the second block, was calculated from the M_n values of the diblock polymer and the first hyperbranched PE block. Polymer dn/dc values were determined on-line from the mass of polymer injected.

[g] Thermal transitions were determined with differential scanning calorimetry (DSC).

significant controllable sizes for the second block have been achieved in both runs, for example, 36 kg/mol at t_2 of 5 h for the second block in run 6. The molecular weight distribution of all block copolymers in both runs is relatively narrow with PDI in the range of 1.03–1.14. These molecular weight data thus confirm that both two-stage runs are "living".

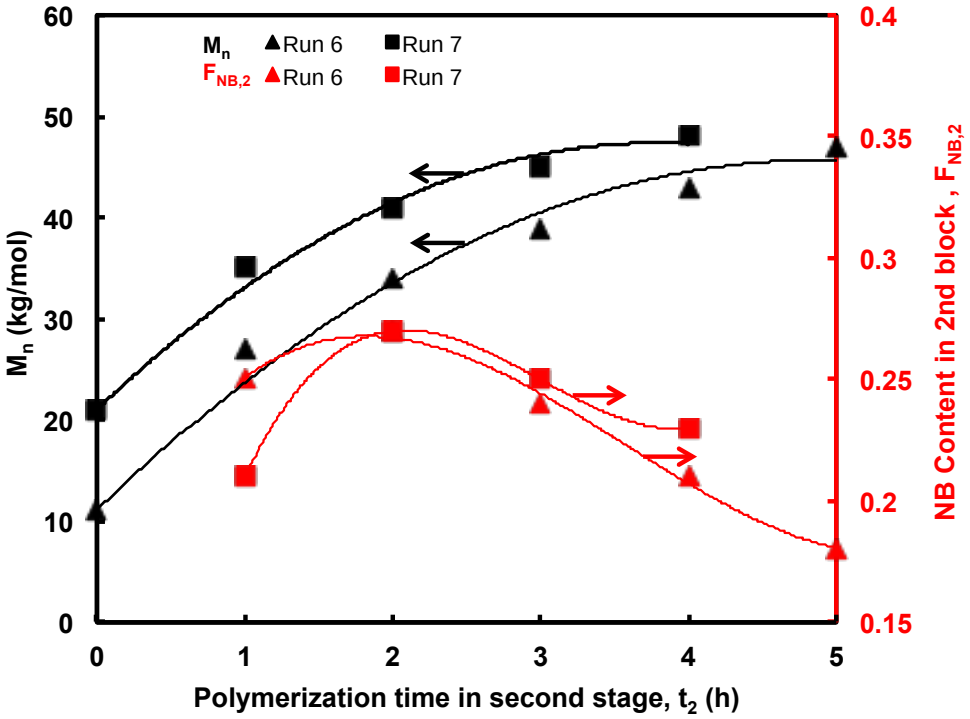

Figure 2.7 M_n of block polymer and NB molar fraction in the second block ($F_{NB,2}$) vs. polymerization time in the second stage (t_2) in the two-stage E-NB copolymerizations (runs 6 and 7 in Table 2.2). Fitting lines are plotted for the purpose of guiding eyes.

Figures S2.3 and S2.4 in Supporting Information display the ^{13}C NMR spectra of the two sets of polymers obtained in runs 6 and 7, respectively. As expected based on the results in the corresponding single-stage run 3 at the same $[NB]_0$, both alternating E-NB units and the isolated NB units are found in the second block of all block

copolymers from the signals in the region of 46–48 ppm. The percentage of alternating NB units among the total incorporated NB units decreases from 74% (at t_2 = 1 h) to 64% (at t_2 = 4 h) with the increase of t_2 in a similar pattern as in run 3. The $F_{NB,0}$ data of the block copolymers were directly calculated from their spectra (see Table 2.2). Since all NB units are incorporated in the second block, its molar fraction in the second block ($F_{NB,2}$) is of more significance. $F_{NB,2}$ is calculated by solving the following balance equation:

$$\frac{M_n F_{NB,0}}{F_{NB,0} M_{NB} + (1 - F_{NB,0}) M_E} = \frac{M_{n,2} F_{NB,2}}{F_{NB,2} M_{NB} + (1 - F_{NB,2}) M_E} \qquad (1)$$

where M_n and $M_{n,2}$ are the molecular weight data for the whole block copolymer and the second block, respectively, and M_{NB} and M_E are the molecular weight of NB and E, respectively. All the data are summarized in Table 2.2. The dependence of $F_{NB,2}$ on t_2 is also plotted in Figure 2.7 for both runs. Unlike the single-stage run 3 where NB content decreases monotonously over time, $F_{NB,2}$ somehow experiences an initial increase within the first 2 h (t_2), followed with continuous decrease afterwards in both runs. In run 6, $F_{NB,2}$ increases from 0.25 (at t_2 = 1 h) to 0.27 (at 2 h), and then decreases gradually to 0.18 (at 5 h). In run 7, the initial increase of $F_{NB,2}$ is even more significant, from 0.21 (at t_2 = 1 h) to 0.27 (at 2 h), but followed with the slower decrease to 0.23 (at 4 h). We reason that the initial increase of $F_{NB,2}$ results from mass diffusion issue in the reaction system since NB added at the end of the first stage has to diffuse through the surrounding hyperbranched PE macromolecular coil to reach the Pd active center for incorporation. The more significant initial increase of $F_{NB,2}$ in run 7 is an indirect evidence supporting this reasoning since the hyperbranched PE block in run 7 is much larger, in turn with enhanced resistance for the NB diffusion. In single stage runs, both E

and NB are well mixed with uniform concentration achieved before the polymerization starts, thus without rendering the initial increase of NB content.

From the trend of change for $F_{NB,2}$, the composition profile in the second block of the diblock polymers in runs 6 and 7 should be more complex compared to the monotonous gradient profile in run 3 polymers. Within the initial period of chain growth (t_2: 0–ca. 2 h), there should be a positive gradient profile with increasing NB content along the direction of chain growth due to the diffusion of NB for polymerization. After that, a negative gradient profile with decreasing NB content should evolve due to the continuous reduction in overall NB concentration. While the first positive gradient is diffusion-caused, the second negative gradient is primarily kinetics-driven.

Figure 2.8 shows the DSC heat flow curves and the associated derivative curves for the polymers synthesized in run 6. In the polymers obtained at t_2 = 1 and 2 h, a broad second glass transition (T_g = 73–80 °C, ΔT_g = 36–44 °C) corresponding to the polymer block of positive gradient composition is observed in addition to the one for the hyperbranched PE block. Because of the incorporation of the negative gradient segment, increasing t_2 to 3 h leads to the further broadening of the former transition to ΔT_g = 57 °C. Further extension of t_2 to 5 h narrows the transition back to ΔT_g = 30 °C. The T_g and ΔT_g values of the hyperbranched PE block are all slightly increased in the block polymers due to the influence from the NB-containing second block. DSC curves for the run 7 polymers are plotted in Figure S2.5 in Supporting Information. Similarly, a relatively broad glass transition corresponding to the E-NB copolymer block (T_g =

78–66 °C, ΔT_g = ca. 36 °C) can be observed in the block polymers obtained at t_2 from 2–4 h. But the changes in the thermal properties with increasing t_2 are less pronounced compared to those in run 6 since the block copolymers in this run have a bigger first PE block and relatively reduced variations of NB composition in the second block.

2.3.4 Triblock Copolymers by Three-Stage "Living" Copolymerization

A three-stage "living" copolymerization (run 8 in Table 2.3) was further carried out to synthesize E-NB triblock copolymers with increasing average NB content from the first to third block. The strategy of sequential feeding of NB was employed while under a fixed ethylene pressure of 1 atm at 15 °C. The first stage was conducted at $[NB]_0$ = 0.11 M (0.5 g NB charged in the beginning of polymerization) for 1 h (t_1). At the end of first stage, a second portion of NB (1 g) was charged (cumulative $[NB]_0$ = 0.31 M) and the second-stage also lasted for 1 h (t_2). The final portion of NB (1 g, giving cumulative $[NB]_0$ = 0.52 M) was added at the end of second stage and the third stage lasted for 4 h in total, with sample taken every hour (t_3). Table 2.3 summarizes the polymerization and polymer characterization results.

During the polymerization, the M_n value of the resulting copolymer increases continuously with the increase of the overall polymerization time (see Figure 2.9) while at maintained relatively low PDI (1.03–1.18, see Table 2.3). The first and second blocks have a M_n value of 12 and 8 kg/mol, respectively. The largest M_n value of the third block achieved in the run is 14 kg/mol at t_3 of 4 h (see Table 2.3), which is calculated by

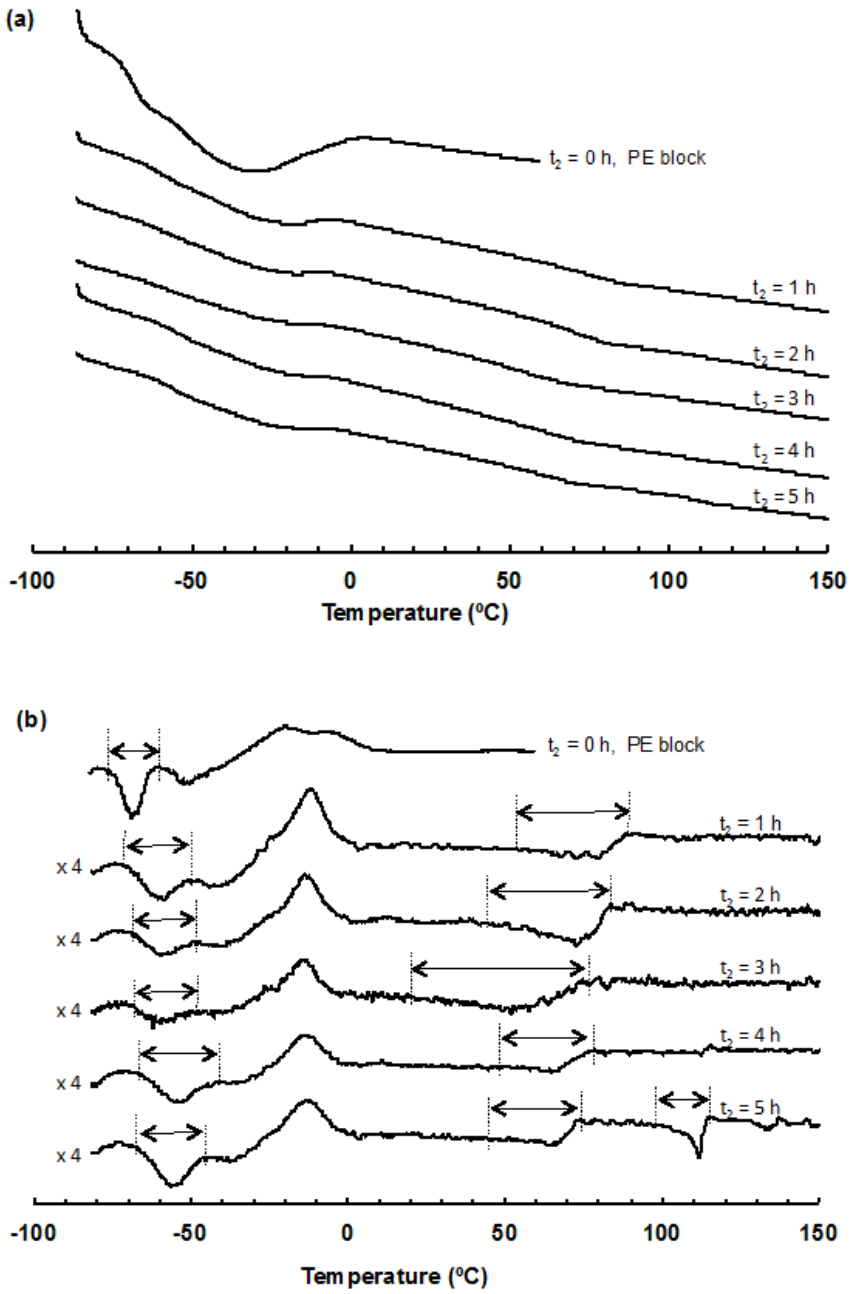

Figure 2.8 DSC heat flow curves (a) and derivatives of the heat flow curves (b) for the set of polymers synthesized in run 6 (see Table 2.2). The heat flow curves were collected during the second heat ramp at 10 °C/min in DSC measurements. The width for each glass transition (ΔT_g) is illustrated with an arrow in the derivative curve.

Table 2.3. Three-stage "living" copolymerization (run 8) of ethylene and norbornene (NB)[a]

t_1 & $[NB]_0$[b]	t_2 & $[NB]_0$[c]	t_3 & $[NB]_0$[d]	Product[e] (kg/mol Pd h)	NMR Characterization[f]					GPC characterization[g]						
				$F_{NB,0}$	$F_{NB,1}$	$F_{NB,2}$	$F_{NB,3}$	Alternat. NB (%)	dn/dc (mL/g)	M_n (kDa)	M_w (kDa)	PDI	$M_{n,1}$ (kDa)	$M_{n,2}$ (kDa)	$M_{n,3}$ (kDa)
1h;0.11 M	0h	0h		0.20	0.20	N/A	N/A	57	0.113	12	12	1.03	12	N/A	N/A
	1h;0.31 M	0h	5.7	0.25	0.20	0.34	N/A	65	0.125	20	21	1.05	12	8	N/A
		1h;0.52 M	3.5	0.26	0.20	0.34	0.29	69	0.127	27	29	1.08	12	8	7
		2h	3.1	0.28	0.20	0.34	0.33	71	0.126	31	34	1.12	12	8	11
		3h	2.8	0.29	0.20	0.34	0.37	72	0.130	32	37	1.17	12	8	12
		4h	2.4	0.30	0.20	0.34	0.40	73	0.133	34	40	1.18	12	8	14

[a] Other conditions: Pd catalyst, 0.1 mmol; solvent, chlorobenzene (50 mL); ethylene pressure, 1 atm; temperature, 15 °C.

[b] Time (t_1) and NB feed concentration in first-stage copolymerization.

[c] Time (t_2) and total cumulative NB feed concentration in second-stage copolymerization.

[d] Time (t_3) and total cumulative NB feed concentration in third-stage copolymerization.

[e] Polymer productivity.

[f] NB molar fraction in the overall tri-block copolymer and each constituting block.

[g] Triple-detection GPC were carried out with THF as eluent at 33 °C. M_n, M_w, and PDI were determined with light scattering detector. $M_{n,1}$, $M_{n,2}$, $M_{n,3}$ are the number-average sizes for the first, second, and third block, respectively. They were calculated from the M_n data of the block copolymers, and the polymers obtained after first- and second-stage copolymerization. Polymer dn/dc values were determined on-line from the mass of polymer injected.

subtracting the M_n value of the triblock polymer with that of the second-stage diblock polymer (i.e., the polymer sampled at the end of second stage). Overall NB molar fraction ($F_{NB,0}$) in each polymer has been determined from their ^{13}C NMR spectra. In particular, the overall NB content (0.20) in the first-stage polymer (i.e., the polymer sampled at the end of first-stage polymerization) corresponds to the average NB content ($F_{NB,1}$) of the first block. The average NB content of the second block ($F_{NB,2}$ = 0.34) is calculated from Eq. 1 by using the M_n and ($F_{NB,0}$) values of both first- and second-stage polymers. The average NB content in the third block ($F_{NB,3}$) is then calculated from the following equation:

$$\frac{M_n F_{NB,0}}{F_{NB,0}M_{NB}+(1-F_{NB,0})M_E} = \frac{M_{n,1}F_{NB,1}}{F_{NB,1}M_{NB}+(1-F_{NB,1})M_E} + \frac{M_{n,2}F_{NB,2}}{F_{NB,2}M_{NB}+(1-F_{NB,2})M_E} + \frac{M_{n,3}F_{NB,3}}{F_{NB,3}M_{NB}+(1-F_{NB,3})M_E} \quad (2)$$

where M_n, $M_{n,1}$, $M_{n,2}$, and $M_{n,3}$ correspond to the molecular weight of the overall triblock copolymer, and the molecular weight of first, second, and third block, respectively. All the molecular weight data and NB content data are summarized in Table 2.3.

In general, $F_{NB,0}$ values of the polymers obtained in this three-stage run shows a continuous increase from the first to the third stage (see Figure 2.9 and Table 2.3), indicating an increase in the average NB content from the first to the third block. This is in good consistency with the increase of the percentage of alternating units among all incorporated NB units (from 57 to 73%, see Table 2.3). Based on the results from the single-stage run 4, the first block in the resulting triblock polymers should have a gradient composition (i.e., negative gradient along the direction of chain growth). Meanwhile, the second block should contain a positive diffusion-caused gradient

followed with a possible kinetics-driven negative gradient from the results in two-stage runs 6 and 7. However, no details on the gradient profiles can be obtained since only a single sample was taken in each of these two stages. As to the third block, we have found that it appears to possess a positive gradient with $F_{NB,3}$ increasing gradually from 0.29 at t_3 = 1 h to 0.40 at t_3 = 4 h. This should also be primarily diffusion-caused. Clearly, the triblock copolymers obtained in this run has very complex composition profiles since each block has its own gradient profile(s).

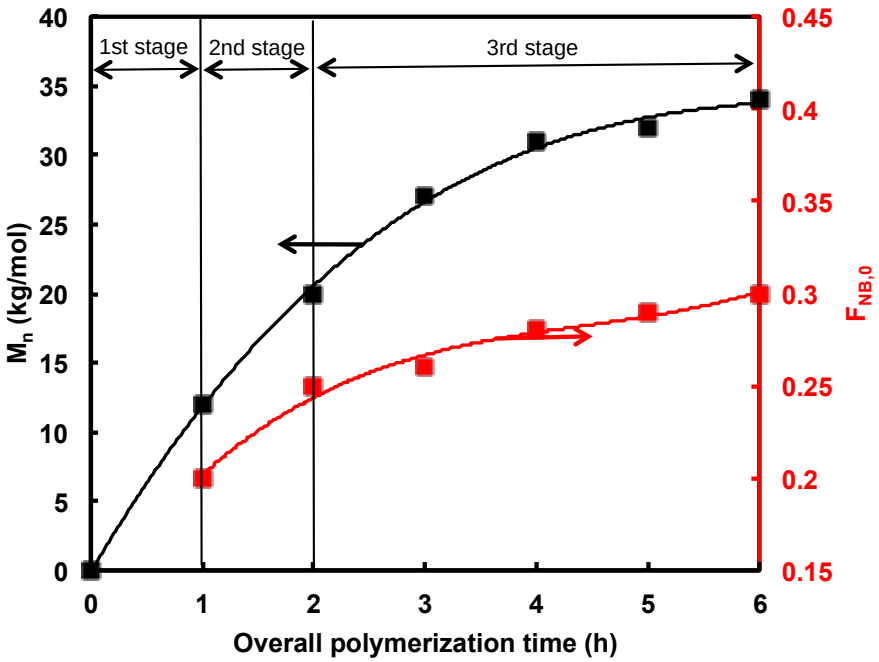

Figure 2.9 Dependences of M_n and overall NB content ($F_{NB,0}$) on overall polymerization time in three-stage copolymerization run 8 (see Table 2.3). Fitting lines are included for the purpose of guiding eyes.

DSC curves of this set of polymers are displayed in Figure 2.10, where T_g and ΔT_g values are also presented. Only a single but very broad glass transition is present in

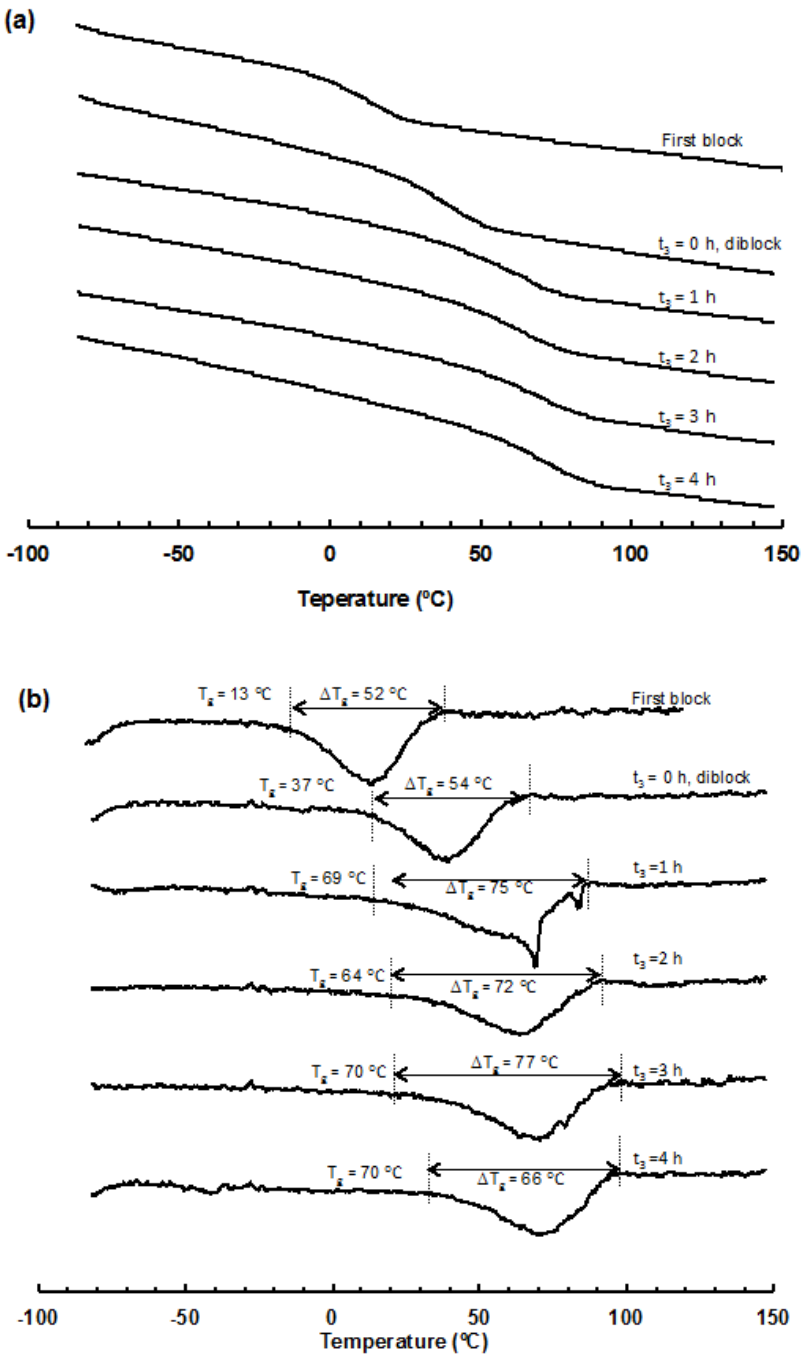

Figure 2.10 DSC heat flow curves (a) and derivatives of the heat flow curves (b) for the set of polymers synthesized in three-stage run 8 (see Table 2.3). The heat flow curves were collected during the second heat ramp at 10 °C/min in DSC measurements. The width for each glass transition (ΔT_g) is illustrated with an arrow in the derivative curve.

all the polymers, without the presence of micro-phase separation even in the block polymers. The transitions corresponding to the hyperbranched PE segments are not clearly observable, suggesting their low/negligible content. With the increase of overall polymerization time, both T_g and ΔT_g values increase significantly. The T_g value increases from 13 °C for the first block to 70 °C for the triblock polymer obtained at t_3 =4 h, with the parallel increase of ΔT_g from 52 to ca. 70 °C, due to the continuous incorporation of chain segments of increasing NB content and the presence of complex composition distribution profiles along the chain. The presence of gradient profile(s) in the first-stage polymer and the second-stage diblock polymer discussed above is confirmed by their high ΔT_g values (52 and 53 °C, respectively). In particular, the very high ΔT_g values (66–77 °C) found with the triblock polymers are appealing and may render some desired damping properties,[4] which are to be investigated.

2.4 Conclusions

We have demonstrated in this work the successful synthesis of a range of narrow-distributed E–NB copolymers featured with various controllable composition distributions, including alternating, gradient, diblock, triblock, and block-gradient structures, through "living" E-NB copolymerization with **1**. In single-stage "living" copolymerization runs 1 and 2 with $[NB]_0$ between 0.42–0.64 M, E-NB alternating copolymers, containing 94% alternating units and 6% isolated NB units, have been obtained, with controllable M_n up to 34 kg/mol. In runs 3 and 4 at lower $[NB]_0$ values (0.11–0.22 M), gradient copolymers featured with different gradient composition

profiles have been synthesized owing to the kinetics-driven reduction in NB concentration over the course of polymerization. Through two-stage copolymerization runs 6 and 7 with NB fed only in the beginning of second stage ($[NB]_0$ = 0.22 M), diblock copolymers containing a first hyperbranched PE block and a second E-NB copolymer block have been designed, with the controllable sizes for both blocks. Containing a significant PE block, these diblock polymers may have enhanced processibility and mechanical impact properties. Meanwhile, a three-stage copolymerization (run 8) has been further demonstrated for the synthesis triblock E-NB copolymers with increasing average NB content from first to third block through sequential feeding of NB. Through extensive DSC characterization, the gradient and block gradient copolymers synthesized herein have been found to have very high ΔT_g values (as high as 119 °C), which may render them with some valuable physical properties (such as damping properties). Meanwhile, the presence of the soft hyperbranched PE segments/blocks in the gradient and block-gradient copolymers can impart the NB-containing polymers with enhanced impact mechanical properties. Further investigations of these properties will be carried out.

2.5 References

1 Ordian, G. *Principle of Polymerization,* 4th Edition, Wiley Interscience: Hoboken, New Jersey, 2004, pp. 464–543.

2 See some representative reviews: (a) Matyjaszewski, K.; Tsarevsky, N. V. *Nature Chem.* **2009**, *1*, 276–288; (b) Matyjaszewski, K.; Xia, J. *Chem. Rev.* **2001**, *101*,

2921–2990; (c) Ouchi, M.; Terashima, T.; Sawamoto, M. *Chem. Rev.* **2009**, *109*, 4963–5050; (d) Hadjichristidis, N; Pitsikalis, M.; Pispas, S.; Iatrou, H. *Chem. Rev.* **2001**, *101*, 3747–3792; (e) Hawker, C. J.; Bosman, A. W.; Harth, E. *Chem. Rev.* **2001**, *101*, 3661–3688.

3 See a review: Beginn, U. *Colloid Polym. Sci.* **2008**, *286*, 1465–1474.

4 Kim, J.; Mok, M. M.; Sandoval, R. W.; Woo, D. J.; Torkelson, J. M. *Macromolecules* **2006**, *39*, 6152–6160.

5 See representative reviews: (a) Tritto, L.; Boggioni, L.; Ferro, D. R. *Coord. Chem. Rev.* **2006**, *250*, 212–241; (b) Janiak, C.; Lassahn, P. G. *J. Mol. Catal., Chem.* **2001**, *166*, 193–209; (c) Makovetskii, K. L. *Polym. Sci, Ser. C* **2008**, *50*, 22–38.

6 Kaminsky, W.; Bark, A.; Arndt, M. *Macromol. Symp.* **1991**, *47*, 83–93.

7 See a review article: Domski, G. J.; Rose, J. M.; Coates, G. W.; Bolig, A. D.; Brookhart, M. *Prog. Polym. Sci.* **2007**, *32*, 30–92.

8 Cherdron, H.; Brekner, M.-J.; Osan, F. *Angew. Makromol. Chem.* **1994**, *223*, 121–133.

9 (a) Jansen, J. C.; Mendichi, R.; Locatelli, P.; Tritto, I. *Macromol. Rapid Commun.* **2001**, *22*, 1394–1398; (b) Jansen, J. C.; Mendichi, R.; Sacchi, M. C.; Tritto, I. *Macromol. Chem. Phys.* **2003**, *204*, 522–530.

10 Thorshaug, K.; Mendichi, R.; Boggioni, L.; Tritto, I.; Trinkle, S.; Friedrich, C.; Mülhaupt, R. *Macromolecules* **2002**, *35*, 2903–2911.

11 (a) Hasan, T.; Shiono, T.; Ikeda, T. *Macromol. Symp.* **2004**, *213*, 123–129. (b) Hasan, T.; Ikeda, T.; Shiono, T. *Macromolecules* **2004**, *37*, 8503–8509.

12 (a) Yoshida, Y.; Saito, J.; Mitani, M.; Takagi, Y.; Matsui, S.; Ishii, S.-i.; Nakano, T.; Kashiwa, N.; Fujita, T. *Chem. Commun.* **2002**, 1298–1299; (b) Yoshida, Y.; Mohri, J.-i.; Ishii, S.-i.; Mitani, M.; Saito, J.; Matsui, S.; Makio, H.; Nakano, T.; Tanaka, H.; Onda, M.; Yamamoto, Y.; Mizuno, A; Fujita, T. *J. Am. Chem. Soc.* **2004**, *126*, 12023–12032.

13 Li, X.-F.; Dai, K.; Ye, W. P.; Pan, L.; Li, Y.-S. *Organometallics* **2004**, *23*, 1223–1230.

14 Wang, W.; Nomura, K. *Macromolecules* **2005**, *38*, 5905–5913.

15 Yoon, J.; Mathers, R. T.; Coates, G. W.; Thomas, E. L. *Macromolecules* **2006,** *39*, 1913–1919.

16 Terao, H.; Iwashita, A.; Ishii, S.; Tanaka, H.; Yoshida, Y.; Mitani, M.; Fujita, T. *Macromolecules* **2009**, *42*, 4359–4361.

17 (a) Boardman, B. M.; Bazan, G. C. *Acc. Chem. Res.* **2009**, *42*, 1597–1606; (b) Diamanti, S. J.; Ghosh, P.; Shimizu, F.; Bazan, G. C. *Macromolecules* **2003**, *36*, 9731–9735; (c) Diamanti, S. J.; Khanna, V.; Hotta, A.; Yamakawa, D.; Shimizu, F.; Kramer, E. J.; Fredrickson, G. H.; Bazan, G. C. *J. Am. Chem. Soc.* **2004**, *126*, 10528–10529; (d) Diamanti, S. J.; Khanna, V.; Hotta, A.; Coffin, R. C.; Yamakawa, D.; Kramer, E. J.; Fredrickson, G. H.; Bazan, G. C. *Macromolecules* **2006**, *39*, 3270–3274; (e) Coffin, R. C.; Diamanti, S. J.; Hotta, A.; Khanna, V.; Kramer, E. J.; Fredrickson, G. H.; Bazan, G. C. *Chem. Commun.* **2007**, 3550–3552; (f) Coffin, R. C.; Schneider, Y.; Kramer, E. J.; Bazan, G. C. *J. Am. Chem. Soc.* **2010**, *132*, 13869–13878.

18 (a) Kiesewetter, J.; Kaminsky, W. *Chem. Eur. J.* **2003**, *9*, 1750–1758; (b) Kiesewetter, J.; Arikan, B.; Kaminsky, W. *Polymer* **2006**, *47*, 3302–3314.

19 (a) Gottfried, A. C.; Brookhart, M. *Macromolecules*, **2001**, *34*, 1140–1142; (b) Gottfried, A. C.; Brookhart, M. *Macromolecules* **2003**, *36*, 3085–3100.

20 Xu, Y.; Xiang, P.; Ye, Z.; Wang, W.-J. *Macromolecules* **2010**, *43*, 8026–8038.

21 Mecking, S.; Johnson, L. K.; Wang, L.; Brookhart, M. *J. Am. Chem. Soc.* **1998**, *120*, 888–899.

22 (a) Zhang, K.; Ye, Z.; Subramanian, R. *Macromolecules* **2009**, *42*, 2313–2316; (b) Xiang, P.; Ye, Z.; Morgan, S.; Xia, X.; Liu, W. *Macromolecules* **2009**, *42*, 4946–4949; (c) Morgan, S.; Ye, Z.; Subramanian, R.; Wang, W.-J.; Ulibarri, G. *Polymer* **2010**, *51*, 597–605; (d) Xia, X.; Ye, Z.; Morgan, S.; Lu, J. *Macromolecules* **2010**, *43*, 4889–4901; (e) Liu, P.; Landry, E.; Ye, Z.; Joly, H.; Wang, W.-J.; Li, B.-G. *Macromolecules* **2011**, *44*, 4125–4139; (f) Dong, Z.; Ye, Z. *Macromolecules* **2012**, *45*, 5020–5031.

23 Ittel, S. D.; Johnson, L. K.; Brookhart, M. *Chem. Rev.* **2000**, *100*, 1169–1204.

24 Guan, Z.; Cotts, P. M.; McCord, E. F.; McLain, S. J. *Science* **1999**, *283*, 2059–2062.

25 (a) Ye, Z.; Zhu, S. *Macromolecules* **2003**, *36*, 2194–2197; (b) Wang, J.; Ye, Z.; Joly, H. *Macromolecules* **2007**, *40*, 6150–6163; (c) Zhang, K.; Wang, J.; Subramanian, R.; Ye, Z.; Lu, J.; Yu, Q. *Macromol. Rapid Commun.* **2007**, *28*, 2185–2191; (d) Wang, J.; Zhang, K.; Ye, Z. *Macromolecules* **2008**, *41*, 2290–2293. (e) Ye, J.; Ye, Z.; Zhu, S. *Polymer* **2008**, *49*, 3382–3392; (f) Xiang, P.; Ye, Z. *Macromol. Rapid Commun.* **2010**, *31*, 1083–1089; (g) Ye, Z.; Li, S.

Macromol. React. Eng. **2010**, *4*, 319–329; (h) Dong, Z.; Ye, Z. *Polym. Chem.* **2012**, *3*, 286–301.

26 Tritto, I.; Marestin, C.; Boggioni, L.; Zetta, L.; Provasoli, A.; Ferro, D. R. *Macromolecules* **2000**, *33*, 8931–8944.

2.6 Supporting Information

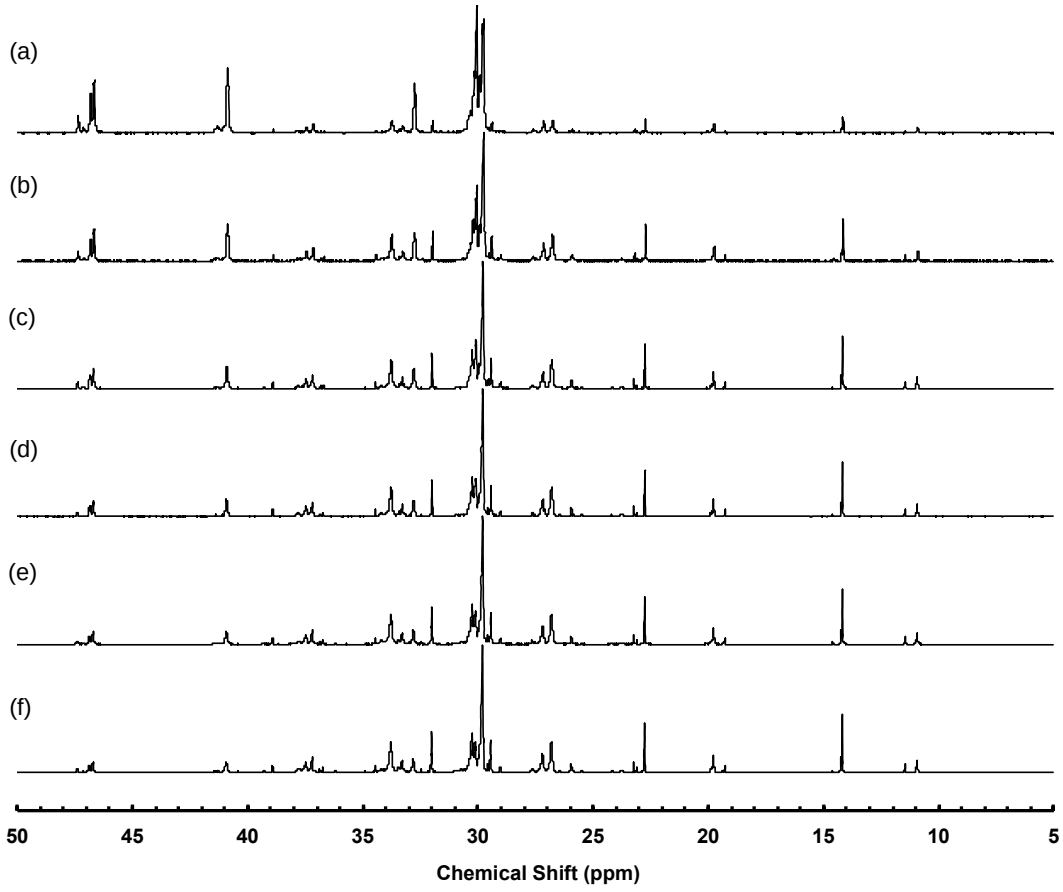

Figure S2.1 ^{13}C NMR (125 MHz) spectra of copolymers synthesized in run 4 (see Table 1) at different polymerization time: (a) 1 h of polymerization; (b) 2 h; (c) 3 h; (d) 4 h; (e) 5 h; and (f) 6 h.

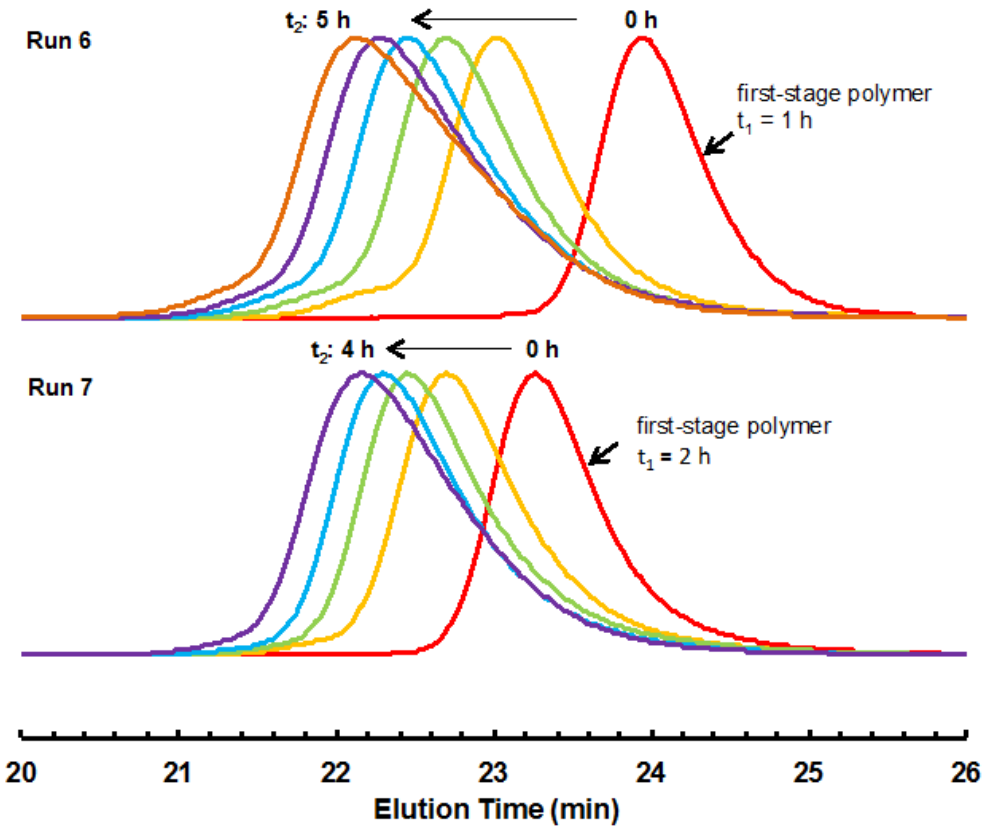

Figure S2.2 GPC elution curves (recorded from DRI detector) of the polymers synthesized in two-stage polymerizations (runs 6 and 7, see Table 2). In the figure, t_2 represents the polymerization time in the second stage polymerization. GPC measurement condition: THF as the eluting phase at 1 mL/min and 33 °C.

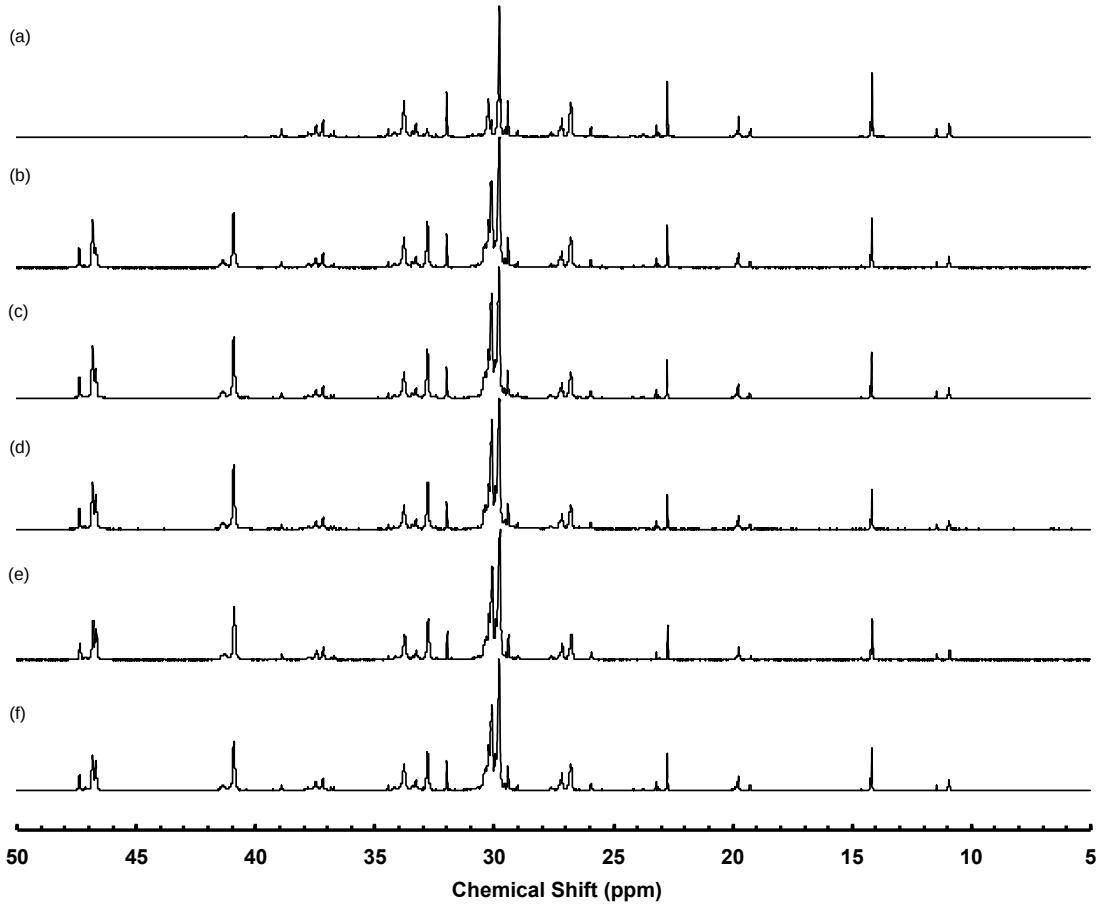

Figure S2.3 ^{13}C NMR spectra (125 MHz) of polymers obtained in run 6 at different polymerization time: (a) t_1=1 h, t_2=0 h, hyperbranched PE block; (b) t_2=1 h; (c) t_2=2 h; (d) t_2=3 h; (e) t_2=4 h; (f) t_2=5 h.

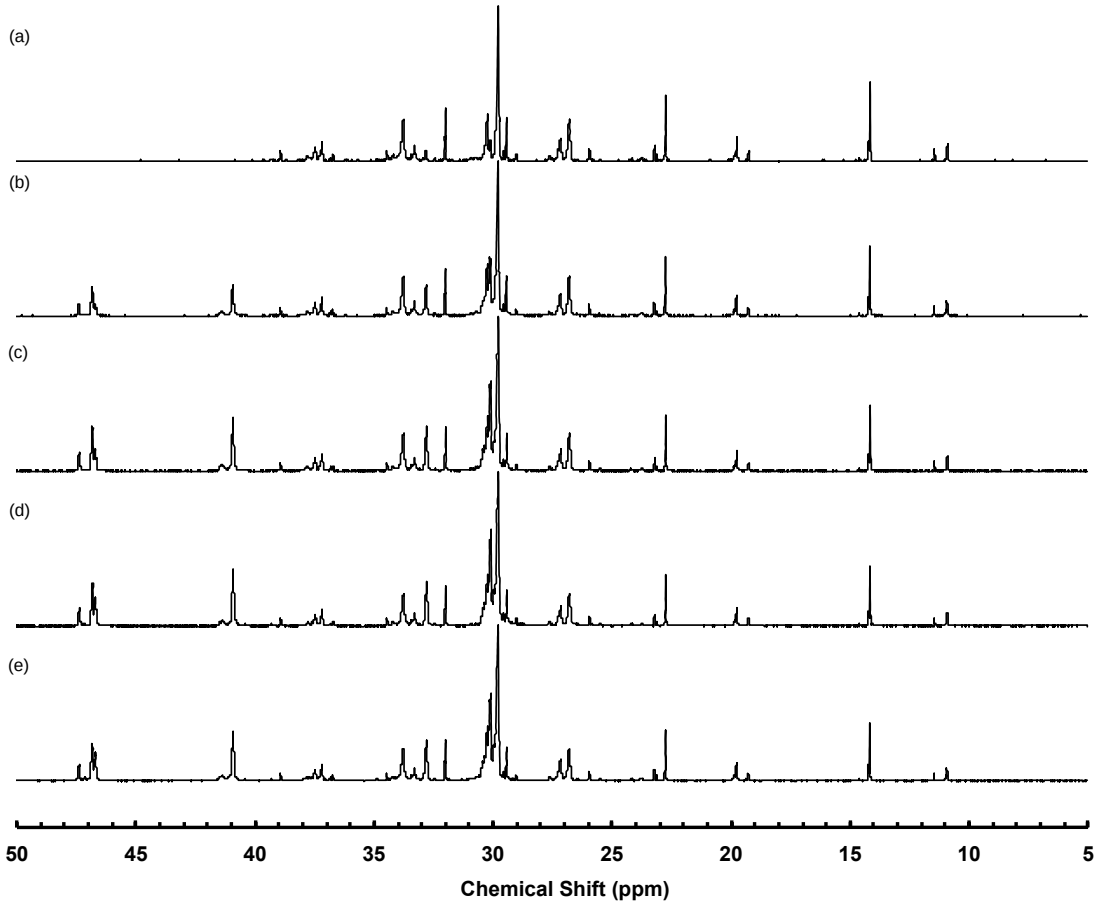

Figure S2.4 ^{13}C NMR spectra (125 MHz) of polymers obtained in run 7 at different polymerization time: (a) t_1=2 h, t_2=0 h, hyperbranched PE block; (b) t_2=1 h; (c) t_2=2 h; (d) t_2=3 h; (e) t_2=4 h.

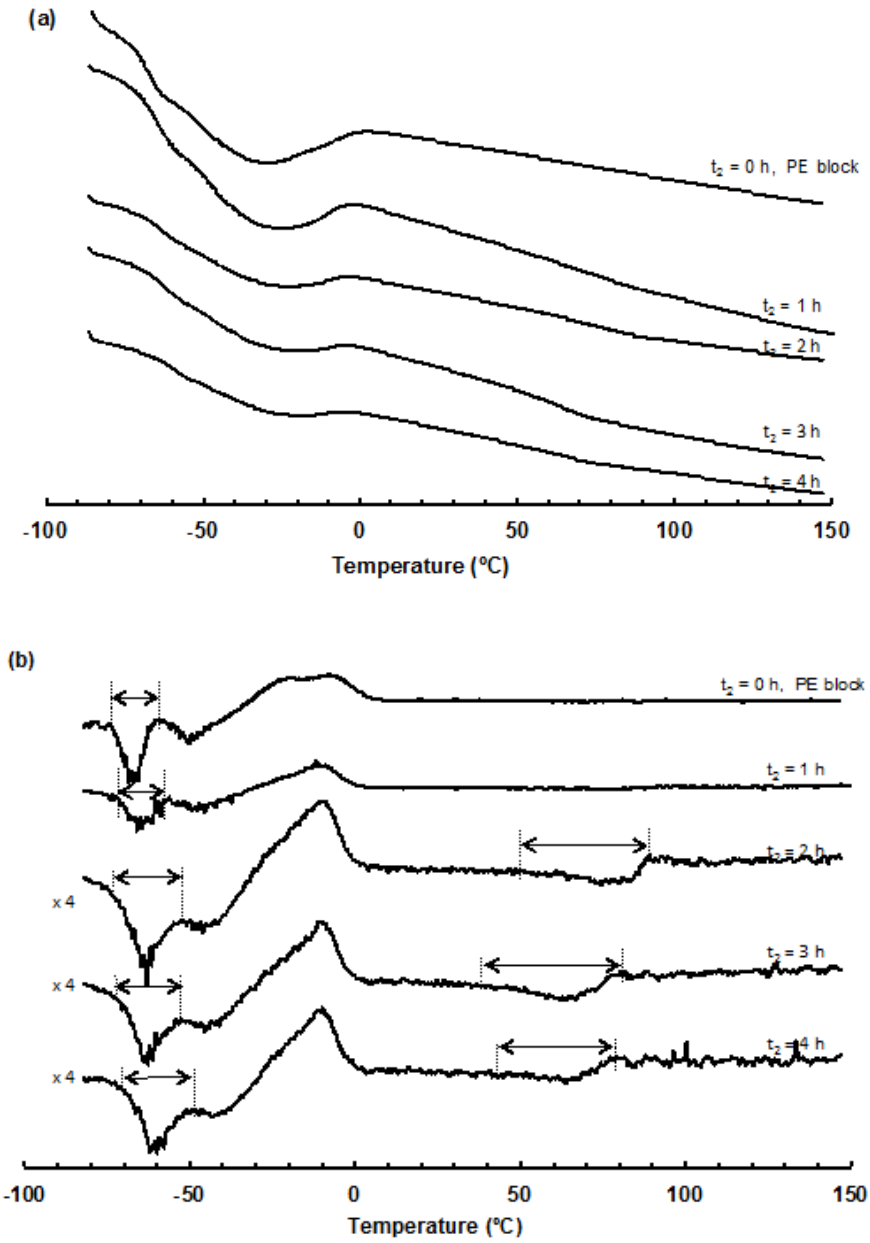

Figure S2.5 DSC heat flow curves (a) and derivatives of the heat flow curves (b) for the set of polymers synthesized in run 7. The heat flow curves were collected during the second heat ramp at 10 °C/min in DSC measurements. The T_g breadth for each glass transition is illustrated with an arrow in the derivative curve.

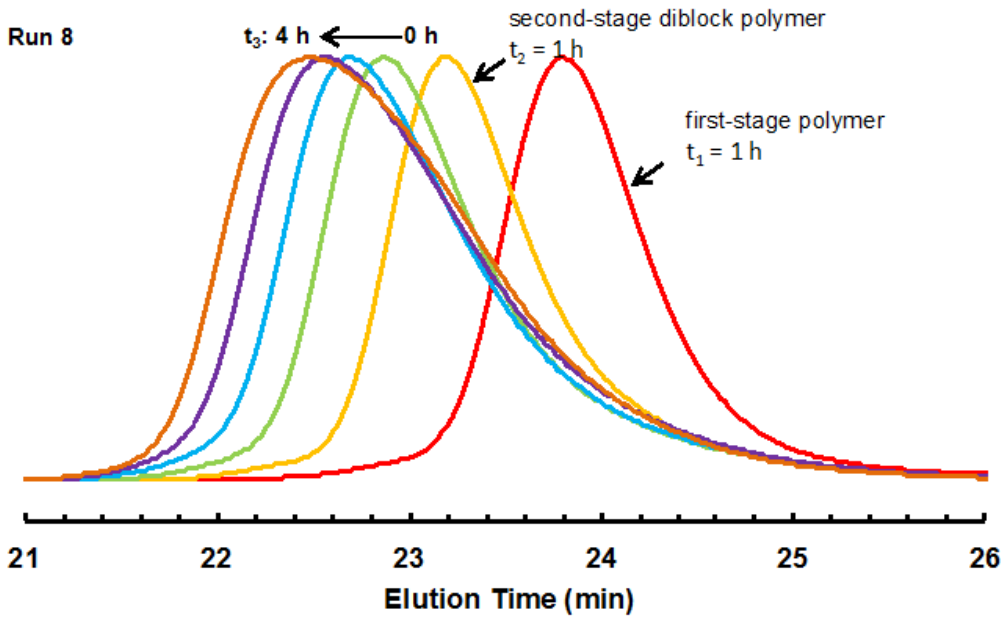

Figure S2.6 GPC elution curves (recorded from DRI detector) of the polymers synthesized in three-stage run 8 (see Table 2.3). In the figure, t_1, t_2, and t_3 represent the polymerization time in the first, second, and third stage, respectively. GPC measurement condition: THF as the eluting phase at 1 mL/min and 33 °C.

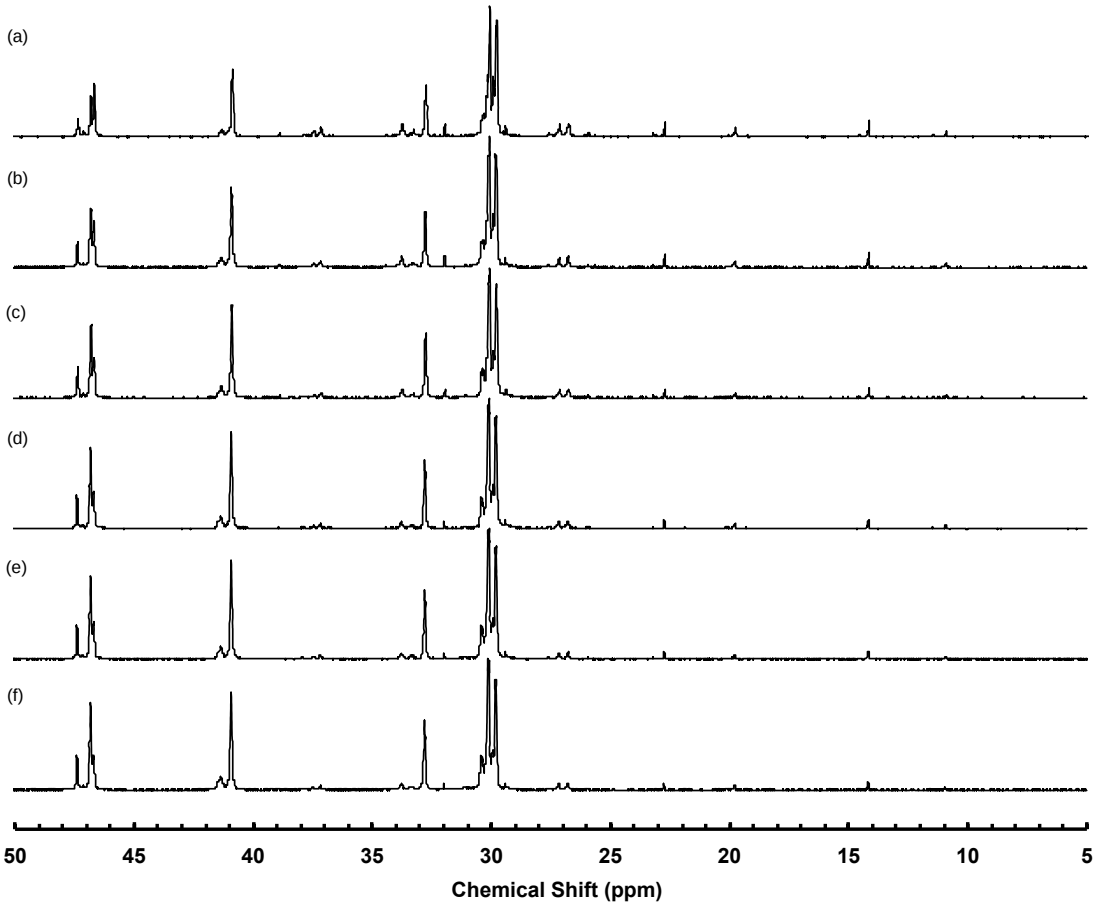

Figure S2.7 ^{13}C NMR spectra (125 MHz) of polymers obtained in run 8 at different polymerization time: (a) t_1 = 1 h, t_2 = 0 h, first block; (b) t_2 = 1 h, t_3 = 0 h, diblock polymer; (c) t_3 = 1 h; (d) t_3 = 2 h; (e) t_3 = 3 h; (f) t_3 = 4 h.

2.7 Sample Calculation of Norbornene (NB) Content in Each Block of the Block Copolymers

A sample calculation procedure is provided as follows for the calculation of the NB content in each block of the triblok copolymer synthesized in run 8 at t_3 = 2 h.

(1) NB content in the first block, $F_{NB,1}$

$F_{NB,1} = F_{NB,0}$ @ t_2 = 0 h = 0.20

(2) NB content in the second block, $F_{NB,2}$

$F_{NB,2}$ is calculated as per the following equation:

$$\frac{M_n F_{NB,0}}{F_{NB,0}M_{NB} + (1 - F_{NB,0})M_E} = \frac{M_{n,1} F_{NB,1}}{F_{NB,1}M_{NB} + (1 - F_{NB,1})M_E} + \frac{M_{n,2} F_{NB,2}}{F_{NB,2}M_{NB} + (1 - F_{NB,2})M_E}$$

where M_n, $M_{n,1}$, and $M_{n,2}$ correspond to the molecular weight of the overall diblock copolymer at t_2 = 1 h & t_3 = 0 h, and the molecular weight of first and second block, respectively; $F_{NB,0}$, $F_{NB,1}$, and $F_{NB,2}$ correspond to the NB average content of the overall diblock copolymer (at t_2 = 1 h & t_3 = 0 h) and the NB average content of first and second block, respectively.

From GPC characterization

M_n = 20 kDa, $M_{n,1}$ = 12 kDa, $M_{n,2}$ = (20 – 12) = 8 kDa;

From NMR characterization

$F_{NB,0}$ = 0.25, $F_{NB,1}$ = 0.20;

Solving the equation renders,

$F_{NB,2}$ = 0.34

(3) NB content in the third block, $F_{NB,3}$

When t_3 = 2h, the average NB content in the third block ($F_{NB,3}$) is calculated from the following equation:

$$\frac{M_n F_{NB,0}}{F_{NB,0}M_{NB}+(1-F_{NB,0})M_E}=\frac{M_{n,1}F_{NB,1}}{F_{NB,1}M_{NB}+(1-F_{NB,1})M_E}+\frac{M_{n,2}F_{NB,2}}{F_{NB,2}M_{NB}+(1-F_{NB,2})M_E}+\frac{M_{n,3}F_{NB,3}}{F_{NB,3}M_{NB}+(1-F_{NB,3})M_E}$$

where M_n, $M_{n,1}$, $M_{n,2}$ and $M_{n,3}$ correspond to the molecular weight of the overall triblock copolymer, and the molecular weight of first, second and third block, respectively; $F_{NB,0}$, $F_{NB,1}$, $F_{NB,2}$ and $F_{NB,3}$, correspond to the NB average content of the overall triblock copolymer and the NB average content of first, second and third block, respectively.

From GPC characterization

M_n = 31 kDa, $M_{n,1}$ = 12 kDa, $M_{n,2}$ = (20 – 12) = 8 kDa; $M_{n,3}$ = (31 – 20) = 11 kDa

From NMR characterization

$F_{NB,0}$ = 0.28, $F_{NB,1}$ = 0.20, $F_{NB,2}$ = 0.34;

Solving the equation renders,

$F_{NB,3}$ = 0.33

Chapter 3

Hyperbranched Polyethylene Ionomers Containing Cationic Tetralkylammonium Ions Synthesized by Pd–Diimine-Catalyzed Direct One-Pot Ethylene Copolymerization with Ionic Liquid Comonomers

This chapter is organized based on a paper published by P. Xiang and Z. Ye in Macromolecules 2015, 48, 6096–6107.*

Abstract

Synthesis of polyolefin-based ionomers through direct catalytic copolymerization of olefin with ionic comonomers has been challenging with no prior success. This Chapter reports the first direct synthesis of a class of hyperbranched polyethylene ionomers containing positively charged tetralkylammonium ions and different counter anions (tetrafluoroborate, hexafluorophosphate, bis(trifluoromethane)sulfonimide, or hexafluoroantimonate) by one-pot copolymerization of ethylene with tetralkylammonium-containing acrylate-type ionic liquid comonomers (**3**–**5, 7**). The use of a Pd–diimine catalyst (**1**), which shows excellent stability towards the highly polar ionic group, is key to the direct synthesis. A detailed study on the catalytic copolymerization and the effects of the polymerization condition on the macromolecular chain parameters of the resulting ionomers has been performed. A range of ionomers differing in ion content and counter anion has been synthesized and characterized. Meanwhile, systematic studies on the structural, thermal, and melt rheological properties of the ionomers have been undertaken. The dramatic effects of ion incorporation on these properties, particularly on the rheological properties,

are demonstrated.

3.1 Introduction

Ionomers are an important class of polymers containing a small fraction of ionic functional groups (typically less than 10 mol%) that are covalently bonded to the polymer backbone as pendant groups. Due to the energetic incompatibility between the polar ionic groups and nonpolar polymer backbone, ionomers are typically featured with microphase separation morphology in the solid state with nanoscale ionic aggregates dispersed within nonpolar polymer matrix. This imparts the ionomers with some enhanced properties, such as toughness, strength, adhesion, barrier properties, surface properties, ion conductivity, *etc.* In consequence, ionomers find use in a variety of applications, including ion transport membranes, fuel cell, thermoplastic elastomers, adhesives, *etc.* [1-4] Among various ionomers, polyolefin-based (such as polyethylene and polypropylene) ionomers are particularly well known for their outstanding chemical stability, superior mechanical properties, and thermoplastic-like processability, as well as their low cost.[1-4] Depending on the charge of ionic groups, ionomers are divided into polyanions with negatively charged groups (*e.g.*, carboxylate, sulfonate, and phosphate) and polycations with positively charged groups (*e.g.*, quaternary amine, imidazolium, and pyridinium). While polyanions are more common with many commercial examples available (such as polyethylene ionomers with metal carboxylate salts ($COO^{-}M^{+}$)),[4] polycations have recently received significant interest.[5]

Ionomers are often synthesized via two routes: (1) direct copolymerization of vinyl-containing ionic or ionic liquid monomers; (2) postpolymerization ionization of electrically neutral polymers.[1-4] In the case of direct polymerization route, polymerization methods insensitive to the functional ionic groups, such as conventional free radical polymerization, controlled/"living" radical polymerization, and condensation polymerization, are often required. For polyolefin based (such as polyethylene and polypropylene) ionomers that are our focus herein, their synthesis by one-step direct copolymerization of olefin with ionic comonomers has been prohibitively challenging though desired given its simplicity and well-defined ionomer composition. This is because polyolefins are synthesized mainly via catalytic coordinative olefin polymerization where the transition metal catalysts (Ziegler-Natta or metallocene catalysts) are often highly sensitive to and easily poisoned by the heteroatoms present in the ionic comonomers.

To date, polyolefin ionomers have been synthesized exclusively by postpolymerization ionization of polyolefins or by alternative metathesis polymerization of special monomers, while with no successful examples reported on their synthesis via direct catalytic olefin copolymerization. In postpolymerization ionization methods, olefin copolymers bearing ionizable functionalities are first prepared either by radical or catalytic polymerization mechanism, followed with ionization.[6-11] In this regard, the well-known polyethylene ionomers with metal carboxylate salts are obtained by postpolymerization neutralization of ethylene copolymers of methacrylic or acrylic acid produced through radical processes. However, the radical processes often require harsh

demanding reaction conditions (*i.e.*, high temperature and high pressure) though functionality tolerant. In contrast, catalytic coordinative processes are much less stringent on reaction conditions, but functionality sensitive. Notably, Chung *et al.* demonstrated the successful use of catalytic coordinative processes mediated with Ziegler-Natta or metallocene catalysts for the synthesis of a range of polyethylene and polypropylene ionomers containing ammonium chloride groups via postpolymerization ionization.[10,11] In their design, ethylene or propylene was copolymerized with α-olefin comonomers containing a silaneprotected amino group to render high-molecular-weight olefin copolymers having ionizable amine groups. Therein, the intelligent use of silane protection chemistry on the functional comonomers provides the key to minimized catalyst poisoning in the coordinative polymerization system.

Alternatively, polyethylene ionomers have also been synthesized via metathesis polymerization methods, including ring-opening metathesis polymerization of cyclic olefin monomers [12,13] and acyclic diene metathesis polymerization.[14-16] In these cases, specially designed ionic olefin monomers, cyclic olefins and α,ω-dienes, respectively, bearing an ionic group, are directly polymerized through the metathesis polymerizations that are insensitive to polar ionic functionalities. Subsequent hydrogenation of resulting metathesis ionomers containing internal double bonds renders polyethylene ionomers. In this stream, Coates *et al.* successfully synthesized cross-linked polyethylene ionomers containing ammonium ions by Ru-catalyzed ring-opening metathesis polymerization of ammonium-containing cyclic olefins.[12,13] Employing the acyclic diene metathesis polymerization technique pioneered by them, Wagener *et al.* demonstrated the synthesis

of a range of precision polyethylene ionomers containing perfectly sequenced imidazolium or carboxylate ions through either direct polymerization of ionic monomers or postpolymerization ionization of neutral metathesis polymers.[14-16] These precision ionomers as model materials provide considerable insights into the nanoscale ionomer morphology.[17-20] Though elegant, the need of sophisticated, specially designed monomers instead of commercially abundant olefin stocks and the requirement of additional hydrogenation step in the synthesis complicate the use of these alternative metathesis polymerization methods.

Tackling the existing synthesis challenge, we report in the article the successful synthesis of a range of hyperbranched polyethylene (HBPE) ionomers containing tetralkylammonium ions coupled with different counter anions [tetrafluoroborate (BF_4^-), hexafluorophosphate (PF_6^-), bis(trifluoromethane)sulfonimide (Tf_2N^-), or hexafluoroantimonate (SbF_6^-)] by direct ethylene copolymerization with unprotected tetralkylammonium-containing acrylate-type ionic liquid comonomers. The polymerization reactions are facilitated with a Pd–diimine catalyst, [(ArN=C(Me)–(Me)C=NAr)Pd(CH_3)(N≡CMe)]$^+SbF_6^-$ (Ar = 2,6–(*i*Pr)$_2$C$_6$H$_3$) (**1**). While the hyperbranched topology of the ionomers results from the well-known chain walking mechanism of the Pd–diimine catalyst,[21-23] the remarkable low oxophilicity and insensitivity of the catalyst towards the tetralkylammonium ions facilitates the effective incorporation of the ionic liquid comonomers while without experiencing severe catalyst poisoning. Meanwhile, the acrylate ionic liquid comonomers with different counter anions (**3**–**7**) used herein are easily obtained from the commercially available analogue

having a chloride anion {[2-(acryloyloxy)ethyl]trimethylammonium chloride, **2**} via simple anion exchange, which adds an additional convenience to this synthesis. To the best of our knowledge, this represents the first synthesis of polyolefin ionomers via direct catalytic olefin copolymerization with ionic liquid comonomers. Besides the synthesis, we have also investigated herein the physical properties of the resulting ionomers (structural, thermal, and rheological) and the unique effects of ion incorporation on these properties.

3.2 Experimental Section

3.2.1 Materials

All manipulations involving air- and/or moisture-sensitive materials were conducted in an N2-filled glovebox or by using Schlenk techniques. The Pd–diimine catalyst, $[(ArN{=}C(Me){-}(Me)C{=}NAr)Pd(CH_3)(N\_CMe)]^+SbF_6^-$ (Ar = 2,6–(iPr)$_2$C$_6$H$_3$) (**1**), was synthesized by following a literature procedure.[24] 1-[2-(Acryloyloxy)ethyl]-3-butyl-imidazolium tetrafluoroborate was synthesized by following the literature procedure employed for a similar methacryloyl analogue.[25] Ultrahigh-purity N_2 (> 99.97%) and polymer-grade ethylene (both obtained from Praxair) were purified by passing sequentially through a 3 Å molecular sieve column and an Oxiclear column before use. Deionized water was obtained from a Barnstead Nanopure II water purification system equipped with reverse osmosis and ion exchange columns. Aqueous solution of [2-(acryloyloxy)ethyl]trimethylammonium chloride solution (**2**, 80 wt% in H_2O),

acetonitrile (anhydrous, 99.8%), sodium tetrafluoroborate ($NaBF_4$, 98%), potassium hexafluorophosphate (KPF_6, > 98%), bis(trifluoromethane)sulfonimide lithium salt ($LiTf_2N$), sodium trifluoromethanesulfonate (NaTfO, 98%), sodium hexafluoroantimonate ($NaSbF_6$, technical grade), trimethylphosphine (97%), sulfuric acid (ACS regent, 95.0–98.0%), and phosphoric acid were obtained from Aldrich and were used directly. Acetone from Fisher Scientific was deoxygenated and dried over molecular sieves before use. Other chemicals, including HPLC-grade tetrahydrofuran (THF), hydrogen peroxide (50 wt% in water), hydrochloric acid (37.4 wt% in water), potassium hydroxide (≥ 90%), *N*, *N*-dimethylformamide (DMF) (HPLC, ≥ 99%), and methanol from Fisher Scientific, were all used as received.

3.2.2 Synthesis of [2-(Acryloyloxy)ethyl]trimethylammonium tetrafluoroborate (3)

In a flask, the commercially obtained aqueous solution of **2** (18.6 g) was washed with excessive acetone and then dried under vacuum, yielding viscous pure ionic liquid **2** (14.7 g, 76 mmol). It was then redissolved in anhydrous acetonitrile (50 mL), followed with the addition of sodium tetrafluoroborate (8.5 g, 77.5 mmol). The mixture was stirred at room temperature for 48 h and then filtered to remove the sodium chloride precipitate. The filtrate was concentrated, and then precipitated in 50 mL of diethyl ether. After three times of wash with diethyl ether, the precipitated white crystal was collected and dried under vacuum at room temperature, rendering **3** (14.4 g, 59 mmol; yield 78%).

3.2.3 Synthesis of [2-(Acryloyloxy)ethyl]trimethylammonium hexafluorophosphate (4)

In a flask, aqueous solution of **2** (12.5 g) was diluted with deionized water (40 mL), followed with the addition of potassium hexafluorophosphate (9.4 g, 51 mmol). The mixture was stirred at room temperature for 48 h and then filtered. The filtered white precipitate was then washed with deionized water (10 mL) and anhydrous THF (10 mL) three times for each. The washed precipitate was then collected and dried under vacuum at room temperature, rendering product **4** (12.6 g, 42 mmol; yield 82%).

3.2.4 Synthesis of [2-(Acryloyloxy)ethyl]trimethylammonium bis(trifluoromethane)sulfonamide (5)

In a flask, aqueous solution of **2** (2.05 g) was washed with excessive acetone and subsequently dried under vacuum, yielding pure **2** (1.64 g, 8.5 mmol). It was redissolved in anhydrous acetonitrile (10 mL), followed with the addition of bis(trifluoromethane)sulfonimide lithium salt (2.43 g, 8.5 mmol). The mixture was stirred at room temperature for 48 h and then stabilized for 1 h. A transparent viscous liquid was separated from the mixture and collected. The collected viscous liquid was then further washed with anhydrous acetonitrile (5 mL $\cdot$ 3), and then dried under vacuum at room temperature to render **5** as a viscous liquid (2.96 g, 6.8 mmol; yield 80%).

3.2.5 Synthesis of [2-(Acryloyloxy)ethyl]trimethylammonium trifluoromethanesulfonate (6)

In a flask, aqueous solution of **2** (1.3 g) was washed with excessive acetone and subsequently dried under vacuum, yielding viscous pure **2** (1.03 g, 5.3 mmol). It was then redissolved in anhydrous acetonitrile (10 mL), followed with the addition of sodium trifluoromethanesulfonate (1.02 g, 5.9 mmol). The mixture was stirred at room temperature for 48 h and then stabilized for 1 h. A transparent viscous liquid was separated from the mixture and collected. The collected viscous liquid was then further washed with anhydrous acetonitrile (5 mL · 3). It was then dried under vacuum at room temperature, rendering **6** (0.90 g, 2.9 mmol; yield 55%).

3.2.6 Synthesis of [2-(Acryloyloxy)ethyl]trimethylammonium hexafluoroantimonate (7)

Aqueous solution of 2 (4.65 g) was washed with excessive acetone and subsequently dried under vacuum, yielding viscous pure 2 (3.72 g, 19.2 mmol). It was then dissolved in anhydrous acetonitrile (10 mL), followed with the addition of sodium hexafluoroantimonate (4.95 g, 19.2 mmol). The mixture was stirred at room temperature for 48 h and then filtered. The filtrate was concentrated to 3 mL, followed with the addition of anhydrous diethyl ether (5 mL) to precipitate out the product as a viscous liquid. The precipitate was further washed with diethyl ether (5 mL × 4), and then dried under vacuum at room temperature, rendering 7 (5.6 g, 14.2 mmol; yield 74%).

3.2.7 Copolymerization of Ethylene with Polymerizable Ionic Liquid Comonomers

All copolymerization reactions of ethylene with the polymerizable ionic liquid comonomers (**2**–**7**) were conducted in a 50 mL Schlenk flask equipped with a magnetic stirrer at room temperature. Representatively, the following procedure was used for the synthesis of I-B-2 listed in Table 3.1 with **3** as comonomer at a feed concentration of 0.3 M. The flask sealed with a rubber septum was first flame-dried under vacuum. After being cooled to room temperature, the reactor was purged with ethylene for at least three times, and then filled with ethylene to 1 atm (absolute pressure). The comonomer solution (0.74 g of **3** in 5 mL acetone) was injected in to the reactor. Subsequently, the polymerization was started upon the injection of the Pd–diimine catalyst solution (0.08 g, 0.1 mmol in 5 mL of acetone). During the polymerization, ethylene pressure was maintained constant by continuous feed from a cylinder. After 24 h, the polymerization was stopped by shutting down ethylene supply and venting the reactor. The black ionomer product containing Pd(0) particles resulting from the decomposition of the Pd–diimine catalyst was precipitated out with a large amount of methanol. The precipitate was washed with methanol three times, and then redissolved in 3 mL THF.

To remove the Pd black trapped within the ionomer, about 5 drops of aqueous mixed solution of HCl and H_2O_2 (containing 0.34 wt% HCl and 45.5 wt% H_2O_2) was added into the black ionomer solution. The solution was stirred at room temperature until the color of the solution turned to red. Subsequently, trimethylphosphine (0.1 mL) was added to the solution. The solution gradually turned to colorless and was then

poured into a large amount of methanol (*ca.* 50 mL) to precipitate out the ionomer product. The precipitated ionomer was redissolved in DMF (5 mL) and 0.2 g of sodium tetrafluoroborate was added to the ionomer solution. The mixture was stirred for 24 h and the product was precipitated out in a large amount of methanol (50 mL) again. After further wash with methanol (20 mL × 3), the product was dried overnight at 70 ℃ under vacuum, yielding I-B-2 (1.1 g).

3.2.8 General Procedure for Basic Hydrolysis of Ionomers

The ionomer (*ca.* 30 mg) and KOH (0.2 g) were dispersed in a solvent mixture containing 3 mL of THF and 1 mL of methanol in a 50 mL flask. The suspension was refluxed for 2 days and was then precipitated out in methanol. The polymer precipitate was redissolved in THF and precipitated in methanol for two cycles. Finally, the hydrolyzed product (*ca.* 20 mg) was dried overnight under vacuum at 70 ℃ and was subsequently characterized.

3.2.9 Characterizations and Measurements

Proton nuclear magnetic resonance (^{1}H NMR) spectra of all samples were collected on a Varian Gemini 2000 spectrometer (200 MHz) with CDCl3 as the solvent. X-ray scattering patterns of the ionomers were recorded on an X_Pert Pro diffractometer with Co radiation (wavelength 1.79 Å) at room temperature. Polymer characterization with gel permeation chromatography (GPC) was carried out on a Polymer Laboratories

PL-GPC220 system equipped with a differential refractive index (DRI) detector (from Polymer Laboratories), a four-bridge capillary viscosity detector, and a three-angle light scattering (LS) detector (high-temperature mini-DAWN from Wyatt Technology). The detection angles of the light scattering detector were 45, 90, and 135°, and the laser wavelength was 687 nm. One guard column (PL# 1110–1120) and three 30-cm columns (PLgel 10μm MIXED-B 300×7.5 mm) were used. The mobile phase was HPLC-grade THF and the flow rate was 1.0 mL/min. The complete GPC system, including the column and detector arrays, was maintained at 33 °C. The mass of the polymers injected into the columns was about 1 mg. Two polystyrene narrow standards (from Pressure Chemicals) with weight-average molecular weights (*M*w) of 30 and 200 kg/mol, respectively, as per the supplier were used for the normalization of light scattering signals at the three angles and the determination of interdetector delay volume and band broadening, respectively. The DRI increment dn/dc value of 0.078 mL/g was used for all cleaved polyethylenes, and the value of 0.185 mL/g was used for polystyrene.

Melt rheological characterization of the polymers was conducted on a TA Instruments AR-G2 rheometer. A parallel plate measurement configuration with a diameter of 20 mm and a gap size of about 1.0 mm was used. The measurements were all carried out in the small amplitude dynamic oscillation mode within a frequency range of 0.01–100 Hz. To establish the linear viscoelastic region for each polymer, a strain sweep was performed at 10 Hz before frequency sweeps. The characterizations were performed in a general temperature range of 35–135 °C with an interval of 10 °C. The temperature was maintained within ± 0.1 °C with the ETC temperature control system

and the measurements were done under N_2 protection. Differential scanning calorimetry (DSC) measurements were performed on a TA Instruments Q100 DSC equipped with a refrigerated cooling system under a N_2 atmosphere. The instrument was operated in the standard DSC mode and was calibrated with an indium standard. A N_2 purging flow of 50 mL/min was used. Samples (*ca.* 5 mg) were heated from room temperature to 250 °C at 10 °C/min and cooled to –90 °C at 5 °C/min, and the data were collected on a subsequent heating ramp from –90 to 250 °C at 10 °C/min.

3.3 Results and Discussion

3.3.1 HBPE Ionomer Synthesis by Direct Ethylene Copolymerization and Macromolecular Characterizations

In the synthesis of HBPE ionomers via direct ethylene copolymerization herein, the tetralkylammonium-containing acrylate-type ionic liquid monomers (**2**–**7**) are chosen and studied as the ionic comonomers (see Scheme 3.1). While **2** with Cl^- anion is commercially available, **3**–**7** with BF_4^-, PF_6^-, Tf_2N^-, trifluoromethanesulfonate (TfO^-), and SbF_6^-, respectively, as the counter anion, are easily prepared from **2** via simple anion exchange. The use of these comonomers bearing different counter anions enables us to investigate the effects of the anion type on their incorporation during the copolymerization. Meanwhile, Pd–diimine catalyst **1** is adopted herein to facilitate the direct copolymerization given their low oxophilicity and high tolerance of functional groups.[22-24,26] Despite their well-known capability in incorporating various acrylate type

comonomers in ethylene polymerization,[22-24,26-32] Pd–diimine catalysts have not been previously investigated for copolymerization of ionic comonomers. The choice of solvent is also important for the copolymerization herein given the use of the highly polar ionic liquid comonomers that often do not dissolve in non-polar or low-polarity solvents. For all copolymerization runs except that with **2** as comonomer, acetone was used as the solvent since it is a good solvent for both catalyst **1** and the other ionic liquid comonomers (**3**–**7**). In the case of **2** as comonomer, acetonitrile was used instead since **2** is only soluble in highly polar solvents (such as water, methanol, and acetonitrile; but not in acetone) and acetonitrile is the optimum among them in consideration of solubility and stability of **1**. All polymerization runs were conducted under a constant ethylene pressure of 1 atm at room temperature (*ca.* 25 ℃).

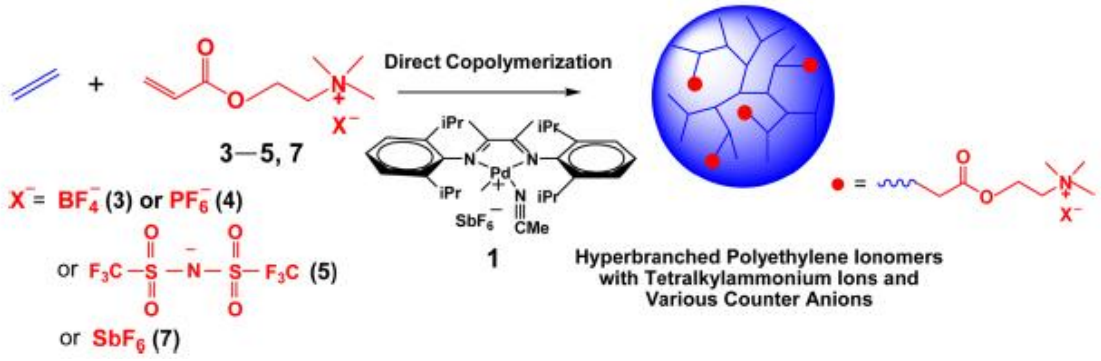

Scheme 3.1 One-step synthesis of hyperbranched polyethylene ionomers containing tetralkylammonium ions and various counter anions by direct chain walking copolymerization of ethylene with polymerizable ionic liquid comonomers.

When the polymerization was carried out with **2** or **6** (with Cl^- and TfO^-, respectively, as counter anion) as comonomer at 0.3 M, the reaction did not occur with

no/negligible polymer produced. On the contrary, successful polymerizations took place in all the other runs performed with **3**–**5** or **7** as the comonomer. Table 3.1 summarizes all the copolymerization reactions undertaken with **3**–**5** or **7**, as well as the characterization results of the resulting ionomers. In the case with **3** or **4** as comonomer, the copolymerizations were carried out under different comonomer concentrations (up to 1.0 M) to investigate the effect of comonomer concentration on their incorporation. In the case with **5**, a single copolymerization was carried out with **5** at 0.3 M. The resulting ionomers are termed correspondingly as I-B-#, I-P-#, I-T-1, and I-S-1, with the first letter I standing for ionomer and the second letter specifying the comonomer varying in counter anion (*i.e.*, B for **3** with BF_4^-, P for **4** with PF_6^-, T for **5** with Tf_2N^-, and S for **7** with SbF_6^-). A control run without the addition of any comonomer was also undertaken, rendering the homopolyethylene control sample, HPE.

For the homopolymerization run undertaken herein in acetone, the polymer yield is significantly lower compared to similar runs carried out in low-polarity solvents (CH_2Cl_2 or chlorobenzene) but at otherwise nearly identical conditions.[27-31,39,59] This may result from both the lower ethylene solubility in acetone as a polar solvent and the coordinating capability of acetone towards the cationic Pd center. Compared to the homopolymerization run, the addition of each ionic liquid comonomer (**3**–**5, 7**) significantly reduces catalyst activity on the basis of the continuously lowered polymer yield upon the increase of comonomer concentration (see Table 3.1). This is indicative of the comonomer incorporation since the incorporation of acrylate comonomers of lower-reactivity often leads to reduced polymerization activity.[27-32] All the as-produced

Table 3.1 Summary of the polymerization results and the characterization data for all polymers[a]

Polymer	Comonomer	$[M]_0$[b] (mol/L)	Polymer yield (g)	C_2H_4 TOF (1/h)	Comonomer content[c] (mol %)	GPC results of hydrolyzed polymers[d]			Branch density[e] (1/1000 C)	Thermal transitions[f]		
						M_w (kg/mol)	PDI	$[\eta]_w$		T_g (℃)	T_m (℃)	ΔH_m (J/g)
HPE	none	0	3.00	44.6	-	36	1.5	16.8	122	–64	–17	25
I-B-1		1	0.77	5.7	2.3	10	3	9.8	94	–58	–26	9
I-B-2	3	0.3	1.29	19.2	1.4	17	1.7	11.5	90	–61	–22	15
I-B-3		0.1	1.89	28.1	0.4	23	1.7	12.3	84	–64	–20	23
I-P-1		0.5	0.84	12.5	0.9	12	1.9	11.0	90	–64	–22	22
I-P-2	4	0.3	1.60	23.8	0.3	19	1.6	13.3	89	–64	–18	17
I-P-3		0.1	1.68	25.0	0.1	59	3.0	17.7	82	–64	–17	25
I-T-1	5	0.3	1.75	26.0	0.5	29	1.5	16.8	88	–64	–20	23
I-S-1	7	0.3	1.40	20.8	0.6				83			

[a] Other polymerization conditions: catalyst 1, 0.2 mmol for I-B-1 and 0.1 mmol for all other runs; solvent, acetone (10 mL); temperature 25 ℃; time 24 h.

[b] Feed concentration of the ionic liquid comonomer.

[c] Molar percentages of comonomer in the ionomer were determined with ^{1}H NMR spectroscopy. according to: comonomer molar content $=4I_1/(9I_2) \times 100\%$, where I1 represents the integration area of the 1H NMR peak (at about 3.25 ppm) for methyl protons on the ammonium ion and I2 represents the total integration area of the peaks (0.7–1.5 ppm) for methyl and methylene protons of incorporated ethylene units..All ionomers synthesized with 3 and 4 were purified by removing Pd black. The ionomer synthesized with **5** and **7**, I-T-1 and I-S-1, respectively, were not purified by removal of Pd black.

[d] Weight-average molecular weight (M_w) and polydispersity index (PDI) of the hydrolyzed polymers were determined with the light scattering detector in triple-detection GPC characterization. Intrinsic viscosity ($[\eta]_w$) was measured using the viscosity detector.

[e] Branching density was determined with ^{1}H NMR spectroscopy.

[f] Thermal transitions were determined with DSC in the second heating ramp at a heating rate of 10 ℃/min.

polymers are black colored due to the presence of Pd black formed by the reductive decomposition of **1** during the polymerization. To obtain purified polymers, the Pd black was removed by digestion with H_2O_2 under slightly acidic conditions, rendering finally nearly white polymers free of Pd black. During the purification, the counter anion in the ionomers was first exchanged to Cl^- temporarily due to the need HCl for digestion of Pd black, and then switched back to the original anion by subsequent simple anion exchange with the respective salt. This confirms that the postpolymerization anion exchange can be conveniently employed to render ionomers having other desired counter anions.

The physical state of the resulting polymers at room temperature changes dramatically upon the use of the ionic liquid comonomer. While HPE appears as low-viscosity oil, the polymers produced in the presence of the ionic liquid comonomers change gradually to higher-viscosity oil (such as I-P-3) to sticky elastic solid (such as I-P-2) and to strongly elastic solid (such as I-P-1) with the increase of comonomer feed concentration. This also suggests the successful incorporation of the ionic comonomer, which leads to the formation of physical cross-linking within the polymers by ionic aggregation.

The resulting polymers were all characterized with ^{1}H NMR spectroscopy to confirm and quantify the comonomer incorporation. Figure 3.1 displays the ^{1}H NMR spectra of representative ionomers, I-B-2, I-P-1, and I-T-1, along with that of HPE for comparison. As expected, the homopolyethylene control sample, HPE, shows only three

characteristic peaks attributed to the methyl, methylene, and methine protons, respectively, of the hyperbranched ethylene sequences in the region of 0.7–1.5 ppm.[22] In addition to these dominant signals from ethylene sequences, characteristic signals (*a–d* in the Figure 3.1(b)) assigned to the incorporated units of **3** can be clearly identified in the spectrum of ionomer I-B-2. Among them, signal *d* at 3.25 ppm corresponds to the protons of the three methyl groups bonded to the ammonium ion; signals *b* and *c* at 4.50 and 3.73 ppm, respectively, correspond to the protons of the two methylene groups in between the ester group and the ammonium ion of the incorporated **3** as assigned in Figure 1(b). Signal *a* at 2.33 ppm, not found in the comonomer, is attributed to the methylene protons (–C*H*$_2$–C(O)O–) of the incorporated acryloyl group.[27-32] The peak is typically found in ethyleneacrylate copolymers synthesized with Pd–diimine catalysts and is indicative of 2,1-insertion of the acrylate comonomer.[27-32] Within the precision limit of 1H NMR spectroscopy, the area integration of the four peaks follows *a* : *b* : *c* : *d* = 2 : 2 : 2: 9. The same four signals are present at correspondingly very similar chemical shifts, though at different intensities, in the spectra of all other copolymers synthesized despite with the use of comonomers of different anion or at different feed concentrations (see the spectra for I-P-1 and I-T-1 in Figure 3.1(d) and (e), respectively). These spectroscopic evidences confirm the successful incorporation of the ionic liquid comonomers during the polymerization.

The molar content of the ionic liquid comonomers in all the ionomers have been quantified from their ^{1}H NMR spectra and the data are summarized in Table 3.1. In each set of ionomers synthesized with the same comonomer, increasing the comonomer feed

concentration leads to its enhanced content in the ionomer. In the I-B set of ionomers produced with **3** as comonomer increasing the feed concentration of **3** from 0.1 to 1 M leads to a pronounced increase of its content from 0.4 to 2.3 mol%. In another set synthesized with **4**, the content of **4** in the ionomers increases from 0.14 to 0.9 mol% with the increase of its feed concentration from 0.1 to 0.5 M. The change of feed concentration of the ionic liquid comonomers thus provides an effective way of tuning the content of the ionic groups in the resulting ionomers.

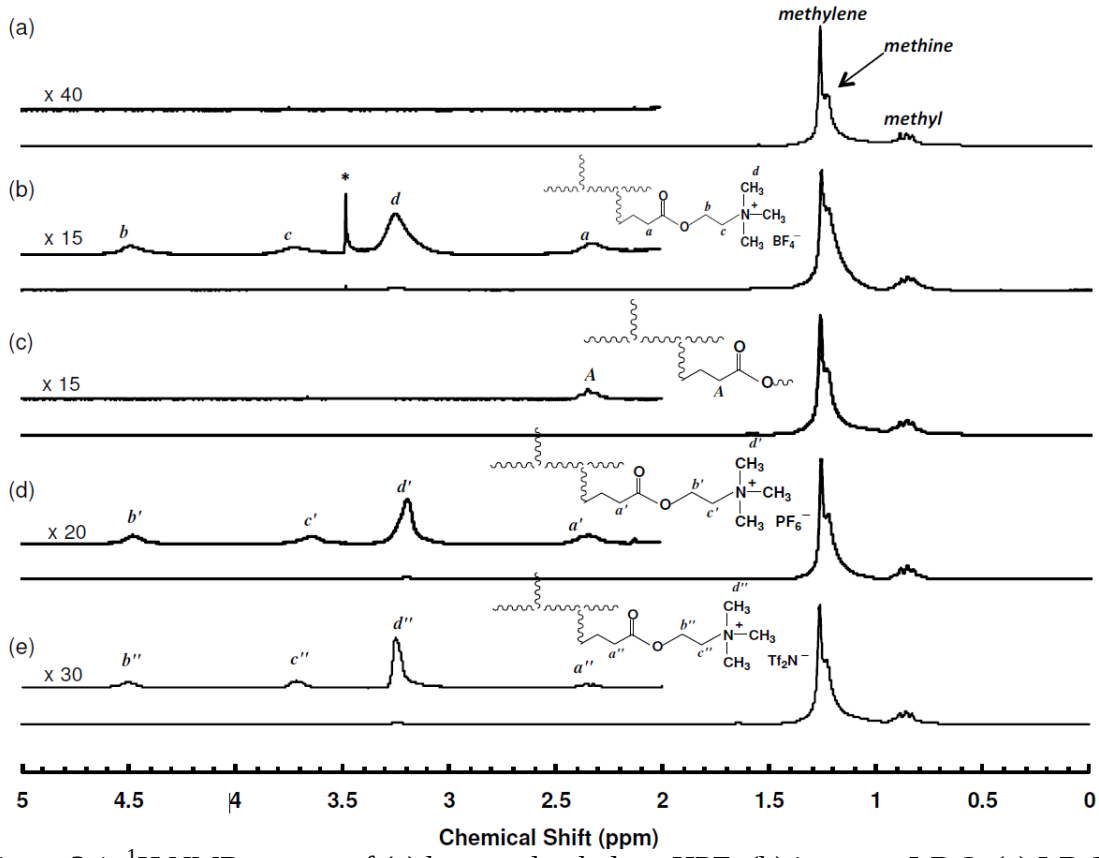

Figure 3.1. ^{1}H NMR spectra of (a) homopolyethylene HPE, (b) ionomer I-B-2, (c) I-B-2 after hydrolysis, (d) ionomer I-P-1, and (e) ionomer I-T-1. The peak denoted with an asterisk (*) results from trace THF residue present in the polymer.

Comparing the ionomers (I-B-2, I-P-2, I-T-1, and I-S-1) synthesized with the four comonomers (**3**–**5, 7**) differing in counter anion but at the same feed concentration (0.3 M), the comonomer content increases in the order: I-P-2 ≈ I-T-1 ≈ I-S-1 < I-B-2. Along with the above-noted failure of polymerization in the presence of **2** or **6**, this result demonstrates the significant effect of the counter anion on the copolymerization. The effect is reasoned to result primarily from the different coordinating power of the anions to the cationic Pd center that catalyzes the polymerization. Though catalyst **1** contains an $SbF6^-$ anion, anion exchange should occur between **1** and the comonomer during the polymerization given the excessive ionic liquid commoner relative to **1**. While BF_4^-, PF_6^-, Tf_2N^- and SbF_6^- are very weakly coordinating anions, TfO^- has been reported to be moderately weak coordinating and Cl^- is strongly coordinating.[33] The complete inhibition of the polymerization in the presence of **2** and **6** with Cl^- and TfO^- respectively, indicates the significant coordination of the anion to the Pd center, which makes ethylene/comonomer coordination/insertion difficult and thus poisons the catalytic center. Though BF_4^-, PF_6^-, Tf_2N^-, and SbF_6^- are generally very weakly coordinating, the different comonomer content data found with I-B-2, I-P-2, I-T-1, and I-S-1 suggest that BF_4^- is least coordinating among the four while PF_6^-, Tf_2N^- and SbF_6^- have similar but slightly higher coordinating power relative to BF_4^-.

Besides the tetralkylammonium-containing comonomers (**2**–**7**) investigated above, we have also attempted to use another imidazolium-containing acrylate-type ionic liquid comonomer with BF_4^- counter anion, 1-[2-(acryloyloxy)ethyl]-3-butyl-imidazolium tetrafluoroborate, in this copolymerization system. However, no

polymerization occurred in the presence of this imidazolium-containing acrylate comonomer, indicating catalyst poisoning by the imidazolium cation. The catalyst poisoning most likely results from the reaction of the imidazolium group with the Pd center in **1** to form N-heterocyclic carbene ligated Pd complex(es). In this regard, azolium salts have been the most versatile precursors for the synthesis of Pd complexes of N-heterocyclic carbenes by their simple reaction with Pd sources.[34] The finding thus excludes the use of imidazolium-containing ionic liquid monomer in this polymerization system.

Branching density (per 1000 carbons) in the ethylene sequences of the ionomers has been quantified from their ^{1}H NMR resonance signals within the region of 0.7–1.5 ppm. The data are also listed in Table 3.1. While the control non-ionic HPE has a branching density of 122 branches per 1000 carbons, all the ionomers have slightly lowered branching density in the range of 82–94 branches per 1000 carbons. This shows that the comonomer incorporation reduces slightly the branching density in the ethylene sequences, which is in agreement with the results noted in other ethylene-acrylate copolymers synthesized with **1** in our earlier works.[27-32] Nevertheless, the high branching density data suggests the hyperbranched chain topology of the ionomers with a hyperbranched polyethylene skeleton tethered with pendant ionic groups (see Scheme 3.1 for a schematic drawing of the ionomer). The hyperbranched topology results from the chain walking mechanism of the Pd–diimine catalyst.[21-23] Previously, ionomers of hyperbranched/dendritic chain topology have been synthesized but in only very limited cases, either through sophisticated multi-step processes with post-polymerization

ionization or through the use of specially designed multifunctional ionic monomers.[35–38] Relative to those reports, the HBPE ionomers are synthesized herein advantageously via a single-step one-pot catalytic polymerization with the use of commercially available monomer stocks.

The incorporation of the polar ionic groups changes dramatically the solvent solubility/dispersibility of the ethylene copolymers. While the non-ionic HPE is only soluble in nonpolar or low-polarity solvents such as toluene, chloroform, THF, *n*-hexane, *etc.*, the ionomers synthesized herein (except I-P-3 with lowest content of ionic groups) are dispersible in highly polar solvents like DMF in addition to the nonpolar or low-polarity solvents. However, the dispersed ionomer chains in these solvents tend to form physical cross-linking due to strong ionic aggregation. We have observed that dilute dispersions (about 2 mg/mL) of the iononomers in THF could not pass through a filtration membrane having pore size of 20 nm while the solution of HPE could. The strong ionic aggregation also makes their molecular weight determination through direct GPC measurement difficult. To facilitate the GPC measurements, we have managed to cleave off the tetralkylammonium ion groups from the ionomers through basic hydrolysis of the ester linkage that connects each tetralkylammonium ion to the hyperbranched backbone, while without affecting the backbone. Representatively, Figure 3.1(c) shows the ^{1}H NMR spectrum of hydrolyzed I-B-2, which confirms the absence of the tetralkylammonium ions. The hydrolyzed ionomers were successfully characterized with triple-detection GPC. Figure 3.2 shows their GPC elution curves recorded with the refractive index detector. Their absolute weight-average molecular

weight (M_w), polydispersity index (PDI), and weight-average intrinsic viscosity ($[\eta]_w$) are summarized in Table 3.1. These molecular weight data, though obtained from their hydrolyzed ones, should well present those of the ionomers given their low content of ionic groups.

All the ionomers, along with HPE, exhibit monomodal GPC elution curve as shown in Figure 3.2. Compared to another homopolyethylene sample (M_w = 115 kg/mol; PDI = 1.3) synthesized with **1** at the same condition but in low-polarity CH_2Cl_2 as solvent,[39] HPE synthesized herein in acetone has a significantly lowered M_w of 36 kg/mol with a PDI of 1.5. This is reasoned to result from the coordinating capability of acetone to the cationic Pd center, rather than the reduced ethylene solubility in acetone. Our earlier results have shown that reducing ethylene pressure in non-coordinating CH_2Cl_2 has no significant effect on polymer molecular weight.[59]

In each set of ionomers, the ionomers generally show reduced M_w value with the increase of the ionic comonomer content due to the enhanced chain breaking reactions after comonomer incorporation. For example, with the increase of comonomer content from 0.4 to 2.3 mol%, the M_w decreases from 23 kg/mol for I-B-3 to 17 kg/mol for I-B-2 and 10 kg/mol for I-B-1. Meanwhile, the ionomers generally show broadened molecular weight distribution compared to HPE with relatively higher PDI values. Figure 3.3 shows the Mark-Houwink plot of the hydrolyzed I-B set of ionomers, along with HPE for comparison, obtained from triple-detection GPC characterization. For brevity, the curves for the other ionomers are not included therein. In general, all the hydrolyzed

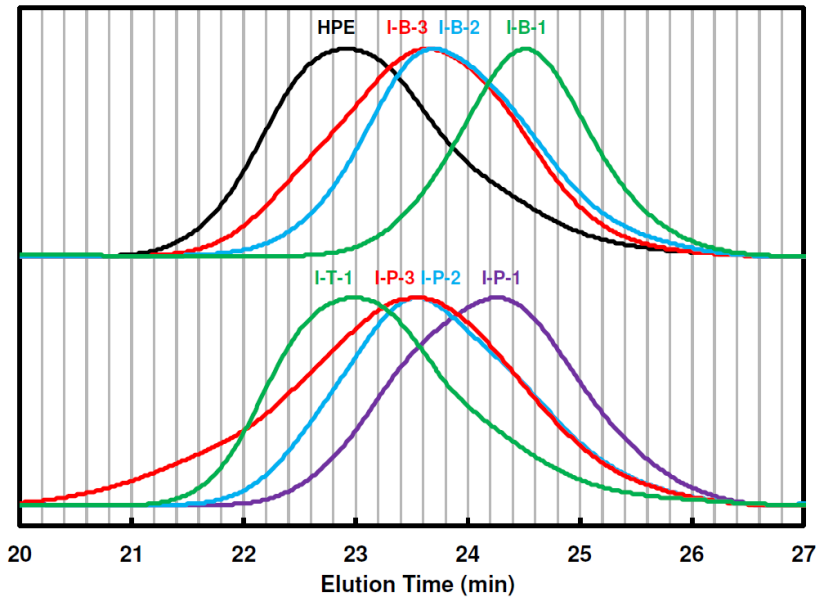

Figure 3.2 GPC elution curves of HPE and the hydrolyzed ionomers recorded with the refractive index detector in their characterization with triple-detection GPC (undertaken with THF as mobile phase at 1 mL/min and 33 ℃).

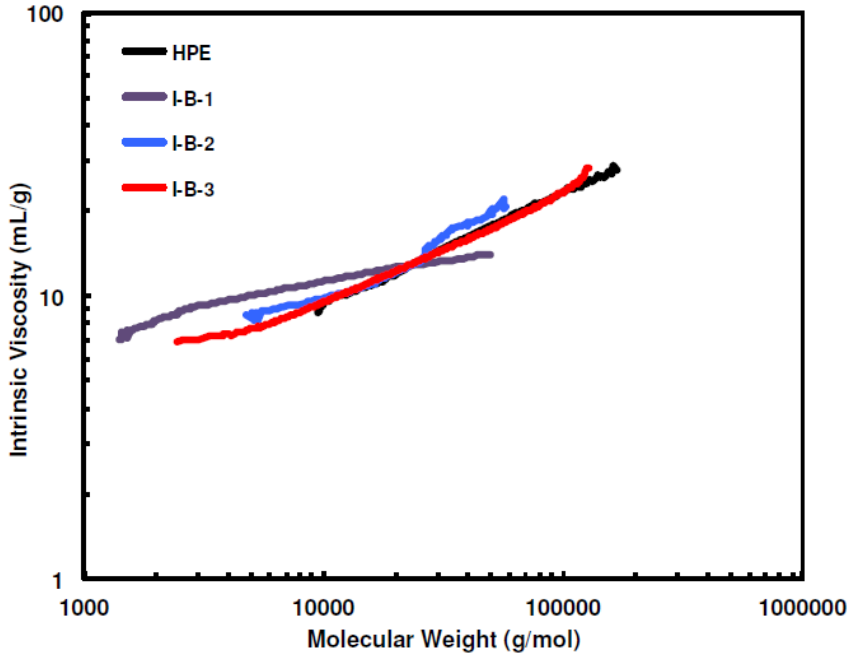

Figure 3.3 Mark-Houwink plot of the hydrolyzed I-B set of ionomers and HPE.

ionomers (including I-P and I-T sets of ionomers) show nearly overlapping intrinsic viscosity curves as HPE within their respective molecular weight range, indicating their similar hyperbranched chain topology. Meanwhile, the results also confirm that the incorporation of the ionic liquid comonomer has negligible effect on catalyst chain walking and copolymer chain topology.

3.3.2 Solid State Structure and Thermal Properties of HBPE Ionomers

Solid state structure/morphology of random ionomers has been extensively studied over the past decades.[1-4,40] Though a number of models have been proposed,[40-45] the exact structure of ionomers has not yet been fully elucidated.[46] Nevertheless, it is generally accepted that ion pairs in ionomers aggregate to form multiplets (quadruplets, sextuplets, and higher aggregates) and, at sufficiently high ion content, large ion-rich clusters may develop. Behaving as a separate phase, the clusters exhibit their own glass transition temperature (T_g).[46] To investigate their nanoscale structure, the HBPE ionomers synthesized herein have been characterized with X-ray scattering, which is widely used in the structural studies of ionomers.[1-4,40-46] Figure 3.4 shows X-ray scattering patterns (intensity of scattered X-rays as a function of scattering vector, q) of two representative ionomers, I-B-1 and I-B-3 with ion content of 2.3 and 0.4 mol%, respectively, as well as that of a hyperbranched homopolyethylene reported in our earlier work[27] for the purpose of comparison. The homopolymer shows only a single "amorphous" polymer peak at 13.6 nm^{-1}, which results from randomly oriented polyethylene backbones and is typically noted for polyethylenes.[14,17-19] Though having

significantly different ion content, the two ionomers show very similar scattering patterns. Both ionomers show two isotropic scattering peaks at correspondingly identical *q* values, with a broad "ionomer" peak centered at *ca.* 4.9 nm^{-1} (*d*-spacing of 1.3 nm) in addition to the same amorphous polymer peak (13.6 nm^{-1}) as observed in the homopolyethylene. Ionomers typically exhibit a broad isotropic scattering peak between 0.5 and 10 nm^{-1}, which is traditionally attributed to interaggregate scattering from the ionic aggregates dispersed in the amorphous region.[17-19,40-48] Herein, the "ionomer" peak confirms the presence of the ionic aggregation in the two ionomers. Increasing the ion content from I-B-3 to I-B-1 leads to a small increase in the relative intensity of the "ionomer" peak in reference to the "amorphous" polymer peak but without changing its shape, indicating the slightly enhanced concentration of ionic aggregates at the higher ion content. On the basis of the nearly identical shape of their "ionomer" peaks, the type/nature of the ionic aggregates (*i.e.*, multiplets or clusters) in the two ionomers is reasoned to remain unchanged from I-B-3 to I-B-1.

Several structural models have been developed to interpret and fit the X-ray scattering data of ionomers.[40-44] Among them, the most prevalent is that proposed by Yarusso and Cooper,[44] which has been used to interpret a wide array of scattering data. This model attributes the "ionomer" peak to interparticle interference between spherical, monodisperse, electron-rich scatters arranged with liquidlike order in a matrix of lower electron density.[44] Fitting of the scattering data with the model renders the radius of ion-rich region and the radius of an excluded volume region surrounding each aggregate that limits the extent to which the ionic aggregates can pack together in space.[44,47,48] Winey

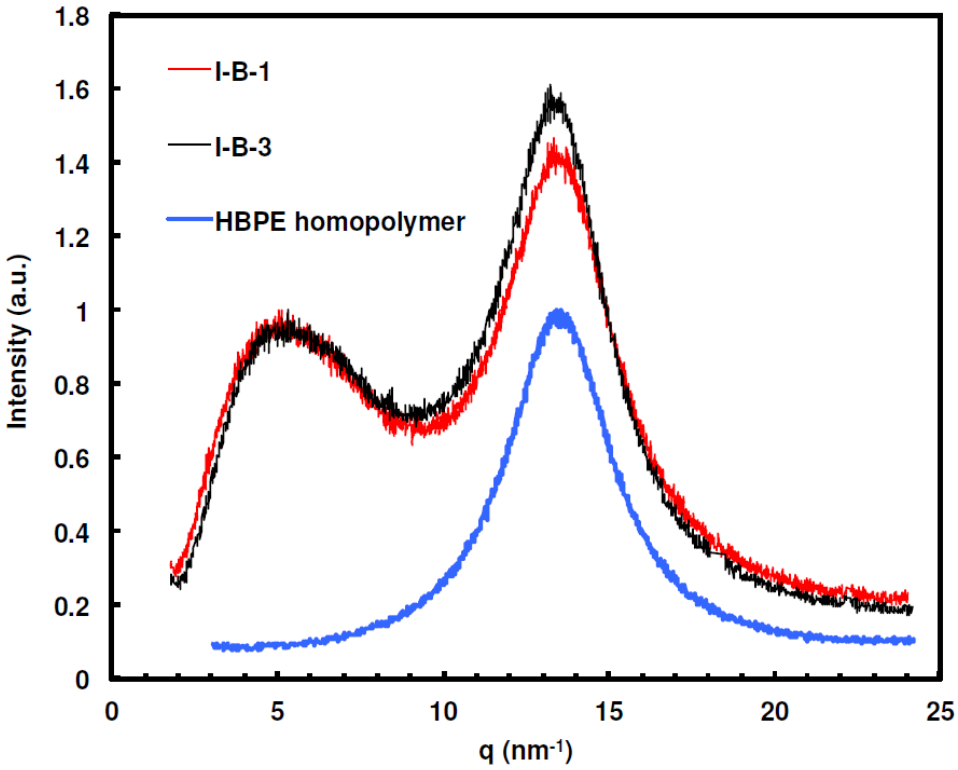

Figure 3.4 X-ray scattering of I-B-1, I-B-3, and a hyperbranched polyethylene homopolymer synthesized in our earlier work.[27]

et al. have demonstrated that the size of spherical ionic aggregates, obtained by fitting the "ionomer" peak with the Yarusso-Cooper model, in an amorphous copper-neutralized poly(styrene-*ran*-methacrylic acid) ionomer agrees well with that measured directly by scanning transmission electron microscopy (STEM).[47,48] Herein, we have attempted to fit the scattering data of I-B-1 and I-B-3 with the Yarusso-Cooper model. However, due to the breath of the "ionomer" peak, we find it is difficult to have much confidence in the size data obtained by fitting.

The ionomers have been characterized with DSC for their thermal properties and the effects of the incorporation of the ionic liquid comonomers. Figure 3.5 plots the

DSC heat flow curves of the various ionomers and HPE. Their thermal transition data are summarized in Table 3.1. Typical of hyperbranched homopolyethylenes,[22] HPE exhibits a glass transition (from −74 to −55 ºC) with the middle of the transition (T_g) at −64 ºC and a weak broad melting endotherm (spanning the temperature range of −58 to 20 ℃) with peak maximum at Tm ≈ −17 ℃ and $\Delta H_m \approx 25$ J/g. Though very close, the two transitions in HPE can be distinguished from each other without severe overlapping. These two thermal transitions, attributed to the hyperbranched polyethylene matrix, are also present in the heat flow curves of the ionomers. However, compared to HPE, a slight increase in T_g and a slight decrease in T_m, along with the weakening and narrowing of the melting endotherm (*i.e.*, a reduction in ΔHm) are found with the ionomers. Such effects become more pronounced with the increase of the content of the ionic liquid comonomer. For example, in the I-B set of ionomers synthesized with **3** as comonomer, T_g increases slightly from −64 ºC for I-B-3 to −61 ºC for I-B-2 and to −58 ℃ for I-B-1. Such a significant change in T_g was not found in hyperbranched ethylene copolymers synthesized with non-ionic acrylates as the comonomer in our earlier works.[27-32] Typically noted in ionomers,[49-53] the increased matrix T_g should result from the suppression of polyethylene segmental motion by the interchain association of the ionic groups, which is increasingly pronounced with the increase in the ion content. Concomitantly, T_m decreases in the I-B set from −20 ºC to −22 and −26 ℃, respectively, along with the reduction of ΔH_m from 23 J/g to 15 and 9 J/g, respectively, indicating that the comonomer incorporation disrupts crystallite formation.[27-32] In addition, an increasingly significant overlapping between the two transitions is noticed with the increase in the ion content. With I-B-1, it becomes difficult to discern the high

temperature end of the glass transition and the low-temperature end of the melting endotherm.

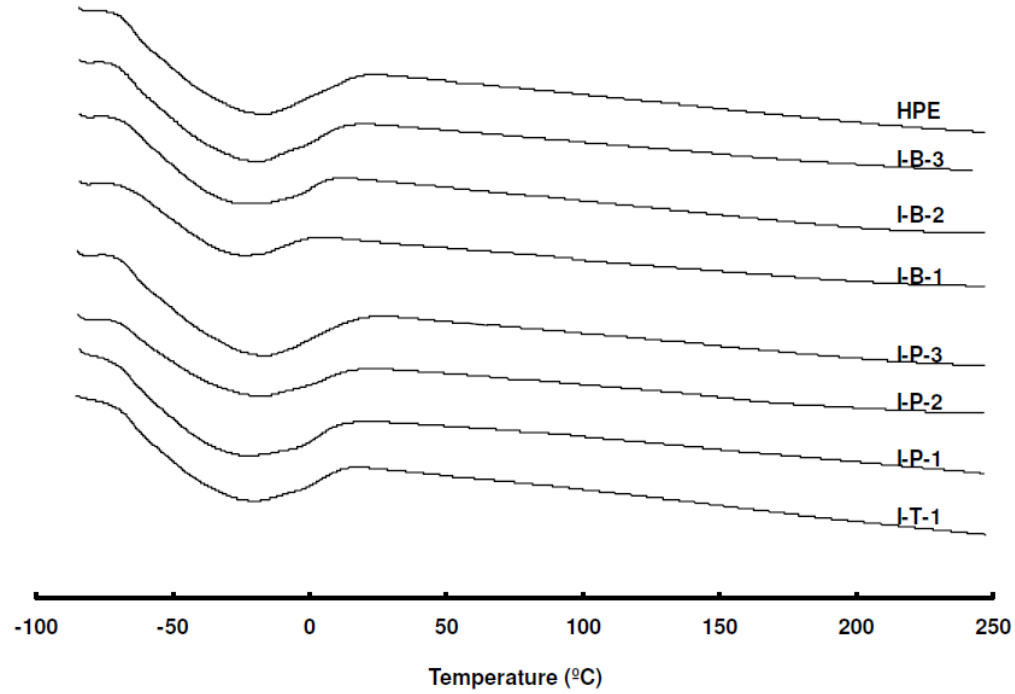

Figure 3.5 DSC heat flow curves of the ionomers and homopolyethylene HPE. The curves were taken from the second heating ramp at 10 ℃/min.

For ionomers containing ion-rich clusters, a second glass transition resulting from the clusters, beside the matrix glass transition, can often be detected through dynamic mechanical analysis (DMA) or DSC. Relative to DSC, DMA is often more sensitive to detect the secondary glass transition.[49-53] In consequence, the observation of the second glass transition with DMA or DSC is often considered as the fingerprint evidence for the presence of ionic clusters in the ionomers. For all the ionomers herein, an obvious second glass transition is not found in their DSC curves (with temperature up to 250 ℃) within the precision limit as shown in Figure 3.5. However, this cannot

completely rule out the existence of the ionic clusters in these ionomers since very weak transitions may not be detected with DSC.[5] We have also attempted to undertake the characterization of the ionomers with DMA. However, ionomer films or bars suitable for common bending or stretching DMA tests could not be prepared, due to their low molecular weight and/or hyperbranched topology.

On the basis of their X-ray scattering data, we reason, nevertheless, that the ionic aggregates in these ionomers should be predominantly multiplets with negligible clusters though we do not have DMA evidence to fully rule out the existence of clusters. It is generally considered that spherical multiplets have a diameter below *ca.* 0.6 nm while the diameter of clusters is on the order of *ca.* 1–10 nm.[44,45] The "ionomer" peak herein is centered at a *d*-spacing of 1.3 nm. This *d*-spacing value is lower than those of typical "ionomer" peaks found in ionomers featured with clusters.[5,17-20,48] For example, the "ionomer" peak of a copper-neutralized poly(styrene-*ran*methacrylic acid) ionomer having a cluster diameter of *ca.* 1.0 nm is centered at 1.7 nm (q = 3.7 nm^{-1}).48 It is thus more reasonable to consider the ionic aggregates in the ionomers herein to be multiplets rather than clusters.

3.3.3 Melt Rheological Properties of HBPE Ionomers

Due to the involvement of strong ionic aggregation, the incorporation of ionic groups has long been demonstrated to significantly impact the flow behaviour of ionomers by increasing enormously melt viscosity and relaxation times. Melt rheology

of ionomers, mainly those with linear backbone and negatively charged ions, have been extensively investigated.[54,55] However, to the best of our knowledge, rheology of ionomers with a hyperbranched backbone has not yet been studied. For ionomers with a linear backbone, their flow behaviour is often affected by both chain entanglements and ionic aggregation unless their backbone chain length is far below the entanglement molecular weight. It is thus difficult to separate the relaxation mechanisms due to chain entanglements and ionic interactions.[56,57] With the HBPE ionomers herein, the effects of chain entanglements on the flow behaviour is eliminated since chain entanglements are absent given their hyperbranched backbone topology and relatively low molecular weight (M_w up to 30 kg/mol for nearly all ionomers). Due to their highly compact chain topology, hyperbranched polyethylenes typically have significantly enhanced entanglement molecular compared to their linear analogues.[58] Previously, we have shown that a high-molecular-weight hyperbranched polyethylene (M_w = 161 kg/mol) exhibits the Newtonian flow behaviour without the involvement of chain entanglements.[59,60] The effect of ionic aggregation on the viscoelastic properties of the ionomers can thus be advantageously isolated and the changes in the flow properties of the HBPE ionomers should thus result solely from the physical cross-linking by ionic aggregation as shown below.

Small amplitude dynamic oscillatory measurements were undertaken on the HBPE ionomers (I-B-1 to I-B-3, I-P-1 and I-P-2) and control non-ionic HPE within the general temperature range of 35–135 ℃ to investigate the effects of the ionic aggregation on their linear viscoelastic properties. Figure 6 shows the master curves of

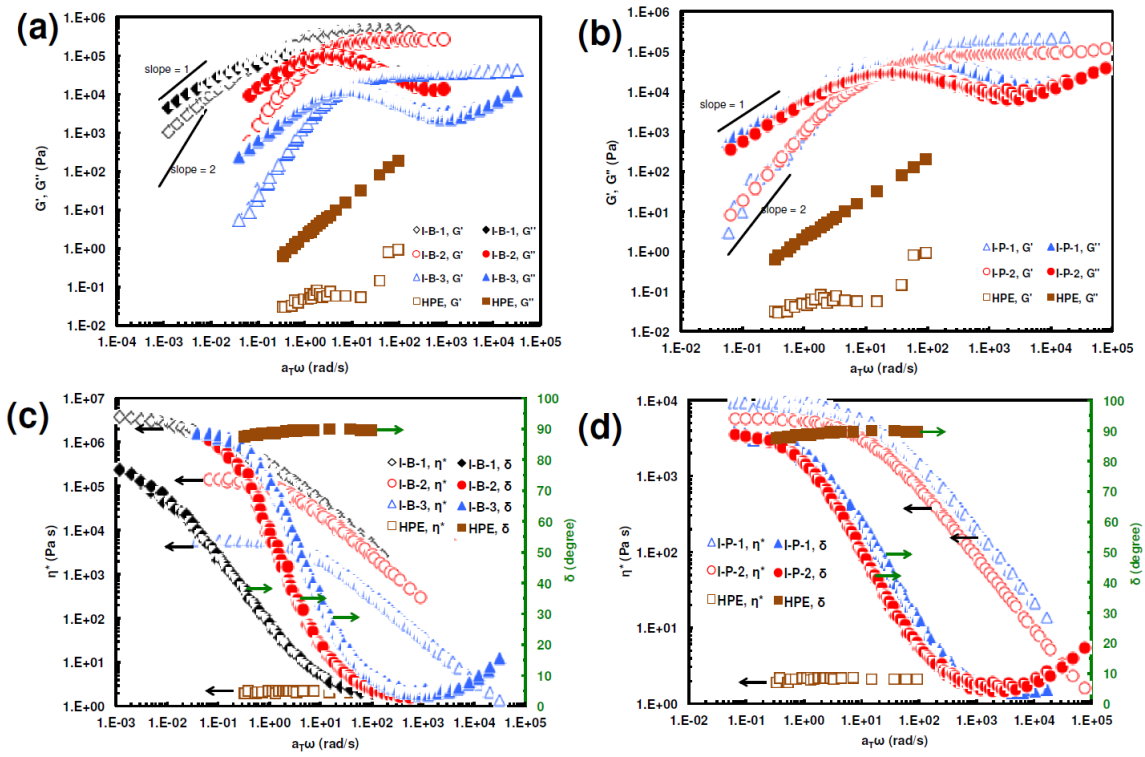

Figure 3.6 Master curves of (a and b) dynamic moduli G′ and G″; (c and d) complex viscosity (η*) and phase angle (δ) for the ionomers and HPE at the reference temperature of 95 ℃. All the master curves were constructed with the data measured at minimum five different temperatures in the general temperature range of 35–135 ℃.

dynamic moduli (G′, G″), complex viscosity (η*), and phase angle (δ) at the reference temperature of 95 ℃. The master curves were constructed by superimposing the data measured at minimum five different temperatures. Time temperature superposition is found to be valid for all the samples characterized, within the temperature and frequency ranges employed herein, despite their different ion content. Previously, time-temperature superposition has been reported[49,50,61-64] for quite a few linear ionomers with neutralized

carboxylate or sulfonate ions below a certain ion content (*e.g.*, 6 mol% for sodium-neutralized poly(styrene-*co*-methacrylic acid) ionomers [61]).

As expected based on our earlier rheological studies on hyperbranched polyethylenes,[59,60] the non-ionic control polymer, HPE, exhibits the typical Newtonian flow behaviour with a low but constant η^* (2.2 Pa s) and a constant δ (90 °) within the precision limit over the full investigated frequency range. Its G'' value ($G'' \propto \omega$) is always dominant over G' within the whole frequency range with no crossover between the two curves, confirming its predominantly viscous flow behaviour with negligible elasticity. Characteristic of hyperbranched and dendritic polymers, this flow behaviour confirms the absence of chain entanglements in HPE. Considering their similar hyperbranched topology and even lower molecular weight relative to HPE, we can conclude that chain entanglements should also be absent in the ionomers herein.

Dramatic changes in the flow behaviour yield upon the incorporation of the tetralkylammonium ions into the ionomers. These include the enormous enhancements in the magnitude of G', G'', and η^*, as well as the changes in the shape of their curves (see Figure 3.6). In both I-B and I-P set of ionomers, the G' and G'' curves are significantly and continuously raised with the gradual increase of ion content. Meanwhile, a rubbery plateau in G' and a relaxation peak in G'' are observed clearly in every ionomer, confirming the concept that the ionic aggregates act as the physical cross-links to impart elastomeric behaviour to these materials.[49,50] With the absence of chain entanglements, the relaxation peak in G'' should result solely from the dynamic

ion association-dissociation process or "ion hopping".[54,65-67] With the I-B set (see Figure 3.6(a)), one can find that the relaxation peak shifts continuously to lower frequency (from 6 to 3 and to 0.7 rad/s) with the increase of the ion content (from I-B-3 to I-B-2 and to I-B-1). The peak position is related to the strength of the forces holding the ionic aggregates. The results thus confirm that the strength or the density of physical cross-linking increases with the increase of the ion content in the ionomers.[49] With the I-P set, the change in the G″ peak position between I-P-1 and I-P-2 is not as evident as those in the I-B set possibly due to the relatively smaller change in the ion content.

A crossover between the G′ and G″ curves is found in each ionomer (see Figure 3.6(a) and (b)). In the I-B set, the crossover frequency (ω_c) is reduced (from 5.3 to 2.2 and to 0.2 rad/s) with the increase in ion content (from I-B-3 to I-B-2 and to I-B-1). In consequence, the terminal relaxation time (τ) calculated from the inverse of ω_c increases concomitantly from 0.19 to 0.45 and to 5 s. The terminal or Newtonian zone with $G' \propto \omega^2$ and $G'' \propto \omega$ is reached at the low frequency end at around 0.06 rad/s for all the ionomers characterized except I-B-1 with the highest ion content. For I-B-1, the terminal zone is not reached yet even at a lower frequency of 0.001 rad/s, with the slopes of its G′ and G″ curves still deviating significantly from those characteristic of terminal flow. These results verify that the ionic association delays terminal relaxation, which occurs via ion hopping, and renders longer terminal relaxation time upon the increase in the strength of ionic association following the increasing ion content.[56,57,65-67]

The plateau modulus (G_N^0 listed in Table 3.2) of the rubbery plateau resulting

from ionic aggregation increases significantly upon the increase in ion content in both sets of ionomers. In the I-B set, it increases by more than one order of magnitude (from 0.037 to 0.46 MPa) from I-B-3 to I-B-1. This confirms the increase of physical cross-linking density since G_N^0 is proportional to the cross-linking density according the theory of rubber elasticity.[56,57]

In sharp contrast to the Newtonian viscosity plateau observed in HPE over the whole frequency range, the distinct shear-thinning is noticed in the η* curve of each ionomer, with the lowfrequency end approaching to the Newtonian zone. The zero-shear viscosity (η_0) has been calculated by fitting the η* curve with the Cross equation,68 with the values listed in Table 3.2. The ion incorporation dramatically enhances η_0. In the I-B set of ionomers, η_0 increases from 6.1×10^3 to 1.5×10^5 and to 4.4×10^6 Pa s with the gradual increase in ion content from I-B-3 to IB-1. Relative to the low η_0 value (2.2 Pa s) of non-ionic HPE having even a higher M_w, the magnitude of increase in η_0 with I-B-3 and I-B-1 is nearly 3 thousand and 2 million times, respectively.

Table 3.2 Rheological parameters of the ionomers and HPE at reference temperature of 95 ℃.

Sample	η_0 (Pa s)	τ (s)	E_a (kJ/mol)	G_N^0 (MPa)
I-B-1	$4.4 \cdot 10_6$	5	124	0.46
I-B-2	$1.5 \cdot 10_5$	0.45	113	0.26
I-B-3	$6.1 \cdot 10_3$	0.19	112	0.037
I-P-1	$8.9 \cdot 10_3$	0.033	92	0.21
I-P-2	$5.8 \cdot 10_3$	0.069	98	0.09
HPE	2.2		50	

The flow activation energy (E_a) of the ionomers was calculated by fitting the

shifting factors, obtained in the course of time-temperature superposition, to the Arrhenius equation. Excellent fitting with R^2 greater than 0.999 was achieved with each ionomer. The E_a values are also listed in Table 3.2. In general, the activation energy increases significantly upon ion incorporation in the ionomers. In the I-B set of ionomer, it increases from 112 to 124 kJ/mol from I-B-3 to I-B-1, which are much higher than the value of 50 kJ/mol found with HPE.

3.4 Conclusions

A direct polymerization strategy has been successfully developed herein for the synthesis of HBPE ionomers containing tetralkylammonium ions, through direct catalytic copolymerization of ethylene with acrylate-type ionic liquid comonomers having different counter anions (**3**–**5**, **7**). The polymerization is facilitated with the use of Pd–diimine catalyst **1**, which shows remarkable stability towards the highly polar tetralkylammonium ions. Four sets of HBPE ionomers (I-B-1 to I-B-3, I-P-1 to I-P-3, I-T-1, and I-S-1) with different tetralkylammonium ion content (up to 2.3 mol%) and different counter anions (BF_4^-, PF_6^-, Tf_2N^-, and SbF_6^-) have been synthesized. With this strategy, the content of the ionic groups in the ionomers can be easily tuned by changing the feed concentration of the ionic liquid comonomers in the copolymerization. The counter anion of the ionic liquid comonomer has been shown to significantly affect the copolymerization. At the same comonomer feed concentration, the highest comonomer incorporation was achieved with **3** having the least coordinating BF_4^- while no polymerization occurred in the case with **2** or **6** having strongly coordinating Cl^- or

moderately coordinating TfO^-. Relative to the non-ionic HPE, the incorporation of the ionic groups has been demonstrated to significantly impact the structural, thermal, and rheological properties of the ionomers due to the formation of ionic aggregates. Through X-ray scattering, ionic aggregates are demonstrated to exist in the ionomers, presumably in the predominant form of multiplets. Through DSC characterization, ion incorporation increases matrix T_g, and reduces Tm and ΔH_m. The most evident impact of ion incorporation is on the melt rheological properties of the ionomers. Acting as physical cross-linkages, the presence of ionic aggregates in the ionomers leads to enormous enhancements in h0 and terminal relaxation times, and imparts the ionomers with typical elastomeric properties. Generally, such effects are increasingly pronounced with the increase of ion content in the ionomers. With their noncrystalline hyperbranched chain topology and possession of the desired positively charged tetralkylammonium ions, we are in the course of investigating various interesting applications of this unique class of polyethylene-based ionomers in nanocomposites and catalysis, with results to be subsequently reported.

3.5 References

1. Eisenberg, A.; Kim, J.-S. *Introduction to Ionomers*; John Wiley & Sons: New York, 1998.
2. *Ionomers: Synthesis, Structure, Properties and Applications*; Tant, M. R.; Mauritz, K. A.; Wilkes, G. L., Eds.; Blackie Acad. Press: London, 1997.
3. *Ionomers: Characterization, Theory, and Applications*; Schlick, S., Ed.; CRC Press:

Boca Raton, FL, 1996.

4. Grady, B. P. *Polym. Eng. Sci.* **2008**, *48*, 1029–1051.
5. Aitken, B. S.; Buitrago, C. F.; Heffley, J. D.; Lee, M.; Gibson, H. W.; Winey, K. I.; Wagener, K. B. *Macromolecules* **2012**, *45*, 681–687.
6. Weiss, R. A.; Agarwal, P. K. *J. Appl. Polym. Sci.* **1981**, *26*, 449–462.
7. Landoll, L. M.; Breslow, D. S. *J. Polym. Sci., Part A: Polym. Chem.* **1989**, *27*, 2189–2201.
8. Dassaud, J. P.; Gallot, B.; Guyot, A.; Spitz, R.; Beautemps, J. P.; Williams, C.; Bourgaux, C.; Eisenberg, A. *Polym. Adv. Tech.* **1994**, *5*, 79–89.
9. Lee, J. A.; Kontopoulou, M.; Parent, J. S. *Polymer* **2005**, *46*, 5040–5049.
10. Zhang, M.; Kim, H. K.; Chalkova, E.; Mark, F.; Lvov, S. N.; Chung, T. C. M. *Macromolecules* **2011**, *44*, 5937–5946.
11. Zhang, M.; Yuan, X.; Wang, L.; Chung, T. C. M.; Huang, T.; deGoot, W. *Macromolecules* **2014**, *47*, 571–581.
12. Clark, T. J.; Robertson, N. J.; Kostalik IV, H. A.; Lobkovsky, E. B.; Mutolo, P. F.; Abruña, H. D.; Coates, G. W. *J. Am. Chem. Soc.* **2009**, *131*, 12888–12889.
13. Robertson, N. J.; Kostalik IV, H. A.; Clark, T. J.; Mutolo, P. F.; Abruña, H. D.; Coates, G. W. *J. Am. Chem. Soc.* **2010**, *132*, 3400–3404.
14. Baughman, T. W.; Chan, C. D.; Winey, K. I.; Wagener, K. B. *Macromolecules* **2007**, *40*, 6564–6571.
15. Aitken, B. S.; Lee, M.; Hunley, M. T.; Gibson, H. W.; Wagener, K. B. *Macromolecules* **2010**, *43*, 1699–1701.
16. Aitken, B. S.; Buitrago, C. F.; Heffley, J. D.; Lee, M.; Gibson, H. W.; Winey, K. I.;

Wagener, K. B. *Macromolecules* **2012**, *45*, 681–687.

17. Seitz, M. E.; Chan, C. D.; Opper, K. L.; Baughman, T. W.; Wagener, K. B.; Winey, K. I. *J. Am. Chem. Soc.* **2010**, *132*, 8165–8174.
18. Buitrago, C. F.; Alam, T. M.; Opper, K. L.; Aitken, B. S.; Wagener, K. B.; Winey, K. I. *Macromolecules* **2013**, *46*, 8995–9002.
19. Buitrago, C. F.; Jenkins, J. E.; Opper, K. L.; Aitken, B. S.; Wagener, K. B.; Alam, T. M.; Winey, K. I. *Macromolecules* **2013**, *46*, 9003–9012.
20. Choi, U. H.; Middleton, L. R.; Soccio, M.; Buitrago, C. F.; Aitken, B. S.; Masser, H.; Wagener, K. B.; Winey, K. I.; Runt, J. *Macromolecules* **2015**, *48*, 410–420.
21. Guan, Z.; Cotts, P. M.; McCord, E. F.; McLain, S. J. *Science* **1999**, *283*, 2059–2062.
22. Dong, Z.; Ye, Z. *Polym. Chem.* **2012**, *3*, 286–301.
23. Ye, Z.; Xu, L.; Dong, Z.; Xiang, P. *Chem. Commun.* **2013**, *49*, 6235–6255.
24. Mecking, S.; Johnson, L. K.; Wang, L.; Brookhart, M. *J. Am. Chem. Soc.* **1998**, *120*, 888–899.
25. Tang, J.; Tang, H.; Sun, W.; Radosz, M.; Shen, Y. *J. Polym. Sci., Part A: Polym. Chem.* **2005**, *43*, 5477–5489.
26. Ittel, S. D.; Johnson, L. K., Brookhart, M. *Chem. Rev.* **2000**, *100*, 1169–1204.
27. Wang, J.; Ye, Z.; Joly, H. *Macromolecules* **2007**, *40*, 6150–6163.
28. Zhang, K.; Wang, J.; Subramanian, R.; Ye, Z.; Lu, J.; Yu, Q. *Macromol. Rapid Commun.* **2007**, *28*, 2185–2191.
29. Wang, J.; Zhang, K.; Ye, Z. *Macromolecules* **2008**, *41*, 2290–2293.
30. Ye, J.; Ye, Z.; Zhu, S. *Polymer* **2008**, *49*, 3382–3392.
31. Morgan, S.; Ye, Z.; Zhang, K.; Subramanian, R. *Macromol. Chem. Phys.* **2008**, *209*,

2232–2240.

32. Xu, Y.; Campeau, P.; Ye, Z. *Macromol. Chem. Phys.* **2011**, *212*, 1255–1262.
33. He, H.; Zhong, M.; Luebke, D.; Nulwala, H.; Matyjaszewski, K. *J. Polym. Chem., Part A: Polym. Chem.* **2014**, *52*, 2175–2184.
34. Kantchev, E. A. B.; O'Brien, C. J.; Organ, M. G. *Angew. Chem. Int. Ed.* **2007**, *46*, 2768–2813.
35. Schwab, E.; Mecking, S. *J. Polym. Sci., Part A: Polym. Chem.* **2005**, *43*, 4609–4617.
36. Tamaki, M.; Taguchi, T.; Kitajyo, Y.; Takahashi, K.; Sakai, R.; Kakuchi, T.; Satoh, T. *J. Polym. Sci., Part A: Polym. Chem.* **2009**, *47*, 7032–7042.
37. Monmoton, S.; Lefebvre, H.; Costa-Torro, F.; Fradet, A. *Macromol. Chem. Phys.* **2008**, *209*, 2382–2389.
38. Schüler, F.; Kerscher, B.; Beckert, F.; Thomann, R.; Mülhaupt, R. *Angew. Chem. Int. Ed.* **2013**, *52*, 455–458.
39. Xiang, P.; Ye, Z.; Morgan, S.; Xia, X.; Liu, W. *Macromolecules* **2009**, 42, 4946–4949.
40. Mauritz, K. A. *J. Macromol. Sci., Rev. Macromol. Chem. Phys.* **1988**, *C28*, 65–98.
41. Marx, C. L.; Caufield, D. L.; Cooper, S. L. *Macromolecules* **1973**, *6*, 344–353.
42. MacKnight, W. J.; Taggart, W. P.; Stein, R. S. *J. Polym. Sci., Polym. Symp.* **1974**, *45*, 113–128.
43. Roche, E. J.; Stein, R. S.; Russell, T. P.; MacKnight, W. J. *J. Polym. Sci., Polym. Phys. Ed.* **1980**, *18*, 1497–1512.
44. Yarusso, D.; Cooper, S. L. *Macromolecules* **1983**, *16*, 1871–1880.
45. Eisenberg, A. *Macromolecules* **1970**, *3*, 147–154.

46. Eisenberg, A.; Hird, B.; Moore, R. B. *Macromolecules* **1990**, *23*, 4098–4107.
47. Benetatos, N. M.; Smith, B. W.; Heiney, P. A.; Winey, K. I. *Macromolecules* **2005**, *38*, 9251–9257.
48. Benetatos, N. M.; Heiney, P. A.; Winey, K. I. *Macromolecules* **2006**, *39*, 5174–5176.
49. Weiss, R. A.; Fitzgerald, J. J.; Kim, D. *Macromolecules* **1991**, *24*, 1071–1076.
50. Weiss, R. A.; Yu, W.-C. *Macromolecules* **2007**, *40*, 3640–3643.
51. Greener, J.; Gillmor, J. R.; Daly, R. C. *Macromolecules* **1993**, *26*, 6416–6424.
52. Kim, J.-S.; Jackman, R. J.; Eisenberg, A. *Macromolecules* **1994**, *27*, 2789–2803.
53. Han, S.-I.; Im, S. S.; Kim, D. K. *Polymer* **2003**, *44*, 7165–7173.
54. Register, R. A.; Prud'homme, R. K. Melt Rheology. In *Ionomers: Synthesis, Structure, Properties and Applications*; Tant, M. R.; Mauritz, K. A.; Wilkes, G. L., Eds.; Blackie Acad. Press: London, 1997.
55. Tant, M. R.; Wilkes, G. L. *J. Macromol. Sci., Rev. Macromol. Chem. Phys.* **1988**, *C28*, 1–63.
56. Weiss, R. A.; Zhao, H. *J. Rheol.* **2009**, *53*, 191–213.
57. Ling, G. H.; Wang, Y.; Weiss, R. A. *Macromolecules* **2012**, *45*, 481–490.
58. Xu, Y.; Xiang, P.; Ye, Z.; Wang, W.-J. *Macromolecules* **2010**, *43*, 8026–8038.
59. Ye, Z.; Zhu, S. *Macromolecules* **2003**, *36*, 2194–2197.
60. Ye, Z.; AlObaidi, F.; Zhu, S. *Macromol. Chem. Phys.* **2004**, *205*, 897–906.
61. Eisenberg, A.; Navratil, M. *Macromolecules* **1973**, *6*, 604–612.
62. Kim, J.-S.; Yoshikawa, K.; Eisenberg, A. *Macromolecules* **1994**, *27*, 6347–6357.
63. Greener, J.; Gillmor, J. R.; Daly, R. C. *Macromolecules* **1993**, *26*, 6414–6424.

64. Nishioka, A.; Takahashi, T.; Masubuchi, Y.; Takimoto, J.; Koyama, K. *J. Rheol.* **2002**, *46*, 1325–1339.

65. Vanhoorne, P.; Register, R. A. *Macromolecules* **1996**, *29*, 598–604.

66. Chen, Q.; Tudryn, G. J.; Colby, R. H. *J. Rheol.* **2013**, *57*, 1441–1462.

67. Colby, R. H.; Zheng, X.; Rafailovich, M. H.; Sokolov, J.; Peiffer, D. G.; Schwarz, S. A.; Strzhemechny, Y.; Nguyen, D. *Phys. Rev. Lett.* **1998**, *81*, 3876–3879.

68. Cross, M. M. *J. Colloid Sci.* **1965**, *20*, 417–437.

Chapter 4

Hyperbranched Polyethylene Ionomers Containing Self-Encapsulated Palladium Nanoparticles as Catalysts for C–C Cross Coupling and Alkyne Semi-Hydrogenation Reactions

Abstract

In this Chapter, the synthesis of HBPE ionomer encapsulating self-supported Pd(0) nanoparticles (NPs) as efficient and recyclable supported Pd catalysts is demonstrated. The Pd(0) NPs were immobilized on the ionomer matrix through ionic interaction directly during the copolymerization of ethylene with polymerizable ionic liquid comonomer using Pd–diimine catalyst [(ArN=C(Me)–(Me)C=NAr)Pd(CH_3)(N≡CMe)]$^+SbF_6^-$ (Ar = 2,6–(*i*Pr)$_2C_6H_3$) (**1**). The resulting ionomer supported Pd(0) catalysts (HBI1–HBI4) have been utilized in carbon-carbon cross coupling reactions (Suzuki and Heck reactions) and semi-hydrogenation of alkynes. In all reactions, the catalysts have shown high catalytic activity and recyclability. For example, in semi-hydrogenation of phenylacetylene (PA), the reaction turnover frequency (TOF) can reach 1015 h^{-1} with the high styrene selectivity of 96%. Semi-hydrogenation reactions of other terminal alkynes including 4-phenyl-1-butyne, 1-ethynylcyclohexene and 1-heptyne were also carried out with supported catalyst HBI2 with high alkene selectivity. Furthermore, the HBI2 Pd catalyst has also shown good activity in both Heck and Suzuki reactions.

4.1 Introduction

Transition metal nanoparticles (NPs), especially palladium (Pd) NPs have been widely used in catalytic applications including carbon-carbon cross-coupling reactions [1] and hydrogenation of unsaturated organic chemicals.[2,15] Owing to highly active surface atoms resulting from their high surface-to-volume ratio and high surface energy, these NPs with outstanding catalytic performance have attracted increasing attention in last ten years. Despite the extensive development of metal NP catalysts in both industry and research areas, the main objective is always to find suitable stabilizers (supports) which could be used to: (1) prevent NPs from aggregation, (2) minimize catalyst leaching in reaction, (3) increase the catalyst recyclability, (4) endow high catalytic selectivity, and (5) render supported metal NPs compatible with different solvents. To achieve above goals, a great variety of materials including carbon, silica, metal oxides, double hydroxides, dendrimers, and polymers have been used as support to immobilize the metal NPs.[3]

In the chemical industry, supported Pd NP catalysts with good catalyst recyclability and reusability are preferred. However, due to the poor contact and the problem of mass transfer between the reactant and catalytic active site on solid supports, the overall catalytic activity and efficiency of these catalysts are usually not high. Moreover, due to differences in the chemical and physical environments on the solid support, the supported catalyst systems always contain multiple catalytic active sites with different catalytic behaviors. Particularly, in the case of semi-hydrogenation of

alkynes with H_2 the over-hydrogenation of desired alkenes to alkanes can easily occur before the complete conversion of reactants by these solid supported Pd NP catalysts in the absence of suppression additives (i.e., Lindlar catalyst).[4] Polymers including both cross-linked and soluble polymers have also been used as supports for Pd NPs. The cross-linked polymers usually have drawbacks similar to those of inorganic solid supports, while soluble polymers-supported Pd NP catalysts allow the catalytic reactions to be carried out under homogeneous conditions thus maximizing the catalyst performance and avoiding different catalytic behaviors caused by multiple active sites.

Usually, immobilization of metal NP catalysts on polymer supports results from electrostatic and/or steric stabilization. Though there are reports on the successful immobilization of Pd NP catalysts on polymer supports through exclusive steric stabilization mechanism,[5] the presence of different functional groups (e.g., thiols, disulfides, amines, nitriles, carboxylic acids and phosphines) on polymers is believed to enhance interactions between supports and metal NPs. To obtain polymer supports containing specific functionalities, special synthesis and/or polymer post-polymerization modification is usually required. Extensive studies have been done with the use of various types of functionalized polymers.[6] Among these, poly(ionic liquids) (PILs) and ionomers, as a special type of polymers containing ionic groups covalently bonded to the polymer backbone, however, have only rarely been used as supports for Pd NP catalysts. In 1976, Hirai has first reported that a colloidal palladium supported on the polyion complex composed of poly(acrylic acid) and poly(ethylene imine) catalyzes highly selective hydrogenation of conjugated diolefions to monoolefins.[7] Twenty years

later, Mu et al. reported the synthesis of ionic copolymers containing imidazolium IL-like units as support for rhodium NPs.[8] The supported NPs showed unprecedented lifetime and activity in arene hydrogenation. Later, Chen et al. developed the first polystyrene (PS)-supported task-specific ionic liquids as efficient metal scavenging (e.g., CuI, $Pd(OAc)_2$, Pd(0), and $IrCl_3$) materials.[9] The Pd-soaked polymers have shown high catalytic activity in the solvent-free hydrogenation of styrene to ethylbenzene. Moreover, Ohtaka et al. successfully stabilized Pd NPs by a polyion complex composed of poly(4-chloromethylstyrene-co-(4-vinylbenzyl)tributylammonium chloride) and poly(arylic acid) for the Suzuki and Heck reactions in water.[10] However, in their case, the multiple-step synthesis of polymers was required and the resulting supported catalysts showed the obvious decrease of activity after only four recycle runs. In another study, Liu et al. synthesized 1-aminoethyl-3vinylimidazolium bromide ([VAIM]Br) grafted on the cross-linked polymer polydivinylbenzene (PDVB) as support to immobilize Pd NPs.[11] Though Heck reactions with different aryl iodides were studied under solvent-free conditions, the catalytic activities were general low in this case due to the problem of mass transfer during the reactions by using the insoluble cross-linked copolymer as support. More recently, Yu et al. prepared and applied a porous copolymer of an IL with divinylbenzene as support for Pd NPs.[12] The supported Pd NP catalyst was extremely active for Suzuki reactions and had excellent recyclability. In all above previous studies, PIL or ionomer-supported Pd NP catalysts with high catalytic activity and recyclability for cross-coupling reactions are difficult to obtain and semi-hydrogenation of alkynes with H_2 by using this type of catalysts has never been reported. Thus, it is important to

find a supported Pd NPs that can be used as a versatile catalyst for most of Pd-catalysed reactions.

Recently, we have demonstrated the facile one-pot synthesis of hyperbranched polyethylene (HBPE) ionomer containing tetralkylammonium ions via chain walking copolymerization of ethylene and polymerizable acrylate-type ionic liquid comonomers, [2-(acryloyloxy)ethyl]trimethylammonium tetrafluoroborate (**3**), by using Pd–diimine catalyst, $[(ArN{=}C(Me){-}(Me)C{=}NAr)Pd(CH_3)(N{\equiv}CMe)]^+SbF_6^-$ (Ar = 2,6–(*i*Pr)$_2$C$_6$H$_3$) (**1**). All synthesized ionomers have shown interesting rheological properties due to the interchain aggregations caused by the incorporated ionic groups. In addition, during the polymerization, it was found that Pd NPs have been autonomously immobilized on the HBPE ionomers through the ionic interactions. In this study, we are utilizing these HBPE ionomers encapsulating self-supported Pd(0) nanoparticles as efficient and recyclable supported Pd catalysts. All ionomer catalysts are found to be dispersible in the common organic solvents (THF, DMF, hexane, etc.). With the unique solubility properties, these catalysts have shown outstanding catalytic performances for the Heck and Suzuki cross-coupling reactions, as well as semi-hydrogenation of alkynes. To the best of our knowledge, this is the first report on the using of ionomer-supported Pd NP catalysts for both cross-coupling and semi-hydrogenation reactions.

4.2 Experimental Section

4.2.1 Materials

All manipulations involving air- and/or moisture-sensitive materials were conducted in an N_2-filled glovebox or by using Schlenk techniques. The Pd–diimine catalyst, $[(ArN{=}C(Me){-}(Me)C{=}NAr)Pd(CH_3)(N{\equiv}CMe)]^+SbF_6^-$ (Ar = 2,6–(iPr)$_2$C$_6$H$_3$) (**1**), was synthesized by following a literature procedure.[13] Ultrahigh-purity N_2 (>99.97%) and polymer-grade ethylene (both obtained from Praxair) were purified by passing sequentially through a 3 Å molecular sieve column and an Oxiclear column before use. Ultrahigh-purity H_2 (>99.999%) was used as received. Deionized Water was obtained from a Barnstead Nanopure II water purification system. Hydrochloric acid (37.4 wt % in water), potassium hydroxide (≥ 90%), K_2CO_3 (granular powder, certified ACS grade), *N, N*-dimethylformamide (DMF) (HPLC, ≥ 99%), HPLC-grade tetrahydrofuran (THF) and methanol were received from Fisher Scientific and all used as received. Acetone from Fisher Scientific were deoxygenated and dried with molecular sieve before use. Natural graphite was purchased from Aldrich (product number 332461). It was sieved through a 500 μm mesh sieve to remove large particles before use. Other chemicals, including, [2-(acryloyloxy)ethyl]trimethylammonium chloride solution (**2**, 80 wt. % in H_2O), acetonitrile (anhydrous, 99.8%), sodium tetrafluoroborate (98%), a palladium atomic absorption standard solution, containing 1,011 ppm of Pd in 5.1 wt% HCl, hydrogen peroxide (50 wt % in water), hexane (anhydrous, 99%), iodobenzene (IPh, 98%), n-butyl acrylate (BA, ≥99%), triethylamine (NEt_3, ≥99%), phenylboronic acid (PBA, >97%), tetrabutylammonium bromide (TBAB, ≥98%), bromobenzene (BrPh, 99%), 2-bromotoluene (99%), 3-bromotoluene (98%), 4-bromotoluneen (98%), 1-bromonaphthalene (97%), 1-bromo-4-nitrobenzene (99%), 4-bromoanisole (99%), 4'-bromoacetophenone (98%), 4-bromoaniline (97%), 2-

bromomesitylene (98%), phenylacetylene (98%), 4-phenyl-1-butyne (97%), 1-ethynylcyclohexene (99%), 1-heptyne (98%), sulfuric acid (ACS regent, 95.0–98.0 %), and phosphoric acid were obtained from Aldrich.

4.2.2 Synthesis of [2-(Acryloyloxy)ethyl]trimethylammonium tetrafluoroborate (3)

In a flask, the commercially obtained aqueous solution of **2** (18.6 g) was washed with excessive acetone and then dried under vacuum, yielding viscous pure ionic liquid **2** (14.7 g, 76 mmol). It was then redissolved in anhydrous acetonitrile (50 mL), followed with the addition of sodium tetrafluoroborate (8.5 g, 77.5 mmol). The mixture was stirred at room temperature for 48 h and then filtered to remove the sodium chloride precipitate. The filtrate was concentrated, and then precipitated in 50 mL of diethyl ether. After three times of wash with diethyl ether, the precipitated white crystal was collected and dried under vacuum at room temperature, rendering **3** (14.4 g, 59 mmol; yield 78%).

4.2.3 Copolymerization of Ethylene with 3 for Synthesis of HBPE Ionomers (HBIs) Encapsulating Self-Supported Palladium Nanoparticles (Pd NPs)

All copolymerizations of ethylene and **3** were conducted in a 50 mL Schlenk flask equipped with a magnetic stirrer at room temperature. The typical polymerization procedure was as follow. The flask sealed with a rubber septum was first flame-dried under vacuum. After being cooled to room temperature, the reactor was purged with ethylene for at least three times, and then filled with ethylene to a pressure of 1 atm. A

solution of Pd–diimine catalyst **1** (0.08 g, 0.1 mmol) in acetone (5 mL) was injected into the reactor, followed with the immediate addition of the comonomer solution (0.74 g of **3** in 5 mL acetone). During the polymerization, ethylene pressure was kept constant by continuous feed from a cylinder. After 24 h, the black ionomer product containing Pd NPs was precipitated out with a large amount of methanol. The precipitate was washed with methanol three times and then dried overnight at 70 ℃ under vacuum, yield HBI2 (1.1 g).

4.2.4 Synthesis of Graphene Oxide (GO)

The synthesis of GO is followed the modified procedure reported by Marcano et al.[42]: A 9:1 mixture of concentrated H_2SO_4/H_3PO_4 was added to a mixture of graphite flakes (3.0 g, 1 wt equiv) and $KMnO_4$ (18.0 g, 6 wt equiv), producing a slight exotherm to 40 ℃. The reaction was then heated to 50 ℃ and stirred for 12 h. The reaction was cooled to room temperature and poured onto ice (400 mL) with 50% H_2O_2 (3 mL). The mixture was then centrifuged (14,000 rpm for 1h) and the supernatant was decanted away. The remaining solid material was then washed in succession with 200 mL of water until the pH of the suspension reached about 7. The suspension was then filtered through glassy carbon fiber. The filtrate obtained after filtration was the aqueous suspension of GO sheets. The final concentration of GO aqueous solution was determined by UV-Vis and ready to use.

4.2.5 Synthesis of GO/HBI Supported Pd NP Catalyst

A 1 mL aqueous suspension containing 8.2 mg of GO sheets was slowly added into 15 mL THF solution containing 2.8 mg of HBI2 under stirring. The suspension was then stirred overnight and subsequently centrifuged. The isolated solid from the centrifugation was further washed with 30 mL of THF three times and dried at room temperature, yielding 11.1 mg of supported Pd NP catalyst GO/HBI2.

4.2.6 Mizoroki-Heck Reactions Catalyzed with HBI2

A typical procedure for Mizoroki-Heck reaction of IPh and BA in DMF is as follows. The catalyst HBI2 (20 mg, containing 1.3 μmol of Pd) was dissolved in 3 mL of DMF in a 20 mL Schlenk tube equipped with a magnetic stirrer, followed with the addition of IPh (2.2 g, 10.6 mmol), BA (2.0 g, 15.9 mmol), and NEt_3 (1.6 g, 15.9 mmol). The tube was sealed with a rubber septum and was subjected to three cycles of vacuum and nitrogen refill. The mixture was then placed in an oil bath set at 100 ℃ to start the reaction. The conversion of the reaction was monitored with ^1H NMR spectroscopy.

The recycling reaction procedure is as follow. The catalyst HBI2 (75 mg. 4.9 μmol of Pd) was dissolved in 1.5 mL of DMF in a glass vial. The DMF solution containing HBI2 was then transferred into a dialysis membrane with cut-off pore size at 1,000 Da. The dialysis membrane with catalyst solution was sealed and immersed into the mixture of IPh (3.61 mmol), BA (5.42 mmol), NEt_3 (5.42 mmol) and DMF (1.5 mL) in a 20 mL Schlenk tube equipped with a magnetic stirrer. The tube was sealed with a rubber septum and was subjected to three cycles of vacuum and nitrogen refill. The tube

was then placed in an oil bath set at 100 ℃ to start the reaction. Samples were taken at specific time intervals from the solution out of the membrane in the tube and were analyzed by ^{1}H NMR spectroscopy to monitor IPh conversions. At the completion of the reaction, the sealed membrane was taken out of the tube and washed with a large amount of DMF (*ca*. 50 mL) through dialysis to remove all products. The washed membrane with HBI2 catalyst was recycled and dried for the next Mizoroki-Heck reaction.

4.2.7 Suzuki-Miyaura Reactions Catalyzed with HBI2

A typical procedure for the Suzuki-Miyaura reactions of IPh is as follows. HBI2 (25 mg, contain 1.6 μmol of Pd), IPh (0.51 g, 2.5 mmol), PBA (0.37 g, 3.0 mmol), K_2CO_3 (0.52 g, 3.75 mmol), DMF (2 mL), and water (3 mL) were combined in a clean test tube with a magnetic stirrer. The test tube was sealed and placed in an oil bath set at 100 ℃ and was stirred for 24 hours. During the reaction, the conversion of IPh was monitored with ^{1}H NMR spectroscopy.

A typical procedure for the Suzuki-Miyaura reactions of different aryl bromides is as follows. HBI2 (15 mg, contain 1.05 μmol of Pd), BrPh (0.39 g, 2.5 mmol), PBA (0.37 g, 3.0 mmol), K_2CO_3 (0.52 g, 3.75 mmol), TBAB (0.81 g, 2.5 mmol) and water (8 mL) were combined in a clean test tube with a magnetic stirrer. The test tube was sealed and placed in an oil bath set at 100 ℃ and was stirred for 24 hours. During the reaction, the conversion of BrPh was monitored by ^{1}H NMR spectroscopy.

A typical procedure for the Suzuki-Miyaura recycling reactions is as follows. HBI2 (31 mg, contain 2.0 μmol of Pd), IPh (0.51 g, 2.5 mmol), PBA (0.37 g, 3.0 mmol), K_2CO_3 (0.52 g, 3.75 mmol), DMF (2 mL), and water (3 mL) were combined in a clean test tube with a magnetic stirrer. The test tube was sealed and placed in an oil bath set at 100 ℃ and was stirred for 1 h. The conversion of IPh was determined with ^{1}H NMR spectroscopy. After reaction, the mixture was cooled down to room temperature and poured into methanol (*ca*. 40 mL). The HBI2 catalyst was precipitated out and dried for the next Suzuki-Miyaura reaction.

4.2.8 Semi-Hydrogenation Reactions Catalyzed with HBI2

All semi-hydrogenation reactions were carried out in a sealed 25 mL Schlenk flask connected to a gas balloon adaptor. A typical procedure is as follows. The reactor was first dried under vacuum. After being cooled to room temperature, the reactor was purged with H_2 for at least three times, and then filed with H_2 to a pressure of 1 atm maintained by a balloon filled with H_2. A solution of HBI2 (3.0 mg, contain 0.19 μmol of Pd) and phenylacetylene (PA, 51 mg, 0.5 mmol) in hexane (5 mL) was injected into the reactor. The conversion of PA was monitored with ^{1}H NMR spectroscopy.

A typical procedure for the semi-hydrogenation recycling reactions is as follows. A sealed 25 mL Schlenk flask connected to a gas balloon adaptor was first dried under vacuum. After being cooled to room temperature, the reactor was purged with H_2 for at least three times, and then filed with H_2 to a pressure of 1 atm maintained by a balloon filled with H_2. A solution of GO/HBI2 (11 mg, contain 0.19 μmol of Pd) and PA (51 mg,

0.5 mmol) in hexane (5 mL) was injected into the reactor. The conversion of PA was monitored with ^{1}H NMR spectroscopy. After the complete conversion of PA, the flask was vented and the GO/HBI2 Pd NP catalyst was isolated from the reaction solution by centrifugation. The isolated GO/HBI2 catalyst was further washed with THF three times and was dried at room temperature for the next semi-hydrogenation reaction.

4.2.9 General Procedure for Pd Content Measurement

To determine the content of Pd encapsulated in HBIs, the following procedure was adopted. HBI1 (10 mg) was dissolved in 1 mL of THF in a 20 mL vial, followed with the addition of 1 mL of HCl (37.5%) and 1 mL of H_2O_2 (30 wt % in water). The mixture was boiled to evaporate all THF and the residue solution was collected. This procedure was repeated at least five times to make sure the complete extraction of Pd(0) NPs encapsulated in HBIs. All collected residuals were diluted with blank solution and analyzed with atomic absorption spectroscopy. To determine the leached Pd present in the recycle reactions (in DMF, methanol and THF, respectively), a sample of the DMF, methanol, or THF solution was added into 5 mL of blank solution, followed with sonication and then measured with ICP-MS.

4.2.10 General Procedure for Cleavage of HBIs

HBI2 (ca. 30 mg) and KOH (0.2 g) were dispersed in a THF (3 mL) and methanol (1 mL) mixture in a 25 mL flask. The suspension was refluxed at 90 ℃ for 2

days and was then precipitated in methanol. The polymer precipitate was redissolved in THF and precipitated in methanol for two cycles. Finally, the cleaved polymer (*ca*. 20 mg) was dried overnight under vacuum at 70 ℃ and was subsequently characterized.

4.2.11 Characterizations and Measurements

Proton nuclear magnetic resonance (^{1}H NMR) spectra of all samples were collected on a Varian Gemini 2000 spectrometer (200 MHz) with $CDCl_3$ as the solvent. Polymer characterization with gel permeation chromatography (GPC) was carried out on a Polymer Laboratories PL-GPC220 system equipped with a differential refractive index (DRI) detector (from Polymer Laboratories) and a three-angle light scattering (LS) detector (high-temperature mini-DAWN from Wyatt Technology). The detection angles of the light scattering detector were 45, 90, and 135 º, and the laser wavelength was 687 nm. One guard column (PL# 1110–1120) and three 30-cm columns (PLgel 10-lm MIXEDB 300 × 7.5 mm) were used. The mobile phase was HPLC-grade THF and the flow rate was 1.0 mL min^{-1}. The complete GPC system, including the column and detector arrays, was maintained at 33 ℃. The mass of the polymers injected into the columns was about 1 mg. Two polystyrene narrow standards (from Pressure Chemicals) with weight-average molecular weights (M_w) of 30 and 200 kg mol^{-1}, respectively, as per the supplier were used for the normalization of light scattering signals at the three angles and the determination of interdetector delay volume and band broadening, respectively. The DRI increment dn/dc value of 0.078 mL g^{-1} was used for all cleaved polyethylenes, and the value of 0.185 mL g^{-1} was used for polystyrene. A Perkin-Elmer

Precisely AAanlyst 400 atomic absorption spectrometer was used to determine the concentration of Pd in HBIs and leached Pd in the coupling reaction solutions. A palladium atomic absorption standard solution, containing 1,011 ppm of Pd in 5.1 wt % HCl was used as the stock solution for the preparation of reference solutions with Pd concentration in the range of 0−10 ppm, which allowed the construction of a calibration curve. An aqueous solution with 11.1 vol % THF, 8.2 vol % H_2O_2 (30 wt % in H_2O), and 6.7 vol % HCl (concentrated) was used as the blank solution. ICP-MS measurement was performed on Varian instrument. UV-vis spectra of HBI samples were obtained on a Thermo Scientific Genesys 10S UV-vis spectrophotometer. HPLC-grade THF was used as the solvent. The measurements were conducted in the wavelength range of 190 to 1000 nm with an optical path length of 1.0 cm. Transition electron microscopy (TEM) images were collected on a JEOL 2010F field emission electron microscope operated at 200 kV.

4.3 Results and Discussion

4.3.1 Synthesis and Characterization of HBPE Ionomers (HBIs) Encapsulating Self-Supported Pd(0) Nanoparticles (NPs)

Pd–diimine catalysts have been extensively studied in our group, which can be used to synthesize HBPEs with unique branch-on-branch architecture.[14] Moreover, featured with low oxophilicity and high tolerance of polar functionalities, various functionalized HBPEs have been synthesized via the copolymerization of ethylene with

functionalized 1-alkene and acrylate using Pd–diimine catalyst.[14a,b] Among them, HBPE ionomer (HBI) containing ammonium ion as one of most interesting HBPEs have recently been successfully synthesized as shown in Chapter 3. It was found that the incorporated ammonium ion in HBIs can directly bind and stabilize Pd NPs formed from the decomposition of Pd–diimine catalyst during the copolymerization, rendering ionomers encapsulating Pd NPs. The resulting black HBIs encapsulating self-supported Pd(0) NPs thus can be directly used as supported Pd NP catalysts to catalyze carbon-carbon cross-coupling reactions and semi-hydrogenation of alkynes without any further treatment.

Four HBIs encapsulating Pd NPs (HBI1–HBI4) were synthesized herein by chain walking copolymerization of ethylene and **3** with a Pd–diimine catalyst **1** under an ethylene pressure of 1 atm and polymerization temperature at room temperature (ca. 25 ℃) (Scheme 4.1). Two catalyst feed amounts (0.1 and 0.375 mmol, respectively) were used for the polymerization. The feed concentration of **3** varied from 0.1 to 0.5 M, rendering HBIs with different ammonium ion content. During the polymerization, HBI gradually precipitated out in acetone. Meanwhile, Pd–diimine catalyst also underwent reductive deactivation during polymerization, providing Pd(0) NPs for the in situ immobilization process. After the completion of the polymerization, methanol as reductant was poured in to the reaction solution mixture to further precipitate HBI and further reduce the remaining Pd(II) species to Pd(0). The black viscous HBI catalyst was then obtained after drying and subsequently characterized. Polymer characterization with ^{1}H NMR spectroscopy confirms the successful incorporation of **3** in the HBIs.

Representatively, Figure S4.1 in Supporting Information shows the ^{1}H NMR spectra of HBI1 to HBI4. In addition to three characteristic peaks of HBPE within the region from 0.7 to 1.5 ppm, signals *a*-*d* in Figure S4.1 showing the incorporated units of **3** can be clearly observed in the ^{1}H NMR spectra of all HBIs. The detailed NMR peak identification has been shown in Chapter 3.

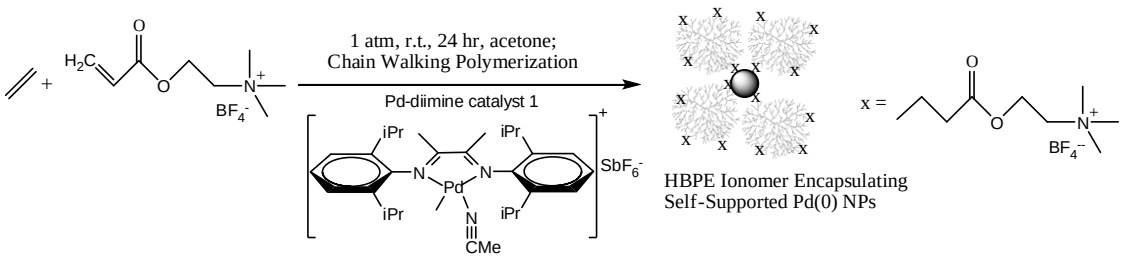

Scheme 4.1 Synthesis of hyperbranched ionomers (HBIs) encapsulating self-supported Pd(0) nanoparticles.

The resonance signal *d* at 3.25 ppm corresponding to methyl protons of the ammonium ion, as well as two resonance signals *b* at 4.49 and *c* at 3.74 ppm corresponding to two methylene units between the ester group and ammonium ion of **3** can be clearly identified. Furthermore, the signals attributable to the acrylate groups are not found, while a new triplet resonance assigned to the methylene protons of the enchained acrylate group, –C*H*$_2$–C(O)O– group at 2.33 ppm is observed in all the ^{1}H NMR spectra. The ratio of area integration of these four signals (*a*-*d*) is about 2:2:2:9 within the precision limit, which further confirms the successful incorporation of **3** in all HBIs. The molar content of **3** in each HBI sample has been calculated based on the ^{1}H NMR spectrum and the data are listed in Table 4.1. It shows that at the same amount of

catalyst **1**, the molar content of ammonium ion increases with the increase of feed concentration of **3**. The highest molar content of 2.7 mol% is found with HBI1 having the highest feed concentration (0.5 M) of comonomer **3** in the polymerization.

The content of encapsulated Pd(0) in all HBIs was determined by using atomic absorption (AA) spectroscopy after their complete extraction with H_2O_2 and HCl acid. All Pd content results determined with AA are summarized in Table 4.1. In the set of HBIs synthesized using catalyst **1** at 0.1 mmol, the Pd(0) content slightly decreases from 7.57×10^{-5} to 6.56×10^{-5} mol per gram of ionomer when the comonomer content decreases from 2.7 to 1.2 mol %. However, as the feed concentration of **3** increased from 0.3 to 0.5 M, the turn-over frequency (TOF) of ethylene dramatically decreased from 19.2 to 5.21 h^{-1}, which is in agreement with the data in Chapter 3. HBI1 has a low Pd encapsulation efficiency of 34%, while HBI2 has a higher Pd encapsulation efficiency of 85%. By increasing the catalyst feed amount to 0.375 mmol, two comonomer feed concentrations (0.1 and 0.3 M, respectively) were used to ensure the productivity of HBIs. It was found that, with the decrease of comonomer content from 1.0 to 0.3 mol %, the Pd content per gram of ionomer was also decreased, while the TOF of ethylene was increased, which gave the similar Pd encapsulation efficiency (about 66%) for both samples. Thus, to maximize the Pd encapsulation efficiency as well as the ethylene TOF, monomer feed concentration of ca. 0.3 M should be the optimum one, giving HBI with relative high comonomer incorporation while without reducing the polymer productivity.

Table 4.1. Summary of the copolymerization conditions, results, and the characterization data for all hyperbranched polyethylene ionomers

Polymer[a]	Comonomer[b]	Catalyst	Yield	C_2H_4 TOF	Comonomer Content[c]	GPC[d]			Pd Content[e]			Branching Density[f]
	(M)	(mmol)	(g)	(1/h)	(mol %)	M_n (kg/mol)	PDI	η_n (mL/g)	Pd content (10^{-5} mol/g)	Pd encap. (%)	N:Pd ratio (mol/mol)	(per 1000 C)
HBI1	0.5	0.1	0.45	5.21	2.7	4	3.7	9.0	7.57	34	11.2	87
HBI2	0.3		1.29	19.20	1.2	12	1.4	10.2	6.56	85	6.5	90
HBI3	0.3	0.375	3.63	14.40	1.0	10	1.4	9.3	6.81	66	5.3	84
HBI4	0.1		4.55	18.06	0.3	11	1.6	9.4	5.49	67	2.0	84

[a] Other polymerization conditions: solvent, acetone, 10 mL; temperature 25 ℃; time 24 h.
[b] Comonomer feed concentration.
[c] Molar percentages of comonomer in the ionomer were determined with ^{1}H NMR spectroscopy.
[d] Number average molecular weight (M_n) and polydispersity index (PDI) were determined through GPC characterization with universal column calibration.
[e] Pd content of each HBI was determined with AA spectroscopy.
[f] Branching density of ionomers was determined with ^{1}H NMR spectroscopy.

To confirm the presence of Pd NPs in HBIs, UV-Vis spectroscopy and high resolution TEM were undertaken. Figure 4.1 shows the UV-Vis spectra of THF solutions of HBIs at the same ionomer concentration of 5 mg/mL. All HBIs have strong absorbance above 500 nm, which are typical for Pd NPs as shown in previous studies.[20] High resolution TEM characterization was undertaken on HBI1 to determine the size and morphology of Pd NPs. The representative TEM images of HBI1 are shown in Figure 4.2. As shown in the Figure 4.2a, Pd NPs with size in the range of *ca*. 1–5 nm are clearly observed. Meanwhile, in Figure 4.2b, a big aggregate composed of many small Pd NPs is also noticed.

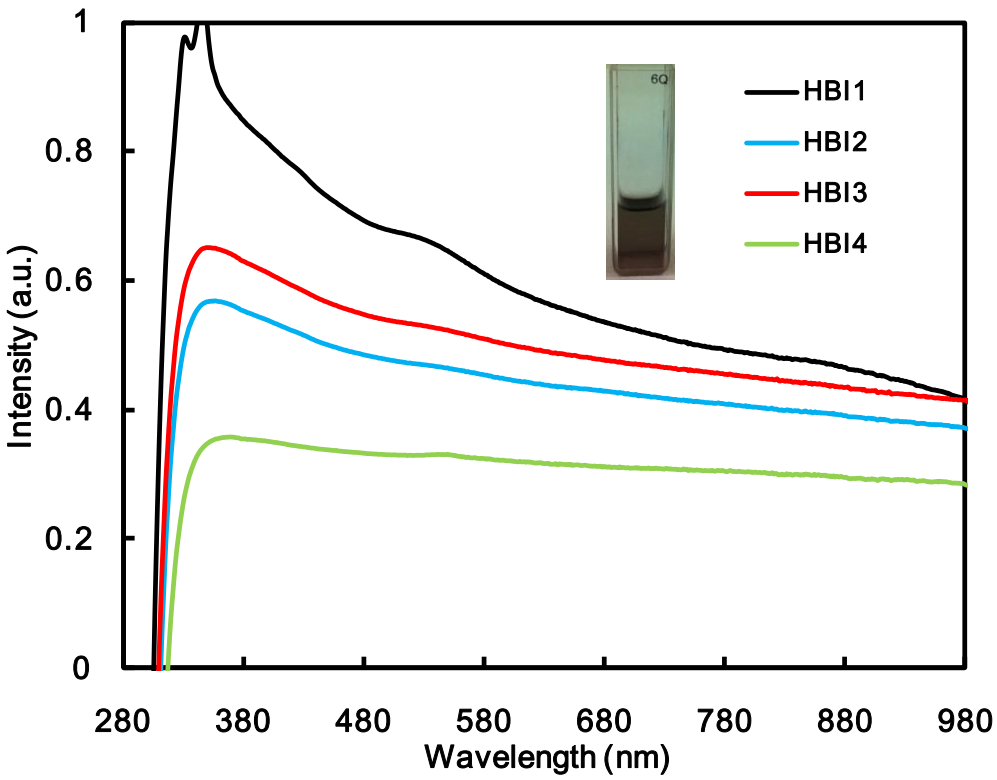

Figure 4.1 UV-Vis spectra of HBIs encapsulating Pd(0) NPs in THF

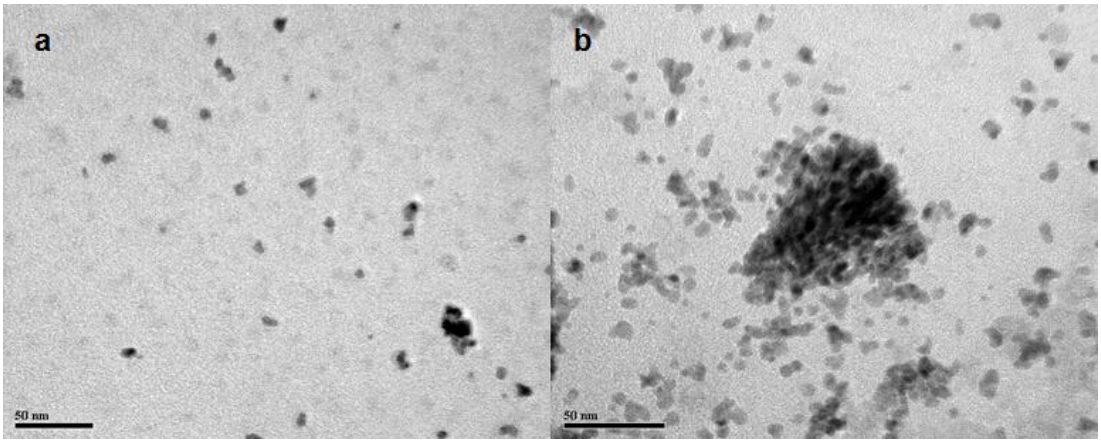

Figure 4.2. TEM micrographs of HBI1 encapsulating Pd NPs (scale bar = 50 nm).

To determine the molecular weight and molecular weight distribution of all HBIs, GPC characterization was undertaken on their cleaved polymers. The incorporated ammonium ions for all HBIs were cleaved and the structures of cleaved HBPEs were confirmed with ^{1}H NMR. A typical ^{1}H NMR spectrum of cleaved HBI1 is also shown in Figure S4.1. All cleaved HBPEs were then characterized with triple-detection GPC equipped with on-line DRI, three-angle light scattering (LS) and capillary viscosity detectors. Figure 4.3 shows the GPC elution curves and all GPC characterization results are summarized in Table 4.1. We can see that HBIs synthesized at lower feed concentration of **3** (0.1 and 0.3 M) have similar molecular weight of ca. 10 kg/mol and polydispersity index of ca. 1.5, while the HBI1 synthesized with at the higher feed concentration of **3** (0.5 M) has a much lower molecular weight of 4 kg/mol and much higher polydispersity index of 3.7. It suggests that increasing feed concentration of **3** will significantly enhance the chain termination and/or chain transfer reactions, reduce the chain propagation rate, and lead to HBI1 with much lower molecular weight and broader molecular weight distribution, and lower TOF.

4.3.2 Catalytic Application of HBIs in Semi-Hydrogenation of Alkynes

Semi-hydrogenation of alkynes to alkenes, without further over-hydrogenation to alkanes, is very important in the synthesis of fine chemicals. Lindlar catalyst ($Pd/CaCO_3$ treated with $Pb(OAc)_2$) as the most known supported Pd catalyst for semi-hydrogenation has been widely used in industry. However, the use of a large amount of toxic lead in the Lindlar catalyst will result the production of harmful wastes, which is undesired.[4] Thus, to develop new types of Pd NP catalyst having less or no toxicity but high selectivity and activity for semi-hydrogenation of alkynes, various supports including carbon, silica, metal oxides, polymers have been extensively studied.[15] For example, Na-Chiangmai et al. employed a mesocellular foam silica with ultra-large pores (MCS) as a support for immobilization of Pd catalysts for the liquid-phase selective hydrogenation of phenylacetylene.[16] However, the styrene selectivity in their case is not high (∼85%). In another study, Lee et al. synthesized a dual catalyst containing Pd and $CuFe_2O_4$ nanoparticles in a silica shell, which enabled > 98% conversion of arylacetylenes to related styrenes with a selectivity greater than 98%.[17] However, in the latter case, the catalyst synthesis was complex and the catalyst activity was not high (TOF of 91 h^{-1}). Most recently, Mitsudome et al. developed highly functionalized core-shell Pd@MPSO/SiO2 catalysts containing Pd NPs in the core and a DMSO-like matrix in the shell.[18] Although the catalysts showed excellent selectivity for the semi-hydrogenation of alkynes, the activity of catalyst was still relatively low (TOF of ca. 85 h^{-1}).

Herein, we synthesized HBIs encapsulating Pd NPs which were utilized for the semi-hydrogenation of alkynes. In the case of semi-hydrogenation of phenylacetylene (PA), all HBIs catalysts showed great styrene selectivity (> 90%) and much higher activity (> 380 h^{-1}) when compared to previously reported supported catalysts. Among these HBIs catalysts, HBI2 having the highest selectivity and activity for semi-hydrogenation of PA were also used for the semi-hydrogenation of other alkynes. The experimental results demonstrate that HBI2 has shown great alkene selectivity and catalytic activity in the hydrogenation of different alkynes. The possible reasons can be: (1) soluble HBIs catalysts allow the easy access to Pd NPs active center; (2) HBIs containing ammonium ion act as macroligand, which provides the active center with high selectivity.

The catalytic activities of HBIs were investigated in the semi-hydrogenation of terminal alkynes, such as PA, which is more reactive than internal alkynes and can be easily over-hydrogenated to alkanes as reported in previous studies. One commercially available Pd on carbon catalyst (Pd/carbon) was also tested for comparison. The hydrogenation conditions and results are summarized in Table 4.2. From the table, all HBIs show higher selectivity for styrene (> 90%) and higher activity in semi-hydrogenation reactions compared to those of Pd/carbon at the same reaction conditions. The use of HBI1 and HBI2 with higher ammonium ion content (2.7 and 1.2 mol %, respectively) showed excellent selectivity of styrene which are greater than 96% at the complete conversion of PA. This is attributed to the higher ammonium/Pd ratios in HBI1 and HBI2, which offers stronger ionic interactions with Pd NPs than in HBI3 and

Table 4.2 Semi-hydrogenation of phenylacetylene to styrene using HBI supported Pd catalysts.

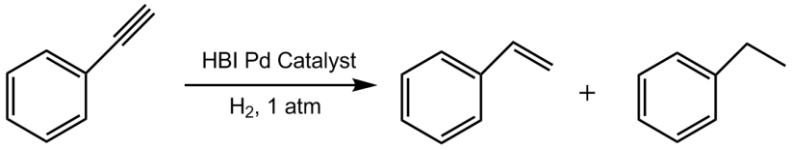

Entry[a]	Catalyst	Catalyst amount (ppm)	Temperature (℃)	Time (min)	Conversion (%)	Selectivity[b] (%)	TOF (h^{-1})
1	HBI1	394	r.t.	210	>99	98	725
2	HBI2	100	r.t.	330	52	>99	945
3	HBI2	250	r.t.	330	96	>99	698
4	HBI2	394	r.t.	150	>99	96	1015
5	HBI2	550	r.t.	90	>99	98	1212
6	HBI2	700	r.t.	60	>99	99	1429
7	HBI2	394	30	150	>99	98	1015
8	HBI2	394	40	105	>99	97	1523
9	HBI3	394	r.t.	150	>99	92	1067
10[c]	HBI3	394	r.t.	240	>99	99	667
11	HBI4	394	r.t.	420	>99	90	380
12	HBPE	1576	r.t.	150	>99	82	254
13	Pd/Carbon	2070	r.t.	45	>99	84	667
14	Pd/Carbon	376	r.t.	360	>99	87	444

[a] Other reaction condition: phenylacetylene (0.5 mmol), hexane (5 mL), H_2 (1 atm).
[b] Selectivity was determined by ^1H NMR spectroscopy.
[c] Phenylacetylene (5 mmol).

HBI4 and leads to greatly suppressed coordination of the reactive terminal alkene. The activity and selectivity of HBI2 at different catalyst feed amounts and different hydrogenation temperatures have also been investigated. As shown in Table 4.2, when the catalyst feed amount was increased, the completion of semi-hydrogenation was faster while with no change in the selectivity. When the reaction temperature was increased from room temperature to 40 ℃ at the same feed of catalyst, the time for complete conversion of PA was decreased from 150 min to 105 min while retained good selectivity. Moreover, when the reaction time was prolonged after the complete conversion of PA, the over-hydrogenation of styrene with HBIs was negligible. On the

contrary, fast over-hydrogenation of styrene to ethylbenzene occurred in the case with Pd/carbon. Figure 4.3 compares the kinetic curves for hydrogenation of PA with the use of HBI2 and Pd/carbon catalysts, respectively. In Figure 4.3a, the complete conversionof PA occurred with HBI2 at 150 minutes, with the yield of styrene remained constant at ～95% without over-hydrogenation to ethylbenzene after additional 90 min of reaction. However, with Pd/carbon, significant over-hydrogenation was observed as from both Figure 4.3b and 4.3c. To test the semi-hydrogenation of PA under a larger scale, one run (run 10) was undertaken with 10 times of loading of both PA (0.51 g) and the catalyst HBI3. The result shows that HBI3 has high selectivity of styrene (99%) in this case, but with slightly lowered activity. This may be attributed to the restricted mass transfer upon scaling up. In addition, pure HBPE without any ionic group but containing Pd particles was also carried out for the semi-hydrogenation of PA as a comparison. However, because of the much lower content of Pd particles in polymer, a large amount of HBPE was adding to the reaction media leading to the much lower activity of this HBPE catalyst (entry 12).

HBI2 was also applicable to the semi-hydrogenation of other terminal alkynes as shown in Table 4.3. Three terminal alkynes were converted into the corresponding alkenes over 93% yields. For example, 4-phenyl-1-butyne and 1-ethynylcyclohexene were obtained in excellent yields (Table 4.3, entries 1 and 2).

Furthermore, with its excellent solubility in most organic solvents (chloroform, THF, dichloromethane, chlorobenzene, DMF, and hexane), the recovery and reuse of the

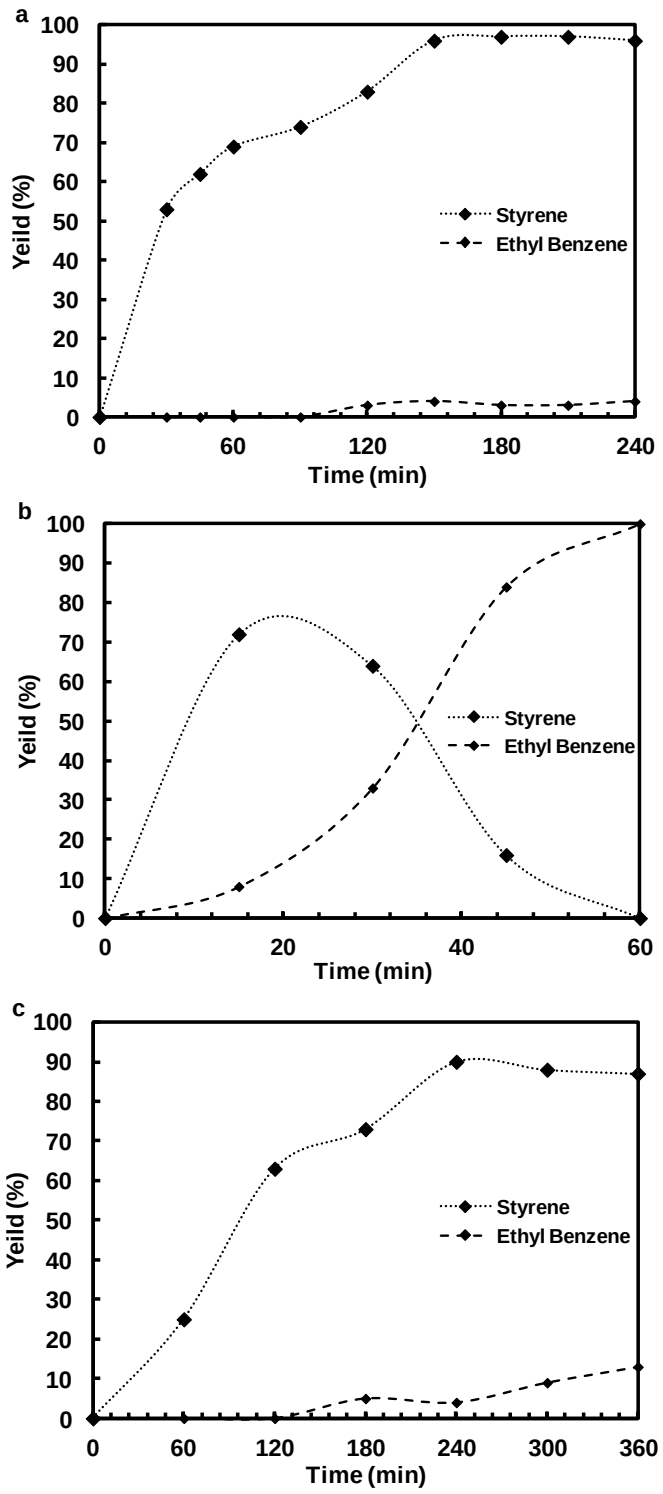

Figure 4.3 Time course for hydrogenation of phenylacetylene (a) entry 4, using HBI2 (394 ppm), (b) entry 13, using Pd/Carbon (2070 ppm), and (c) entry 14, Pd/carbon (376 ppm).

Table 4.3 Semi-hydrogenation of terminal alkynes using HBI2 Pd catalyst

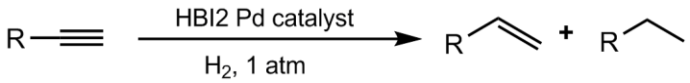

Entry[a]	Substrate	Product	Time (min)	Conversion (%)	Selectivity[b] (%)	TOF (h^{-1})
1	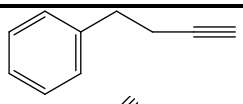	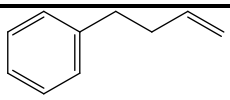	120	>99	>99	1269
2	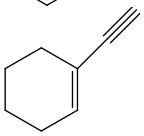	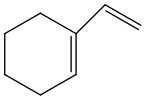	150	>99	>99	1015
3	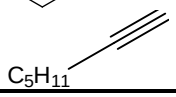	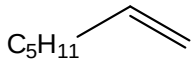	150	95	93[c]	965

[a] Other reaction condition: alkyne (0.5 mmol),HBI2 (2.9 mg, Pd: 394 ppm), hexane (5 mL), H_2 (1 atm), room temperature.
[b] Selectivity was determined by ^{1}H NMR spectroscopy.
[c] Determined by GC.

ionomer-supported HBI Pd NP catalysts is difficult. Thus we immobilized HBI2 Pd catalyst onto the graphene oxide (GO) to render recyclable heterogeneous GO/HBI supported Pd catalyst. In the case of the heterogeneous catalyst, HBI2 was tethered to the GO flakes through both ionic and CH-π interactions. It was then subsequently used for many cycles of semi-hydrogenation of PA. After each reaction, the supported catalyst was easily recycled by centrifugation. After washing three times with THF and dried, the GO/HBI2 Pd catalyst could be utilized in next semi-hydrogenation reaction. To test the recyclability of GO/HBI Pd catalyst, a six-cycle recycling experiment was carried out for the semi-hydrogenation of PA. The reaction conditions and results are summarized in Table 4.4. From the table, it shows that the styrene selectivity of each recycling reaction remained high, but with continuously decreasing activity. For example, the TOF for semi-hydrogenation of PA decreased from 1316 h^{-1} (recycling reaction entry 1) to 434 h^{-1} (recycling reaction entry 6). The reason herein may be due to

the loss of Pd NPs during the washing step. When we washed GO/HBI Pd catalyst with THF, there was always a small amount of leached free HBI which cannot be centrifuged. The free HBI with Pd NPs in the supernatant was then collected and subsequently characterized with ICP-MS to determine the Pd amount. In each recycling reaction, it shows 0.12 to 1.2 μg of Pd NPs leached out by washing. To determine the weight fraction of HBI in GO/HBI catalyst before and after recycling reaction, TGA characterization was carried out. Representatively, Figure 4.4 shows the TGA curve of GO/HBI2 catalyst before and after recycling reaction as well as the fresh pure GO sample. As seen from the curves, the weight loss in the temperature range of 400–500 ℃ is mainly due to the weight loss of HBI2. From this TGA weight loss data, the mass of tethered HBI2 has been calculated. It shows that after six recycling reactions, the bonded HBI2 on the GO is only about 1.51 mg. Compared to the fresh GO/HBI2 catalyst, 1.29 mg (46 wt %) of HBI2 was lost during the washing procedure.

Table 4.4 Recycling semi-hydrogenation of PA with GO/HBI2 Pd catalyst.

Entry[a]	Time (min)	Conversion (%)	Selectivity[b] (%)	TOF (h^{-1})	Pd Leached[c] (μg)	[Pd] Leached (%)
1	120	>99	98	1316	1.19	5.9
2	210	>99	98	752	1.22	6.0
3	230	>99	95	686	0.70	3.5
4	165	>99	98	956	0.12	0.6
5	160	>99	98	987	0.30	1.5
6	120	33	>99	434	0.56	2.8

[a] Other conditions: phenylacetylene (0.5 mmol), hexane (5 mL), H_2 (1 atm), HBI2 (2.9 mg, 380 ppm), GO (8.2 mg), room temperature.
[b] Selectivity was determined by ^{1}H NMR spectroscopy.
[c] Pd leached results were determined by ICP-MS.

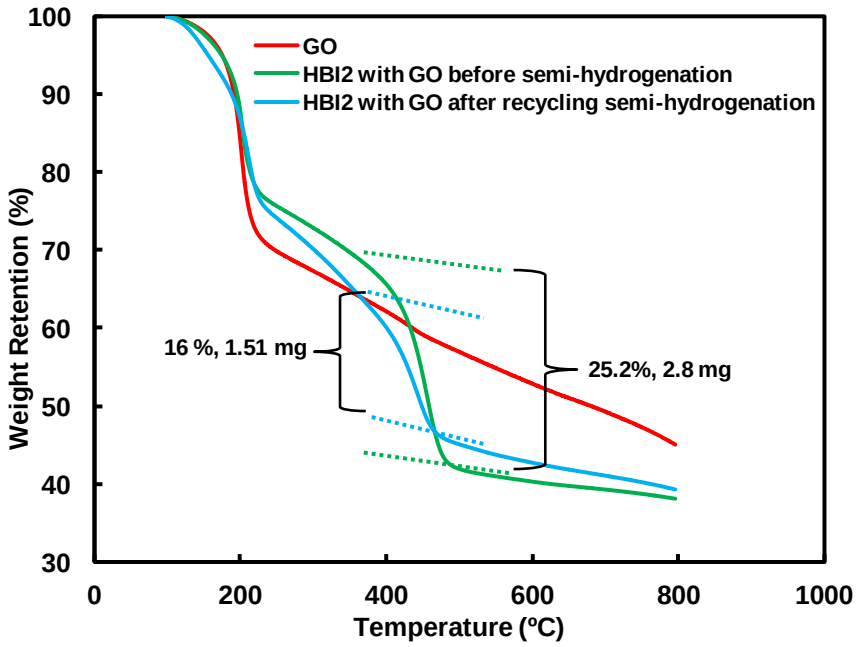

Figure 4.4 TGA curves of GO supported HBI2 before and after recycling semi-hydrogenation.

4.3.3 Catalytic Application of HBIs in Heck and Suzuki Reactions

HBI2 encapsulating Pd NPs were also used for the Heck reaction of iodobenzene (IPh) with n-butyl acrylate (BA). To investigate the catalyst activity of HBI2 in this case, a series of Heck reactions with different catalyst amounts were undertaken. The reaction conditions and results are summarized in Table 4.5. From the table we can see that the Heck reaction can be completed with HBI2 at as low as 6.2 ppm and the TOF is up to about 9,000 h^{-1}. The kinetic plots of the Heck reactions of IPh and BA are also shown in Figure 4.5. To test the recyclability of HBI catalysts, an eight-cycle recycling experiment was carried out for the Heck reaction of IPh and BA with HBI2 in a dialysis membrane with cut-off pore size at 1,000 Daltons. In each cycle, samples were taken at

specific time intervals from the solution out of the membrane in the tube and were analyzed by ^{1}H NMR spectroscopy to monitor IPh conversions. At the completion of the reaction, the sealed membrane was taken out of the tube and washed with a large amount of DMF (ca. 50 mL) through dialysis to remove all products. The washed membrane with HBI2 catalyst was recycled and dried for next Heck reaction. Table 4.6 summarizes the results obtained in the recycling experiment. From the table, in all eight runs, the conversion of > 99% was achieved in less than 6.5 h, although there was small amount of Pd leached out (from 0.36 to 2.18 wt %) in each recycle reaction. Moreover, the catalyst activity of HBI2 for Heck reaction of IPh and BA by using dialysis membrane (from 100 to 350 h^{-1}) is much lower than those without membrane (larger than 1500 h^{-1}) due to the mass transfer limitation imposed by the membrane. However, by using dialysis membrane, the recycle of the HBI2 was much easier and the additional filtration steps can be eliminated. Filtrations were usually used in previous studies with other type of Pd-based catalysts.

Table 4.5. Heck reaction of iodobenzene (IPh) and n-butyl acrylate (BA) using HBI2.

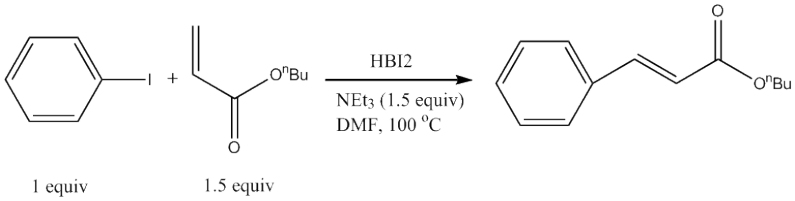

Entry[a]	Catalyst amount (ppm)	Time (h)	Conversion[b] (%)	TON	TOF (h^{-1})
1	619	1	>99	1616	1616
2	124	2	>99	8078	4039
3	31	7	>99	32320	4617
4	6.2	18	>99	161600	8978

[a] Other conditions: $[IPh]_0$ = 3.5 M, $[IPh]_0 : [BA]_0 : [NEt_3]_0$ = 1 : 1.5 : 1.5, 3 mL of DMF as solvent, T = 100 ℃.

[b] Conversion was determined by ^{1}H NMR.

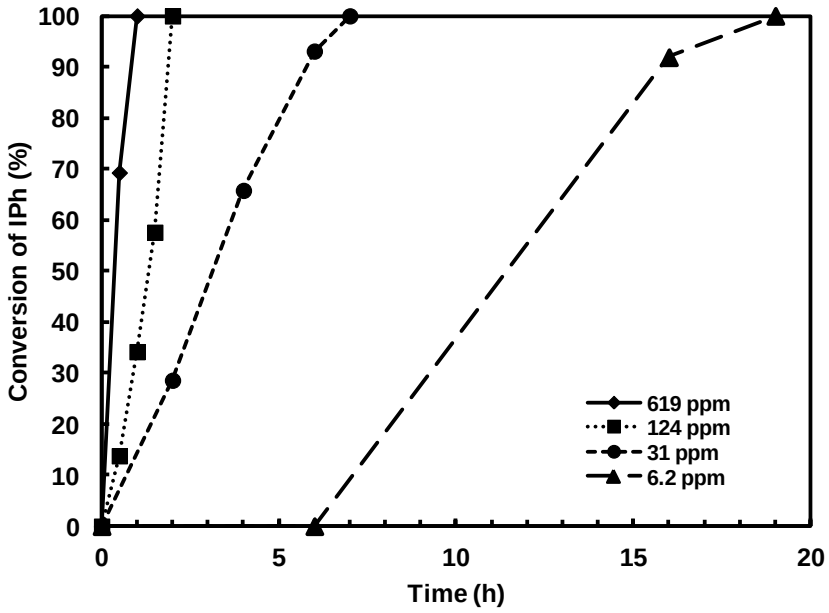

Figure 4.5 Conversion of IPh as a function of reaction time in the Heck reactions of IPh and BA with HBI2 at different Pd amounts.

Table 4.6. Eight-Cycle Recycling Heck Reactions with HBI2

Cycle[a]	Membrane (1000 Da Cut off)				
	Time (h)	Conversion[b] (%)	TOF (h^{-1})	Pd Leached[c] (μg)	[Pd] Leached (%)
1	6.5	>99	110	9.1	1.74
2	5	>99	143	5.5	1.05
3	6	>99	119	1.9	0.36
4	6.5	>99	110	4.3	0.82
5	2	>99	357	1.8	0.34
6	3	>99	238	2.5	0.48
7	4	>99	179	2.7	0.52
8	6	>99	119	11.4	2.18

[a] Other conditions: 75 mg of HBI2, $[IPh]_0$ = 1.2 M, $[Pd]_0/[IPh]_0$ = 0.14%, $[IPh]_0 : [BA]_0 : [NEt_3]_0$ = 1 : 1.5 : 1.5, 3 mL of DMF as solvent, T = 100 ℃.

[b] Conversion was determined by ^1H NMR.

[c] Pd leached results were determined by ICP-MS.

Suzuki coupling reaction of IPh and phenylboronic acid was also conducted with HBI2. In the reaction, a mixture of DMF (2 mL) and deionized water (3 mL) was used as the solvent with K_2CO_3 as the base. Similar to Heck reaction, different amount of

HBI2 were used to investigate the catalyst activity in Suzuki reaction. The reaction conditions and results are summarized in Table 4.7. Generally, the TOF of the Suzuki reaction in this case is above 1000 h^{-1}, which is higher than previous studies of other supported Pd NP catalysts.[5c,19] To further test the activity of HBI2 for Suzuki reaction, less active aryl bromides and PBA were used. All reaction conditions and results are summarized in Table 4.8. It clearly shows that HBI2 can successfully catalyze the Suzuki reaction of most aryl bromides with PBA. The TOF can reach as high as 833 h^{-1} with most reactive aryl bromide, 4′-bromoacetophenone.

Table 4.7 Suzuki reaction of iodobenzene (IPh) and phenylboronic acid (PBA) using HBI2.

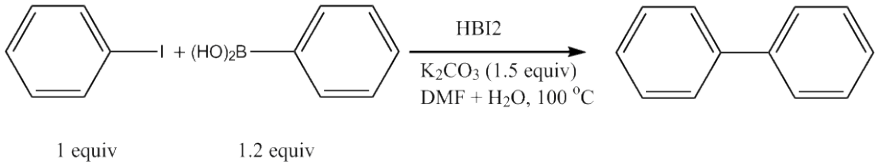

Entry[a]	Catalyst amount (ppm)	Time (h)	Conversion[b] (%)	TON	TOF (h^{-1})
1	822	1	>99	1217	1217
2	20	24	93	46500	1938
3	11	48	90	81820	1704

[a] Other conditions: $[IPh]_0$ = 0.5 M, $[IPh]_0 : [PBA]_0 : [K_2CO_3]_0$ = 1 : 1.2 : 1.5, a mixture of DMF (2 mL) and H_2O (3 mL) as solvent, T = 100 ℃.
[b] Conversion was determined by ^1H NMR.

Recycling reactions were also carried out for Suzuki reaction of IPh and PBA. The reaction conditions and results are shown in Table 4.9. Form the table, we can see that there is no reduction in catalyst activity and the leached Pd amount is also low. In this case, when we recycled the HBI2 catalyst after Suzuki reaction by precipitating the polymer in methanol, a small amount of HBI2 having ammonium ion with Pd NPs can dissolve in methanol.

Table 4.8 Suzuki coupling of aryl bromides and phenylboronic acid

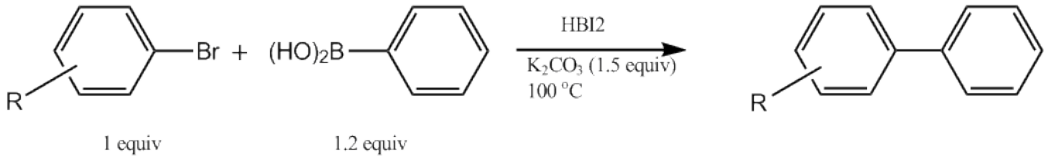

Entry[a]	R	Time (h)	Conversion[c] (%)	TON	TOF (h^{-1})
1	H	6	89	2282	380
2	4-Me	24	96	2461	103
3	3-Me	24	92	2359	98
4	2-Me	24	85	2179	91
5	1-Naphthyl	8	>99	2564	321
6	4-NO_2	24	82	2103	88
7	4-MeO	24	>99	2564	107
8	4-NH_2	24	<1	-	-
9	1,3,5-Me_3	24	6	154	6
10[b]	4-MeCO	24	>99	2000	833

[a] Other conditions: 15 mg of HBI2, $[IPh]_0$ = 0.5 M, $[Pd]_0/[IPh]_0$ = 0.039%, $[IPh]_0 : [PBA]_0 : [K_2CO_3]_0 : [TBAB]$ = 1 : 1.2 : 1.5 : 1, 8 mL of H_2O as solvent, T = 100 ℃.
[b] $[Pd]_0/[IPh]_0$ = 0.005%
[c] Conversion was determined by ^1H NMR.

Table 4.9 Recycling Suzuki Reactions with HBI2

Entry[a]	Time (h)	Conversion[b] (%)	Pd Leached[c] (μg)	[Pd] Leached (%)
1	1	>99	4.8	2.22
2	1	>99	0.6	0.29
3	1	>99	0.8	0.37
4	1	>99	0.5	0.25
5	1	>99	6.5	2.98
6	1	>99	0.2	0.10
7	1	>99	14.3	6.54
8	1	>99	1.7	0.78
9	1	>99	6.2	2.86

[a] Other conditions: 31 mg of HBI2, $[IPh]_0$ = 0.5 M, $[Pd]_0/[IPh]_0$ = 0.08%, $[IPh]_0 : [PBA]_0 : [K_2CO_3]_0$ = 1 : 1.2 : 1.5, a mixture of DMF (2 mL) and H_2O (3 mL) as solvent, T = 100 ℃.
[b] Conversion was determined by ^1H NMR.
[c] Pd leached results were determined by ICP-MS.

4.4 Conclusion

The synthesis of hyperbranched polyethylene ionomers encapsulating self-supported Pd(0) NPs as efficient and recyclable supported Pd catalysts have been

demonstrated. The HBI Pd catalysts with ionomer as the support can be obtained directly from the ethylene/ionic liquid copolymerization with Pd–diimine catalyst. The Pd(0) NPs herein are immobilized on ionomer support by ionic interactions with ammonium ions. These HBI Pd catalysts have been utilized in both carbon-carbon coupling reactions and semi-hydrogenation of alkynes. They have shown good catalytic activity and recyclability in all Pd-catalysed reactions. For example, in semi-hydrogenation of PA, the TOF can reach as high as 1015 h^{-1}, while with high styrene selectivity of 96%. In addition, semi-hydrogenation of three terminal alkynes was also carried out with HBI2. The selectivity of alkene products in these reactions was high (the lowest selectivity is observed in the semi-hydrogenation of 1-heptyne with 93% 1-heptene selectivity). The HBI2 Pd catalyst has also shown high activity in the Heck reaction of IPh with n-BA (as high as 8978 h^{-1}) and in the Suzuki reaction of IPh with PBA (as high as 1938 h^{-1}). Furthermore, three different catalyst recycling methods have been used in the recycling reactions which are: (1) immobilization of HBI Pd catalyst on GO flakes, (2) using dialysis membrane, and (3) directly precipitation of HBI Pd catalyst in methanol after each reaction. Three methods have their own advantages, however, they all suffered with the loss of a small amount of Pd NP catalyst after each recycling reaction.

4.5 References

1. See some representative reviews: (a) Moreno-Manas, M.; Pleixates, R. *Acc. Chem. Res.* **2003**, *36*, 638–643; (b) Farina, V. *Adv. Synth. Catal.* **2004**, *346*, 1553–1582; (c)

Astruc, D. *Inorg. Chem.*, **2007**, *46*, 1884–1894; (d) Balanta, A.; Godard, C.; Claver, C. *Chem. Soc. Rev.*, **2011**, *40*, 4973–4985; (e) Fihri, A.; Bouhrara, M.; Nekoueishahraki, B.; Basset, J.-M.; Polshettiwar, V. *Chem. Soc. Rev.*, **2011**, *40*, 51815203. (f) Perez-Lorenzo, M. *J. Phys. Chem. Lett.*, **2012**, *3*, 167–174.

2. See some representative examples on semi-hydrogenation (a) Witte, P. T.; Berben, P. H.; Boland, S.; Boymans, E. H.; Vogt, D.; Geus, J. W.; Donkervoort, J. G. *Top Catal.* **2012**, *55*, 505511; (b) Tew, M. W.; Emerich, H.; van Bokhoven, J. A. *J. Phys. Chem. C* **2011**, *115*, 8457–8465; (c) Hori, J.; Murata, K.; Sugai, T.; Shinobara, H.; Noyori, R.; Arai, N.; Kurono, N.; Ohkuma, T. *Adv. Synth. Catal.* **2009**, *351*, 3143–3149; (d) Mori, S.; Ohkubo, T.; Ikawa, T.; Kume, A.; Maegawa, T.; Monguchi, Y.; Sajiki, H. *J. Mol. Catal. A: Chemical* **2009**, *307*, 77–81; (e) Studt, F.; Abild-Pedersen, F.; Bligaard, T.; Sørensen, R.; Christensen, C. H.; Nørskov, J. K. *Science* **2008**, *320*, 1320–1322; (f) Teschner, D.; Borsodi, J.; Wootsch, A.; Revay, Z.; Havecker, M.; Knop-Gericke, A.; Jackson, D.; Schlogl, R. *Science* **2008**, *320*, 86–89; (g) Sajiki, H.; Mori, S.; Ohkubo, T.; Ikawa, T.; Kume, A.; Maegawa, T.; Monguchi, Y. *Chem. Eur. J.* **2008**, *14*, 5109–5111; (h) Mastalir, A.; Kiraly, Z.; Patzko, A.; Dekany, I.; L'Argentiere, P. *Carbon* **2008**, *46*, 1631–1637; (i) Kluwer, A. M.; Koblenz, T. S.; Jonischkeit, T.; Woelk, K.; Elsevier, C. J. *J. Am. Chem. Soc.* **2005**, *127*, 15470–15480; (j) Evrard, D.; Groison, K.; Mugnier, Y.; Harvey, P. D. *Inorg. Chem.* **2004**, *43*, 790–796; (k) Hamilton, C. A.; Jackson, S. D.; Kelly, G. J.; Spence, R.; de Bruin, D. *Applied Catalysis A: General*, **2002**, 201–214; (l) Niessen, H. G.; Eichhorn, A.; Woelk, K.; Bargon, J. *J. Mol. Catal. A: Chemical*, **2002**, *182–183*, 463–470; (m) Van Laren, M. W.; Duin, M. A.; Klerk, C.; Naglia, M.; Rogolino, D.;

Pelagatti, P.; Bacchi, A.; Pelizzi, C.; Elsevier, C. J. *Organometallics* **2002**, *21*, 1546–1553; (n) Molnar, A.; Sarbany, A.; Varga, M. *J. Mol. Catal. A: Chemical.* **2001**, *173*, 185–221.

3. (a) Yin, L.; Liebscher, *J. Chem. Rev.* **2007**, *107*, 133–173; (b) Polshettiwar, V.; Len, C.; Fihri, A. *Coord. Chem. Rev.* **2009**, *253*, 2599–2626; (c) Molnar, A. *Chem. Rev.* **2011**, *111*, 2251; (d) Albeniz, A. C; Carrera, N. *Eur. J. Inorg. Chem.* **2011**, *15*, 2347–2360.
4. (a) Lindlar, H. Helv. *Chim. Acta.*, **1952**, *34*, 446–450; (b) Pattison, F. L. M; Dear, R. E. A *Nature* **1961**, *192*, 1284–1285; (c) Lindlar, H.; Dubuis, R. *Org. Synth.* **1966**, *46*, 89. (d) Rajaram, J.; Narula, A. P. S.; Chawla, H. P. S.; Dev, S. *Tetrahedron* **1983**, *39*, 2315–2322; (e) Nicolaou, K. C.; Xu, J.-Y.; Kim, S.; Ohshima, T.; Hosokawa, S.; Pfefferkon, J. *J. Am. Chem. Soc.* **1997**, *119*, 11353–11354; (f) Rzasa, R. M.; Shea, H. A.; Romo, D. *J. Am. Chem. Soc.* **1998**, *120*, 591–592.
5. (a) Kralik, M.; Biffis, A. *J. Mole. Catal. A: Chem.* **2001**, *177*, 113–138; (b) Cho, J. K.; Najman, R.; Dean, T. W.; Ichibara, O.; Muller, C.; Bradley, M. *J. Am. Chem. Soc.*, **2006**, 128, 6276–6277; (c) Liu, P.; Dong, Z.; Ye, Z.; Wang, W.-J.; Li, B.-G. *J. Mater. Chem. A*, **2013**, 1, 15469–15478.
6. (a) Jin, M.; Zhang, H.; Xie, Z.; Xia, Y. *Angew. Chem., Int. Ed.* **2011**, 50, 7850–7854; (b) de Luna Martins, D.; Alvarez, H. M.; Aguiar, L. C. S. *Tetrahedron Lett.* **2010**, 51, 6814–6818; (c) Coulter, M. M.; Dinglasan, J. A.; Goh, J. B.; Nair, S.; Anderson, D. J.; Dong, V. M. *Chem. Sci.* **2010**, 1, 772–775; (d) Ohtaka, A.; Teratani, T.; Fujii, R.; Ikeshita, K.; Kawashima, T.; Tatsumi, K.; Shimomura, O.; Nomura, R. *J. Org. Chem.* **2011**, 76, 4052–4060; (e) Biffis, A.; Sperotto, E. *Langmuir*, **2003**, *19*,

9548–9550; (f) Ogasawara, S.; Kato, S. *J. Am. Chem. Soc.* **2010**, 132, 4608. (f) Pathak, S.; Greci, M. T.; Kwong, R. C.; Mercado, K.; Prakash, S. G. K.; Olah, G. A.; Thompson, M. E. *Chem. Mater.* **2000**, 12, 1985–1989; (g) Price. K. E.; Mcquade, D. T. *Chem. Commun.* **2005**, 1714–1716.

7. Nakamura, Y.; Hirai, H. *Chem. Lett.* **1976**, 1197–1201.
8. Mu, X.; Meng, J.; Li, Z.-C.; Kou, Y. *J. Am. Chem. Soc.* **2005**, *127*, 9694–9695.
9. Chen, W.; Zhang, Y.; Zhu, L.; Lan, J.; Xie, R.; You, J. *J. Am. Chem. Soc.* **2007**, *129*, 13879–13886.
10. Ohtaka, A.; Tamaki, Y.; Igawa, Y.; Egami, K.; Shimonmura, O.; Nomura, R. *Tetrahedron*, **2010**, *66*, 5642–5646.
11. Liu, N.; Liu, C.; Jin, Z. *Green Chem.* **2012**, *14*, 592–597.
12. Yu, Y.; Hu, T.; Chen, X.; Xu, K.; Zhang, J.; Huang, J. *Chem. Commun.* **2011**, *47*, 3592–3594.
13. Johnson, L. K.; Killian, C. M.; Brookhart, M. *J. Am. Chem. Soc.*, **1995**, 117, 6414–6415.
14. (a) Ye, Z.; Xu, L.; Dong, Z.; Xiang, P. *Chem. Commun.* **2013**, *49*, 6235–6255; (b) Dong, Z.; Ye, Z. *Polym. Chem.* **2012**, *3*, 286–301; (c) Ye, Z.; Li, S. *Macromol. React. Eng*. **2010**, *4*, 319–332.
15. See some representative examples on semi-hydrogenation with supported Pd catalysts (a) Weerachawanasak, P.; Mekasuwandumrong, O.; Arai, M.; Fujita, S.-I.; Praserthdam, P.; Panpranot, J. *Journal of Catalysis* **2009**, *262*, 199–205; (b) Dominguez-Dominguez, S.; Berenguer-Murcia, A.; Pradhan, B. K.; Linares-Solano, A.; Cazorla-Amoros, D. *J. Phys. Chem. C* **2008**, *112*, 3827–3834; (c) Dominguez-

Dominguez, S.; Berenguer-Murcia, A.; Linares-Solano, A.; Cazorla-Amoros, D. *Journal of Catalysis* **2008**, *257*, 87–95; (d) Drelinkiewicz, A.; Knapik, A.; Stanuch, W.; Sobczak, J.; Bukowska, A.; Bukowski, W. *Reactive & Functional Polymers* **2008**, *68*, 1652–1664; (e) Marin-Astorga, N.; Pecchi, G.; Pinnavaia, T. J.; Alves-Manoli, G.; Reyes, P. *J. Mol. Catal. A: Chemical* **2006**, *247*, 145–152; (f) Nishio, R.; Sugiura, M.; Kobayashi, S. *Org. Biomol. Chem.* **2006**, *4*, 992–995; (g) Dominguez-Dominguez, S.; Berenguer-Murcia, A.; Cazorla-Amoros, D.; Linares-Solano, A. *Journal of Catalysis* **2006**, *243*, 74–81; (h) Papp, A.; Molnar, A.; Mastalir, A. *Applied Catalysis A: General* **2005**, *289*, 256–266; (i) Marin-Astorga, N.; Alvez-Manoli, G.; Reyes, P. *J. Mol. Catal. A: Chemical*, **2005**, *226*, 81–88; (j) Mastalir, A.; Kiraly, Z.; Berger, F. *Applied Catalysis A: General*, **2004**, *265*, 161–169; (k) Roelofs, J. C. A. A.; Berben, P. H. *Chem. Commun.* **2004**, 970–971; (l) Mastalir, A.; Kiraly, Z. *Journal of Catalysis*, **2003**, *220*, 372–381.

16. Na-Chiangmai, C.; Tiengchad, N.; Kittisakmontree, P.; Mekasuwandumrong, O.; Powell, J.; Panpranot, *J. Catla. Lett.* **2011**, *141*, 1149–1155.
17. Lee, K. H.; Lee, B.; Lee, K. R.; Yi, M. H.; Hur, N. H. *Chem. Commun.* **2012**, *48*, 4414–4416.
18. Mitsudome, T.; Takahashi, Y.; Ichikawa, S.; Mizugaki, T.; Jitsukawa, K.; Kaneda, K. *Angew. Chem. Int. Ed.* **2013**, *52*, 1481–1485.
19. (a) Wen, F.; Zhang, W.; Wei, G.; Wang, Y.; Zhang, J.; Zhang, M.; Shi, L. *Chem. Mater.* **2008**, *20*, 2144–2150; (b) Zhang, L.; Wang, L.; Li, H.; Li, P. *Synth. Commun.* **2008**, *38*, 1498–1511; (c) Bergbreiter, D. E.; Oshurn, P. L.; Wilson, A.; Sink, E. M. *J. Am. Chem. Soc.* **2000**, *122*, 9058–9064.

20. (a) Liu, P.; Ye, Z.; Wang, W.-J.; Li, B.-G. *Macromolecules* **2013**, *46*, 72–82; (b) Liu, P.; Dong, Z.; Ye, Z.; Wang, W.-J.; Li, B.-G. *J. Mater. Chem. A* **2013**, *1*, 15469–15478.

4.6 Supporting Information:

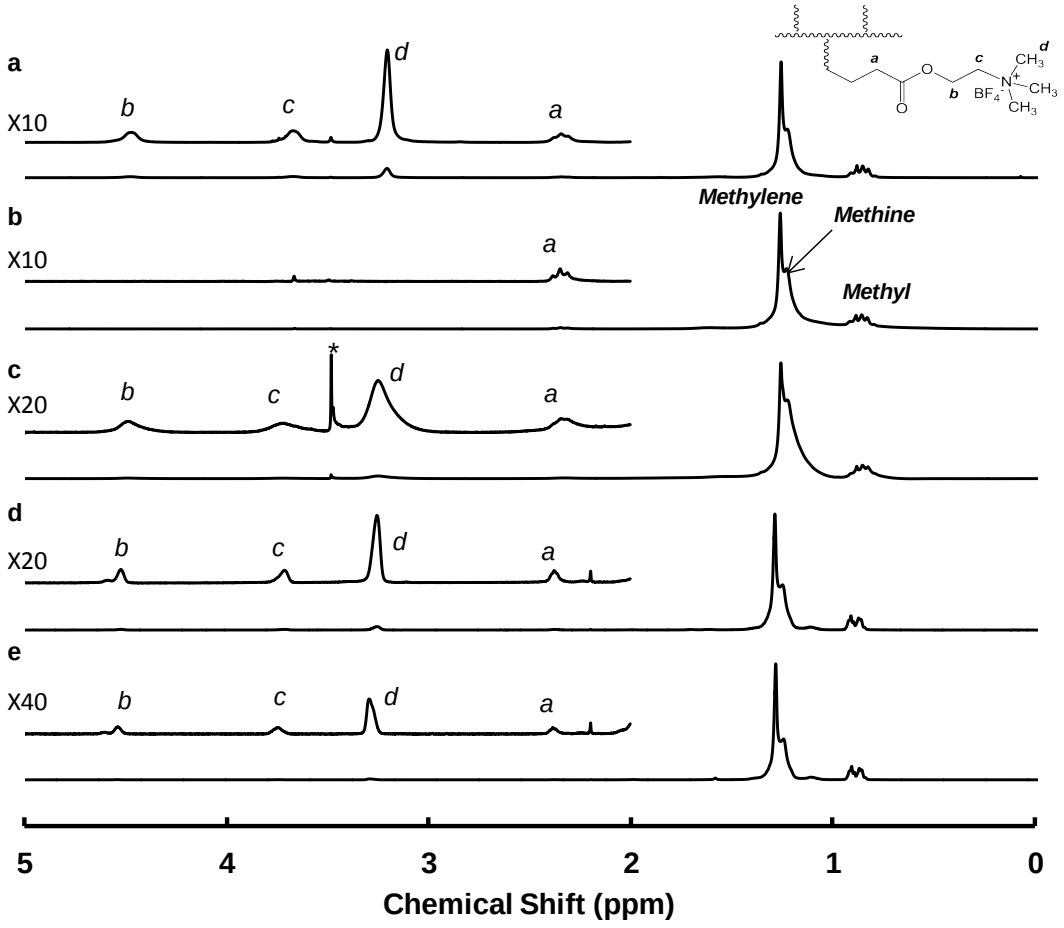

Figure S4.1 ^{1}H NMR spectrum of (a) HBI1, (b) cleaved HBI1, (c) HBI2, (d) HBI3, and (e) HBI4.

NMR Spectra (200 MHz, $CDCl_3$) and Data of the Semi-hydrogenation Products

Styrene: δ = 5.23 (d, *J* = 10.8 Hz, 1H), 5.74 (d, *J* = 17.6 1H), 6.69 (dd, *J* =17.6 Hz, *J*` = 10.8 Hz, 1H), 7.50–7.10 (m, 5H),

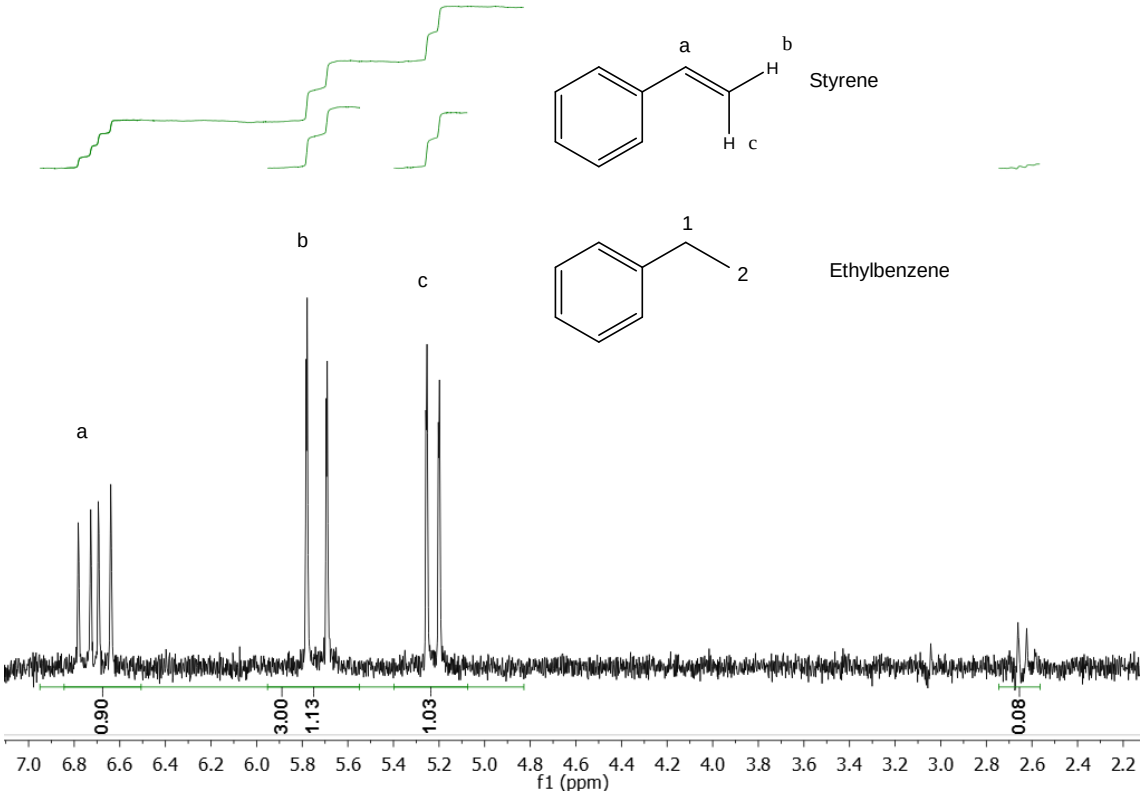

Figure S4.2 ^{1}H NMR spectrum of semi-hydrogenation of PA entry 4 after 150 min

4-phenyl-1-butene

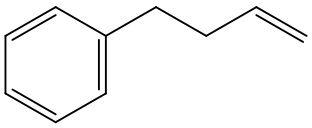

δ = 2.38 (d, 2H), 2.69 (d, *2*H), 4.97 (t, 2H), 5.84 (m, 1H) 7.44–7.00 (m, 5H),

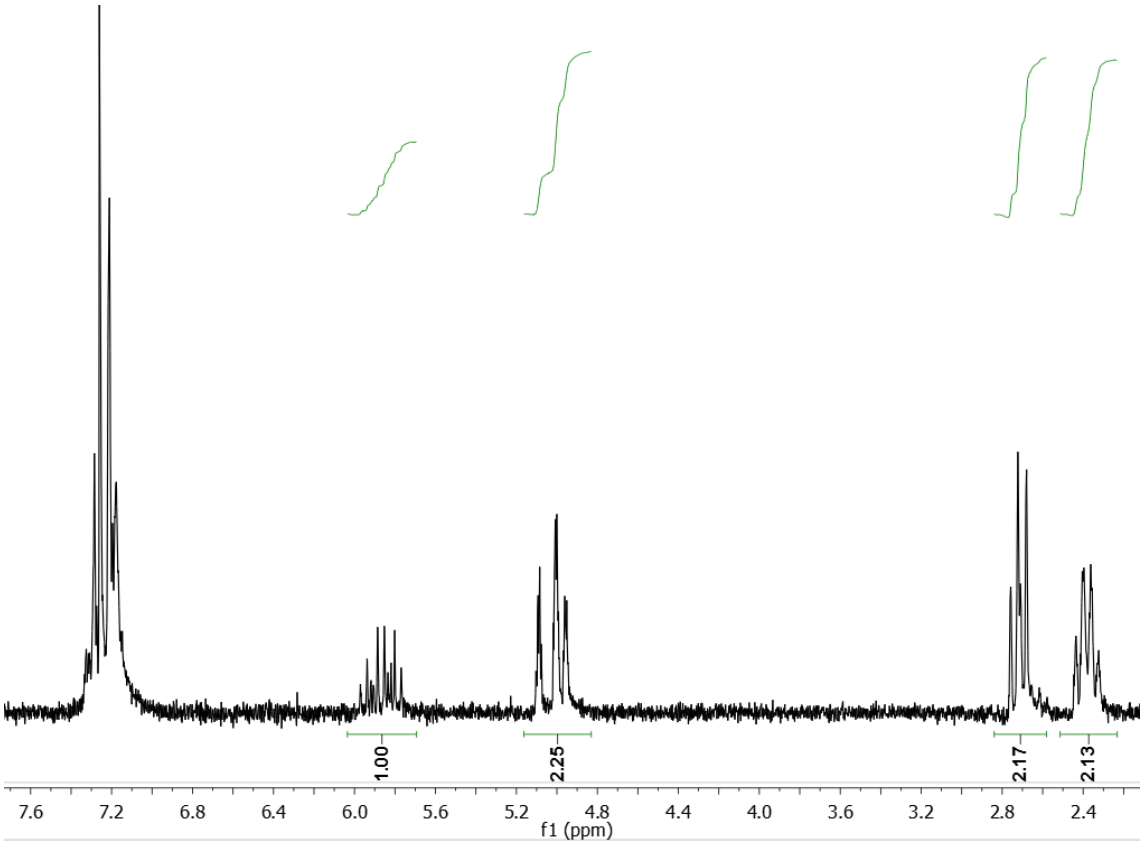

Figure S4.3 ^{1}H NMR spectrum of semi-hydrogenation of 4-phenyl-1-butyne after 120 min

1-vinylcyclohex-1-ene: δ = 1.60–1.72 (m, 4H), 2.14 (d, *J*= 4.4 Hz, 4H), 4.90 (d, *J* = 10.80 Hz, 1H), 5.07 (d, *J* = 17.6 Hz, 1H), 5.77 (s, 1H), 6.35 (dd, *J* = 17.60, 10.80 Hz, 2H).

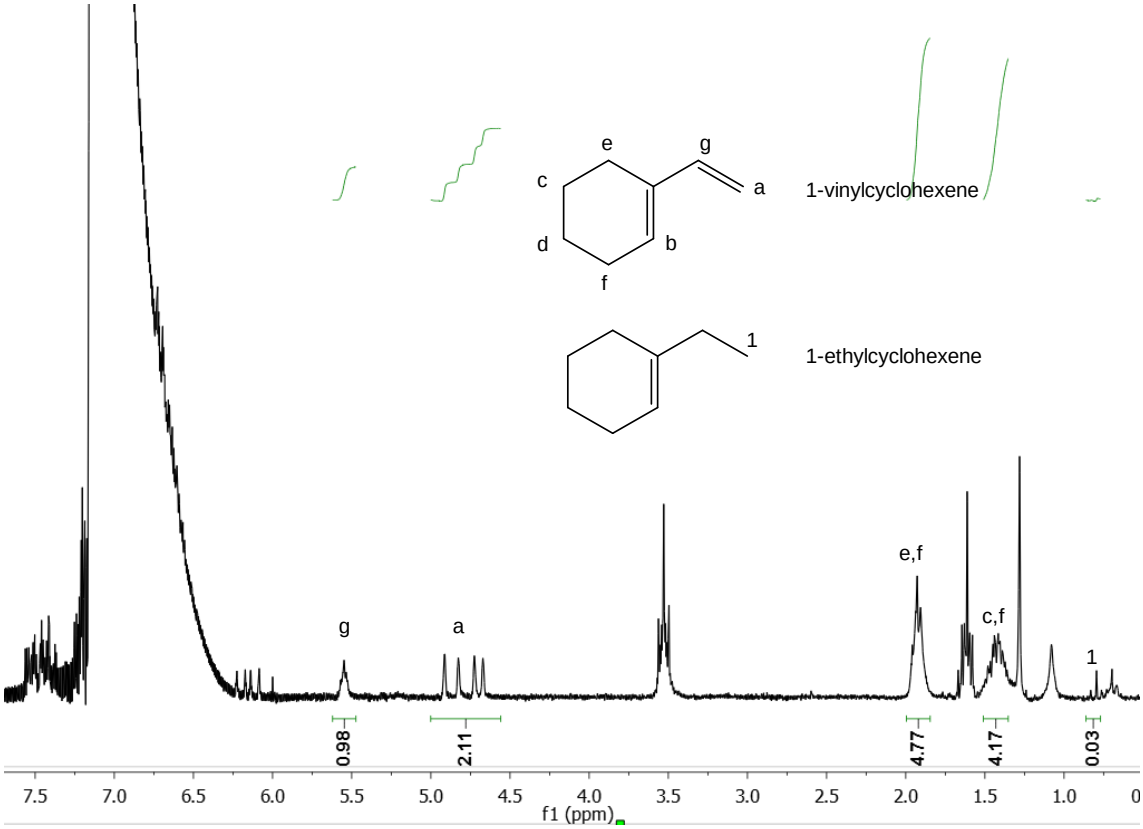

Figure S4.4 ^{1}H NMR spectrum of semi-hydrogenation of 1-ethynylcyclohexene after 150 min

NMR Spectra (500 MHz, $CDCl_3$) and Data of the Cross-Coupling Products

Butyl cinnamate

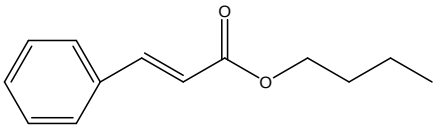

δ = 0.97 (t, *J* = 7.4 Hz, 3H), 1.44 (d, *J* = 7.6 Hz, 2H), 1.72–1.67 (m, 2H), 4.21 (t, *J* = 6.6 Hz, 2H), 6.44 (d, *J* = 16.0 Hz, 1H),7.38 (m, 3H),7.55–7.51 (m, 2H), 7.68 (d, *J* = 16.0 Hz, 1H).

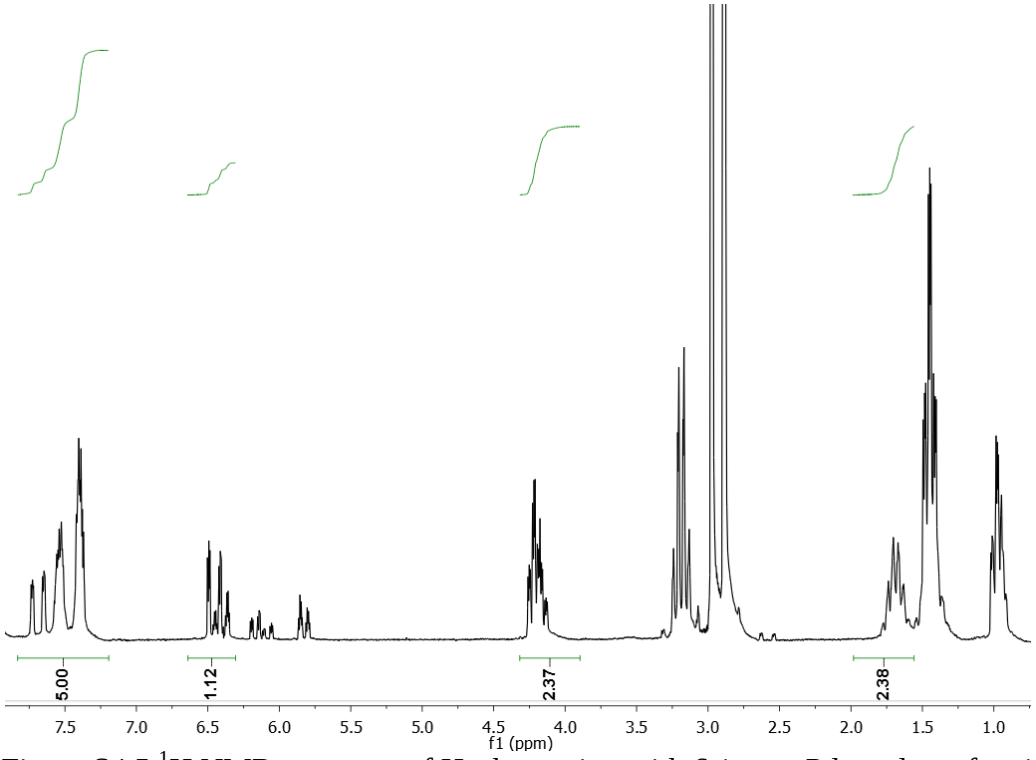

Figure S4.5 ^{1}H NMR spectrum of Heck reaction with 6.1 ppm Pd catalyst after 18 h

Biphenyl

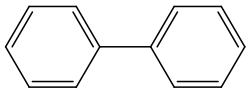

δ = 7.36 (t, *J* = 7.4 Hz, 2H), 7.46 (t, *J* = 7.7 Hz, 4H), 7.61 (d, *J* = 7.4 Hz, 4H).

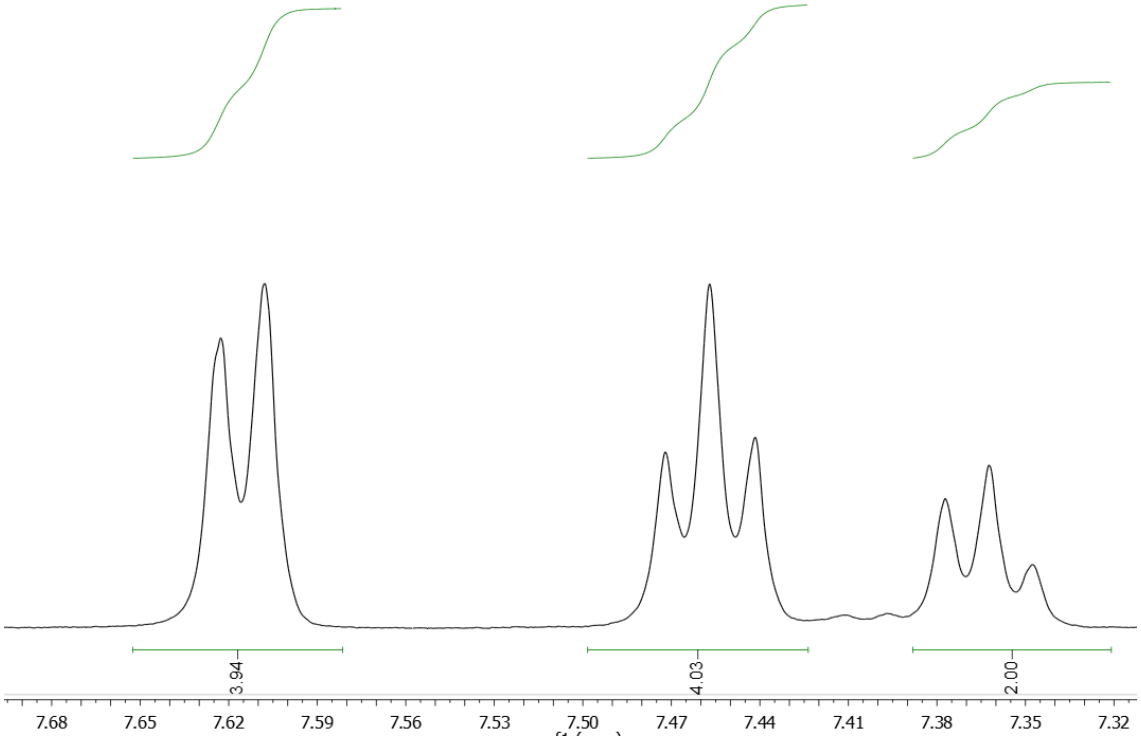

Figure S4.6 ^{1}H NMR spectrum of recycling Suzuki reaction entry 2 after 1h

4-Methylbiphenyl: δ = 2.39 (s, 3H), 7.25 (d, *J*= 8.0 Hz, 2H), 7.31 (t, *J* = 7.4 Hz, 1H), 7.42 (t, *J* = 7.4 Hz, 2H), 7.49 (d, *J* = 8.0 Hz, 2H), 7.58 (d, *J* = 8.0 Hz, 2H).

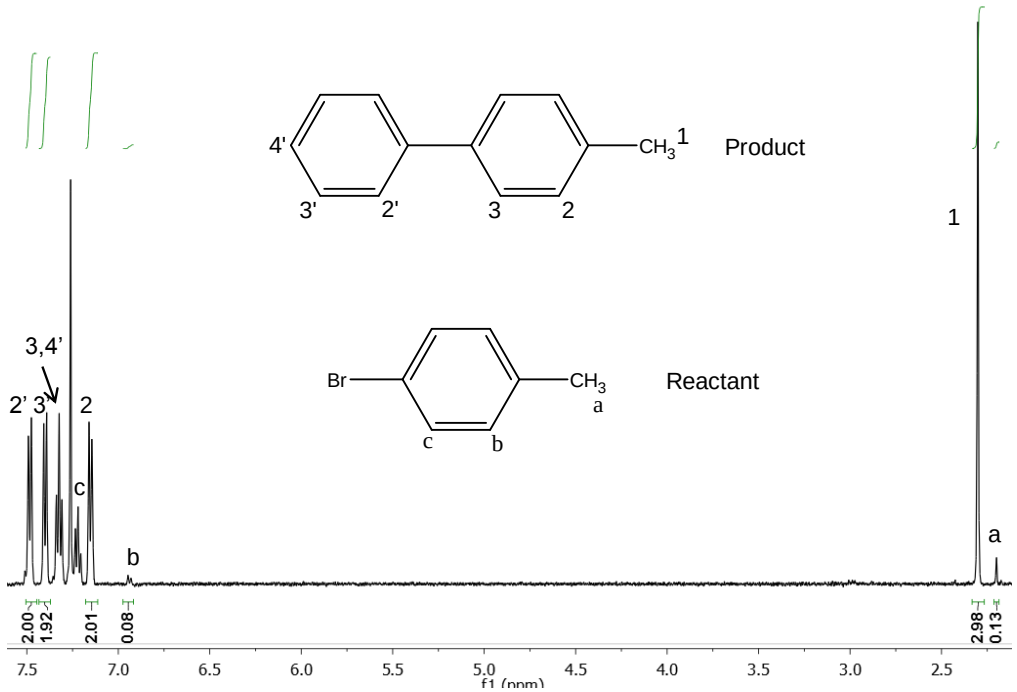

Figure S4.7 ^{1}H NMR spectrum of Suzuki coupling of aryl bromides and phenylboronic acid entry 2 after 24 h

3-Methylbiphenyl: δ =2.37 (s, 3H), 7.11 (d, *J* = 7.5 Hz, 1H), 7.28 (t, *J* = 7.6 Hz, 1H), 7.40–7.33 (m, 4H), 7.53 (d, *J* = 7.6 Hz, 1H)

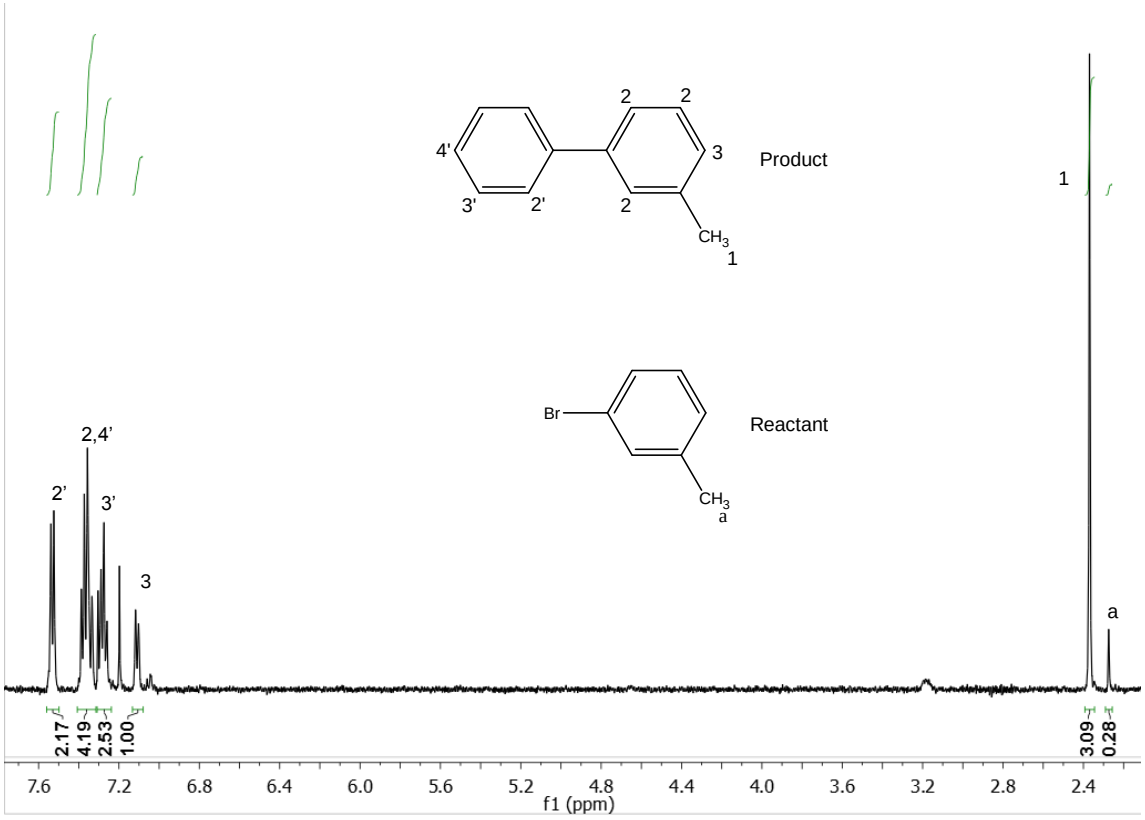

Figure S4.8 ^{1}H NMR spectrum of Suzuki coupling of aryl bromides and phenylboronic acid entry 3 after 24 h

2-Methylbiphenyl: δ = 2.25 (s, 3H), 7.20–7.24 (m, 4H), 7.29–7.33 (m, 3H), 7.38 (t, *J* = 7.4 Hz, 2H).

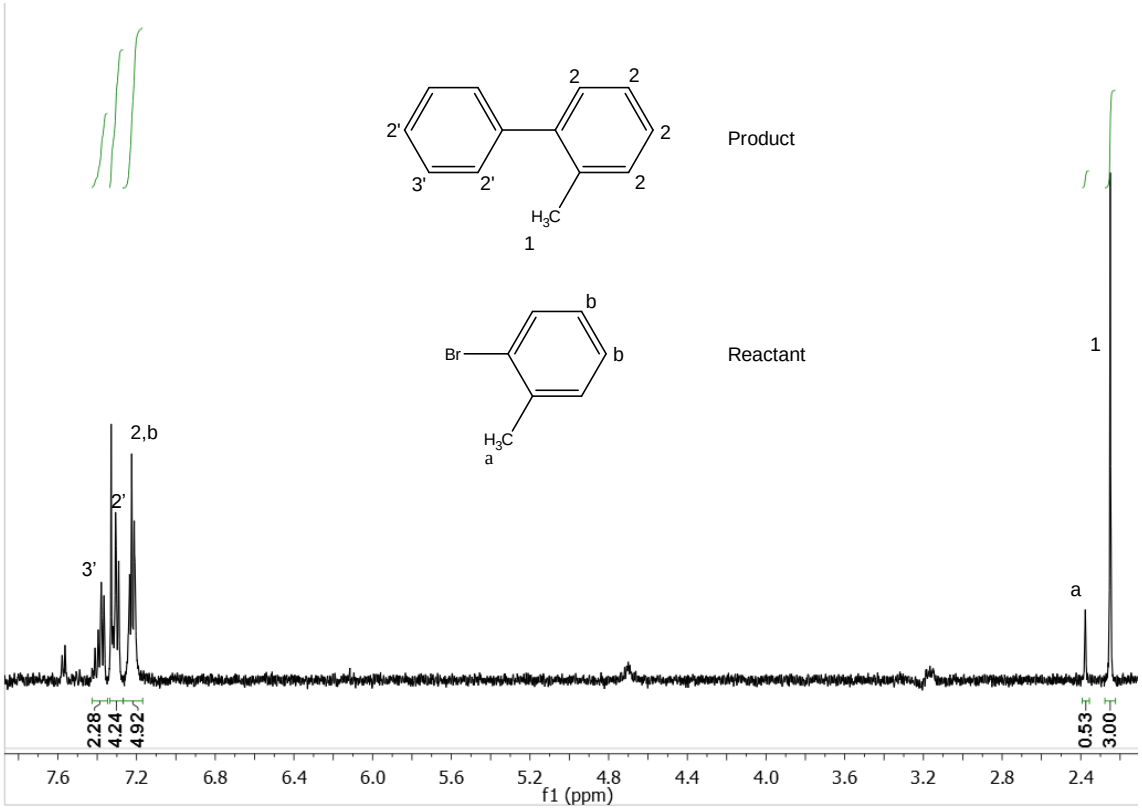

Figure S4.9 ^{1}H NMR spectrum of Suzuki coupling of aryl bromides and phenylboronic acid entry 4 after 24 h

1-phenyl-nathphalene

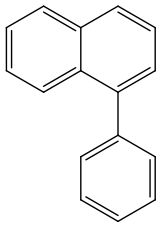

δ =7.35–7.30 (m, 3H), 7.45–7.36 (m, 6H), 7.85–7.77 (m, 3H).

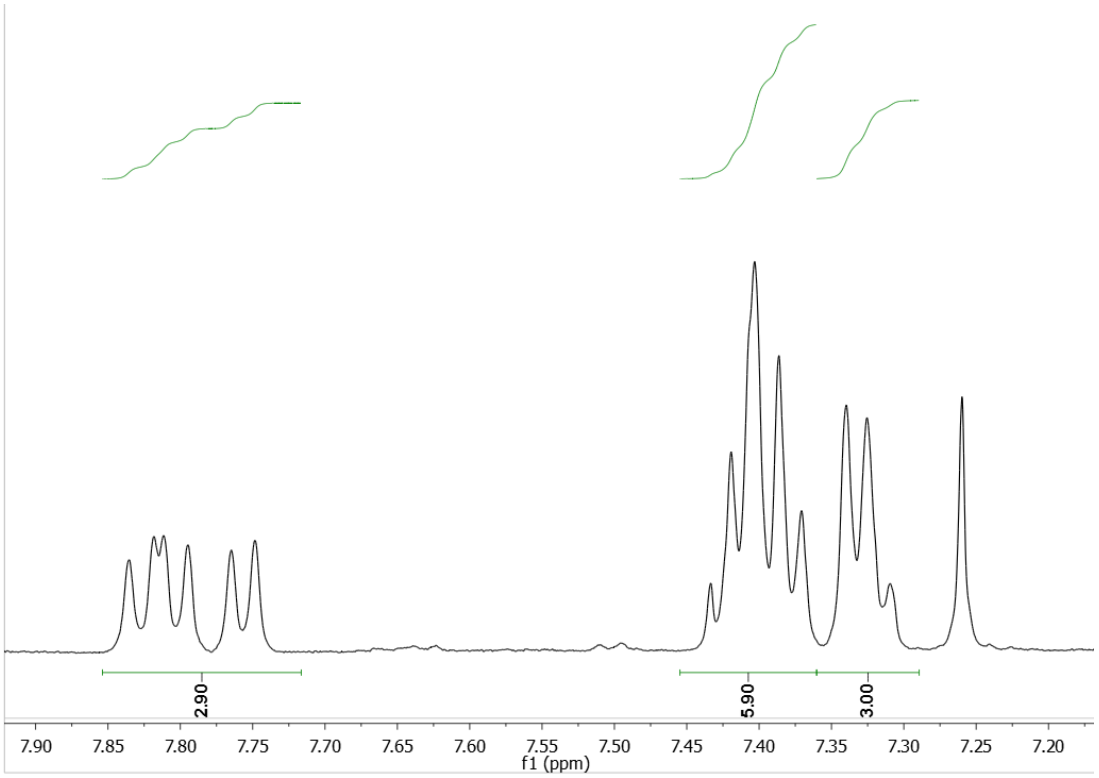

Figure S4.10 ^{1}H NMR spectrum of Suzuki coupling of aryl bromides and phenylboronic acid entry 5 after 8 h

4-Nitro-1,1'-biphenyl: δ = 7.44 (t, *J* = 7.4 Hz, 1H), 7.50 (t, *J* = 7.4 Hz, 2H), 7.62 (d, *J* = 7.1 Hz, 1H), 7.73 (d, *J* = 8.8 Hz, 2H), 8.29 (d, *J* = 8.8 Hz, 2H).

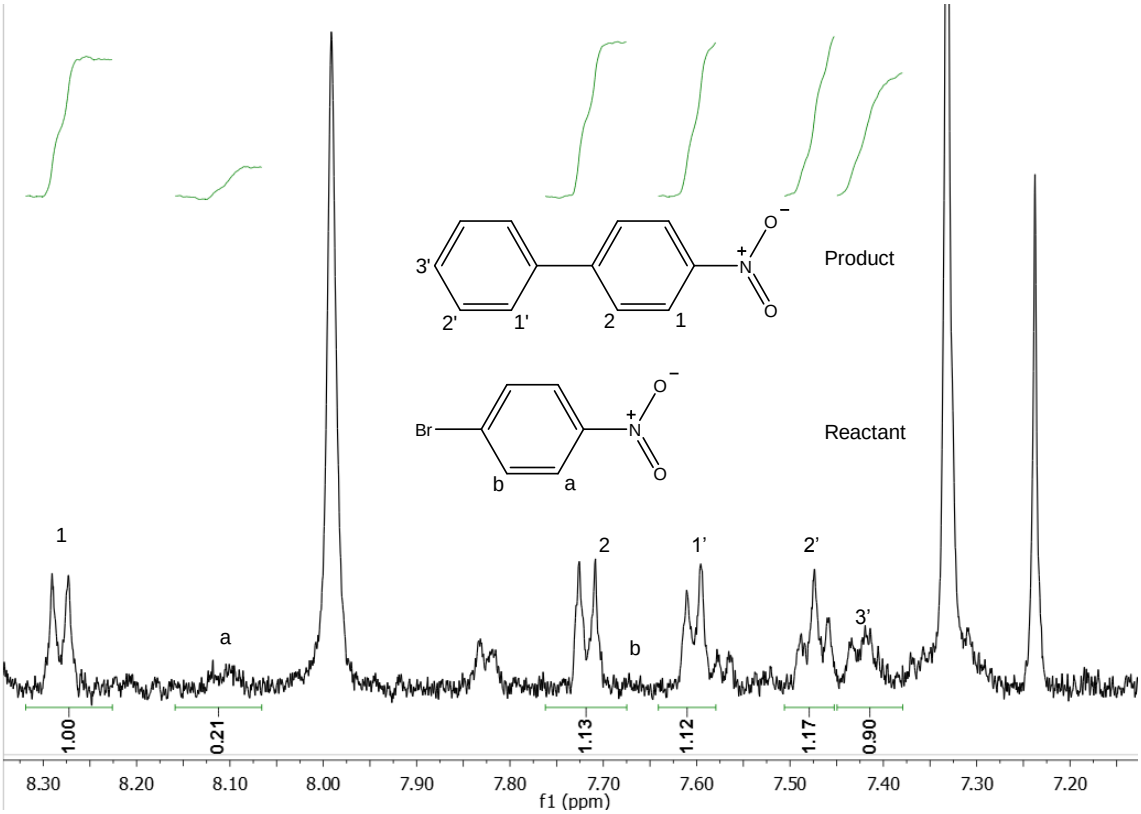

Figure S4.11 ^{1}H NMR spectrum of Suzuki coupling of aryl bromides and phenylboronic acid entry 6 after 24 h

4-Methoxybiphenyl: δ = 3.83 (s, 3 H), 6.97 (d, *J*= 8.6 Hz, 2 H), 7.30 (t, *J* = 8.0 Hz, 1 H), 7.42 (t, *J* = 8.0 Hz, 2 H), 7.51–7.55 (m, 4 H).

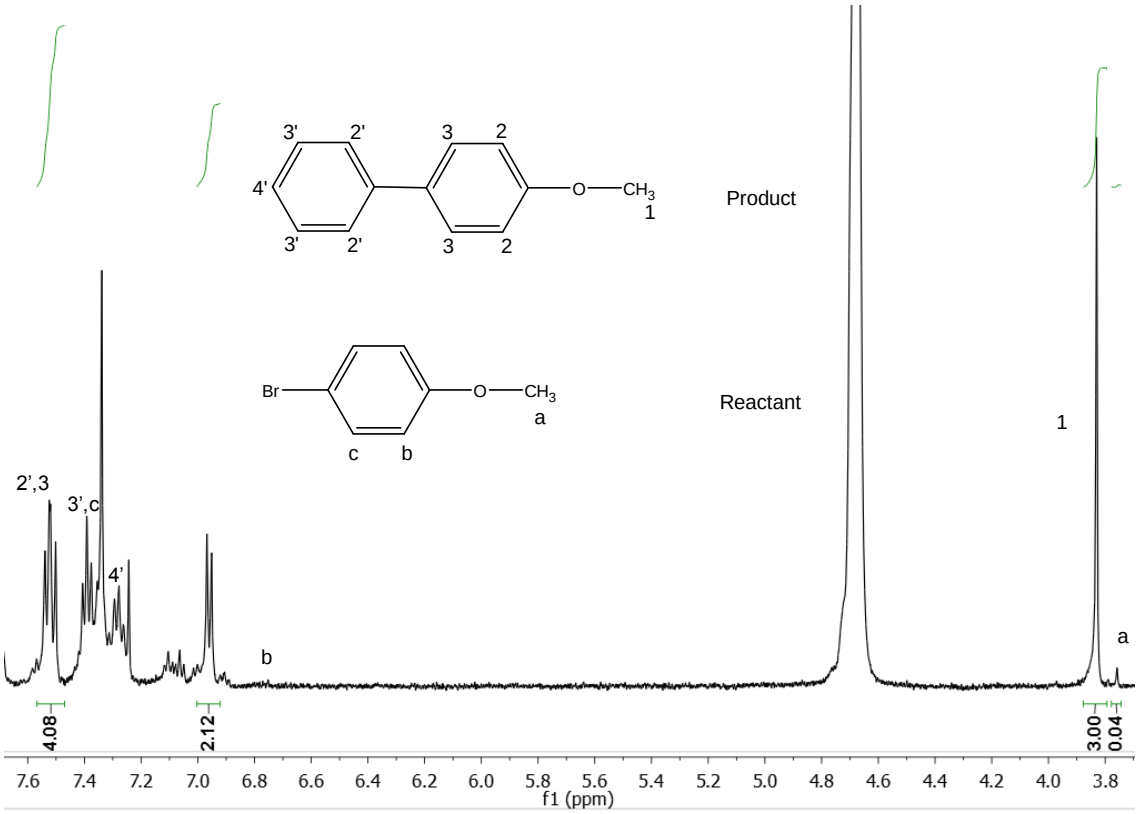

Figure S4.12 ^{1}H NMR spectrum of Suzuki coupling of aryl bromides and phenylboronic acid entry 7 after 24 h

2,4,6-Trimethyl-biphenyl: δ = 2.02 (s, 6H), 2.35 (s, 3H),6.96 (s, 2H), 7.16 (d, *J* = 7.0 Hz, 2H), 7.35 (d, *J* = 7.3 Hz, 1H), 7.43 (t, *J* = 7.0 Hz, 2H).

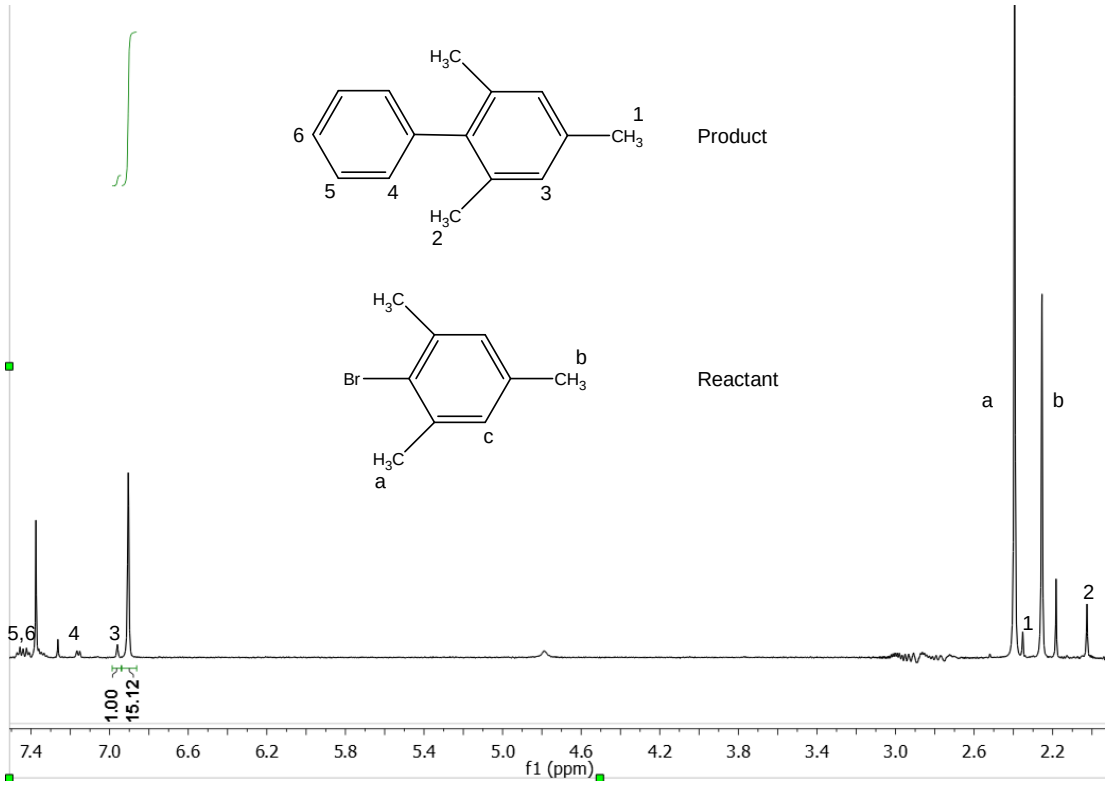

Figure S4.13 ^{1}H NMR spectrum of Suzuki coupling of aryl bromides and phenylboronic acid entry 9 after 24 h

4-Acetyl-1,1'-biphenyl

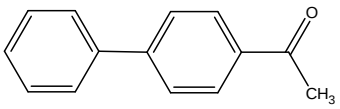

δ = 2.64 (s, 3 H), 7.40 (t, *J* = 7.4 Hz, 1H),7.47(t, *J* = 7.4 Hz, 2 H), 7.63 (d, *J* = 7.3 Hz, 2H), 7.69 (d, *J* = 8.5 Hz,2H), 8.04 (d, *J* = 8.5 Hz, 2 H).

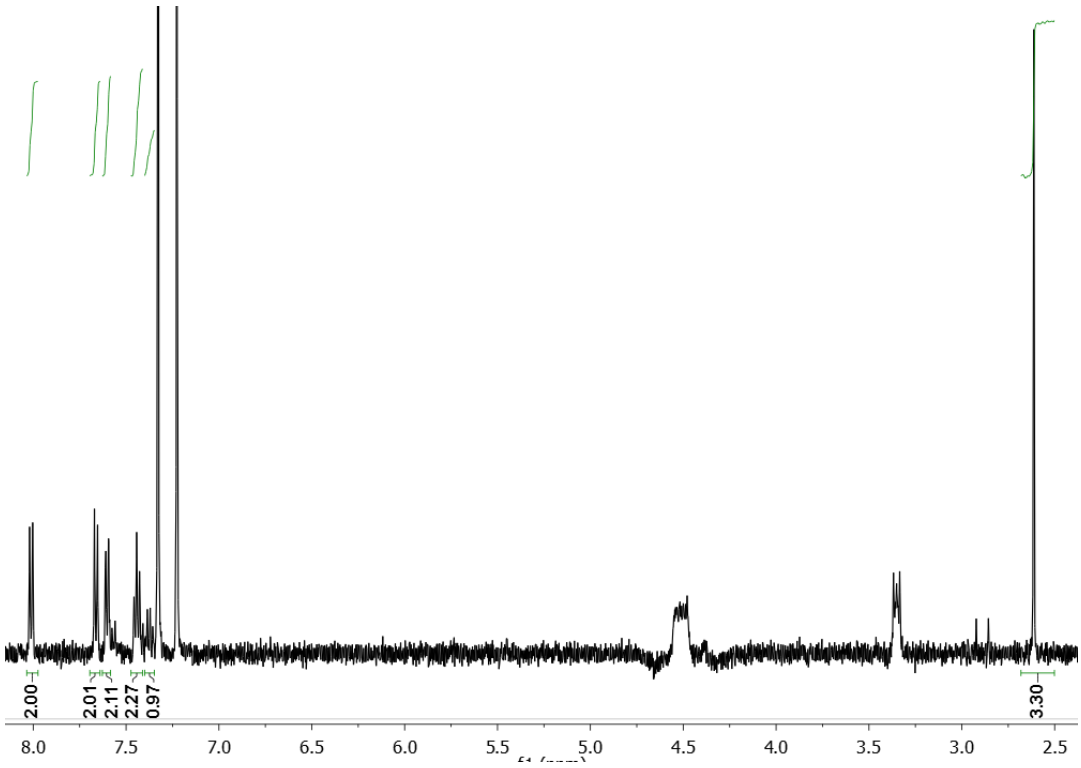

Figure S4.14 ^{1}H NMR spectrum of Suzuki coupling of aryl bromides and phenylboronic acid entry 10 after 24 h

Chapter 5

Tuning Structural Parameters of Polyethylene Brushes in Surface-Initiated Ethylene "Living" Polymerization from Silica Nanoparticles and Effects on Nanocomposite Properties

This chapter is organized based on a paper published by P. Xiang, K. Petrie, M. Kontopoulou, Z. Ye, R. Subramanian in Polym. Chem. 2013, 4, 1381–1395. Part of the work on the preparation and characterization of the nanocomposites was carried out by K. Petrie and M. Kontopoulou at Queen's University through research collaboration with the silica nanofillers containing PE brushes prepared at Laurentian University.*

Abstract

Our group has previously demonstrated the first surface-initiated ethylene "living" polymerization with surface-tethered Pd–diimine catalyst for successful covalent surface functionalization of silica nanoparticles with polyethylene (PE) brushes. This Chapter further reports on the successful tuning of structural parameters of PE brushes in surface-initiated ethylene "living" polymerization from two types of nonporous silica nanoparticles (Silica-I as a precipitated silica and Silica-II as a fumed silica). The brush parameters that are controlled herein include brush length, density, and topology. To control/reduce the brush density, the density of the surface-tethered acryloyl groups for catalyst immobilization is adjusted by using mixed silane agents comprised of an effective one (3-acryloxypropyltrichlorosilane) and an inert dummy one (ethyltrichlorosilane) at different compositions, which in turn adjusts the density of immobilized catalysts and PE brushes. This approach is demonstrated to be successful,

rendering PE brushes of controllable densities at the polymerization condition of 27 atm/5 ℃: 0.022–0.055 chains/nm^2 for Silica-I and 0.07–0.17 chains/nm^2 for Silica-II. Simultaneously, the brush length can be controlled by adjusting the polymerization time, with the highest length of about 45 kg/mol achieved at 6 h of polymerization at 27 atm/5 ℃. Different from the linear brushes with short branch structures obtained at 27 atm/5 ℃, hyperbranched PE brushes with compact topology are obtained at 1 atm/25 ℃, benefiting from the chain walking mechanism of the Pd–diimine catalyst. The PE-grafted silicas with varying brush density and length are subsequently used as nanofillers to construct polymer nanocomposites with an elastomeric ethylene-olefin copolymer (EOC) as the matrix polymer. The effects of brush length and density on the nanofiller dispersion, rheological properties, and tensile properties of the composites are examined.

5.1 Introduction

Surface-initiated "living"/controlled polymerization techniques have been extensively developed for controlled "grafting-from" surface modification of various inorganic or metal nanoparticles with covalently tethered polymer brushes.[1] The presence of the covalently surface-tethered polymer shell renders the modified nanoparticles with some enhanced properties, such as processability, dispersion, stability in selected solvents, and interfacial compatibility with matrix polymer in polymer nanocomposites, as well as some value-added functional properties.[1] Most "living"/controlled polymerization techniques developed to date have been successfully

employed for surface-initiated polymerization. These include the traditional "living" polymerization techniques (anionic polymerization,[2] cationic polymerization,[2c,3] ring-opening polymerization,[4] and ring-opening metathesis polymerization[5]) and the recently developed most popular controlled radical polymerization techniques[1] (atom-transfer radical polymerization (ATRP),[6] nitroxide-mediated radical polymerization,[7] and reversible addition-fragmentation chain transfer polymerization[8]). In all these surface-initiated polymerization techniques, design and covalent immobilization of corresponding initiating species on the substrate surface to form a self-assembled monolayer (SAM) is often the critical first step to successfully achieve subsequent surface-initiated "living"/controlled polymerization.[1] The monomer stocks used for constructing the brushes have included typical monomers polymerizable with the above polymerization techniques, such as methacrylates, acrylates, methacrylamides, acrylamides, styrenics, cycloolefins, etc. A large variety of inorganic or metal nanoparticles, including silica nanoparticles, gold nanoparticles, metal oxide nanoparticles, quantum dots, carbon nanotubes, and magnetic nanoparticles, have been used as substrates.[1]

The chain structural parameters of the polymer brushes, including length, density, composition, and architecture, have been shown to greatly affect the properties of the resulting polymer modified particles. Their precise control is thus very important. Strategies have been developed with each specific surface-initiated "living"/controlled polymerization for the control of these structural parameters.[1] In particular, control of polymer brush density is often achieved by adjusting immobilization density of the

initiating species in SAM.[9] Two common methods have been used for reducing/controlling the polymer brush density: (1) controlling initiator concentration or the length of time used for immobilization of initiator and (2) immobilization of a mixture of the initiator and its corresponding inert (dummy) analogue on the substrate surface.[9] The aim of both methods is to limit the density of active initiator in SAM, thus controlling the resulting polymer brush density. While the first method requires detailed kinetics of the initiator immobilization process, the second one is insensitive to the kinetics and is thus more convenient.[9]

In sharp contrast to the tremendous advancements achieved with the above-mentioned surface-initiated "living"/controlled polymerization techniques, little progress somehow has been made to date with the surface-initiated "living" olefin coordination polymerization for grafting polymer brushes from olefin monomer stocks (like ethylene). Though metal-catalyzed "living" olefin polymerization technique has advanced significantly over the past two decades with a number of well-behaved transition metal catalysts discovered,[10] it has rarely been developed for surface-modification with polyolefins. The major hurdle limiting the developments is the difficulty of finding versatile transition metal catalysts, which can be covalently immobilized onto substrate surface through their initiating sites and can subsequently catalyze surface-initiated chain growth.[11] To this end, our research group has recently demonstrated the first example of surface-initiated "living" ethylene polymerization from both silica nanoparticles and mesoporous silicas.[11,12] Our success benefits from the use of a Brookhart Pd–diimine catalyst,[13]

[(ArN=C(Me)–(Me)C=NAr)Pd(CH_3)(N≡CMe)]$^+SbF_6^-$(**1**, Scheme 5.1), which has been discovered by us to uniquely meet the stringent requirements. In this technique, catalyst **1** is covalently immobilized onto acryloyl-functionalized silica surface through 2,1-insertion of the surface-tethered acryloyl double bond into Pd–Me bond to render surface-mounted Pd chelate catalysts (Scheme 1).[11,12] This immobilization chemistry has been verified with a homogeneous model supported catalyst.[14] With the Pd–CH_2 bond in the chelate centers serving as the initiating site for chain growth,[11,12,14,15] successful surface-initiated "living" ethylene polymerization occurs at 27 atm (ethylene pressure) and 5 ℃, giving rise to covalent surface grafting of low-polydispersity polyethylene (PE) brushes of controllable length through the ester linkage.[11]

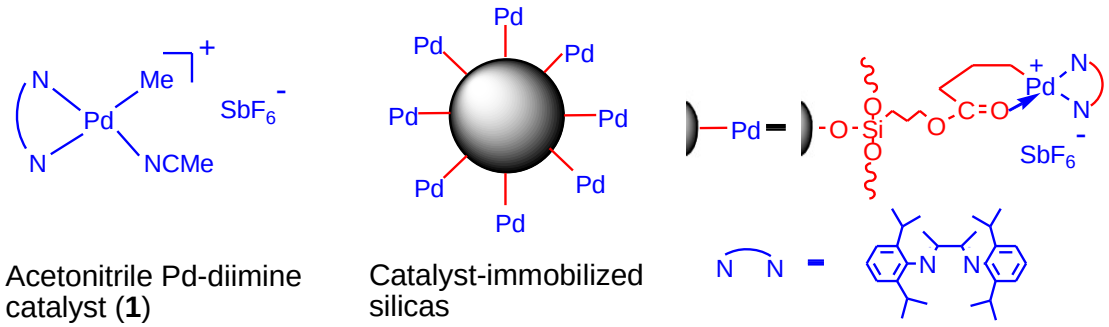

Scheme 5.1 Homogeneous and covalently immobilized Pd–diimine catalysts.

In our previous works, the control of PE brush density and chain topology on silica particles somehow has not been demonstrated though we have shown that the length of the low-polydispersity brushes can be conveniently tuned by changing the polymerization time.[11] Herein, we further report on the successfully control of brush density and topology with this surface-initiated polymerization technique from two

types of silicas (precipitated and fumed silicas). Two ranges of silicas containing PE brushes at different structural parameters have been prepared. Meanwhile, polymer nanocomposites with PE-grafted silicas dispersed in a polyethylene elastomer (ethylene-octene copolymer, EOC) as the matrix polymer have been compounded. The effects of brush length and density on nanofiller dispersion and mechanical properties of the compounded nanocomposites have been investigated.

5.2 Experimental Section

5.2.1 Materials

All manipulations of air- and/or moisture-sensitive compounds were performed in a N_2-filled glovebox or using Schlenk techniques. The acetonitrile Pd–diimine complex, $[(ArN{=}C(Me){-}(Me)C{=}NAr)Pd(CH_3)(N{\equiv}CMe)]^+SbF_6^-$ (**1**), was synthesized according to a literature procedure.[13a,b] 3-Acryloxypropyltrichlorosilane (ATCS) and ethyltrichlorosilane (ETCS) were obtained from Gelest Inc. and were used as received. Two types of silica particles, Silica-I (a precipitated silica synthesized by sol gel method, aggregates of silica nanoparticles at an average diameter of about 10 nm, obtained from Aldrich, catalog # 637238) and Silica-II (a hydrophilic fumed silica, AEROSIL 200, average nanoparticle size of about 12 nm, obtained from Evonik), were used in this work. The silica particles were washed with a large amount of methanol and then dried in vacuo at 220 ℃ overnight before use. Ultrahigh-purity N_2 and polymer-grade ethylene (both obtained from Praxair) were purified by passing through 3 Å/5 Å

molecular sieve and Oxiclear columns to remove moisture and oxygen, respectively, before use. The EOC used herein as the matrix polymer for the compounding of polymer nanocomposites is Engage 8130 obtained from Dow Chemical. It has a density of 0.864 g/cm^3, a melt flow index of 13 g/min (at 190 ℃), and a comonomer content of 42 wt%. Its melting and crystallization temperatures are 67 and 40 ℃, respectively.[18] Other chemicals, including chlorobenzene (99%, Aldrich), anhydrous dichloromethane (99.8%), tetrahydrofuran (THF) (>99%), triethylsilane (97%), triethylamine (minimum, 99%), toluene (ACS reagent, ≥99.5%), methanol (ACS reagent, ≥99.8%), HCl acid (regent grade, 37%), KOH (regent grade, ≥ 90%, flakes) and H_2O_2 solution (50 wt%), were obtained from either Aldrich and were all used as received.

5.2.2 Preparation of Acryloyl-Functionalized Silicas

Representatively, the following is the procedure used for the preparation of acryloyl-functionalized silica that was used subsequently for preparation of Pd-Silica-I-3 in Table 5.1. Type I dried bare Silica-I particles (6.6 g) were dispersed, under ultrasonication, in anhydrous CH_2Cl_2 (80 mL) in a Schlenk flask under a N_2 atmosphere. ATCS (1.48 g, 5.9 mmol), ETCS (9.76 g, 59.7 mmol), and triethylamine (5.0 mL, 35.8 mmol) were subsequently added into the solution. The solution was stirred for 7 days at room temperature under a N_2 atmosphere. The particles were then isolated from the solution by centrifugation (14,000 rpm, 22,800 g), and were consecutively washed twice with CH_2Cl_2 (80 mL), twice with methanol (80 mL each), once with methanol-water mixture (v/v, 1/1, 80 mL each), twice with acetone (80 mL each), and once with diethyl

ether (ca. 30 mL). The product (6.4 g) was obtained after drying overnight in vacuo at room temperature.

5.2.3 Preparation of Catalyst-Immobilized Silicas

Representatively, the following procedure was used for the preparation of Pd-Silica-I-3 in Table 5.1. The acryloyl-functionalized silica particles prepared above (6.0 g), catalyst **1** (1.20 g, 1.49 mmol), and dichloromethane (80 mL) were added into a Schlenk flask under N_2 protection. The solution was stirred for 5 days at room temperature under a N_2 atmosphere, and then centrifuged (14,000 rpm, 22,800 g). The resulting silica particles were then washed with anhydrous CH_2Cl_2 (80 mL) under ultrasonication followed with centrifugation (14,000 rpm, 22,800 g). The washing and centrifugation procedure was repeated for at least five cycles until the supernatant liquid after centrifugation turned to colorless. The catalyst-immobilized silica particles (5.01 g) were then obtained after drying overnight in vacuo at room temperature.

5.2.4 Ethylene Polymerization with Homogeneous and Immobilized Catalysts

All polymerizations (at both 1 and 27 atm) were carried out in a 500 mL Autoclave Engineers Zipperclave reactor equipped with a MagneDrive agitator and a removable heating/cooling jacket. The reactor temperature was controlled by passing a water/ethylene glycol mixture through the jacket using a refrigerating/heating circulator set at the desired temperature. The following is a typical procedure used for ethylene

polymerization with Pd-Silica-I-3. Similar procedure was used for all the other catalysts. Prior to each polymerization, the reactor was washed using toluene and acetone, respectively. It was then heated at ca. 75 ℃, subject to at least three cycles of vacuum and nitrogen purge, and then cooled down to room temperature under a positive N_2 pressure. The immobilized catalyst, Pd-Silica-I-3 (1.2 g) suspended in anhydrous chlorobenzene (60 mL), was injected into the autoclave under N_2 protection, and the reactor was then cooled down to the desired temperature (5 or 25 ℃) under agitation. After establishing thermal equilibrium, the polymerization was started by quickly pressurizing the reactor to a desired ethylene pressure of (27 or 1 atm). During the polymerization, ethylene pressure was maintained constant by continuous feed of ethylene from a cylinder, and the reactor temperature was kept constant by using the circulator.

After the prescribed polymerization time (2, 4, or 6 h), ethylene pressure was released. The polymerization suspension was then transferred out from the reactor and was quenched by adding Et_3SiH (0.5 mL) under stirring. After stirring for about 1 h, each suspension was centrifuged (14,000 rpm, 22,800 g), yielding the black PE-grafted silicas. To remove the possible untethered free polymer, the products were redispersed in toluene (60 mL) followed by the centrifugation. This wash-centrifugation cycle was repeated for two more times. To remove the black Pd(0) resulting from the deactivated Pd-diimine catalysts, the products were redispersed in toluene (ca. 30 mL), which was subsequently charged with HCl acid (37%, 5 mL) and H_2O_2 solution (50 wt %, 5 mL). After stirring for 1 h, the solution was precipitated in a large amount of methanol, and

the precipitated solids were further washed with excess methanol. Finally, the PE-grafted silica particles were obtained after drying overnight in vacuo at 70 ℃.

5.2.5 General Procedure for Cleavage of PE Brushes

PE-grafted silica particles (ca. 60 mg) and KOH (0.3 g) were dispersed in THF (3 mL) and methanol (1 mL) mixture in a 50 mL flask. The suspension was refluxed at 90 ℃ for 3 days and was then filtered using a 0.2 μm syringe filter. The cleaved polymer was obtained from the filtrate by precipitation in methanol. The polymer precipitate was redissolved in THF and filtered again followed with precipitation in methanol. Finally, the cleaved polymer (about 10 mg) was dried overnight in vacuo at 70 ℃ and was subsequently characterized.

5.2.6 Compounding of Polymer Nanocomposites

All silica samples (both bare silicas and PE-grafted silicas) were vacuum dried at 120 ℃ for 2 h prior to the compounding to remove possible residual solvent or moisture. The samples were slightly grinded with a mortar and pestle in an attempt to break up the large aggregates. Premixing of EOC and the silica sample was carried out with a Carver press for 1 min at 150 ℃. The product was folded and repressed five times to ensure even particle distribution in the resulting EOC sheet. After being cut into smaller pieces, the sheet was then compounded with co-rotation in a DSM micro 5cc twin-screw compounder for 8 min at 120 rpm and 120 ℃. The filler loading in the compounded

nanocomposites was 7 wt% (percentage of actual dry silica in the nanocomposites) for bare Silica-I and PE-grafted Silica-I samples, and 5 wt% (percentage of actual dry silica in the nanocomposites) for bare Silica-II and PE-grafted Silica-II samples.

5.2.7 Characterizations and Measurements

^{1}H nuclear magnetic resonance (NMR) spectra of cleaved polymers were obtained on a Varian Gemini 2000 spectrometer (200 MHz) at ambient temperature. $CDCl_3$ (δ 7.26) was used as the solvent. Differential scanning calorimetry (DSC) measurements were performed on a TA Instruments Q100 DSC equipped with a refrigerated cooling system (RCS) under a N_2 atmosphere. The instrument was operated in the standard DSC mode and was calibrated with an indium standard. A N_2 purging flow of 50 mL/min was used. Samples (ca. 10 mg) were heated from room temperature to 200 ℃ at 10 ℃/min and cooled to –90 ℃ at 5 ℃/min, and the data were collected on a subsequent heating ramp from –90 to 200 ℃ at 10 ℃/min. Thermogravimetric analysis (TGA) was performed on a TA Instruments Q50 thermogravimetric analyzer. Measurements were carried out in a N_2 atmosphere with a continuous N_2 flow of 60 mL/min. In a typical run, the sample (ca. 10 mg) was heated from 100 to 700 ℃ at a heating rate of 20 ℃/min. Brunauer-Emmett-Teller (BET) measurements were performed on Micrometrics ASAP2010 apparatus. Typically, 50–250 mg of bare silica samples were degassed in vacuo at 100 ℃ for 8 h prior to the N_2 adsorption/desorption test under liquid N_2 conditions.

Polymer characterization with triple-detection gel permeation chromatography (GPC) was performed on a Polymer Laboratories PL-GPC220 system equipped with a triple detection array, including a differential refractive index (DRI) detector (from Polymer Laboratories), a three-angle laser light scattering (LS) detector (high-temperature miniDAWN from Wyatt Technology), and a four-bridge capillary viscosity detector (from Polymer Laboratories). The detecting angles of the miniDAWN LS detector were 45, 90, and 135°, and the laser wavelength was 687 nm. One guard column (PL# 1110-1120) and three 30 cm columns (PLgel 10 μm MIXED-B 300 mm × 7.5 mm) were used for polymer fractionation. This triple-detection GPC technique has been used extensively in our previous works[15b-d,19] and a similar methodology is employed herein. The mobile phase was HPLC-grade THF and the flow rate was 1.0 mL/min. The complete GPC system, including the column and detector arrays, was maintained at 33.0 ℃. The mass of the polymers injected into the columns was about 1 mg. Astra software from Wyatt Technology was used to collect and analyze the data from all three detectors. Two polystyrene narrow standards (from Pressure Chemicals) with weight-average molecular weight (M_w) of 30 and 200 kg/mol, respectively, as per the supplier were used for the normalization of light scattering signals at the three angles, and the determination of inter-detector delay volume and band broadening, respectively. The DRI increment dn/dc value of 0.078 mL/g was used for all cleaved polyethylenes, and the value of 0.185 mL/g was used for polystyrene. As a demonstration, the above two polystyrene standards were measured to have a typical M_w value of 31.0 and 207.5 kg/mol, respectively, which are in agreement with the data provided by the supplier.

Dynamic light scattering (DLS) measurement of the dilute dispersions of bare silicas and PE-grafted silica samples was performed on a Malvern Zeta-Sizer Nano S90 apparatus with the detection angle of 90 °. All the dispersions were prepared at a concentration of ca. 0.1 mg/mL in either THF (for bare silicas) or toluene (for PE-grafted silicas). All the dispersions were sonciated for at least 3 h. Measurements were conducted both right after the sonication and after leaving the sonciated samples stand still for 20–24 h. All the measurements were carried out at 25 ℃.

Transmission electron microscopy (TEM) characterization of the EOC nanocomposites was performed on a FEI Tecna 20 transmission electron microscope. The nanocomposites were hot pressed into discs having a diameter of 20 mm and a thickness of 1 mm using a Carver press at 150 ℃ for 1 min. The samples were then cut into ultrathin sections using a Leica ultra microtome for measurement. Image analysis was performed using SigmaScan Pro 5 software to measure the area and Feret diameter of silica aggregates. Rheological characterization of the composites by small amplitude dynamic oscillation was conducted on a Rheologica ViscoTech rheometer equipped with a 20 mm parallel plate fixture at a gap of 1 mm using a nitrogen purge. Stress-controlled frequency sweeps were carried out from a frequency of 0.04 to 157.7 rad/s at 190 ℃.

Tensile properties of nanocomposites were examined using an Instron 3369 universal tester. All experiments were carried out with a crosshead speed of 200 mm/min. A type V die according to ASTM D638 was used to cut dog-bone shaped

samples from a sheet with an average thickness of 1.5 mm. The sheets were prepared by compression molding in a Carver press at approximately 150 ℃. A minimum of 5 repeat trials were performed for each specimen, and the average is reported.

5.3 Results and Discussion

5.3.1 Surface Functionalization of Bare Silicas and Covalent Catalyst Immobilization

Two different commercially available bare silica particles, Silica-I (a precipitated silica synthesized via sol gel method) and Silica-II (a hydrophilic fumed silica, AEROSIL 200), are employed in this work. Both bare silicas exhibit as aggregates of solid silica nanoparticles (with average nanoparticle size of 10 and 12 nm, respectively, as per the suppliers). On the basis of N_2 adsorption-desorption measurements, Silica-I and Silica-II have a specific surface area of 550 and 200 m^2/g, respectively, with negligible pore structures. As shown schematically in Scheme 5.2, this surface modification technique herein involves a three-step procedure consisting of (1) covalent surface functionalization of bare silica with acryloyl groups; (2) immobilization of Pd–diimine catalyst **1** by reacting with the surface-tethered acryloyl groups; (3) surface-initiated ethylene polymerization.[11,12] To achieve a control of the brush density, we choose to adjust the density of the surface-tethered acryloyl groups and in turn the density of immobilized Pd catalysts since the acryloyl groups serve as the specific sites for catalyst anchoring. To control the density of acryloyl groups, we employ the strategy

of mixed silane compounds, 3-acryloxypropyltrichlorosilane (ATCS, the effective one) and ethyltrichlorosilane (ETCS, the inert dummy one) at different compositions, in the surface functionalization step, attempting to obtain SAM having reactive acryloyl groups diluted with inert ethyl groups at different ratios. Table 5.1 summarizes the details in the preparation of the surface-functionalized silicas and the corresponding catalyst-immobilized silicas, along with the characterization results.

In the surface-functionalization step, the total dosage of the two silane compounds is in large excess relative to the surface silanol groups (2.2 and 6.0 mol per mole of silanol for Silica-I and Silica-II, respectively, with the assumption of 5 silanol groups per nm^2 surface in both dry bare silicas[6b]) to maximize the conversion of the silanol groups. The molar feed fraction of ATCS ($f_{ATCS,0}$) in the mixed silane compounds was varied from 0.17 to as low as 0.06 (see Table 5.1) in order to investigate its effect on the grafting density of the resulting PE brushes. In our previous studies that employed surface functionalization with sole ATCS, we have found that the percentage of the surface-tethered acryloyl groups usable for catalyst immobilization is often small (30% or lower) due to the bulky structure of the Pd–diimine catalyst, which covers more surface area than an acryloyl group.[11,12] Our preliminary experiments have shown that brush density changes negligibly when the $f_{ATCS,0}$ value is reduced from 1 to 0.33 due to this reason. Considering this, we intentionally choose herein low $f_{ATCS,0}$ values in order to achieve a pronounced tuning of the brush density. Control experiments employing ATCS alone ($f_{ATCS,0} = 1$) were also undertaken with both bare silicas. Meanwhile, an

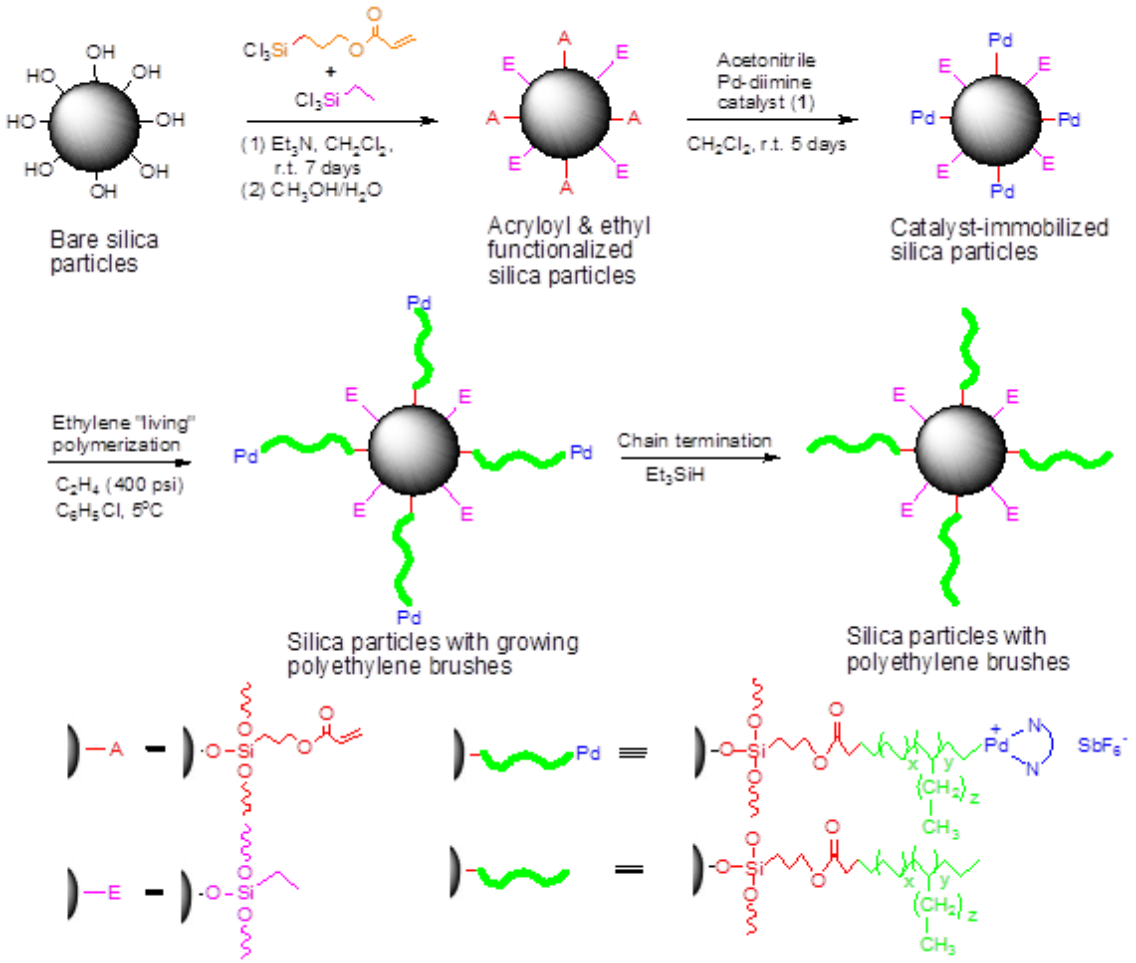

Scheme 5.2 Three-step procedure for surface modification of silica nanoparticles with polyethylene brushes via surface-initiated ethylene polymerization.

additional surface-functionalization was carried out on Silica-I with the use of ETCS alone as the sole silane compound (i.e, $f_{ATCS,0} = 0$).

The resulting surface-functionalized silicas were characterized with TGA for the determination of weight fraction of the surface-tethered organic moieties. Figure 5.1 shows the TGA curves of these surface-functionalized silicas as well as those of the bare

Table 5.1 Synthesis of surface-functionalized silicas and corresponding catalyst-immobilized silicas.

Catalyst-Immobilized Silica Sample	Bare Silica and Weight Loss at 700 ℃[a]	Surface Functionalization with Silane Compounds						Catalyst Immobilization	
		Total Silane Feed Dosage (ATCS+ETCS)		ATCS Feed Fraction, $f_{ATCS,0}$ (mol/mol)	Weight Loss at 700 ℃[a] (%)	Total Density of Functionalization[c] (molecules/nm^2)	Density of Acryloyl[d] (molecules/nm^2)	**1**/Acryloyl (mol/mol)	Weight Loss at 700 ℃[a] (%)
		mmol/g silica	mol/mol silanol[b]						
Pd-Silica-I-1	Silica-I, 2.4%	10	2.2	1	12.8	1.2	1.2	1.2	16
Pd-Silica-I-2				0.17	11.3	2.6	0.4	1.5	12
Pd-Silica-I-3				0.09	9.6	2.4	0.2	1.5	11
-				0	10.6	3.5	0	-	-
Pd-Silica-II-1	Silica-II, 0.7%	10	6.0	1	5.1	1.2	1.2	1.2	11
Pd-Silica-II-2				0.09	3.2	2.1	0.2	1.5	6.8
Pd-Silica-II-3				0.06	4.6	3.6	0.2	1.5	7.1

[a] Weight loss at 700 ℃ was determined with TGA in N_2 at a heating rate of 20 ℃/min.

[b] Total silane dosage per surface silanol group is estimated from the BET surface area (550 and 200 m^2/g for Silica-I and Silica-II, respectively) with the assumption of 5 silanol groups/nm^2 of silica surface.

[c] Total density of functionalization = $\frac{\left(\frac{W_{\text{Fuctionalized Silica}}}{100-W_{\text{Fuctionalized Silica}}}-\frac{W_{Silica}}{100-W_{Silica}}\right)\times N_A}{S_{sp}\left(M_{Acryloyl}f_{ATCS,0}+M_{Ethyl}(1-f_{ATCS,0})\right)}$ where $W_{\text{Functionalized Silica}}$ and W_{Silica} are the percentage weight loss of surface-functionalized silica and corresponding bare silica, respectively, at 700 ℃; N_A is the Avogadro's number; $S_{\mathbf{sp}}$ is the specific area of the bare silica; M_{Acryloyl} (113 g/mol) and M_{Ethyl} (29 g/mol) are the molecular weight data for the surface-tethered acryloyl group and ethyl group, respectively, and $f_{\text{ATCS,0}}$ is the molar feed fractions of ATCS in the mixed silane compounds.

[d] Grafting density of acryloyl groups = total density of functionalization × $f_{\text{ATCS,0}}$.

silicas. With each silica, decreasing $f_{ATCS,0}$ (from 1 to 0.09 for Silica-I; from 1 to 0.06 for Silica-II) generally leads to reduced weight loss at 700 ℃. For example, for Silica-I, the percentage of weight loss is reduced from 12.8% ($f_{ATCS,0}$ = 1) to 9.6% ($f_{ATCS,0}$ = 0.09). This trend of change is expected given the higher molecular weight of ATCS relative to ETCS. For those functionalized with mixed silane compounds, two distinct weight-loss regions (one centered at around 400 ℃ and the other centered at around 560 ℃) can be identified though with some overlap. This is better illustrated in their derivative thermogravimetric curves (see Figure S5.1 in Supporting Information). For those functionalized with ATCS or ETCS alone, only one of the two regions is found. From this comparison, it can be inferred that the former region results from weight loss of the tethered acryloyl groups (from ATCS) and the latter results from weight loss of the tethered ethyl groups (from ETCS). With the decrease of $f_{ATCS,0}$, the weight loss in the latter region is clearly enhanced relative to that in the former region (see Figure 5.1).

The total density of surface functionalization and the density of acryloyl groups have been estimated (see Table 5.1) from the relative TGA weight loss data (at 700 ℃) in reference to the dry bare silicas. For silicas functionalized with mixed silane compounds, we have assumed in the estimation that the two silane compounds have equal chemical reactivity with silanol groups given their similar structures, i.e., the molar ratio of the two types of surface-tethered groups equals the feed ratio of ATCS/ETCS. From the estimation, decreasing $f_{ATCS,0}$ with both silicas renders the expected decrease in the density of acryloyl group and a concomitant increase in the

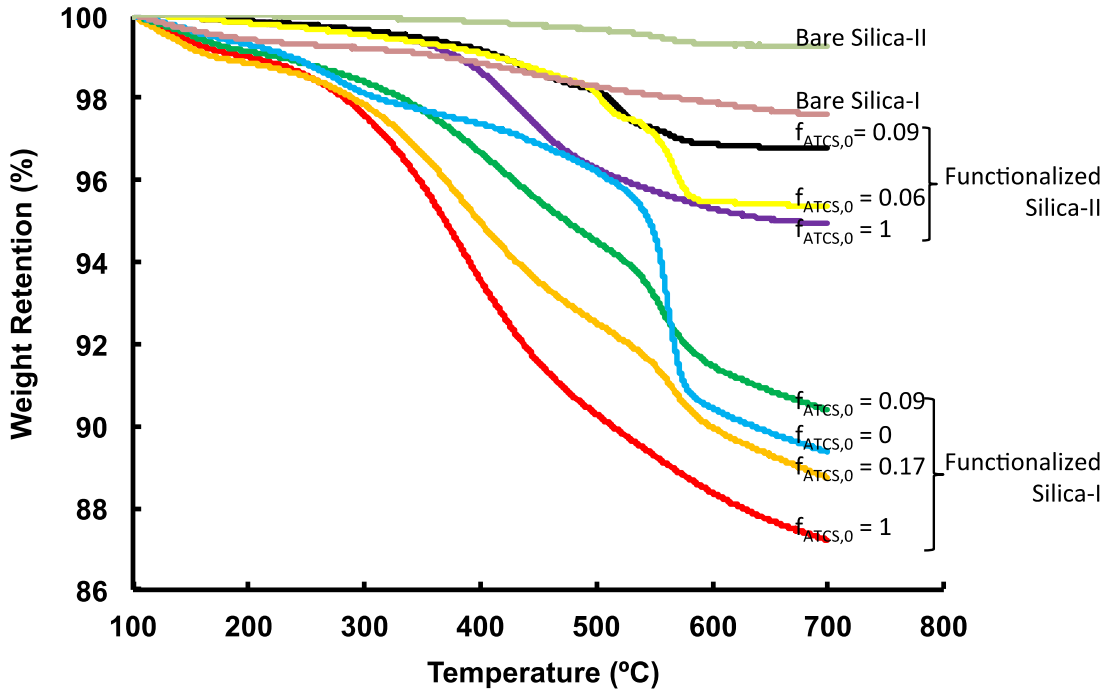

Figure 5.1 Thermogravimetric curves of bare silicas and surface-functionalized silicas.

total density of surface functionalization. With Silica-I, the acryloyl density decreases gradually from 1.2 (at $f_{ATCS,0}$ = 1) to 0.2 molecules/nm^2 (at $f_{ATCS,0}$ = 0.09) while the total density increases from 1.2 (at $f_{ATCS,0}$ = 1) to 3.5 molecules/nm^2 (at $f_{ATCS,0}$ = 0). With Silica-II, the acryloyl density decreases from 1.2 (at $f_{ATCS,0}$ = 0) to 0.2 molecules/nm^2 (at $f_{ATCS,0}$ = 0.06) and the total density increases correspondingly from 1.2 to 3.6 molecules/nm^2. The increase in the total density with the decreasing $f_{ATCS,0}$ should be attributed to the smaller surface coverage of the tethered ethyl group relative to acryloyl group as a result of its smaller size. Despite their different specific surface area, we find that both total density and acryloyl density data achieved with the two different silicas are very similar at the same $f_{ATCS,0}$, indicating that the two bare silicas have similar density of surface silanol groups.

Covalent immobilization of catalyst **1** was subsequently carried out with the surface-functionalized silicas to render catalyst-immobilized silicas. To maximize catalyst loading, an excess amount of **1** (1.2 or 1.5 equiv. see Table 5.1) relative to surface-tethered acryloyl groups was used in each immobilization with a total reaction time of 5 days. Extensive wash was subsequently undertaken to remove possible unsupported homogeneous catalyst residue. As expected, TGA characterization shows their enhanced percentage weight loss at 700 ℃ compared to the corresponding acryloyl-functionalized silicas due to the additional tethering of the organometallic catalyst having bulky organic ligand. Given that the exact char composition of the immobilized Pd catalyst in TGA analysis is not known, the TGA weight loss data was not used for estimating Pd immobilization density. We attempted to quantify the immobilization density of the covalently tethered Pd(II) centers through ICP-MS after digestion of the immobilized catalyst with HF and HNO_3 acids. However, this method was found to be unsuccessful with inconsistent results obtained despite several trials. It perhaps results from the uncontrollable decomposition of **1** in the long catalyst immobilization procedure to render Pd(0) physically deposited on silica surface, causing inaccurate overestimated results. Nevertheless, this difficulty in the estimation of Pd immobilization density should not affect our subsequent determination of the density of PE brushes, which is accurately determined from the relative mass and molecular weight data of PE brushes (see the next section). As per our previous studies, the density of tethered Pd(II) centers should be very close to the density of PE brushes.[11,12]

5.3.2 Surface-Initiated Ethylene "Living" Polymerization at 27 atm and 5 ℃ for Synthesis of Silicas Grafted with Linear PE Brushes at Different Length and Density

Surface-initiated ethylene polymerizations were carried out with the various catalyst-immobilized silicas at 27 atm and 5 ℃, at which the polymerization should behave typically "living" with cationic Pd–diimine catalysts.[11,12,14,15,19e] With the different catalyst-immobilized silicas synthesized above, PE brushes at different densities are expected to yield. With each silica, polymerization time was varied from 2 to 6 h in order to obtain PE brushes at different length. During the polymerization, the growing PE brushes resulting from the covalently immobilized catalysts should be covalently tethered onto the silica surface through the ester linkage originally present in the acryloyl groups.[11,12] The length of PE brushes should be "linearly" dependent on the polymerization time for a "living" polymerization. For the purpose of comparison, control polymerizations with homogeneous catalyst **1** were also carried out (run 21 in Table 5.2). All the polymerization runs are summarized in Table 5.2. The resulting PE-grafted silicas were subject to extensive wash and centrifugation to remove possible free untethered polymers resulting from physically adsorbed catalyst **1**. However, the quantities of such free polymers have been found to be negligible (less than 5%) in all the products synthesized at this polymerization condition.

The PE-grafted silicas were characterized with TGA to determine the relative mass percentage of the PE brushes. Representatively, Figure 5.2 shows the TGA curves

of the PE-grafted silicas synthesized with Pd-Silica-I-1 (Figure 5.2a, samples 1–3) and Pd-Silica-I-3 (Figure 5.2b, samples 8–10), along with the curves for bare Silica-I, corresponding surface-functionalized silicas and catalyst-immobilized silicas for comparison. From the curves, their weight loss occurs mainly in the temperature region of 400–500 ℃. From the TGA weight loss data (at 700 ℃), the mass of grafted PE brushes relative to bare silica has been calculated. These data are summarized in Table 2. Figure 5.3 plots the dependencies of relative mass of PE brushes on the polymerization time with the six supported catalysts. A linear increase of the relative brush mass with polymerization time is found with each supported catalyst, hinting "living" growth of the PE brushes.

To determine the length and chain structures of the PE brushes, cleavage of the brushes off the silica surface was carried out through hydrolysis (under basic condition) of the ester linkage connecting the brushes to the silica surface. The cleaved brushes were then characterized with triple-detection GPC for their molecular weight and chain topology, and with ^{1}H NMR spectroscopy for their branching density. Representatively, Figure 5.4 shows the GPC elution curves of the cleaved PE brushes obtained with Pd-Silica-I-1. Additional GPC curves of other cleaved brushes are displayed in Figure S5.2 in Supporting Information. Narrow elution peaks are generally observed for the cleaved brushes obtained with all supported catalysts at 27 atm and 5 ℃. Meanwhile, the peaks move continuously towards to the left (i.e., reduced elution volume) with the increase of polymerization time, indicating the continuous growth of the brushes over time. The absolute number-average molecular weight ($M_{n,LS}$) and polydispersity index (PDI_{LS})

Table 5.2 Surface-initiated ethylene polymerizations with catalyst-immobilized silicas and characterization results.

Run	Catalyst & amount	T (℃)	C_2H_4 (atm)	Time[a] (h)	TGA Characterization[b]			GPC-LS-VIS Characterization[e]			NMR Characterization[f]	DLS Characterization[g]	
					Weight Loss @700 ℃ (%)	Relative Mass of Grafted PE to Silica[c] (g/100g silica)	Brush Density[d] (chains/nm^2)	$M_{n,LS}$ (kD)	PDI_{LS}	$[\eta]_w$ (mL/g)	Branches (1/1000 C)	R_h (nm)	PDI
1	Pd-Silica-I-1, 1.0 g	5	27	2	48	79	0.053	16	1.01	27	89	231	0.25
2		5	27	4	62	149	0.056	29	1.05	40	108	222	0.18
3		5	27	6	69	212	0.058	40	1.10	44	94	308	0.28
4		25	1	2	51	88	-	37	1.77	29	93	307	0.28
5	Pd-Silica-I-2, 1.0 g	5	27	2	44	67	0.044	16	1.02	24	Not Measured	205	0.12
6		5	27	4	57	119	0.041	32	1.02	31		242	0.20
7		5	27	6	64	166	0.044	42	1.06	46		283	0.22
8	Pd-Silica-I-3, 1.2 g	5	27	2	30	33	0.024	15	1.02	24	89	218	0.30
9		5	27	4	34	42	0.018	25	1.10	35	90	275	0.34
10		5	27	6	46	76	0.022	38	1.29	44	93	242	0.21
11		25	1	2	56	115	-	29	2.50	27	101	236	0.23
12	Pd-Silica-II-1, 0.85 g	5	27	2	48	87	0.157	17	1.12	26	84	107	0.11
13	Pd-Silica-II-1, 0.90 g	5	27	4	62	155	0.175	27	1.35	36	84	130	0.06
14	Pd-Silica-II-3, 3.50 g	5	27	6	72	250	0.184	41	1.02	38	87	153	0.35
15	Pd-Silica-II-2, 1.5 g	5	27	2	41	66	0.111	18	1.01	21	Not Measured	103	0.14
16	Pd-Silica-II-2, 1.2 g	5	27	4	55	117	0.116	31	1.02	36		113	0.10
17	Pd-Silica-II-2, 1.2 g	5	27	6	66	190	0.136	42	1.01	45		125	0.14
18	Pd-Silica-II-3, 0.90 g	5	27	2	30	39	0.078	15	1.02	25	93	125	0.36
19	Pd-Silica-II-3, 0.93 g	5	27	4	42	68	0.076	27	1.06	34	99	123	0.31
20	Pd-Silica-II-3, 0.74 g	5	27	6	49	93	0.059	47	1.06	47	98	130	0.26
21	**1**, 0.08 g	5	27	2 4 6	N/A	N/A	N/A	17 30 42	1.01 1.04 1.09	24 32 39	87 87 86	N/A	N/A
22	**1**, 0.08 g	25	1	2	N/A	N/A	N/A	47	1.09	19	102	N/A	N/A

[a] Other polymerization conditions: solvent, C_6H_5Cl; total volume, 240 mL for run 14 and 60 mL for other runs.

[b] Thermogravimetric analysis (TGA) was carried out in N_2 at a heating rate of 20 ℃/min.

[c] The relative mass of PE brushes to dry bare silica is calculated from TGA weight loss data according to the following equation:
relative PE mass = $\frac{W_{\text{PE–Silica}}}{100-W_{\text{PE–Silica}}} - \frac{W_{\text{Functionalized Silica}}}{100-W_{\text{Functionalized Silica}}}$ where $W_{\text{PE–Silica}}$ and $W_{\text{Functionalized Silica}}$ are the percentage weight loss of PE–grafted silica and corresponding surface-functionalized silica, respectively, at 700 ℃.

[d] Polyethylene grafting density = $\frac{m_{\text{PE–relative}}\,N_A}{100M_nS_{sp}}$ where $m_{\text{PE-relative}}$ is the relative mass of PE brushes; N_A is the Avogadro's number; M_n is the number–average molecular weight of PE brushes; S_{sp} is the specific surface area of the bare silica.

[e] The absolute number– and weight–average molecular weights (M_n and M_w) and polydispersity index (PDI_{LS}) of the cleaved polyethylene grafts were determined with light scattering detector of the triple–detection GPC. The weight–average intrinsic viscosity ($[\eta]_w$) data were determined with the viscosity detector of the triple–detection GPC.

[f] The branching density data of the cleaved PE brushes were determined with ^{1}H NMR spectroscopy.

[g] The hydrodynamic radius (R_h) and polydispersity index were determined with DLS in toluene (sample concentration: 0.1 mg/mL) at room temperature.

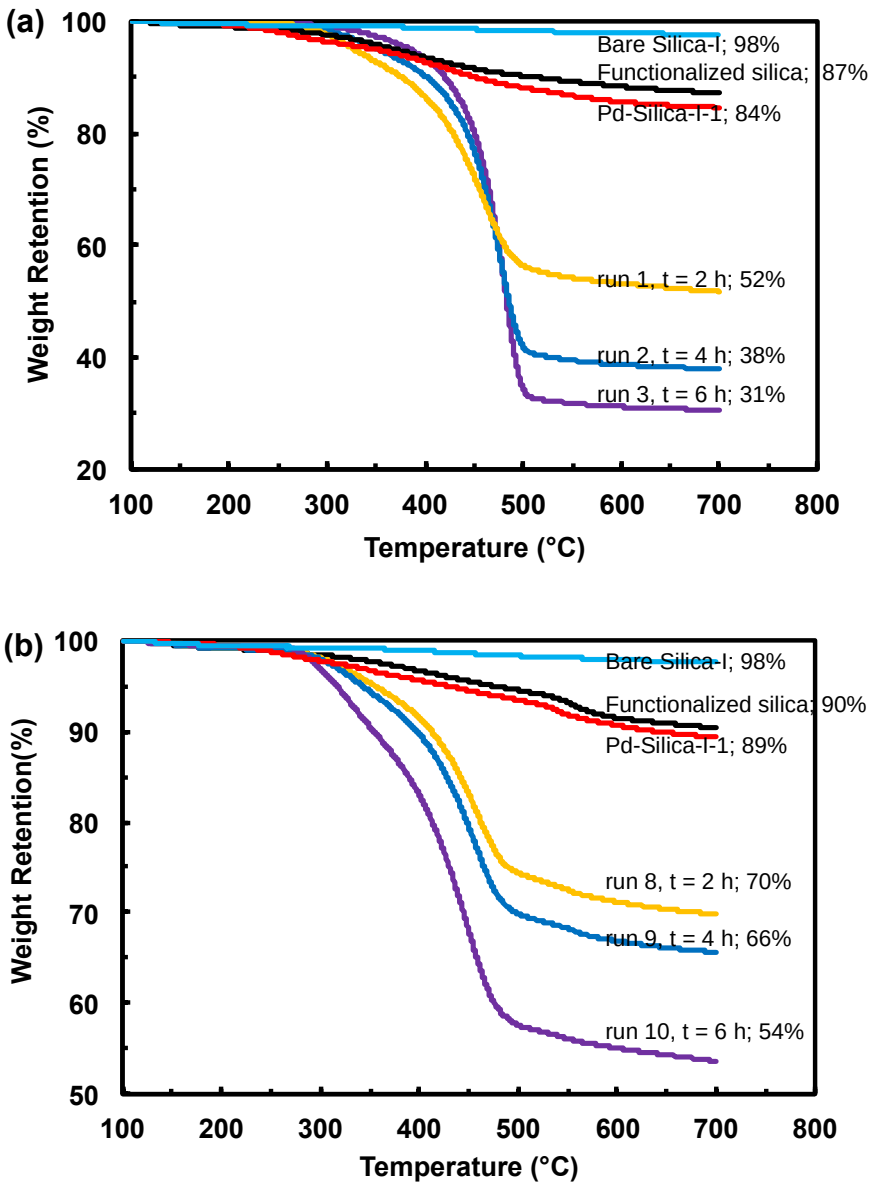

Figure 5.2 Thermogravimetric curves of PE-grafted silicas synthesized with Pd-Silica-I-1 (a) and Pd-Silica-I-3 (b) for different polymerization time (2, 4, and 6 h) at 27 atm and 5 ℃ (runs 1–3 with Pd-Silica-I-1 and runs 8–10 in Table 2). The corresponding curves for bare Silica-I, functionalized silica, and catalyst-immobilized silica are included for comparison. The final percentage weight retention data at 700 ℃ are listed.

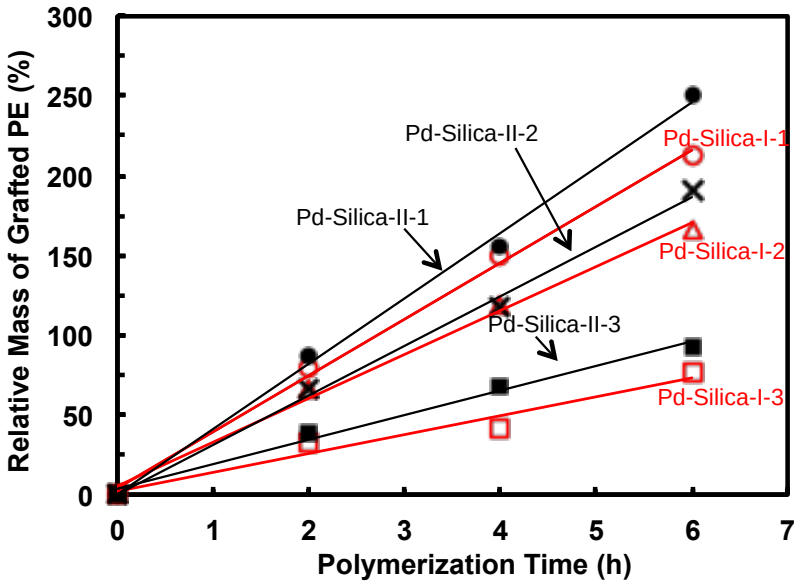

Figure 5.3 Dependencies of relative mass of PE brushes on polymerization time at the polymerization condition of 27 atm and 5 ℃.

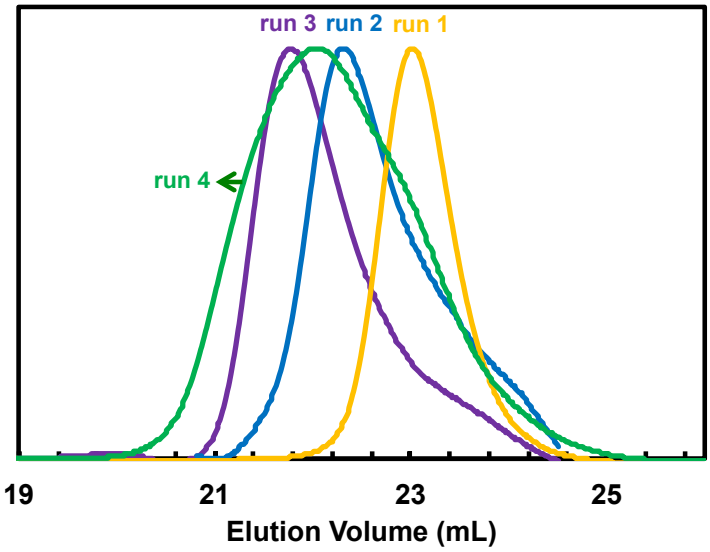

Figure 5.4 GPC elution traces (recorded from DRI detector) of cleaved PE brushes from PE-grafted silicas obtained with Pd-Silica-I-1 in runs 1, 2, and 3 carried out at 27 atm and 5 ℃, and in run 4 carried out 1 atm and 25 ℃. GPC eluent: THF at 1 mL/min and at 33 ℃.

data of the cleaved brushes have been determined with the light scattering detector and are summarized in Table 5.2. Figure 5.5 plots the dependencies of $M_{n,LS}$ on polymerization time. Nearly linear increase of $M_{n,LS}$ over time is found with all supported catalysts. Meanwhile, the $M_{n,LS}$ values obtained with all the supported catalysts and homogeneous catalyst **1** at a given time are generally very close though with small variations. This confirms that the ethylene incorporation is not impeded by the heterogeneous silica support since the Pd centers move progressively away from the surface with the growth of PE brushes.[11] The PDI values of the cleaved brushes are generally low (in the general range of 1.00–1.29), but with slight increase upon the increase of polymerization time. Along with the above linear increase of relative brush mass over time, the linear dependence of the $M_{n,LS}$ values of the brushes on time and low PDI values confirm that the surface-initiated ethylene polymerization with all the supported catalysts is "living" at this polymerization condition. Adjusting the polymerization time can thus enable the effective control of the brush length (up to about 45 kD herein).

With the relative mass and $M_{n,LS}$ data of the brushes, the brush density data have been calculated and are listed in Table 5.2. For the PE-grafted silica samples obtained with a given supported catalyst, the brush density is found to remain nearly constant despite their different polymerization time, confirming the consistency and reliability of the results. For example, the brush density obtained with Pd-Silica-I-1 is 0.053, 0.056, and 0.058 chains/nm^2 at the polymerization time of 2, 4, and 6 h, respectively. For a given type of silica, the brush density decreases with the decrease of $f_{ATCS,0}$ in the silica

surface functionalization step. In the set with Silica-I, it decreases from 0.055 chains/nm ^{2} for Pd-Silica-I-1 ($f_{ATCS,0}$ = 1) to 0.044 chains/nm^2 for Pd-Silica-I-2 ($f_{ATCS,0}$ =0.17) and to 0.022 chains/nm^2 for Pd-Silica-I-3 ($f_{ATCS,0}$ = 0.09). In the other set with Silica-II, it decreases from 0.17 chains/nm^2 for Pd-Silica-II-1 ($f_{ATCS,0}$ = 1) to 0.12 chains/nm^2 for Pd-Silica-II-2 ($f_{ATCS,0}$ = 0.09) and to 0.07 chains/nm^2 for Pd-Silica-II-3 ($f_{ATCS,0}$ = 0.06).

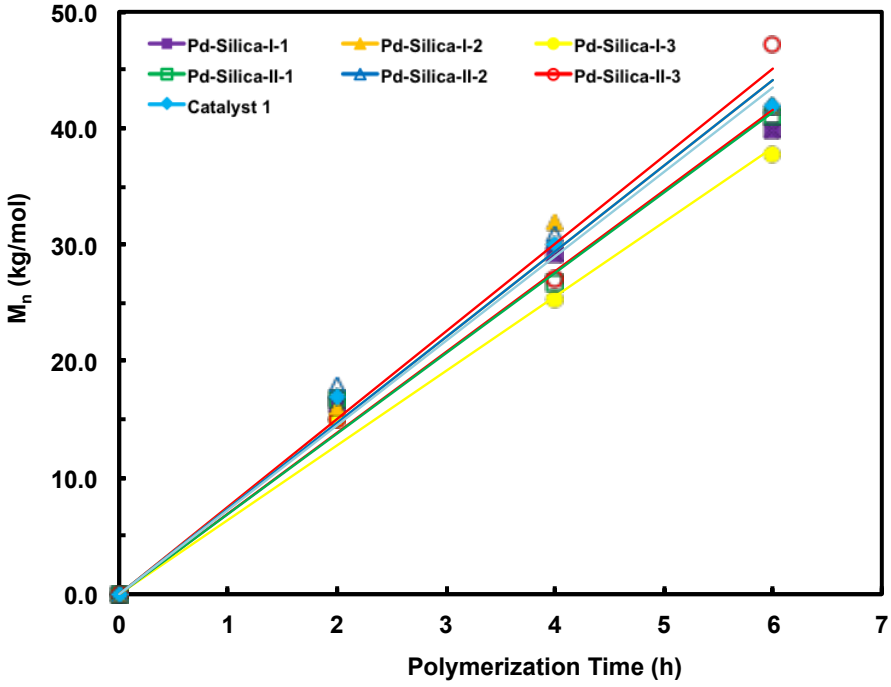

Figure 5.5 Dependencies of M_n on polymerization time for the cleaved PE brushes synthesized with the six different catalyst-immobilized silicas and the polymers synthesized with catalyst **1** at 27 atm/5 ℃. The M_n data were determined with light scattering detector in triple-detection GPC characterization.

For the silicas functionalized with ATCS alone (i.e., $f_{ATCS,0}$ = 1), the brush density data achieved herein (0.055 and 0.12 chains/nm^2 for Silica-I and Silica-II,

respectively) are lower than the value (0.15 chains/nm^2) obtained in our previous work with solid silica nanoparticles, possibly due to some variations in experimental procedures.[11,12] In consistency with our hypothesis, the above results confirm that significant reduction in the brush density can only be achieved at low $f_{ATCS,0}$ values. For instance, the density is reduced by half only when $f_{ATCS,0}$ is reduced dramatically to about 0.09 or 0.06 for Silica-I and Silica-II, respectively. Comparing the brush density data with the two types of silicas, we find that the density achieved with Silica-II is significantly greater than the counter one achieved with Silica-I at the same $f_{ATCS,0}$. This indicates higher catalyst immobilization density data with Silica-II. However, as shown in our previous discussion, the acryloyl density data are similar in two sets of surface-functionalized silicas (see Table 5.1). The precise reason leading to this difference in the brush density with the two silicas is unknown. Despite this, the results obtained herein with both types of silicas confirm the successful control of PE brush density by adjusting $f_{ATCS,0}$ in the silica surface functionalization step.

^{1}H NMR spectra of some representative cleaved brushes are shown in Figure S5.3 in Supporting Information. In addition to the dominant peaks (methyl, methylene, and methane) from the branched ethylene sequences, the resonance peak (signal *a* in the figure) assigned to CH_2 protons next to the terminal ester functionality is clearly present in all the spectra. This confirms the end tethering of the brushes to the silica surface through the ester linkage. From the spectra, the cleaved brushes all have a branching density of about 90 per 1000 carbons, which is typical for PE synthesized with homogenous catalyst **1**. The formation of such branching structures should result from

the intrinsic chain walking mechanism of the Pd–diimine catalysts.[16,17] Despite their high branching density, the brushes should possess a linear chain topology with primarily short side branches due to the short chain walking distance at this polymerization condition on the basis of our previous studies.[15,17,18c-e] Figure 5.6 shows the Mark-Houwink plots of the cleaved PE brushes, where the weight-average intrinsic viscosity ($[\eta]_w$) is plotted against the weight-average molecular weight ($M_{w,LS}$) for these narrow-distributed polymers. In the figure, a reference curve ($\log[\eta]_w = 0.0603 \log M_w - 1.19$)[15b-d,19e] for linear polymers synthesized with homogeneous catalyst **1** has also been included. Compared to polymers of equal molecular weight obtained with **1**, the cleaved brushes exhibit similar $[\eta]_w$ values, confirming their possession of similar linear chain topology as those synthesized with **1**. At this polymerization condition, the silica supports show negligible effect on chain growth, catalyst chain walking, and polymer topology on the basis of their molecular weight and intrinsic viscosity data.

5.3.3 Surface-Initiated Ethylene Polymerization at 1 atm and 25 ℃ for Synthesis of Silicas Grafted with Hyperbranched PE Brushes

A remarkable feature of Pd–diimine catalysts in ethylene polymerization is their capability of rendering branched polyethylenes of tunable chain topologies, ranging from highly compact hyperbranched to linear, through changing the polymerization temperature and pressure.[16,17,19a-g] This feature is also utilized herein for tuning the topology of PE brushes. As a demonstration, two ethylene polymerization runs (runs 4 and 11 in Table 5.2) were carried out with Pd-Silica-I-1 and Pd-Silica-I-3, respectively,

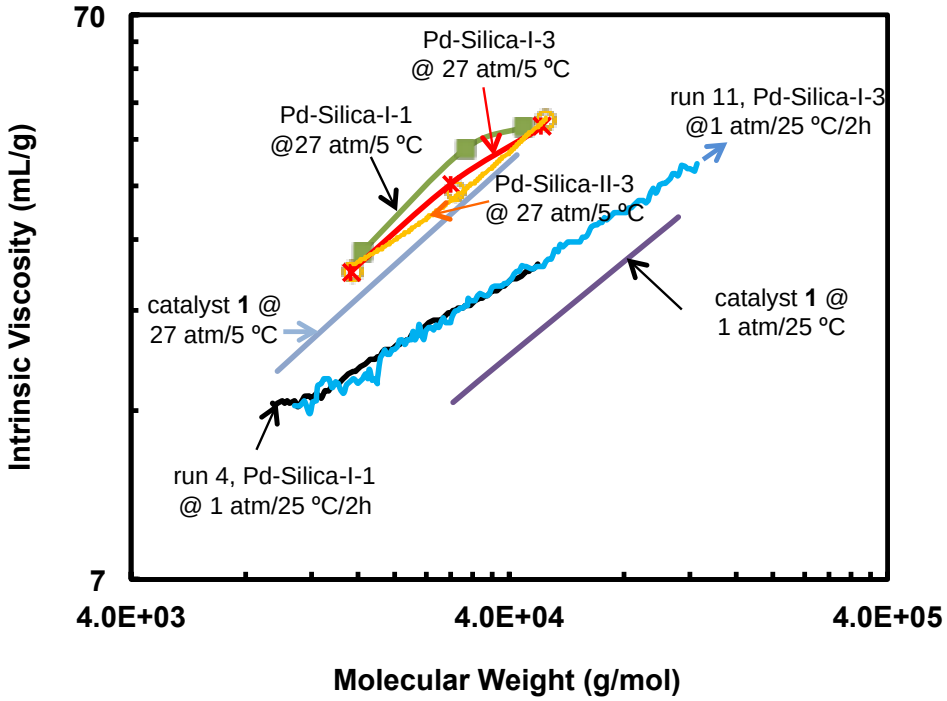

Figure 5.6 Mark-Houwink plot (intrinsic viscosity vs. molecular weight) for cleaved PE brushes. Two reference curves ($[\eta]= 0.0646M^{0.603}$ and $[\eta]= 0.0525M^{0.548}$)[19e] for PEs synthesized with homogeneous catalyst **1** at 27 atm/5 ℃ and 1 atm/25 ℃, respectively, are included for comparison.

for 2 h at 1 atm and 25 ℃. At this condition, catalyst chain walking distance should be significantly enhanced, giving rise to hyperbranched topology.[16,17,19a-g] From triple-detection GPC characterization, the resulting cleaved PE brushes have much higher $M_{n,LS}$ (37 and 29 kg/mol, respectively, as opposed to 16 kg/mol) and broader molecular weight distribution (PDI_{LS} of 1.77 and 2.50, respectively, as opposed to 1.02) compared to those synthesized at 27 atm and 5 ℃ for 2 h of polymerization. As a demonstration, the GPC elution curve for the cleaved brush in run 4 is also displayed in Figure 5.4. The

elution peak is much broader. Meanwhile, significantly higher amounts of untethered free polymers (about 30%) have been found. These evidences indicate the deterioration in the "living" behavior of the surface-initiated polymerization with the appreciable occurrence of chain transfer reactions at this condition. As investigated in our earlier studies with catalyst **1**, the higher temperature (25 ℃) should be the primary reason leading to the enhanced chain transfer.[19e]

The intrinsic viscosity curves of the two cleaved brushes are also included in Figure 5.6. Because of their high PDI values, the curves are plotted across their molecular weight distribution. The two curves are overlapping nearly in their entire molecular weight region, which confirms their virtually identical chain topology. Meanwhile, the reference curve for the polymer synthesized with **1** at the same condition is also displayed in the figure. Compared to the other brushes synthesized at 27 atm and 5 ℃, the two brushes have significantly downshifted curves (i.e., much reduced intrinsic viscosity at a given molecular weight) with reduced slope. These evidences prove their more compact chain topologies than the linear brushes obtained 27 atm and 5 ℃, confirming the success of achieving the brush topology control by adjusting the polymerization conditions. This strategy, employing the chain walking mechanism of the tethered Pd catalysts to achieve hyperbranched brush topology, is fundamentally different from the conventional strategies for generating hyperbranched brushes, which often involve multistep procedures and/or functional monomer stocks.[20] Due to their broad molecular weight distribution, accurate determination of the density for these two hyperbranched brushes is difficult. Suppose their density should

approximately equal the values (0.055 and 0.022 chains/nm^2, respectively) accurately determined above for the two supported catalysts at 27 atm and 5 ℃.

Compared to the hyperbranched analogue polymer by **1** that even has a further downshifted intrinsic viscosity curve, the brushes, however, still have less compact chain topology. This deviation suggests the presence of the significant hindering effect of the silica surface on the catalyst chain walking at this polymerization condition, which reduces appreciably catalyst chain walking distance and chain compactness. Such an effect should be particularly pronounced at the beginning of brush growth since at that time the Pd centers are closest to the silica surface. As the Pd centers move gradually away from the surface following continuous brush growth, this hindering effect should progressively weaken. This is proved to be the case by investigating the gap between the intrinsic viscosity curves of the brushes and the reference curve. From Figure 5.6, the curves have different slopes. The gap between them is most significant at the low-molecular-weight end and it is gradually reduced with the increase of molecular weight. Since the chain conformation of polymer brushes often shows a dependence on brush density,[1a] the steric crowdedness exerted by the neighboring brushes hypothetically may also affect the chain topology of the growing brushes particularly at high brush densities. This effect, however, appears to be insignificant given the overlapping intrinsic viscosity curves found for the two brushes having significantly different densities. Perhaps the difference in brush density herein is not significant enough to show this effect.

5.3.4 Thermal Properties of PE-Grafted Silicas

Thermal properties of the various PE-grafted silicas synthesized above were characterized with DSC. Representative DSC thermograms of those synthesized with Pd-Silica-I-1 and Pd-Silica-I-3 are shown in Figure S5.4 in Supporting Information. Highly branched PEs synthesized with Pd–diimine catalysts typically show two transitions, a glass transition with T_g at around –67 °C and a broad but weak melting endotherm with T_m at around –34 °C.[17,19a-g,i] Compared to those of untethered PEs, thermograms of PE-grafted silicas (particularly, those with lower relative polymer contents) are generally less well-defined, with a slow gradual decrease of heat capacity in a very broad temperature range (from about –70 °C to about 30 °C). This should result from the restricted segmental movement of the brushes due to their covalent end-tethering on the silica surface.[11,12] By comparing the different samples, the variations in brush length, density, and topology do not appear to have a distinct effect on the thermal transitions.

5.3.5 Effect of PE Brushes on Silica Dispersion in Solution and Particle Size

DLS measurements were performed on the dispersion of the PE-grafted silicas in toluene to study the effect of PE brushes on their solution dispersibility and particle size. The measurements were carried out both immediately after sonication and after leaving the sonicated dispersion stand still for 20–24 h to investigate the stability of the dispersion. Compared to the bare silicas, the PE-grafted silicas show much enhanced

solution dispersability due to the presence of PE brushes that have good solubility in toluene. For all the PE-grafted silicas, their profiles of particle size distribution obtained after sonication and after long standing are nearly identical (see Figure S5.5 in Supporting Information), confirming the good stability of the dispersion and the absence of aggregation among the particles. Hydrodynamic radius (R_h) and PDI data of the PE-grafted silicas are listed in Table 5.2. In general, the samples based on Silica-I have higher R_h values (205–308 nm) than the others based on Silica-II (103–153 nm). In each set synthesized with the same catalyst-immobilized silica, increasing the polymerization time at 27 atm/5 ℃ generally leads to a noticeable increase in R_h. However, the change in brush density does not show a clear trend of effect on R_h.

For the bare silicas, DLS measurements could not be carried out in toluene since DLS signals were very unstable due to the immediate particle aggregation following sonication. Relatively more stable signals were obtained in THF as the solvent due to its higher polarity. However, their profiles of particle size distribution obtained right after sonication and after long standing are dramatically different (see Figure S5.5). Significant broadening of the profile and increase in the average particle size are observed after long standing due to the aggregation of the particles having highly hydrophilic surface.

5.3.6 Compounding of Elastomer Nanocomposites and Effect of PE Brushes on Nanofiller Dispersion

Silica nanoparticles have long been used as nanofillers for constructing polymer nanocomposites. Due to their high tendency to aggregate as a result of the highly hydrophilic surface, the uniform dispersion of silica nanoparticles and their strong interactions with the polymer matrix are critical to achieve optimally enhanced nanocomposite properties.[21] Surface modification of silica nanoparticles by covalently grafting polymer brushes has been shown to affect their dispersion and interactions with polymer matrix.[22-25] Given their well-defined brush structural parameters (length and density), the PE-grafted silicas synthesized herein are subsequently used as nanofillers to compound polymer nanocomposites. The effects of brush length and density on the nanofiller dispersion and mechanical properties (rheological and tensile properties) of the nanocomposites are investigated.

An EOC elastomer (Engage 8130) is chosen here as the matrix polymer for compounding nanocomposites with PE-grafted silicas and bare silicas (as control) as nanofillers. Due to limited amounts of the PE-grafted silicas, the composites were formulated with the content of actual dry bare silica fixed at 7 wt% in the case with Silica-I and PE-grafted Silica-I samples, or 5 wt% in the case with Silica-II and PE-grafted Silica-II samples. Containing high branching density (estimated at about 56 branches per 1000 carbons), the EOC matrix polymer should have good compatibility with the highly branched PE brushes herein. It has been previously used in our recent works as the matrix polymer to compound nanocomposites with multiwall carbon nanotubes, which were noncovalently surface-functionalized with hyperbranched PE, as

nanofillers.[26] Significantly enhanced nanotube dispersion has been achieved therein because of the good compatibility between EOC and the hyperbranched PE.

Figure 5.7 shows the TEM images of the sets of composites compounded with bare Silica-I and PE-grafted Silica-I samples of different brush density and length (runs 1–3 at the higher brush density of 0.055 chains/nm^2, and runs 8–10 at the lower brush density of 0.022 chains/nm^2, see Table 4.2). It can be seen that the composites with bare Silica-I and run 3 sample, which has longest brush length and higher brush density in the set, contain large aggregates. With the increase of brush length at a given density, the size of aggregates tends to increase. Detailed image analysis was performed with the TEM images. Feret diameter measurements were used to statistically determine the diameter of the aggregates since many of them generally followed a spherical shape. Figure 5.8 confirms the above trend. Among this set of nanofillers, bare Silica-I and run 3 sample render the largest average aggregate areas and Feret diameters with the largest standard deviation. For samples from runs 1–3 having the same higher brush density, increasing the brush length renders the significant increases in the average aggregate areas and Feret diameter. For samples from run 8–10 at the same lower brush density, aggregation of the nanofillers is reduced, and average aggregate area and Feret diameter show marginal increases with the increase of brush length.

While the formation of large aggregates with bare Silica-I is expected due to the presence of strong silica-silica interactions, the significantly enhanced filler aggregation with the increase of brush length from run 1 to 3 is surprising. With PE-grafted silicas,

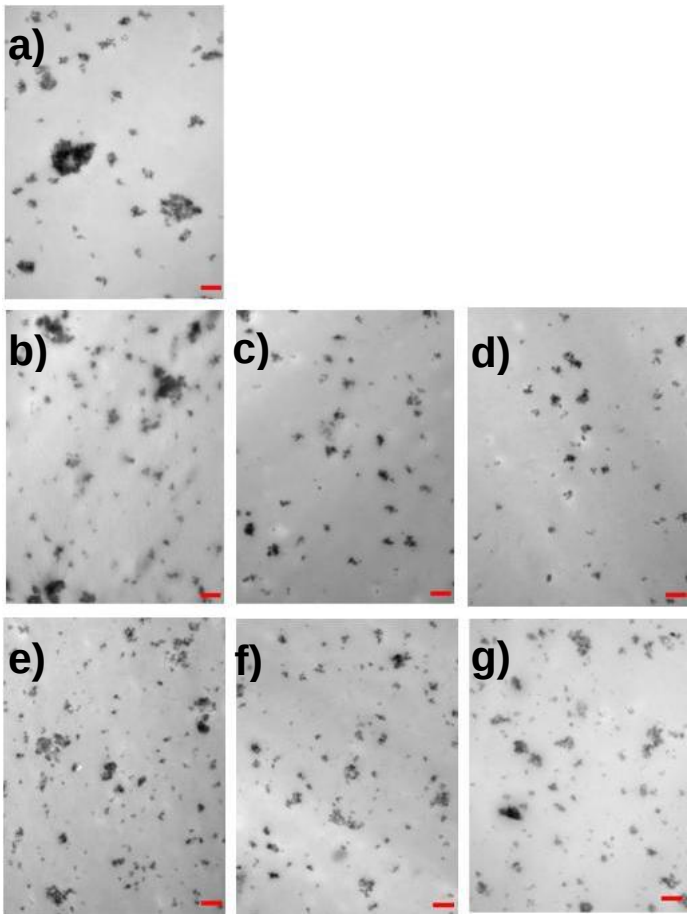

Figure 5.7 TEM images of the EOC composites with bare Silica-I (a), PE-grafted Silica-I synthesized in run 1 (see Table 5.2) (b), run 2 (c), run 3 (d), run 8 (e), run 9 (f), and run 10 (g). The content of dry bare silica in the composites is 7 wt%. All images were taken at a magnification of 19,000 at 200 kV. Scale bar = 500 nm.

the increases in both the length and density of polymer brushes are supposed to induce an enhanced steric repulsion between the silica particles and weaken more significantly the silica-silica interactions, rendering disaggregation. The unexpected finding with samples from runs 1–3 herein suggests the existence of attractive interactions between the grafted brushes on the fillers, which are enhanced with the increase in brush length

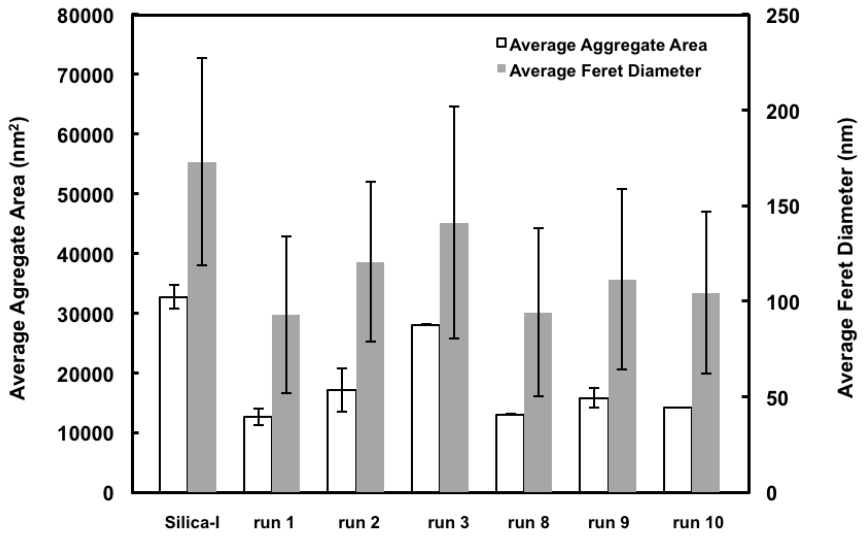

Figure 5.8 Average aggregate area and Feret diameter of the EOC composites with bare Silica-I, PE-grafted Silica-I samples synthesized in runs 1–3 and 8–10. The results were obtained by performing image analysis on the TEM images shown in Figure 5.7. Error bars correspond to standard deviation.

or density. Chain entanglements among the brushes can be one type of such interactions that tend to promote the aggregations of the PE-grafted silicas.

Figure 5.9 displays the TEM images of the composites compounded with bare Silica-II and PE-grafted Silica-II samples (runs 12 and 13, and runs 18–20 in Table 5.2). Large aggregates with poor filler dispersion can be seen in the composite containing bare Silica-II, while improved more uniform filler dispersion is found in the composites with PE-grafted Silica-II samples. Figure 5.10 confirms that the average aggregate area and Feret diameter with bare Silica-II are significantly larger than those with PE-grafted ones. Meanwhile, it can also be concluded that there is no significant differences in

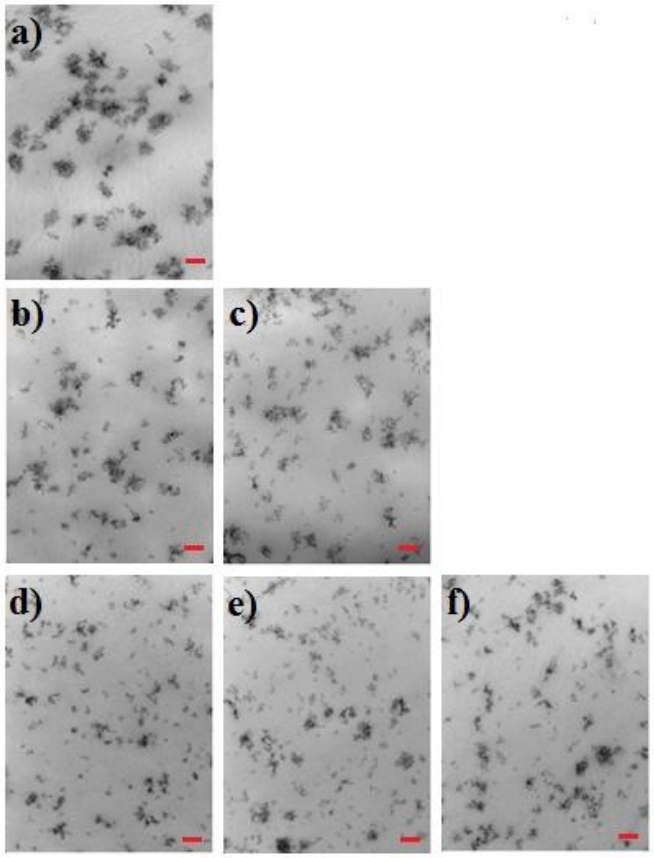

Figure 5.9 TEM images of the EOC composites with bare Silica-II (a), PE-grafted Silica-II sample in run 12 (see Table 2) (b), run 13 (c), run 18 (d), run 19 (e), and run 20 (f). The content of dry bare silica in the composites is 5 wt%. All images were taken at a magnification of 50,000 at 200 kV. Scale bar = 100 nm.

average aggregate area and Feret diameter of the composites containing the PE-grafted Silica-II samples, though they are significantly different in brush density and/or length. Covalent grafting of PE brushes on Silica-II thus improves filler dispersion, but with no significant effects from brush length and density. This is in contrast to the above finding with the set of Silica-I samples. This difference is reasoned to result from the use of different types of silicas which differ in surface properties (precipitated Silica-I vs.

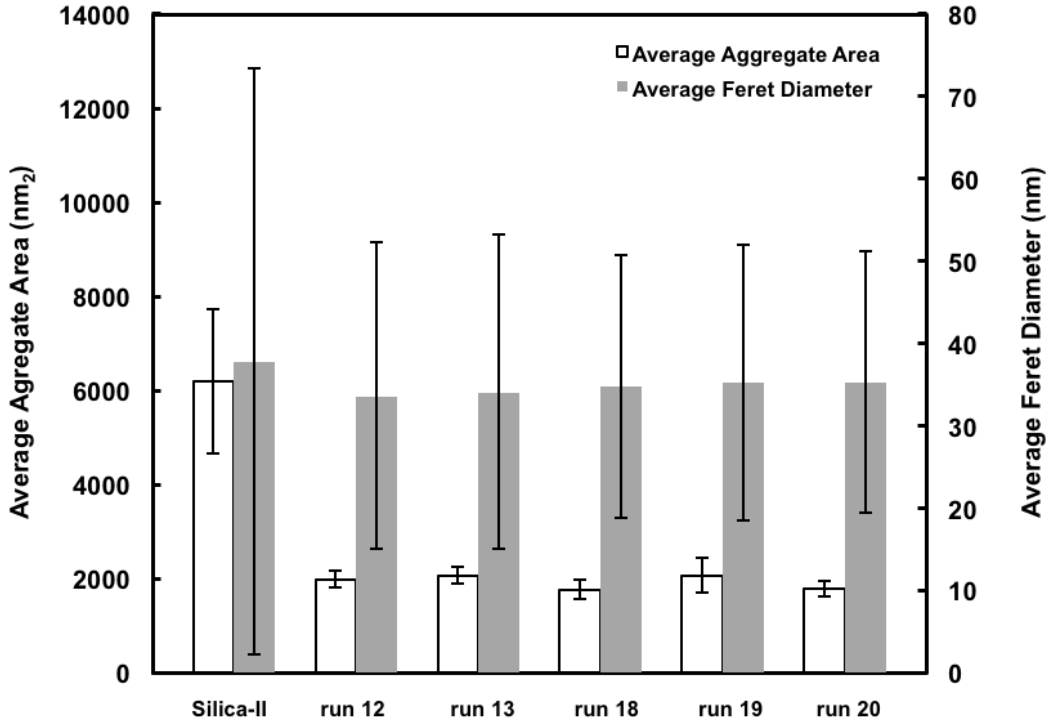

Figure 5.10 Average aggregate area and Feret diameter of the EOC composites with bare Silica-II, PE-grafted Silica-II samples synthesized in runs 12, 13, and 18–20. The results were obtained by performing image analysis on the TEM images shown in Figure 9. Error bars correspond to standard deviation.

fumed Silica-II). It has been previously noted in the literature that the silica type has an effect on the properties of compounded nanocomposites.[22]

5.3.7 Rheological Properties of Nanocomposites

Rheological properties of the above nanocomposites were investigated with small amplitude dynamic oscillatory rheometry at 190 ℃. The storage modulus (G ′)

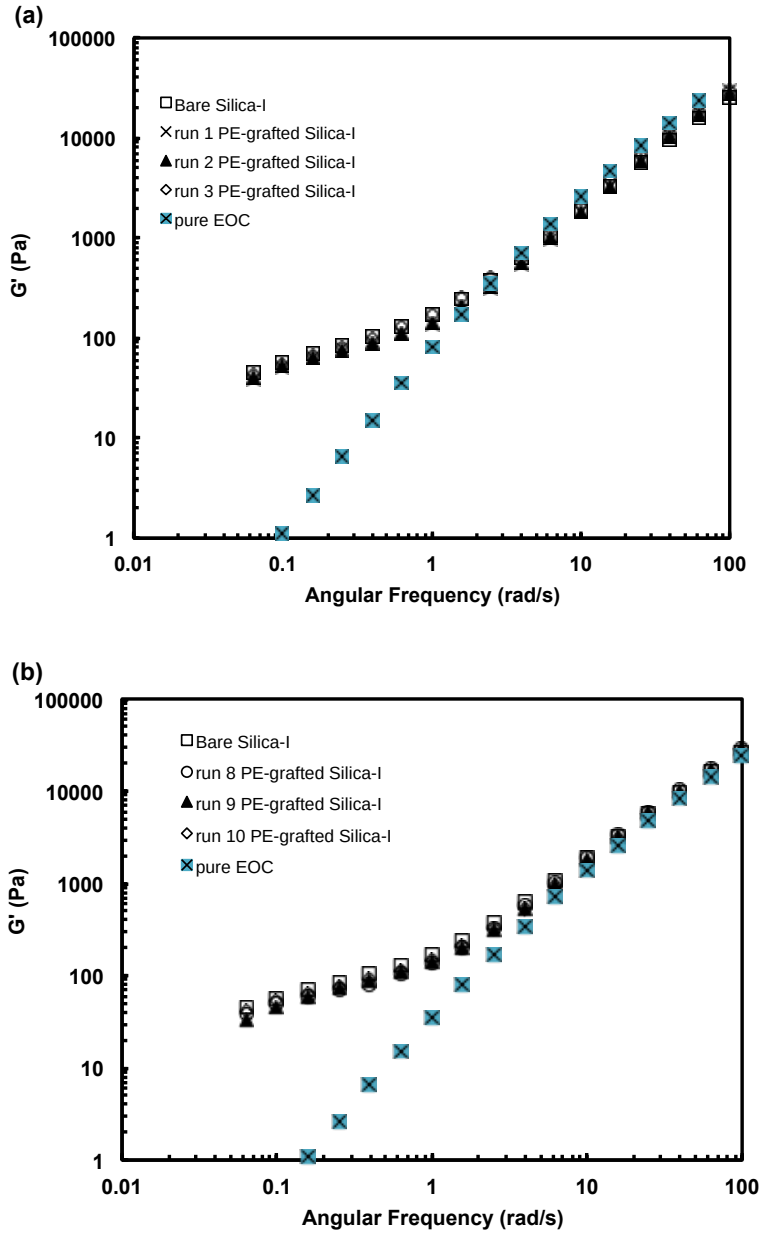

Figure 5.11 Storage modulus (G′) curves (at 190 ℃) for the EOC composites compounded with various PE-grafted Silica-I samples as fillers: (a) PE-grafted Silica-I samples synthesized in runs 1–3; (b) PE-grafted Silica-I samples synthesized in runs 8–10. The curves for pure EOC and the composite compounded with bare Silica-I are also included. The filler loading is designed with the dry bare silica content in the composites being 7 wt%.

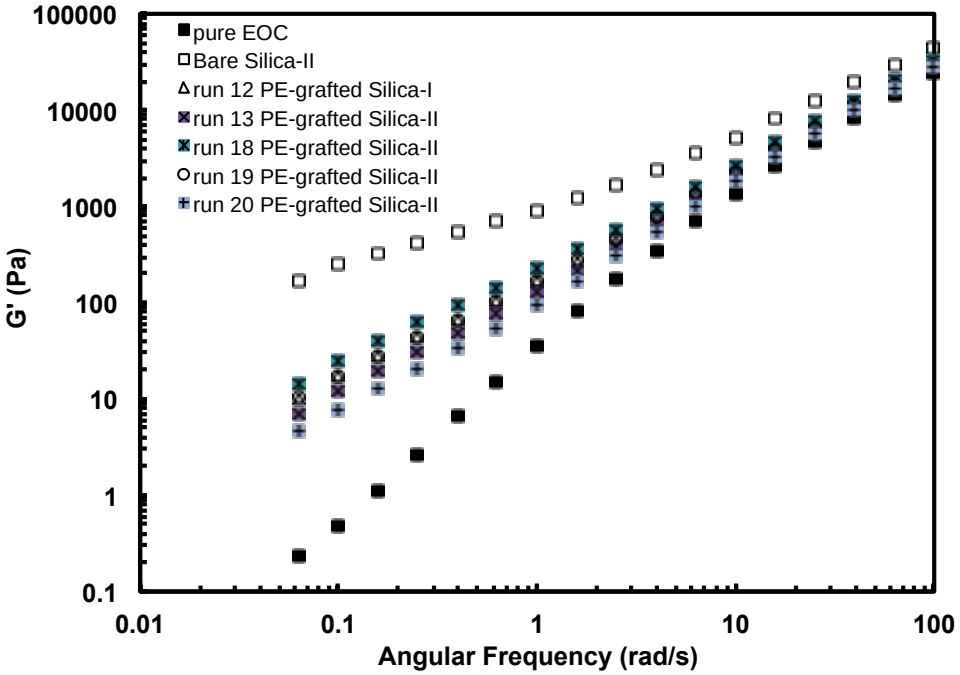

Figure 5.12 Storage modulus (G´) curves (at 190 ℃) for the EOC composites compounded with various PE-grafted Silica-II samples (synthesized in runs 12, 13, and 18–20) as fillers. The curves for pure EOC and the composite compounded with bare Silica-II are also included. The filler loading is designed with the dry bare silica content in the composites being 5 wt%.

curves displayed in Figure 5.11 and 5.12 reveal that the addition of either bare or PE-grafted silica results in a gel-like behavior with significantly raised G´values compared to the matrix polymer in the terminal flow region. Often observed in polymer/silica nanocomposites, this gel-like behavior is indicative of the presence of a physical filler network in the nanocomposites. Meanwhile, there is often a sensitive dependence of the G´value on filler dispersion at a given filler loading, with poorer dispersion (i.e., larger aggregates) often rendering more elevated G´values.[18,22,24,25] To better illustrate the differences, Figures 5.13 compares the G´values at 0.0628 rad/s for the two respective

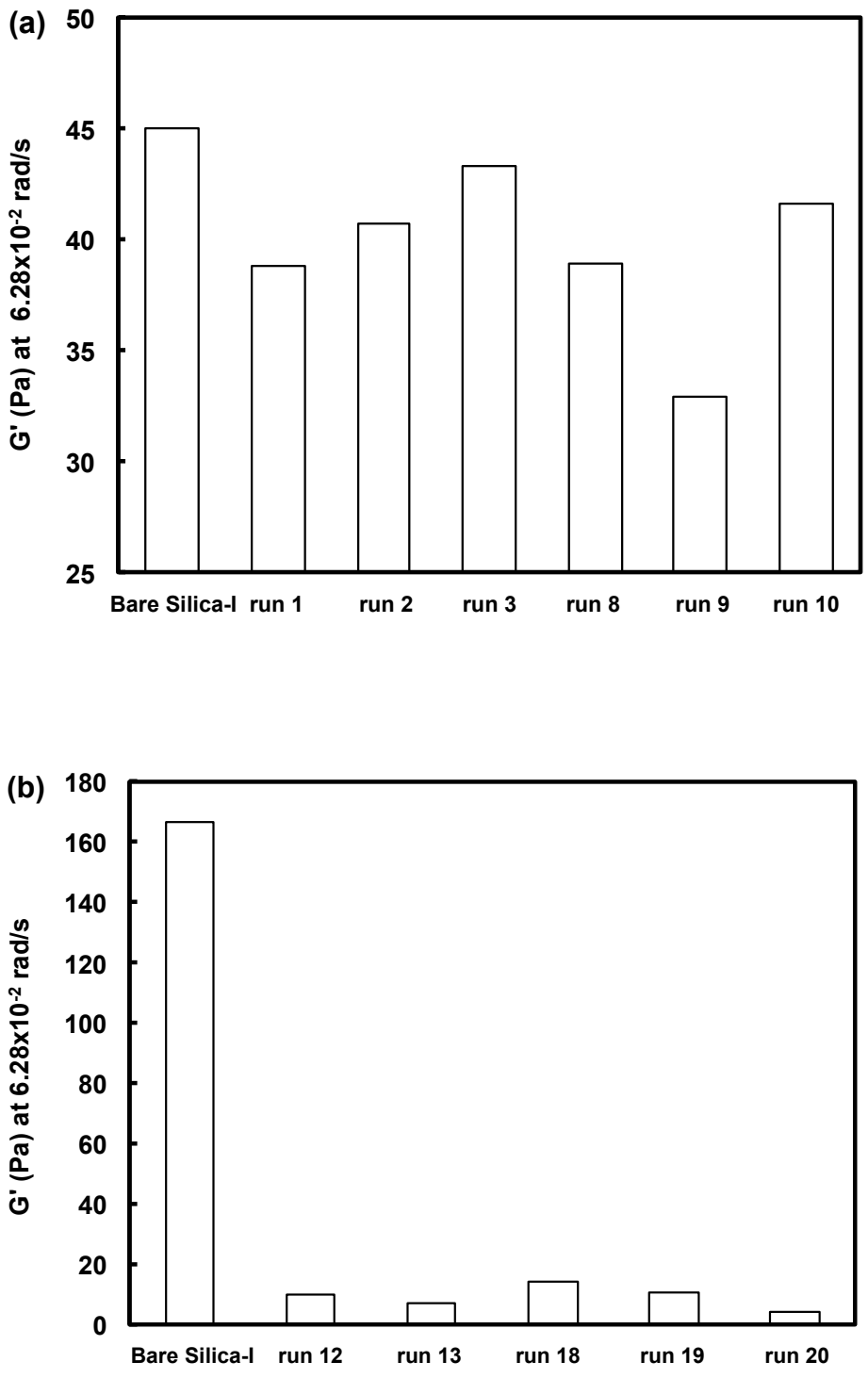

Figure 5.13 G ´values at 6.28×10^{-2} rad/s (at 190 °C) for the two sets of composites: (a) the set with Silica-I series of samples as fillers; (b) the set with Silica-II series of samples as fillers.

sets of composites. In each set, the composite with the highest average aggregate area and Feret diameter (i.e., those with bare silica) displays the highest G´value. In the set with Silica-I, increasing the brush length at a given density (for example, comparing samples 1–3 in Figure 5.13a) leads to enhanced G´, which is consistent with the deteriorated filler dispersion upon increasing brush length found above. In the other set with Silica-II, much reduced G´values (around 10 Pa, see Figure 5.13b) are noted in those with PE-grafted silicas compared to that (ca. 100 Pa) with bare Silica-II. In agreement with the finding from the TEM image analysis, this further confirms the significantly enhanced filler dispersion after polymer modification of Silica-II. Meanwhile, increasing brush length causes a trend of decrease in G´(for example, comparing runs 12 and 13 samples, and runs 18–20 samples), indicative of enhanced filler dispersion upon increasing brush length for Silica-II. However, the change in brush density does not seem to have a significant effect on the filler dispersion with no clear trend of change in G´found.

5.3.8 Tensile Properties of Nanocomposites

Due to limited sample amounts, tensile properties were only determined for the nanocomposites compounded with PE-grafted silica samples obtained in runs 12 and 14 (see Table 5.2), besides bare Silica-II, at the bare silica loading of 5 wt%. Figure 14 shows the tensile elongation at breakage and modulus of the composites. Compared to pure EOC, the addition of bare Silica-II at this dosage does not seem to change the ductility of the composite despite the filler aggregation demonstrated above, but with a

clearly enhanced modulus. Both polymer-grafted silicas give rise to similarly enhanced ductility compared to the unfilled EOC. Meanwhile, modulus of the composites also shows a trend of increase with the increase of PE brush length. Both the reinforcement and the increase in ductility with the PE-grafted Silica-II are attributed to the improved filler dispersion resulting from the presence of the PE brushes.

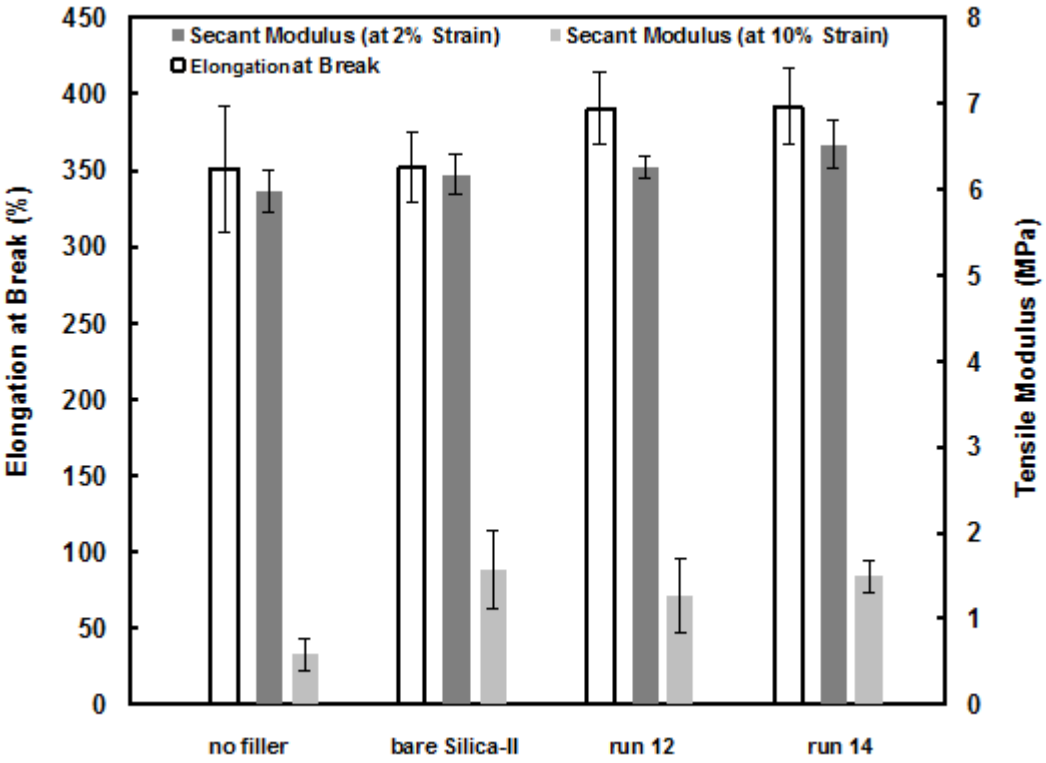

Figure 5.14 Elongation at breakage and tensile modulus of the composites compounded with Silica-II series samples (bare Silica-II, runs 12 and 14 samples) as fillers.

5.4 Conclusions

We have demonstrated in this work the successful control of the PE brush density, length, and topology in surface-initiated ethylene polymerization from both types of silica particles, Silica-I and Silica-II. The approach of using mixed silane agents (ATCS and ETCS at different $f_{ATCS,0}$ values) is confirmed effective in rendering different brush densities through adjusting the density of surface-tethered acryloyl groups in surface-functionalized silicas and in turn the density of immobilized Pd catalysts in catalyst-immobilized silicas. The brush density achieved herein is in the range of 0.022–0.055 chains/nm^2 for Silica-I and 0.07–0.17 chains/nm^2 for Silica-II. At the polymerization condition of 27 atm/5 ℃, the surface-initiated polymerization behaves typically "living" with nearly linear increase of brush length with polymerization time for all the catalyst-immobilized silicas. This thus enables the control of brush length by adjusting the polymerization time, with the highest value of about 45 kg/mol achieved herein at 6 h of polymerization. The brush topology tuning is achieved by adjusting the polymerization condition. At 1 atm/25 ℃, hyperbranched brushes with compact topology yields as opposed to the linear topology featured in those synthesized at 27 atm/5 ℃.

From both morphological and rheological properties of EOC nanocomposites compounded with various PE-grafted silicas, the presence of PE brushes on silica particles is found to generally improve nanofiller dispersion in the composites, but with different effects from the change of brush length in the two sets of silica samples. In the set with Silica-I series of fillers, increasing brush length leads to deteriorated filler dispersion. On the opposite, enhanced filler dispersion yields with the increase of brush

length. The change in brush density in both sets of samples shows negligible effect on the filler dispersion. Tensile testing of the composites compounded with PE-grafted Silica-II samples indicates that the PE grafting improves both ductility and modulus of the composites, which is more pronounced at increased brush length.

5.5 References

1. See representative review papers: (a) Zhao, B.; Brittain, W. *J. Prog. Polym. Sci.* **2000**, *25*, 677–710; (b) Pyun, J.; Matyjaszewski, K. *Chem. Mater.* **2001**, *13*, 3436–3448; (c) Kato, K.; Uchida, E.; Kang, E.-T.; Uyama, Y.; Ikada, Y. *Prog. Polym. Sci.* **2003**, *28*, 209–259; (d) Barbey, R.; Lavanant, L.; Paripovic, D.; Schüwer, N.; Sugnaux, C.; Tugulu, S.; Klok, H.-A. *Chem. Rev.* **2009**, *109*, 5437–5527; (e) Orski, S. V.; Fries, K. H.; Sontag, S. K.; Locklin, J. *J. Mater. Chem.* **2011**, *21*, 14135–14149; (f) Olivier, A.; Meyer, F.; Raquez, J.-M. Damman, P.; Dubois, P. *Prog. Polym. Sci.* **2012**, *37*, 157–181; (g) Azzaroni, O. J. *Polym. Sci. Part A: Polym. Chem.* **2012**, *50*, 3225–5258; (h) Radhakrishnan, B.; Ranjan, R.; Brittain, W. J. *Soft Matter* **2006**, *2*, 386–396.
2. Some examples on surface-initiated anionic polymerization: (a) Jordan, R.; Ulman, A.; Kang, J. F.; Rafailovich, M. H.; Sokolov, J. *J. Am. Chem. Soc.* **1999**, *121*, 1016–1022; (b) Advincula, R.; Zhou, Q.; Park, M.; Wang, S.; Mays, J.; Sakellariou, G.; Pispas, S.; Hadjichristidis, N. *Langmuir* **2002**, *18*, 8672–8684; (c) Advincula, R. *Adv. Polym. Sci.* **2006**, *197*, 107–136.

3. Some examples on surface-initiated cationic polymerization: (a) Jordan, R.; Ulman, A. *J. Am. Chem. Soc.* **1998**, *120*, 243–247; (b) Zhao, B.; Brittain, W. J. *J. Am. Chem. Soc.* **1999**, *121*, 3557–3558; (c) Zhao, B.; Brittain, W. J. *Macromolecules* **2000**, *33*, 342–348.
4. Some examples on surface-initiated ring-opening polymerization: (a) Jaworek, T.; Neher, D.; Wegner, G.; Wieringa, R. H.; Schouten, A. J. *Science* **1998**, *279*, 57–60; (b) Husemann, M.; Mecerreyes, D.; Hawker, C. J.; Hedrick, J. L.; Shah, R.; Abbott, N. L. *Angew. Chem. Int. Ed.* **1999**, *38*, 647–649; (c) Kratzmüller, T.; Appelhans, D.; Braun, H.-G. *Adv. Mater.* **1999**, *11*, 555–558; (d) Choi, I. S.; Langer, R. *Macromolecules* **2001**, *34*, 5361–5363; (e) Zeng, H.-L.; Gao, C.; Yan, D.-Y. *Adv. Funct. Mater.* **2006**, *16*, 812–818.
5. Some examples on surface-initiated ring-opening metathesis polymerization: (a) Weck, M.; Jackiw, J. J.; Rossi, R. R.; Weiss, P. S.; Grubbs, R. H. *J. Am. Chem. Soc.*, **1999** *121*, 4088–4089; (b) Kim, N. Y.; Jeon, N. L.; Choi, I. S.; Takami, S.; Harada, Y.; Finnie, K. R.; Girolami, G. S.; Nuzzo, R. G.; Whitesides, G. M.; Laibinis, P. E. *Macromolecules* **2000**, *33*, 2793–2795; (c) Juang, A.; Scherman, O. A.; Grubbs, R. H.; Lewis, N. S. *Langmuir* **2001**, *17*, 1321–1323; (d) Harada, Y.; Girolami, G. S.; Nuzzo, R. G. *Langmuir* **2003**, *19*, 5104–5114; (e) Skaff, H.; Ilker, M. F.; Coughlin, E. B.; Emrick, T. *J. Am. Chem. Soc.* **2002**, *124*, 5729–5733.
6. Some examples on surface-initiated atom-transfer radical polymerization: (a) Pyun, J.; Kowalewski, Matyjaszewski, T.; K. *Macromol. Rapid Commun.* **2003**, *23*, 1043–1059; (b) Werne, T. von; Patten, T. E. *J. Am. Chem. Soc.* **2001**, *123*, 7497–7505; (c) Pyun, J.; Matyjaszewski, K.; Kowalewski, T.; Savin, D.; Patterson, G.; Kickelbick,

G.; Huesing, N. *J. Am. Chem. Soc.* **2001**, *123*, 9445–9446; (d) Baskaran, D.; Mays, J. W.; Bratcher, M. S. *Angew. Chem. Int. Ed.* **2004**, *43*, 2138–2142; (e) Li, D.; Sheng, X.; Zhao, B. *J. Am. Chem. Soc.* **2005**, *127*, 6248–6256; (f) T. Gelbrich, M. Feyen, A. M. Schmidt, *Macromolecules* 2006, **39**, 3469–3472; (g) Fu, G. D.; Shang, Z.; Hong, L.; Kang, E. T.; Neoh, K. G. *Macromolecules* **2005**, *38*, 7867–7871; (h) Husseman, M.; Malmström, E. E.; McNamara, M.; Mate, M.; Mecerreyes, D.; Benoit, D. G.; Hedrick, J. L.; Mansky, P.; Huang, E.; Russell, T. P.; Hawker, C. J. *Macromolecules* **1999**, *32*, 1424–1431; (i) Kruk, M.; Dufour, B.; Celer, E. B.; Kowalewski, T.; Jaroniec, M.; Matyjaszewski, K. *Macromolecules* **2008**, *41*, 8584–8591; (j) Chen, R.; Zhu, S.; Maclaughlin, S.; *Langmuir* **2008**, *24*, 6889–6896; (k) Pasetto, P.; Blas, H.; Audouin, F.; Boissière, C.; Sanchez, C.; Save, M.; Charleux, B. *Macromolecules* **2009**, *42*, 5983–5995; (l) Lego, B.; François, M.; Skene, W. G.; Giasson, S. *Langmuir* **2009**, *25*, 5313–5321. For a comprehensive list, see the relevant references cited in the review papers in Ref. 1.

7. Some examples on surface-initiated nitroxide-mediated radical polymerization: (a) Matsuno, R.; Yamamoto, K.; Otsuka, H.; Takahara, A. *Macromolecules* **2004**, *37*, 2203–2209; (b) Sill, K.; Emrick, T. *Chem. Mater.* **2004**, *16*, 1240–1243; (c) Blomberg, S.; Ostberg, S.; Harth, E.; Bosman, A. W.; Van Horn, B.; Hawker, C. J. *J. Polym. Sci., Part A: Polym. Chem.* **2002**, *40*, 1309–1320; (d) Bartholome, C.; Beyou, E.; Bourgeat-Lami, E.; Chaumont, P.; Zydowicz, N. *Macromolecules* **2003**, *36*, 7946–7952; (e) Blas, H.; Save, M.; Boissière, C.; Sanchez, C.; Charleux, B. *Macromolecules* **2011**, *44*, 2577–2588. For a comprehensive list, see the relevant references cited in the review papers in Ref. 1.

8. Some examples on surface-initiated reversible addition-fragmentation chain transfer polymerization: (a) Li, C.; Benicewicz, B. C. *Macromolecules* **2005**, *38*, 5929–5936; (b) Li, C.; Han, J.; Ryu, C. Y.; Benicewicz, B. C. *Macromolecules* **2006**, *39*, 3175–3183; (c) Zhao, Y.; Perrier, S. *Macromolecules* **2006**, *39*, 8603–8608; (d) Hong, C.-Y.; You, Y.-Z.; Pan, C.-Y. *Chem. Mater.* **2005**, *17*, 2247–2254; (e) Lowe, A. B.; Sumerlin, B. S.; Donovan, M. S.; McCormick, C. L. *J. Am. Chem. Soc.* **2002**, *124*, 11562–11563. For a comprehensive list, see the relevant references cited in the review papers in Ref. 1.
9. Bao, Z.; Bruening, M. L.; Baker, G. L. *Macromolecules* **2006**, 39, 5251–5258.
10. See two representative review papers: (a) Coates, G. W.; Hustad, P. D.; Reinartz, S. *Angew. Chem. Int. Ed.* **2002**, *41*, 2236–2257; (b) Domski, G. J.; Rose, J. M.; G. W.; Coates, Bolig, A. D.; Brookhart, M. *Prog. Polym. Sci.* **2007**, *32*, 30–92.
11. Zhang, Y.; Ye, Z. *Macromolecules* **2008**, *41*, 6331–6338.
12. Xu, L.; Ye, Z.; Cui, Q.; Gu, Z.; Mercier, L. *Polymer* **2011**, *52*, 5961–5974.
13. (a) Johnson, L. K.; Killian, C. M.; Brookhart, M. *J. Am. Chem. Soc.* **1995**, *117*, 6414–6415; (b) Mecking, S.; Johnson, L. K.; Wang, L.; Brookhart, M. *J. Am. Chem. Soc.* **1998**, *120*, 888–899; (c) Ittel, S. D.; Johnson, L. K. *Chem. Rev.* **2000**, *100*, 1169–1204.
14. Zhang,Y.; Ye, Z. *Chem. Commun.* **2008**, 1178–1180.
15. (a) Zhang, K.; Ye, Z.; Subramanian, R. *Macromolecules* **2008**, *41*, 640–649; (b) Zhang, K.; Ye, Z.; Subramanian, R. *Macromolecules* **2009**, *42*, 2313–2316; (c) Xia, X.; Ye, Z.; Morgan, S.; Lu, J. *Macromolecules* **2010**, *43*, 4889–4901; (d) Liu, P.;

Landry, E.; Ye, Z.; Joly, H.; Wang, W.-J.; Li, B.-G. *Macromolecules* **2011**, *44*, 4125–4139.

16. (a) Guan, Z.; Cotts, P. M.; McCord, E. F.; McLain, S. J. *Science* **1999**, *283*, 2059–2062; (b) Guan, Z. *Chem.–Eur. J.* **2002**, *8*, 3086–3092.
17. (a) Ye, Z.; Li, S. *Macromol. React. Eng.* **2010**, *4*, 319–332; (b) Dong, Z.; Ye, Z. *Polym. Chem.* **2012**, *3*, 286–301.
18. Bailly, M.; Kontopoulou, M.; Mabrouk, K. El *Polymer* **2010**, *51*, 5506–5515.
19. (a) Morgan, S.; Ye, Z.; Zhang, K.; Subramanian, R. *Macromol. Chem. Phys.* **2008**, *209*, 2232–2240; (b) Ye, J.; Ye, Z.; Zhu, S. *Polymer* **2008**, *49*, 3382–3392; (c) Xiang, P.; Ye, Z.; Morgan, S.; Xia, X.; Liu, W. *Macromolecules* **2009**, *42*, 4946–4949; (d) Morgan, S.; Ye, Z.; Subramanian, R.; Wang, W.-J.; Ulibarri, G. *Polymer* **2010**, *51*, 597–605; (e) Xu, Y.; Xiang, P.; Ye, Z.; Wang, W.-J. *Macromolecules* **2010**, *43*, 8026–8038; (f) Xu, Y.; Campeau, P.; Ye, Z. *Macromol. Chem. Phys.* **2011**, *212*, 1255–1262; (g) Xiang, P.; Ye, Z.; Subramanian, R. *Polymer* **2011**, *52*, 5027–5039; (h) Dong, Z.; Ye, Z. *Macromolecules* **2012**, *45*, 5020–5031; (i) Zhang, Z.; Ye, Z. *Chem. Commun.* **2012**, *48*, 7940–7942.
20. (a) Bergbreiter, D. E.; Kippenberger, A. M. *Adv. Polym. Sci.* **2006**, *198*, 1–49; (b) Matsuda, T. *Adv. Polym. Sci.* **2006**, *197*, 67–106.
21. Zou, H.; Wu, S.; Shen, J. *Chem. Rev.* **2008**, *108*, 3893–3957.
22. Bartholome, C.; Beyou, E.; Bourgeat-Lami, E.; Cassagnau, P.; Chaumont, P.; David, L.; Zydowicz, N. *Polymer* **2005**, *46*, 9965–9973.
23. Ver Meer, M. A.; Narasimhan, B.; Shanks, B. H.; Mallapragada, S. K. *ACS Appl. Mater. Interfaces* **2010**, *2*, 41–47.

24. Chevigny, C.; Jouault, N.; Dalmas, F.; Bouéé F.; Jestin, J. *J. Polym. Sci. Part B: Polym. Phys.* **2011**, *49*, 781–791.

25. Chevigny, C.; Dalmas, F.; Cola, E. D.; Gigmes, D.; Bertin, D.; Bouéé F.; Jestin, J. *Macromolecules* **2011**, *44*, 122–133.

26. (a) Petrie, K.; Docoslis, A.; Vasic, S.; Kontopoulou, M.; Morgan, S.; Ye, Z. *Carbon* **2011**, *49*, 3378–3382; (b) Osazuwa, O.; Petrie, K.; Kontopoulou, M.; Xiang, P.; Ye, Z.; Docoslis, A. *Composite Sci. Eng.* **2012**, *73*, 27–33.

5.6 Supporting Information

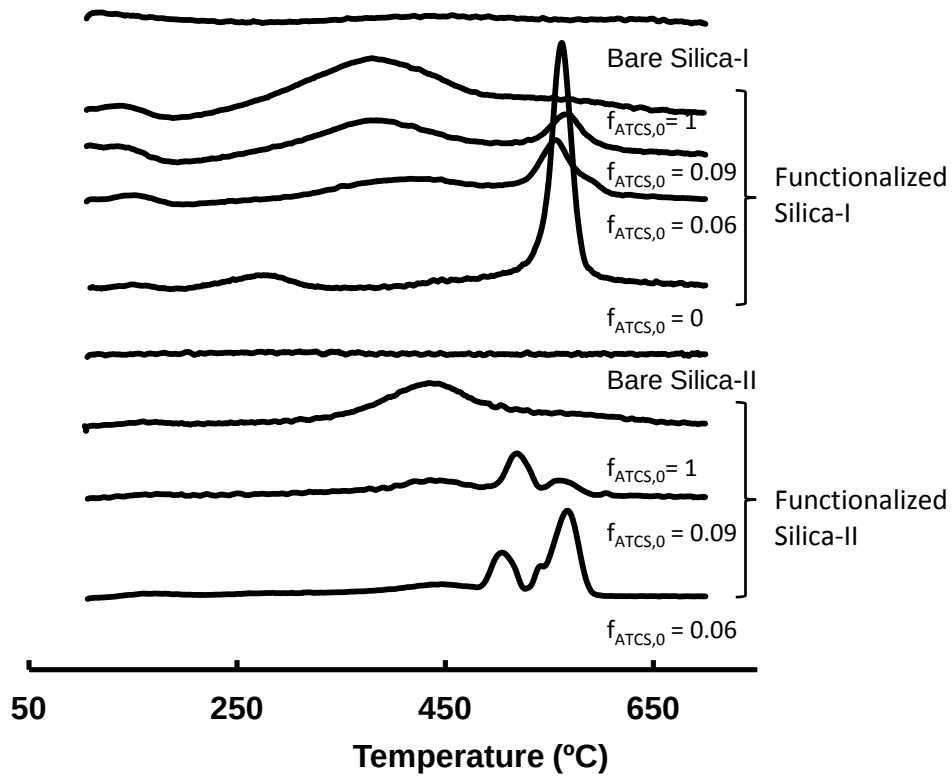

Figure S5.1. Derivative thermogravimetric curves of bare silicas and surface-functionalized silicas.

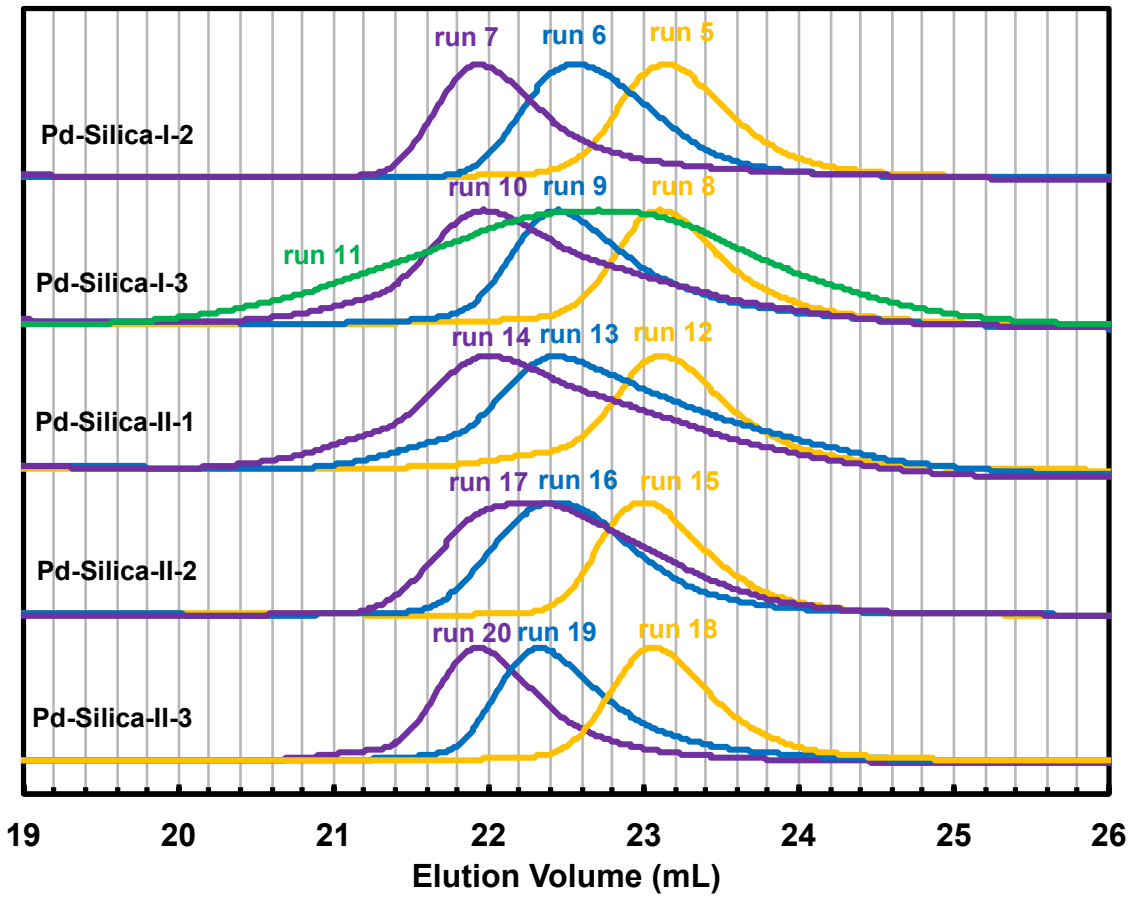

Figure S5.2 GPC elution curves (recorded from DRI detector) of cleaved PE brushes from PE-grafted silicas obtained in runs 5–18 with the various catalyst-immobilized silicas. GPC eluent: THF at 1 mL/min and at 33 ℃.

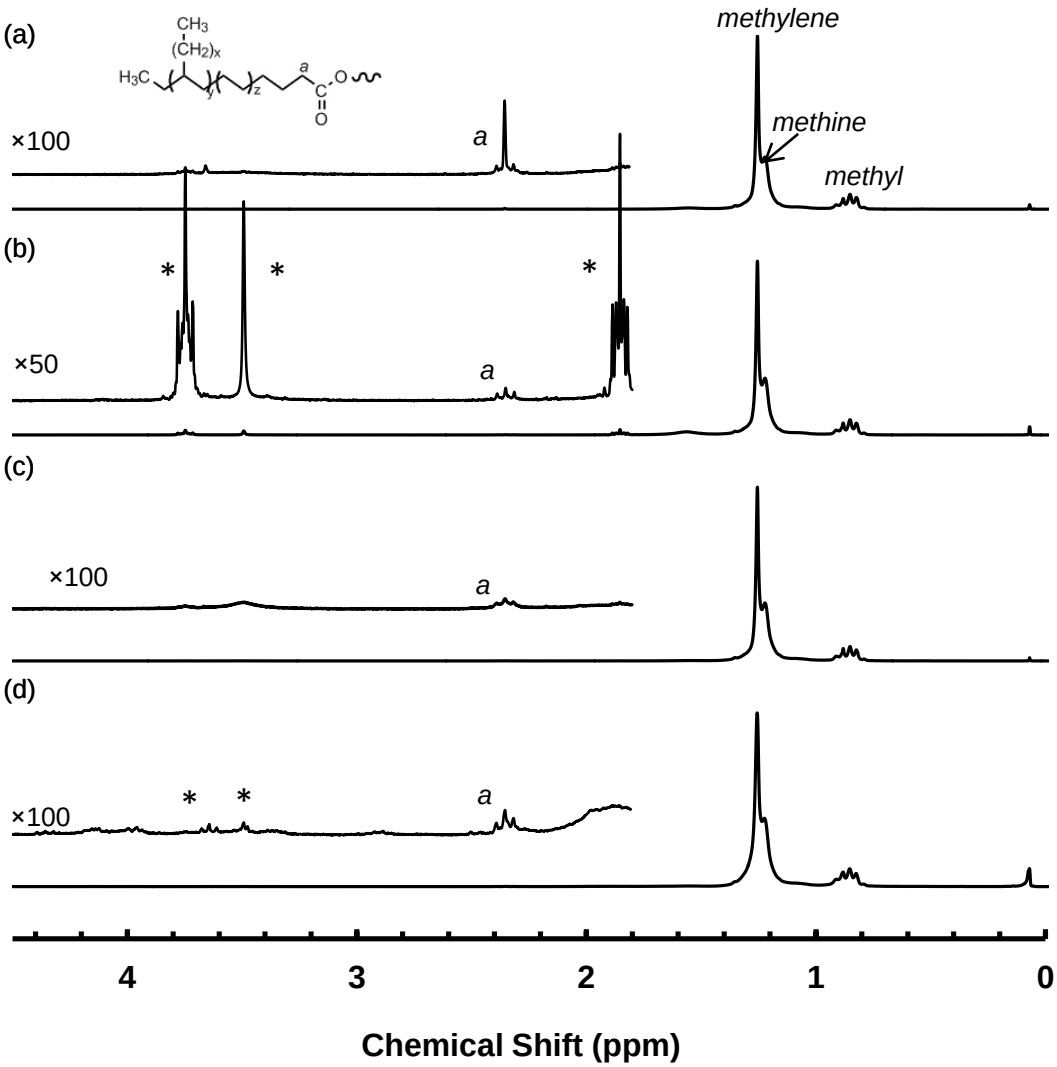

Figure S5.3 ^{1}H nuclear magnetic resonance spectra of cleaved polyethylene brushes from run 1 synthesized with Pd-Silica-I-1 (a), from run 8 synthesized with Pd-Silica-I-3 (b), from run 12 synthesized with Pd-Silica-II-1 (c), from run 18 synthesized with Pd-Silica-II-3. These runs were all carried out at 27 atm and 5 ℃ (see Table 2). The signals marked with an asterisk (*) result from trace solvent residue (methanol or THF) present in the cleaved brushes.

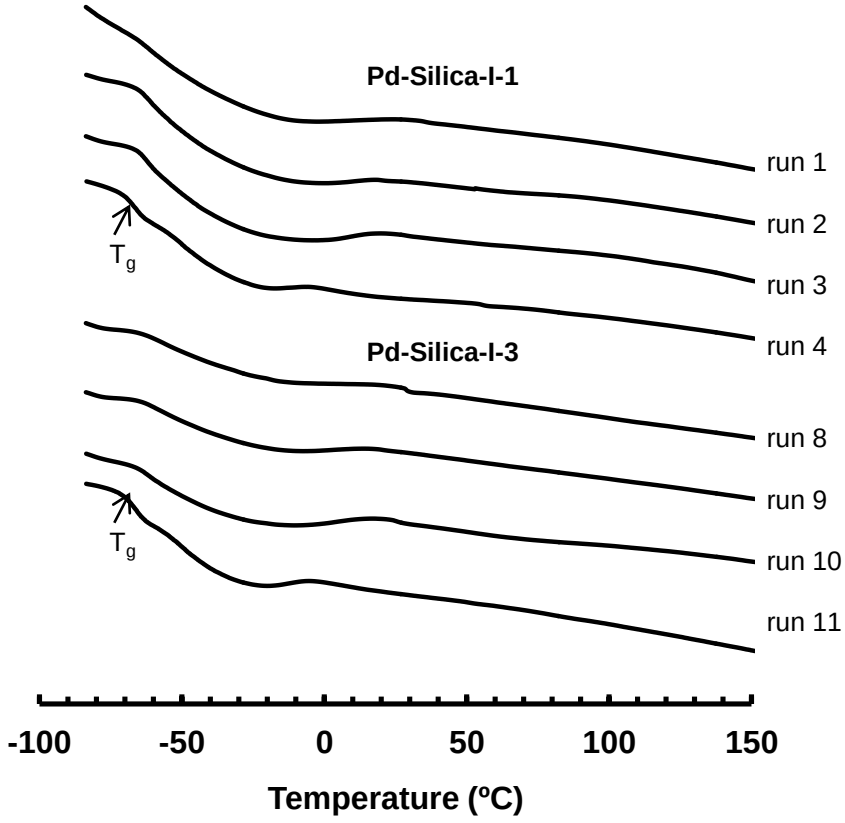

Figure S5.4 DSC thermograms of the PE-grafted silicas synthesized with Pd-Silica-I-1 and Pd-Silica-I-3, respectively.

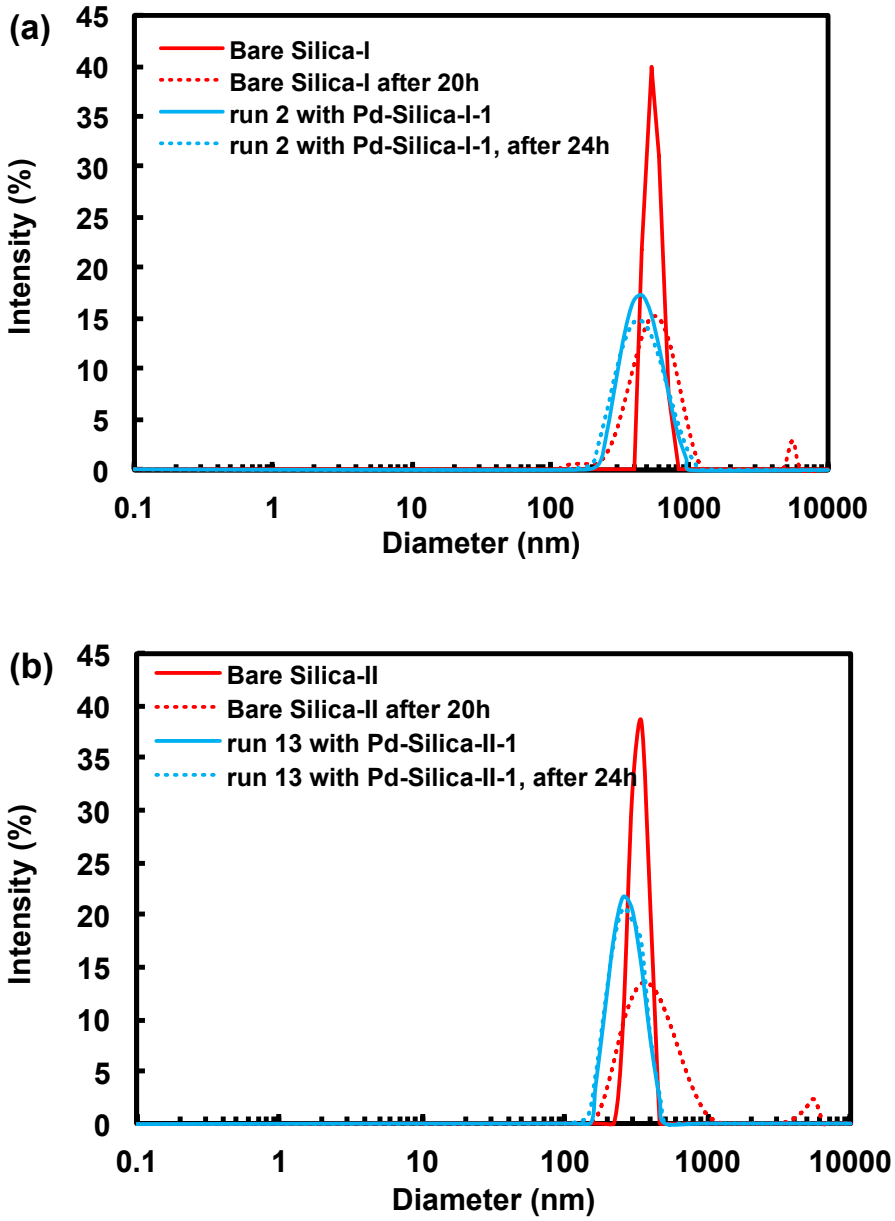

Figure S5.5 Particle size distribution of bare silicas and PE-grafted silicas determined from their dispersions with DLS at room temperature. The dispersions of bare silicas were prepared in THF and those of PE-grafted silicas were prepared in toluene.

Chapter 6

Significant Research Contributions and Recommendations for Future Developments

6.1 Significant Research Contributions of Thesis Work

To develop polymers with special chain topology or containing valuable functional group and inorganic nanoparticles with grafted polymer arms, ethylene homopolymerization/copolymerizations with Pd–diimine catalysts were carried out in this thesis. The resulting polymer/polymer-inorganic hybrid materials with unique structures and outstanding properties were characterized and some of them were utilized for various applications. A number of significant contributions to the research area on synthesis of ethylene polymerization have been made. These contributions are respectively summarized as follows.

In Chapter 2, we demonstrate the facile synthesis of a broad class of low-polydispersity E-NB copolymers having various controllable comonomer composition distributions, including gradient, alternating, diblock, triblock, and block-gradient, through "living"/quasi-living E-NB copolymerization facilitated with a single Pd–diimine catalyst. In this work, we have greatly expanded the family of E-NB copolymers and all the copolymers have controllable molecular weight and relatively low polydispersity. Some of the gradient and block-gradient copolymers have been found to

exhibit the characteristic broad glass transitions as a result of their possession of broad composition distribution.

In Chapter 3, we demonstrate the one-pot synthesis of hyperbranched HBPE ionomers containing ammonium ions via chain walking copolymerization of ethylene with polymerizable acrylate type ionic liquid comonomers by using Pd–diimine catalyst. HBPE ionomers with various ammonium ion contents have been efficiently synthesized. All ionomers have shown the hyperbranched chain architecture with branching density of ca. 90 branches per 1000 carbon. Cleaved ionomers possess narrow-distributed molecular weight distribution with different molecular weight varying from 4,000 to 22,000 g/mol. The ionic aggregation behavior in the ionomer is also discussed and the rheological characterization shows that the small amount incorporation of ammonium ions will effectively increase the complex viscosity about five factors.

In Chapter 4, we demonstrate the synthesis of HBPE ionomer encapsulating self-supported Pd(0) NPs as efficient and recyclable supported Pd catalysts. The Pd(0) nanoparticles (NPs) were immobilized on the ionomer matrix through ionic interaction directly during the copolymerization of ethylene with polymerizable ionic liquid using Pd–diimine catalyst. The resulting ionomer supported Pd(0) catalysts have been utilized in C–C coupling reactions and semi-hydrogenation of alkynes. In all semi-hydrogenation reactions of alkynes, they have shown outstanding catalytic activity and selectivity to alkenes. The HBI2 Pd catalyst has also shown great activity in both Heck and Suzuki reactions.

In Chapter 5, we further report on the successful tuning of structural parameters of PE brushes in surface-initiated ethylene "living" polymerization from two types of nonporous silica nanoparticles. We can effectively control the brush parameters including brush length, density, and topology. The PE-grafted silicas with varying brush density and length are subsequently used as nanofillers to construct polymer nanocomposites with an elastomeric EOC as the matrix polymer. The effects of brush length and density on the nanofiller dispersion, rheological properties, and tensile properties of the composites are examined.

6.2 Recommendations for Future Research

The polymers and polymer-silica nanoparticles synthesized and developed in this thesis have great potentials for various applications. Some recommendations for future research are provided in the following section.

6.2.1 Mechanical and Rheological Property Characterization of E-NB copolymer

We have synthesized a broad class of low-polydispersity E-NB copolymers having various controllable comonomer composition distributions, including gradient, alternating, diblock, triblock, and block-gradient, through "living"/quasi-living E-NB copolymerization facilitated with a single Pd–diimine catalyst. However, in Chapter 2, the mechanical and rheological properties of these polymers have not been characterized. DMA, tensile test and rheology characterization of these materials should be conducted

in the future work. The lack of these results will restrict the potential applications of these copolymers.

6.2.2 Synthesis of Artificial-Nacre Nanocomposites

Developing new lightweight materials with high mechanical and/or electrical performances is one of the major challenges in research area nowadays. Organic-inorganic biological materials such as tooth, bone and nacre with unique hierarchical microstructures have shown superior mechanical properties and biocompatibility. Thus, the synthesis of bio-inspired hybrid nanocomposites mimicking biological materials has attracted more attention in past ten years. In Chapter 3, the HBPE ionomer containing ammonium ion can bond with GO through electrical interaction mimic nature nacre resulting polymer nanocomposites material with superior mechanical strength. The successful synthesis of this artificial-nacre material will be important in both research and industrial areas.